

Second Annual Technical Progress Report

IMPROVED TECHNIQUES FOR FLUID DIVERSION IN OIL RECOVERY

Contract Number: DE-AC22-92BC14880

New Mexico Petroleum Recovery Research Center
New Mexico Institute of Mining and Technology
Socorro, New Mexico

Date of Report: October 1, 1994

Contract Date: September 17, 1992

Anticipated Completion Date: September 30, 1995

Program Manager: Randall S. Seright

Principal Investigator: Randall S. Seright

Contracting Officer's Representative: Jerry F. Casteel

Reporting Period: October 1, 1993 through September 30, 1994

PRRC Report 94-43

ABSTRACT

This report describes work performed during the second year of the project, "Improved Techniques for Fluid Diversion in Oil Recovery." This project is directed at reducing water production and increasing oil recovery efficiency. In the United States, more than 20 billion barrels of water are produced each year during oilfield operations. An average of 7 barrels of water are produced for each barrel of oil. Today, the cost of water disposal is typically between \$0.25 and \$0.50 per bbl. Therefore, there is a tremendous economic incentive to reduce water production if that can be accomplished without sacrificing hydrocarbon production. Environmental considerations also provide a significant incentive to reduce water production during oilfield operations.

This three-year project has two technical objectives. The first objective is to compare the effectiveness of gels in fluid diversion (water shutoff) with those of other types of processes. Several different types of fluid-diversion processes are being compared, including those using gels, foams, emulsions, and particulates. The ultimate goals of these comparisons are to (1) establish which of these processes are most effective in a given application and (2) determine whether aspects of one process can be combined with those of other processes to improve performance. Analyses and experiments are being performed to verify which materials are the most effective in entering and blocking high-permeability zones.

The second objective of the project is to identify the mechanisms by which materials (particularly gels) selectively reduce permeability to water more than to oil. A capacity to reduce water permeability much more than oil or gas permeability is critical to the success of gel treatments in production wells if zones cannot be isolated during gel placement.

Topics covered in this report include (1) comparisons of the use of gels, foams, emulsions, and particulates as blocking agents, (2) propagation of aluminum-citrate-HPAM gels through porous rock, (3) gel properties in fractured systems, (4) gel placement in unfractured anisotropic flow systems, and (5) an investigation of why some gels can reduce water permeability more than oil permeability.

This project receives financial support from the U.S. Department of Energy, the State of New Mexico, and a consortium of 10 oil companies. The technology developed in this project has been transferred to the oil industry in several ways. First, project review meetings are held regularly, with 20 people from 10 oil companies attending the most recent review (November 10, 1994). Second, technical progress reports are issued quarterly and annually. Third, papers are regularly presented at meetings of the Society of Petroleum Engineers (SPE) and are published in SPE and other journals (see Appendix J). Fourth, in conjunction with SPE's Distinguished Lecture Series, the presentation, "Cost-Effective Methods to Reduce Water Production," has been given in 40 locations throughout the world.

TABLE OF CONTENTS

ABSTRACT	iii
LIST OF FIGURES	ix
LIST OF TABLES	xiii
ACKNOWLEDGEMENTS	xv
EXECUTIVE SUMMARY	xvi
1. INTRODUCTION	1
Project Objectives.....	1
Report Content	1
2. USE OF FOAMS AS BLOCKING AGENTS.....	2
Some Key Features of Foam Flow Through Porous Media	2
Limiting Capillary Pressure.....	5
Minimum Pressure Gradient for Foam Generation.....	9
Minimum Pressure Gradient for Foam Mobilization	12
Linear Flow	12
Radial Flow	13
Reservoir Simulation Using the Limiting-Capillary-Pressure Concept.....	15
Foams as Blocking Agents to Reduce Gas Coning.....	15
Permeability Reduction Provided by Foams	16
Foamed Polymers and Gels	18
Field Applications of Foam Blocking Agents.....	19
Conclusions	19
3. USE OF EMULSIONS AS BLOCKING AGENTS	21
Some Key Features of Emulsion Flow Through Porous Media	21
Dilute Oil-in-Water Emulsions	21
Concentrated Oil-in-Water Emulsions	22
Concentrated Water-in-Oil Emulsions	22
Models of Emulsion Flow Through Porous Media.....	22
Using Emulsions as Blocking Agents.....	23
Potential Improvements.....	27
Patent Literature.....	27
Emulsion/Polymer and Emulsion/Gelant Combinations	28
Analogy with Foams	28
Field Application	29
Conclusion.....	29
4. USE OF PARTICULATES AS BLOCKING AGENTS.....	30
Formation Damage From Particulate Invasion.....	30
Selective Plugging Using Preformed Xanthan Gels	31
Selective Plugging Using Particulates In Unfractured Wells	32

Exploiting Differences In Transient Times For Selective Placement.....	34
Selective Plugging Using Particulates In Fractured Wells	36
Exploiting Gravity For Selective Placement.....	36
Shallow Plugging-Selective Re-Entry Technique.....	38
Theoretical Model.....	39
Basic Assumptions	39
Effects of Particulates on Gelant Placement	42
Particulates with a Monodisperse Size	42
Particulates with a Size Distribution.....	45
Conclusions	50
5. PROPAGATION OF AN ALUMINUM-CITRATE-HPAM "COLLOIDAL-DISPERSION" GEL THROUGH BEREA SANDSTONE	51
Importance of the Suggested Behavior	51
Experimental.....	52
Injection of Polymer Solution Without Aluminum	52
Injection of Polymer Solution With Aluminum.....	58
Summary.....	58
Consideration of Literature Reports.....	62
Tiorco Laboratory Data	62
Other Literature Data	62
Tiorco Field Data	62
Conclusions	64
6. FLOW OF ONE-DAY-OLD GELS THROUGH FRACTURES.....	65
Core Properties	65
Gels Examined.....	68
Coreflood Sequence.....	68
Discussion of Results	85
Cr(III)-Acetate-HPAM.....	85
Resorcinol-Formaldehyde	86
Cr(III)-Xanthan.....	86
Cr(III)-Acetate-PAM/AMPS.....	86
Cr(VI)-Redox-PAM/AMPS.....	86
Al-Citrate-HPAM.....	87
Conclusions	87
7. EFFECTS OF GEL CURING AND MECHANICAL BREAKDOWN ON GEL PROPAGATION THROUGH FRACTURED CORES.....	88
Curing Effects for a Cr(III)-Acetate-HPAM Gel.....	88
Curing Effects for a Hydroquinone-Hexamethylenetetramine-HPAM Gel.....	89
Performance of a Sheared Cr(III)-Acetate-HPAM Gel.....	94
Recycling of a Cr(III)-Acetate-HPAM Gel Through a Fractured Core.....	98
Recycling of a Cr(III)-Acetate-HPAM Gel Through a Series of Fractured Cores	101
Conclusions	113

8. GEL PLACEMENT IN ANISOTROPIC FLOW SYSTEMS	114
Models Used.....	114
Analysis Using Model 1.....	114
Streamlines.....	114
Permeability Distribution.....	115
Areal Flow Profile During Gelant Injection	115
Effect of Resistance Factor	117
Injectivity Expressions	117
Comparison of Linear Flow with Anisotropic Radial Flow	119
Effect of Distance of Gelant Penetration	121
Conclusions for Model 1.....	121
Analysis Using Model 2.....	121
Model Description.....	121
Pressure Profile Before Gel Placement	123
Pressure Profile After Gel Forms	126
Limitations Associated with Using Numerical Methods in Model 2	126
Conclusions	126
9. DISPROPORTIONATE PERMEABILITY REDUCTION.....	129
Experimental Procedures.....	129
Gelants Studied.....	129
Rock and Fluids Used	129
Coreflood Sequence.....	130
Endpoint Permeabilities Before Gel Treatments.....	131
Gelant Placement in Cores	133
Permeability Reduction Using Cr(III)-Acetate-HPAM Gels.....	134
Effects of Permeability and Lithology on the Disproportionate Permeability Reduction.....	136
Possible Mechanisms For Disproportionate Permeability Reduction.....	137
Water and Oil Pathway Constrictions and Wettability Effects.....	137
Segregated Oil and Water Pathways	138
Conclusions	142
Future Work	143
NOMENCLATURE	144
REFERENCES	147
APPENDIXES	
A Effect of Formation Permeability on Degree of Permeability Reduction by Particulates	159
B Derivation of Eq. 37.....	161
C Derivation of Eq. 38.....	163
D Derivations of Eqs. 39, 40, and 41.....	166
E Derivation of Eq. 42.....	169

F	A Fortran Program to Determine the Profile of the Gelant Front: Supplement to Chapter 8.....	173
G	Pressure Expression After Gel Forms for Near-Wellbore Gelant Placement: Supplement to Chapter 8.....	179
H	Pressure Expression After Gel Forms When the Gelant Reaches the Outer Boundary in the x-Direction: Supplement to Chapter 8.....	185
I	Data Supplement to Chapter 9.....	196
J	Technology Transfer	218

LIST OF FIGURES

Figure 1.	Distinction between a blocking agent and a mobility-control agent.....	3
Figure 2.	Simplified view of foam flow	4
Figure 3.	Concept of limiting capillary pressure in foam flow	6
Figure 4.	Permeability dependence of capillary pressures	7
Figure 5.	Permeability dependence of gas mobility	8
Figure 6.	Replotted data from Lee, Heller & Hoefler.....	10
Figure 7.	Minimum pressure gradient for foam generation	11
Figure 8.	Blocking agent entering two non-communicating zones	14
Figure 9.	In production wells, foams may collapse in oil zones more rapidly than in water zones.....	17
Figure 10.	Effect of particle size and filter-cake permeability on the degree of gelant penetration for particulates with a monodisperse size	43
Figure 11.	Effect of filtration coefficient on the degree of gelant penetration for particulates with a monodisperse size.....	44
Figure 12.	Particulates with a normal size distribution.....	46
Figure 13.	Effect of standard deviation on the degree of gelant penetration	47
Figure 14.	Effect of mean particle size on degree of gelant penetration	48
Figure 15.	Effect of permeability contrast on the maximum standard deviation for a given selectivity.....	49
Figure 16.	Viscosity vs. shear rate and HPAM concentration	53
Figure 17.	Viscosity vs. time since gelant preparation.....	54
Figure 18.	Resistance factor vs. throughput for HPAM: first 13 PV.....	55
Figure 19.	Resistance factor vs. throughput for HPAM: first 15 PV.....	56
Figure 20.	Resistance factor vs. velocity for HPAM.....	57
Figure 21.	Resistance factor vs. throughput for first 10 PV of Al-citrate-HPAM injection	59

Figure 22.	Resistance factor vs. throughput for first 20 PV of Al-citrate-HPAM injection	60
Figure 23.	Residual resistance factor vs. throughput for Al-citrate-HPAM gel.....	61
Figure 24.	Schematic of a fractured core	66
Figure 25.	Tracer results in fractured vs. unfractured Berea sandstone cores	67
Figure 26.	Apparent mobility before, during, and after placement of a Cr(III)-acetate-HPAM gel.....	69
Figure 27.	Tracer results before vs. after placement of a Cr(III)-acetate-HPAM gel.....	70
Figure 28.	Permeability reduction vs. pressure gradient after placement of a Cr(III)-acetate-HPAM gel.....	71
Figure 29.	Apparent mobility before, during, and after placement of a resorcinol-formaldehyde gel.....	72
Figure 30.	Tracer results before vs. after placement of a resorcinol-formaldehyde gel.....	73
Figure 31.	Apparent mobility before, during, and after placement of a Cr(III)-xanthan gel.....	74
Figure 32.	Tracer results before vs. after placement of a Cr(III)-xanthan gel.....	75
Figure 33.	Permeability reduction vs. pressure gradient after placement of a Cr(III)-xanthan gel.....	76
Figure 34.	Apparent mobility before, during, and after placement of a Cr(III)-acetate-PAM/AMPS gel.....	77
Figure 35.	Tracer results before vs. after placement of a Cr(III)-acetate-PAM/AMPS gel.....	78
Figure 36.	Permeability reduction vs. pressure gradient after placement of a Cr(III)-acetate-PAM/AMPS gel.....	79
Figure 37.	Apparent mobility before, during, and after placement of a Cr(VI)-redox-PAM/AMPS gel.....	80
Figure 38.	Tracer results before vs. after placement of a Cr(VI)-redox-PAM/AMPS gel.....	81
Figure 39.	Permeability reduction vs. pressure gradient after placement of a Cr(VI)-redox-PAM/AMPS gel.....	82
Figure 40.	Apparent mobility before, during, and after placement of an Al-citrate-HPAM gel.....	83
Figure 41.	Tracer results before vs. after placement of an Al-citrate-HPAM gel.....	84
Figure 42.	Tracer results before vs. after placement of Cr(III)-acetate-HPAM gels in fractured cores.....	90

Figure 43.	Tracer results before vs. after placement of hydroquinone-hexamethylenetetramine-HPAM gels in fractured cores.....	93
Figure 44.	Resistance factors and pressure gradients during placement of a sheared Cr(III)-acetate-HPAM gel.....	95
Figure 45.	Residual resistance factors and pressure gradients during brine injection after placement of a sheared Cr(III)-acetate-HPAM gel.....	96
Figure 46.	Tracer results before vs. after placement of a sheared Cr(III)-acetate-HPAM gel.....	97
Figure 47.	Resistance factors during the first and second cycles of gel injection.....	99
Figure 48.	Resistance factors during the third, fourth, and fifth cycles of gel injection.....	100
Figure 49.	Resistance factors during the sixth, seventh, and eighth cycles of gel injection	102
Figure 50.	Tracer results before vs. after placement of a Cr(III)-acetate-HPAM gel in Fractured Core 25	103
Figure 51.	Resistance factors during the first cycle of gel injection into a series of five fractured cores.....	105
Figure 52.	Resistance factors during the first two cycles of gel injection into five fractured cores	106
Figure 53.	Resistance factors in the first, third, and fifth fractured cores through 12 cycles of gel injection.....	107
Figure 54.	Resistance factors in the second and fourth fractured cores through 12 cycles of gel injection.....	108
Figure 55.	Residual resistance factors during brine injection into five fractured cores	111
Figure 56.	Tracer results after gel placement for Fractured Cores A, B, C, D, and E.....	112
Figure 57.	Plan view of the gelant front. $F_r=1$	116
Figure 58.	Degree of gelant penetration in direction i vs. permeability ratio when gelant reaches the outer boundary in the most-permeable direction	118
Figure 59.	Comparison of injectivity ratio for linear flow and anisotropic radial flow when $r_{px}=50$ ft.....	120
Figure 60.	Injectivity ratios in anisotropic radial flow for different radii of gelant penetration	122
Figure 61.	Pressure profile during brine injection before gel placement when $\rho_x/\rho_y=10$	124

Figure 62.	Plan view of the gelant front in the first quadrant when gelant reached the outer boundary in the x-direction.....	125
Figure 63.	Pressure profiles during brine injection after gel placement when $r_{px}=5$ ft and $\Delta p_x/\Delta p_y=10$	127
Figure 64.	Pressure profiles during brine injection after gel placement when $r_{px}=50$ ft and $\Delta p_x/\Delta p_y=10$	128
Figure 65.	Apparent rheology during oil and water injection.....	139
Figure 66.	Segregated water and oil pathways.....	140

LIST OF TABLES

Table 1.	Radial Flow System.....	25
Table 2.	Linear Flow System.....	26
Table 3.	Example Rock and Fluid Properties for Transient Time Calculations.....	35
Table 4.	Example Fluid Properties for Exploiting Gravity for Selective Placement Calculations	38
Table 5.	Rock and Fluid Properties for Degree of Penetration Calculations	42
Table 6.	Core and Fracture Permeabilities.....	65
Table 7.	Gel Compositions.....	68
Table 8.	Properties in Fractured Cores with One-Day-Old Gels.....	85
Table 9.	Injection of a Cr(III)-Acetate-HPAM Gel into Fractured Cores.....	89
Table 10.	Injection of a Hydroquinone-Hexamethylenetetramine-HPAM Gel into Fractured Cores	91
Table 11.	Properties of Fractured Cores Mounted in Series.....	104
Table 12.	Resistance Factors During Gel Injection into a Series of Five Fractured Cores	109
Table 13.	Gelant Compositions and Viscosities (at 41°C).....	129
Table 14.	Rock and Fluid Properties	130
Table 15.	Sequence Followed During Oil/Water Core Experiments.....	131
Table 16.	Summary of Residual Saturations (S_{wr} , S_{or}) and Endpoint Permeabilities (k, k) Obtained Before Gel Treatment. Core: Strongly Water-Wet Berea Sandstone (SSL-68), 41°C	132
Table 17.	Summary of Residual Saturations (S_{wr} , S_{or}) and Endpoint Permeabilities (k, k) Obtained Before Gel Treatment. Core: Indiana Limestone (LSH-67), 41°C	132
Table 18.	Gelant Placement Data (41°C).....	133
Table 19.	Summary of Residual Resistance Factors. Core: High-Permeability Berea Sandstone (SSH-S2) Gel: 0.5% HPAM (Alcoflood 935®), 0.0417% Cr(III)-Acetate, 1% NaCl.....	134
Table 20.	Summary of Residual Resistance Factor and Tracer Results. Core: High-	

	Permeability Berea Sandstone (SSH-71). Gel: 0.5% HPAM (Alcoflood 935®), 0.0417% Cr(III)-Acetate, 1% NaCl.....	135
Table 21.	Summary of Residual Resistance Factors. Core: High-Permeability Berea Sandstone (SSH-75). Gel: 1% HPAM (Alcoflood 935®), 0.0834% Cr(III)- Acetate, 1% NaCl.....	135
Table 22.	Summary of Residual Resistance Factors. Core: High-Permeability Berea Sandstone (SSH-77). Gel: 0.75% HPAM (Alcoflood 935®), 0.0625% Cr(III)- Acetate, 1% NaCl.....	136
Table 23.	Summary of Residual Resistance Factors. Core: High-Permeability Berea Sandstone (SSH-78). Gel: 0.75% HPAM (Alcoflood 935®), 0.0625% Cr(III)- Acetate, 1% NaCl.....	136
Table 24.	Effects of Permeability and Lithology on the Disproportionate Permeability Reduction	137
Table 25.	Impact of Wettability on Gel Performance.....	138
Table 26.	Summary of F_{ro} and F_{rw} Values for Dilute Oil-Based Gels	141
Table 27.	Summary of F_{ro} and F_{rw} Values for a Concentrated Oil-Based Gel.....	142

ACKNOWLEDGEMENTS

This work was financially supported by the United States Department of Energy, the State of New Mexico, Arco Exploration and Production Technology Co., British Petroleum Company, Chevron Petroleum Technology Co., Conoco Inc., Exxon Production Research Company, Marathon Oil Co., Mobil Research and Development Corp., Phillips Petroleum Co., Texaco Inc., and Unocal. This support is gratefully acknowledged. I greatly appreciate the efforts of those individuals who contributed to this project. Dr. Jenn-Tai Liang played the major role in the work described in Chapters 4 and 9. Richard Schrader performed the experimental work described in Chapters 5, 6, and 7. Rowelyn Lansangan helped Richard during some of this work. John Hagstrom and Haiwang Sun performed the experiments described in Chapter 9. Mei Ye was principally responsible for performing and reporting the work in Chapter 8. I thank J.P. Heller, A.R. Kovscek, C.J. Radke, and W.R. Rossen for helpful discussions regarding Chapter 2. Hassan Nimir also contributed to the work described in Chapter 2. I also thank K. Stanley and her staff for reviewing the report. I especially appreciate the thorough review of the manuscript by Julie Ruff.

EXECUTIVE SUMMARY

This report describes work performed during the second year of the project, "Improved Techniques for Fluid Diversion in Oil Recovery." This three-year project has two general objectives. The first objective is to compare the effectiveness of gels in fluid diversion with those of other types of processes. Several different types of fluid-diversion processes are being compared, including those using gels, foams, emulsions, and particulates. The second objective of the project is to identify the mechanisms by which materials (particularly gels) selectively reduce permeability to water more than to oil.

Use of Foams as Blocking Agents. We examined the use of foams as blocking agents. In concept, several phenomena could allow foams to be superior to gels as blocking agents, however, only in certain circumstances. At present, these circumstances are hypothetical; very few conditions have been verified experimentally or in field applications. Two phenomena (the limiting capillary pressure and the minimum pressure gradient for foam generation) could allow low-mobility foams to form in high-permeability zones but not in low-permeability zones. Exploiting these phenomena during foam placement requires that (1) under given reservoir conditions, a gas/liquid composition must be identified that will foam in high-permeability zones but not in low-permeability zones, (2) the foam must not easily collapse or wash out from the high-permeability zones, and (3) the aqueous phase must not contain a gelant or other reactive blocking agent.

The following is a list of several other ideas where foams, foamed polymers, or foamed gels could have advantages over gels as blocking agents. However, all of these concepts require further development and experimental verification.

1. When oil wells are returned to production after foam injection, foams could collapse more rapidly in oil zones than in water zones. Foam washout from the water zones could be reduced by incorporating a polymer or gel into the foam. If a gelant is used, the foam must be produced from the oil zones before gelation occurs; otherwise, the oil zones could be damaged.
2. Preformed foamed gels may be effective blocking agents for plugging fractures. Because gelation occurs before injection, leakoff from fractures could be minimized using foamed gels. Because they are foams, foamed gels may propagate through fractures more effectively than preformed gels (i.e., foamed gels may be less likely to screen out or develop excessively high pressure gradients during injection).
3. Because of their high gas content, foamed gels formed using "strong" gels may allow more control in achieving low or intermediate residual resistance factors.
4. In cyclic steam projects, foam placement could be aided by gravity effects combined with very large mobility contrasts between the foam and the displaced oil.
5. For foams, residual resistance factors for gas can increase with increasing permeability. This behavior could be exploited when using foam as a gas blocking agent. A similar phenomenon has not been observed for water residual resistance factors in the presence of foam. Gels and foams are known to show different permeability reductions for different phases. Experimental work is needed to establish the permeability reduction properties of foamed polymers and foamed gels.

Use of Emulsions as Blocking Agents. We also examined the use of emulsions as blocking agents to improve reservoir sweep efficiency. Although several features of emulsion flow through porous media

remain unanswered, our analysis of the literature indicates that emulsions or emulsion/gel combinations will not perform significantly better than gels as blocking agents, particularly in the areas of placement characteristics and permeability-reduction properties.

Use of Particulates as Blocking Agents. We also examined the use of particulates as blocking agents. Petroleum and patent literature was surveyed to investigate whether particulates have potential advantages over gels for use as blocking agents. Most of the literature surveyed made unsubstantiated claims that particulates can selectively plug high-permeability thief zones without damaging oil productivity. Critical analyses of these claims reveal that most of the proposed schemes suffer from the same placement limitations that gels experience. Particulates small enough to penetrate into the formation can cause significant damage to the formation permeability. The degree of permeability reduction increases with decreasing formation permeability.

We developed a theoretical model to examine the feasibility of using particulates to prevent gelant penetration into low-permeability zones. Our theoretical analyses revealed that, when used in conjunction with gels, monodisperse particulates could prevent gelant leakoff into the rock matrix during the placement process. To achieve selective placement, the size of the particulates must be small enough to penetrate readily into high-permeability zones but large enough not to enter low-permeability zones.

For economic and technical reasons, particulates used in field applications usually have a size distribution. To achieve selective placement using particulates with a normal size distribution, a maximum standard deviation exists that should not be exceeded for a given permeability contrast. The maximum standard deviation for selective placement decreases with decreasing permeability contrast. For a given standard deviation, maximum selectivity is achieved by choosing the average of the critical particle sizes of the high- and low-permeability zones as the mean particle size.

Propagation of an Aluminum-Citrate-HPAM "Colloidal-Dispersion" Gel Through Berea Sandstone. We studied the ability of an aluminum-citrate-HPAM "colloidal-dispersion" gel to propagate through Berea sandstone. Our experimental results indicate that this formulation basically behaves like other gels and gelants. Early in the gelation process, it propagates through sandstone like a polymer solution without crosslinker. After some point (presumably when gel aggregates grow to the size of pore throats), gel propagation is extremely slow or negligible. Although we observed an unusual behavior during the second day of gelant injection, we do not expect aluminum-citrate-HPAM formulations to propagate through porous rock like a "super polymer" after gel formation.

An objective analysis of the literature supports these findings. Claims to the contrary were based largely on field results that assumed the wells were not fractured. The field and laboratory results can be explained if the reservoir is assumed to be naturally fractured. Alternatively, the results could be explained by assuming that gelation never occurred because the aluminum crosslinker did not propagate through the formation.

Flow of One-Day-Old Gels Through Fractures. Preformed gels were forced through fractured cores. Using several different types of gels, the objectives of these experiments were to (1) determine whether excessive pressure gradients would develop during gel injection, (2) assess how effectively the gels "heal" fractures, and (3) determine whether the gels wash out easily during brine injection after gel placement.

Our data indicates both hope and caution concerning the injection of gels into fractured systems. Our tracer studies indicated that some gels can effectively heal fractures under the right circumstances. However, the high resistance factors and pressure gradients exhibited during placement raise concern

about our ability to propagate these gels deep into a fracture system. We suspect that the ability of a given gel to propagate effectively through a fracture depends on (1) the composition of the gelant, (2) the degree of gelation or gel curing, (3) the fluid velocity (or pressure gradient) in the fracture, and (4) the width, conductivity, and tortuosity of the fracture. Thus, at this point, we are not suggesting that one gel is necessarily better than other gels for fracture applications. More work will be needed to establish the best circumstances for propagation of gels in fractures.

Effects of Gel Curing and Mechanical Breakdown on Gel Propagation Through Fractured Cores. In this work, we report results from studies involving two gels, including a Cr(III)-acetate-HPAM gel and a hydroquinone-hexamethylenetetramine-HPAM gel. An interesting feature of the latter gel is that a high temperature (e.g., 110°C) is required for the gelation reaction to proceed at a rapid rate. At the temperature of our core experiments (41°C), the gelation rate is negligible. Therefore, the gelation reaction can be allowed to proceed to a desired point at 110°C and then quenched and studied at 41°C.

For hydroquinone-hexamethylenetetramine-HPAM gels that were aged for 1 day or more at 110°C, these gels effectively healed fractures at 41°C, but they exhibited high resistance factors and pressure gradients during injection. For gels that were aged for 0.5 to 0.75 days at 110°C, low resistance factors and pressure gradients were observed during injection, but the gel treatments did not improve sweep efficiency in the fractured cores.

For Cr(III)-acetate-HPAM gels that were aged 10, 24, and 72 hrs before injection into short fractured cores, gel treatments effectively healed the fractures without damaging porous rock. For Cr(III)-acetate-HPAM gels that were aged 24 hrs before injection (at 200 ml/hr), gel resistance factors were typically about 3,000 in fractures with conductivities ranging from 53.8 to 1,560 darcy-cm. This result suggests that resistance factors may be independent of fracture conductivity for a gel with a fixed velocity and a fixed degree of gelation or curing. Also, during gel injection, the pressure gradient may be inversely proportional to the fracture conductivity.

A five-day-old mechanically blended (sheared) Cr(III)-acetate-HPAM gel exhibited lower than usual resistance factors and pressure gradients in a fractured core. Although this gel treatment did not heal the fracture, it did significantly improve sweep efficiency.

Experiments were performed where Cr(III)-acetate-HPAM gels were recycled through a single fractured core and through a series of fractured cores. In these experiments, the gel showed plugging behavior in some cores but not others. The plugging behavior did not correlate with fracture conductivity or with fracture position in a series of fractured cores. Additional work is needed to determine why the gel heals some fractures more effectively than others.

Gel Placement in Anisotropic Flow Systems. Two theoretical models were developed to determine flow profiles before and after gel placement in anisotropic reservoirs. The primary question addressed in this work is, How anisotropic must an unfractured reservoir be to achieve an acceptable gel placement and profile modification during unrestricted gelant injection? Both analytical and numerical methods were applied to solve the problem. We studied how the effectiveness of gel treatments are influenced by permeability variation, distance of gelant penetration, anisotropic pressure distributions, resistance factor, and residual resistance factor.

Our analyses showed that k_x/k_y must be greater than 1,000 (and usually greater than 10,000) before anisotropy can be exploited to achieve a satisfactory gel placement in unfractured wells. We doubt that any unfractured wells or reservoirs exist with this degree of anisotropy. In contrast, in wells and

reservoirs where anisotropic flow is due to fractures, the linear flow geometry and the extreme permeability contrast between the fracture and the porous rock can aid gel placement substantially.

Disproportionate Permeability Reduction. A capacity to reduce water permeability much more than oil permeability is critical to the success of gel treatments in production wells if zones cannot be isolated during gel placement. Although several researchers have reported polymers and gels that provide this disproportionate permeability reduction, the explanation for the phenomenon was unclear. In our first annual report, we examined several possible mechanisms for why some gels can reduce water permeability more than oil permeability. We demonstrated that the disproportionate permeability reduction is not caused by gravity or lubrication effects. Also, gel shrinking and swelling are unlikely to be responsible for the phenomenon. In this report, we continue our study of the disproportionate permeability reduction. Our experimental results indicate that wettability effects may play a role that affects the disproportionate permeability reduction. However, they do not appear to be the root cause for water permeability being reduced more than oil permeability. Results from experiments with an oil-based gel suggest that segregation of oil and water pathways through a porous medium may play the dominant role in causing the disproportionate permeability reduction. Experiments are continuing to verify this concept. We also examined the effects of permeability and lithology on the disproportionate permeability reduction. Disproportionate permeability reduction was observed in both a low-permeability Berea sandstone core and an Indiana limestone core with a water-based gel. Because we were not able to force multiple pore volumes of gelant into the low-permeability Berea sandstone core and the Indiana limestone core, we have not yet established the effects that permeability and lithology have on the disproportionate permeability reduction. Additional work will be required to address this issue.

1. INTRODUCTION

In any oil recovery process, fractures and high-permeability streaks can cause early breakthrough of injected fluid and reduce oil recovery efficiency. They can also aggravate production of excess water or gas in reservoirs with water-drive or gas-drive recovery mechanisms. Several different types of processes have been proposed to reduce channeling of fluids through fractures and streaks of very high permeability. Processes that use crosslinked polymers or other types of gels have been most common. However, processes using emulsions, foams, suspended solids, precipitates, and microorganisms have also been proposed or tested. Although many of these fluid-diversion (or water or gas shutoff) projects have been very successful, many other projects have been technical failures. At present, there is no consensus on where or how the various treatments should be applied.

Project Objectives

This three-year project has two general objectives. The first objective is to compare the effectiveness of gels in fluid diversion with those of other types of processes. Several different types of fluid-diversion processes are being compared, including those using gels, foams, emulsions, and particulates. The ultimate goals of these comparisons are to (1) establish which of these processes are most effective in a given application, and (2) determine whether aspects of one process can be combined with those of other processes to improve performance. Analyses and experiments are being performed to verify which materials are the most effective in entering and blocking high-permeability zones. Another objective of the project is to identify the mechanisms by which materials (particularly gels) selectively reduce permeability to water more than to oil.

Report Content

This report describes work performed during the second year of the project. (Work performed during the first year of the project was documented in Ref. 1). The use of foams, emulsions, and particulates as blocking agents are investigated in Chapters 2, 3, and 4, respectively. In Chapter 5, we examine the ability of an aluminum-citrate-HPAM "colloidal-dispersion" gel to propagate through Berea sandstone.

Chapters 6 and 7 documents result of experiments in which preformed gels were forced through fractured cores. Using several different types of gels, the objectives of these experiments were to (1) determine whether excessive pressure gradients would develop during gel injection, (2) assess how effectively the gels "heal" fractures, and (3) determine whether the gels wash out easily during brine injection after gel placement.

In Chapter 8, we examine how anisotropic an unfractured reservoir must be to achieve an acceptable gel placement during unrestricted gelant injection.

Finally, Chapter 9 documents the latest results from our investigation of why some gels can reduce water permeability more than oil permeability.

2. USE OF FOAMS AS BLOCKING AGENTS

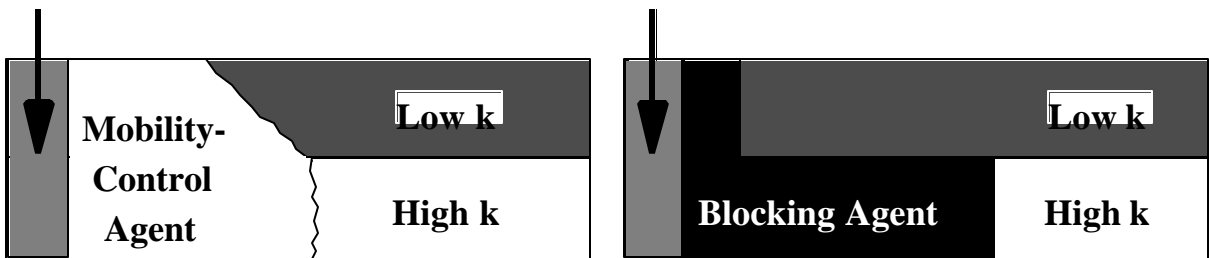
A considerable volume of theoretical, laboratory, and field work has been performed to evaluate the use of foams as mobility-control agents during steam and high-pressure gas floods. Much less work has been done to evaluate the use of foams as blocking agents. The distinction between a blocking agent and a mobility-control agent is an important concept to understand (see Fig. 1). A mobility-control agent should penetrate as much as possible into the less-permeable zones so that oil can be displaced from poorly swept zones. In contrast, we wish to minimize penetration of blocking agents into the less-permeable, oil-productive zones. Any blocking agent that enters the less-permeable zones can hinder subsequent injected fluids (e.g., water, CO₂, steam) from entering and displacing oil from those zones.

In this chapter, we examine the use of foams as blocking agents. A foam is a gas dispersed in a liquid. Also, we define a foamed polymer to be a foam where the aqueous liquid phase is a polymer solution, and a foamed gel is the product that results from a foam where the liquid phase contains a gelant. The basic question that we want to answer in this analysis is, Can foams be made to work better than gels as blocking agents? Thus, we will use the performance of gels as a basis of comparison. This analysis will use experimental, theoretical, and field results from the literature. Although much of the literature focuses on the use of foams as mobility-control agents, we will consider whether the reported properties of foams can be exploited during placement of these materials in blocking applications. Three concepts that we will investigate in this regard are (1) the limiting-capillary-pressure concept, (2) the concept of a minimum pressure gradient for foam mobilization, and (3) the concept of a minimum pressure gradient for foam generation.

Some Key Features of Foam Flow Through Porous Media

In the 1960s, researchers demonstrated that foam transport through porous media should not be treated as the transport of a single phase (i.e., "foam").^{2,4} Instead, propagation of gas and water should be considered separately. Bernard *et al.*³ found that at a given water saturation, S_w , the relative permeability to water, k_{rw} , is independent of surfactant concentration in the aqueous phase. For example, at any given water saturation in a core, k_{rw} is the same when no surfactant is present as when the aqueous phase contains 1% surfactant. In contrast, gas mobility is very dependent on the surfactant concentration. Gas mobility is quite low in the presence of the 1% surfactant solution because an effective foam is generated. When no surfactant is present, gas mobility remains high.

Fig. 2 presents a simplified view of foam flow in porous media, as proposed by Radke and co-workers.^{5,6} In this view, water wets the rock and also fills the smallest pores. Consistent with the findings of Bernard *et al.*³, k_{rw} is strictly a function of water saturation. The primary means by which foams affect k_{rw} is by increasing the trapped gas saturation (thereby decreasing S_w).³ Between 85% and 99% of the gas saturation is effectively immobile (trapped) and is located primarily in the pores of intermediate sizes.^{6,7} The effective permeability of this "phase" is zero. The third "phase" shown in Fig. 2 is that of flowing gas, which primarily propagates through the largest pores. This gas flows as a train of bubbles (lamellae) that continually form and coalesce as they propagate. In typical reservoir rocks, these lamellae are at least as large as the pores through which they flow.⁵ The mobility of the flowing gas is a quantity that presents a challenge to predict.



- For a mobility control agent, penetration into low-k zones should be maximized.

- For a blocking agent, penetration into low-k zones should be minimized.

Fig. 1. Distinction between a blocking agent and a mobility-control agent.

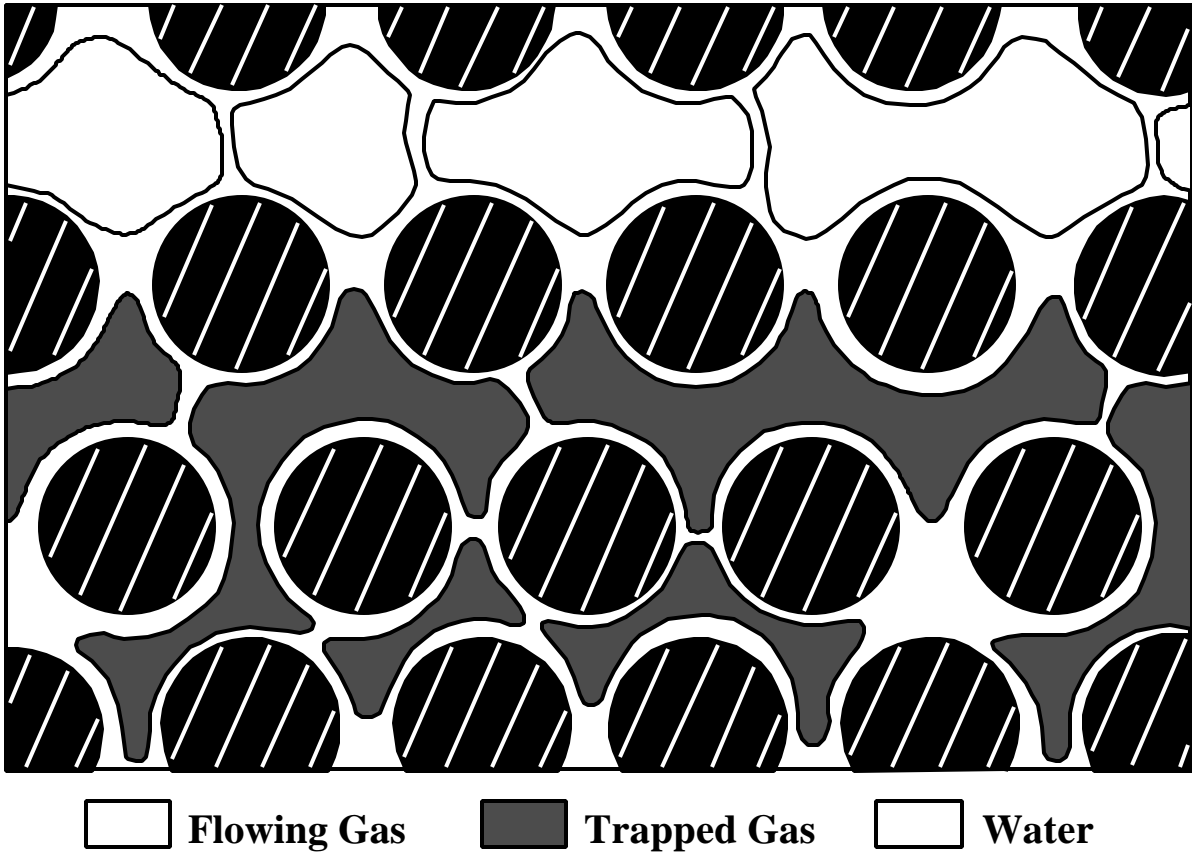


Fig. 2. Simplified view of foam flow (from Radke and Gillis⁶).

Limiting Capillary Pressure

Khatib *et al.*⁸ applied the concept of limiting capillary pressure to predict foam flow through porous media. To explain this concept, consider two gas bubbles that are flowing through a water-wet porous medium, as shown in Fig. 3. Because of their close proximity, these bubbles are separated by a film of water. A pressure difference, called the capillary pressure, exists between the gas phase and the liquid phase. The limiting-capillary-pressure concept recognizes that if the capillary pressure is too great, water will be sucked away from the film, the film separating the bubbles will collapse, and the bubbles will coalesce. The capillary pressure at which this coalescence occurs is called the limiting capillary pressure. According to Khatib *et al.*⁸, this capillary pressure could depend on (1) the type and concentration of surfactant and electrolyte, (2) the gas velocity, and (3) the rock permeability. (Radke *et al.*¹⁰ argue that the limiting capillary pressure is, at best, a very weak function of rock permeability)

We are interested specifically in how the limiting capillary pressure affects foam placement in heterogeneous reservoirs. This can be understood by considering Figs. 4 and 5, which were taken from Figs. 11 and 12 of Ref. 8. Fig. 4 illustrates how the limiting capillary pressure varies with permeability, as speculated by Khatib *et al.*⁸ (In contrast, Radke *et al.*¹⁰ argue that the limiting capillary pressure is basically independent of permeability.) This figure also shows how the capillary entry pressure varies with permeability. The capillary entry pressure is the injection pressure that must be exceeded to overcome capillary forces and allow the non-wetting phase to enter the porous medium. For the surfactant/brine system considered by Khatib, Fig. 4 indicates that the capillary entry pressure exceeds the limiting capillary pressure in low-permeability rock. In this situation, water films between flowing gas bubbles will always be unstable and bubbles will coalesce very rapidly. As a result, normal gas and liquid flow behavior will be observed—that is, gas mobility will increase linearly with increasing rock permeability. The case of normal gas-liquid flow through porous media is illustrated by the top dashed line in Fig. 5. Khatib *et al.*⁸ point out that gas mobility in the presence of surfactant solutions in low-permeability rock may be lower than that in the absence of surfactant because the surfactant solutions can increase the trapped gas saturation. Thus, they predict that until the limiting capillary pressure exceeds the capillary entry pressure, gas mobility increases linearly with increased rock permeability, as indicated by the first linear portion of the solid curve in Fig. 5. If the capillary entry pressure exceeds the limiting capillary pressure for all zones in a reservoir, no placement advantage exists for foams over gelants. Since both foams and gelants exhibit analogous flow behavior in this situation, their placement characteristics in heterogeneous reservoirs will be similar (if gravity effects are neglected).

If the limiting capillary pressure exceeds the capillary entry pressure (e.g., for permeabilities above 800 md in Fig. 4), Khatib *et al.*⁸ predict that gas mobility should decrease with increasing permeability up to a point (see the middle part of the solid curve in Fig. 5). This property promotes foam as a mobility-control agent. Foams will penetrate more efficiently into the less-permeable zones because the foams can exhibit a higher mobility in low-permeability rock than in high-permeability rock. However, this behavior is opposite of the desired performance for a blocking agent. We want to minimize penetration of blocking agents into the less-permeable zones. If the injectant was a foamed gelant that behaved as shown in the middle part of the solid curve in Fig. 5, the low-permeability zones could be seriously damaged after the gel forms. Thus, if all zones in a reservoir are in this regime of behavior, a placement disadvantage exists for foam blocking agents when compared to gelants.

In very high-permeability porous media, Khatib *et al.*⁸ predict that gas mobility again increases linearly with increased permeability (Fig. 5). Following the same argument that was given earlier, if all zones in a reservoir fall in this regime of behavior, no placement advantage exists for foams over gelants.

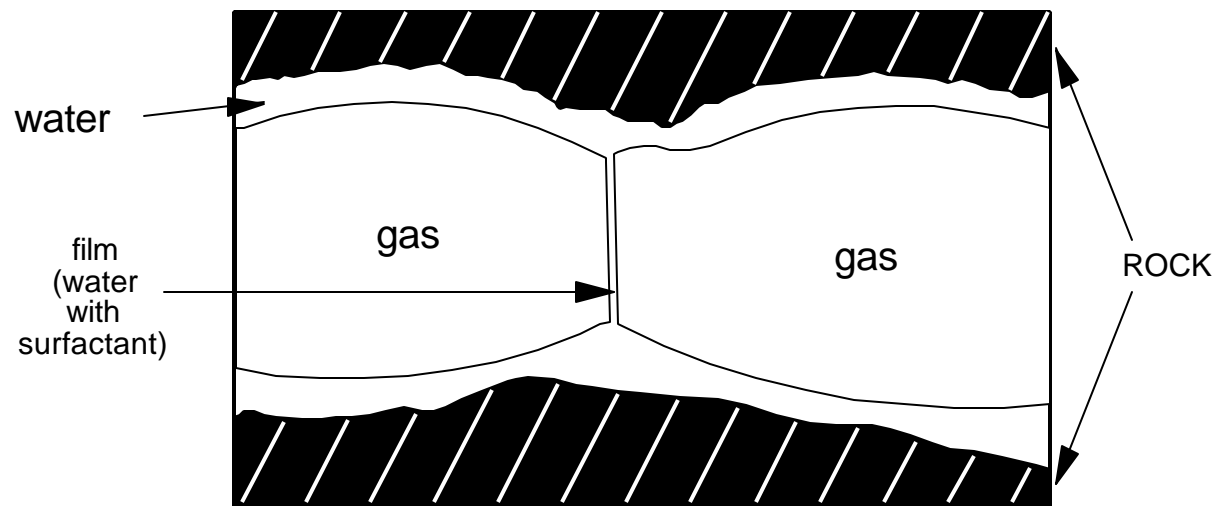


Fig. 3. Concept of limiting capillary pressure in foam flow.⁸

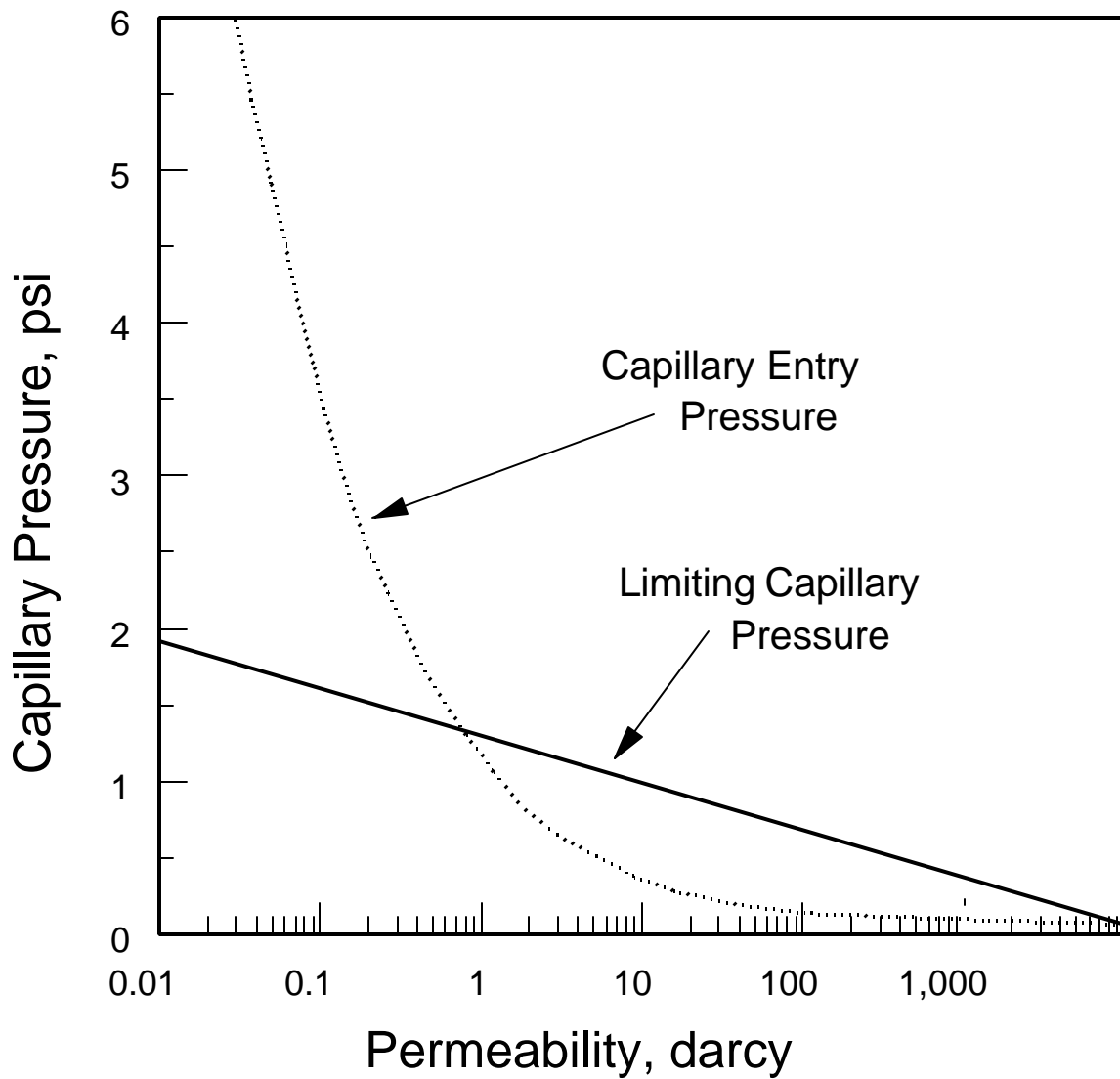


Fig. 4. Permeability dependence of capillary pressures (from Khatib et al.⁸).

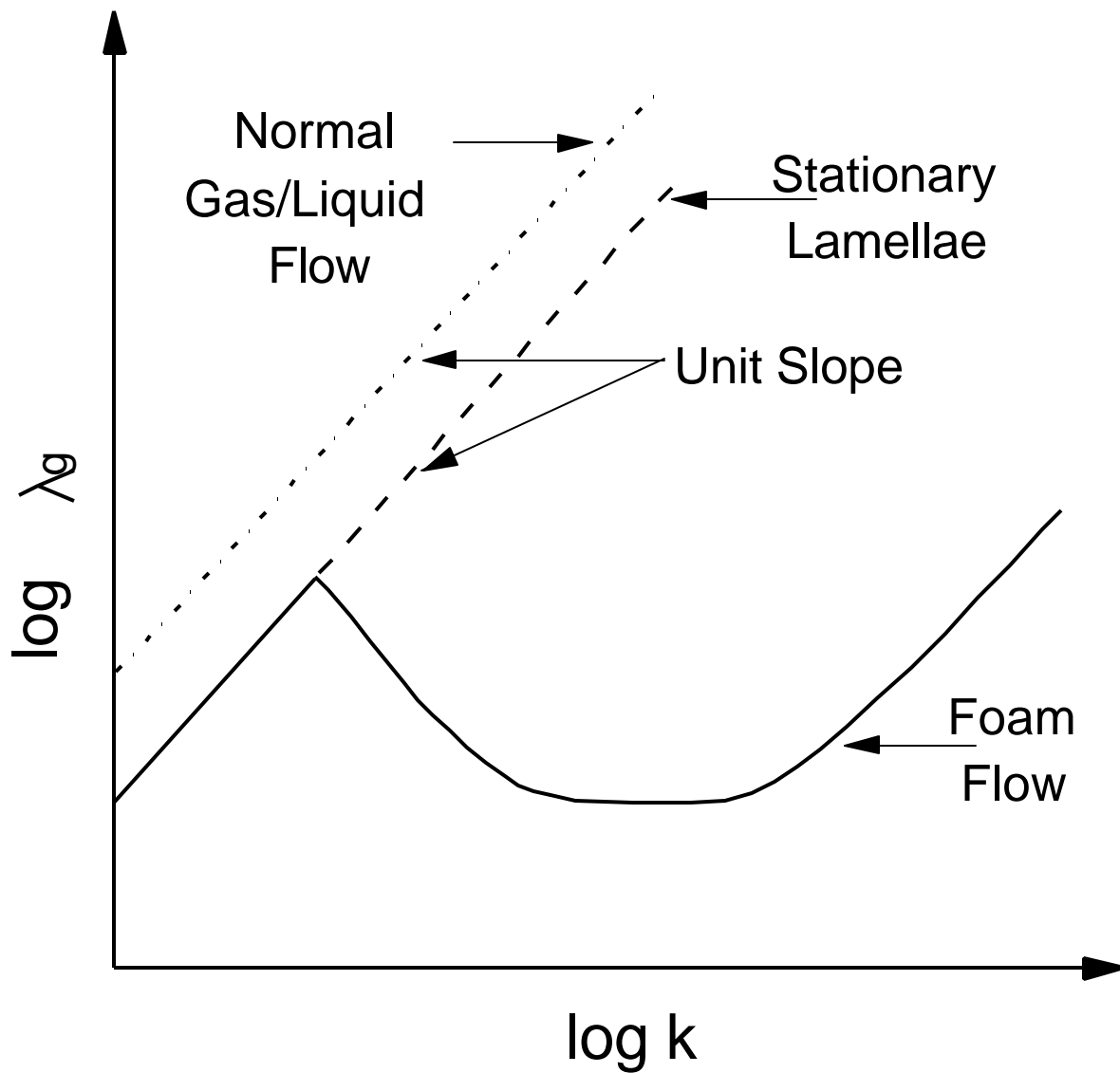


Fig. 5. Permeability dependence of gas mobility (from Khatib et al.⁸).

Using the limiting-capillary-pressure concept, one circumstance can be identified where a foam blocking agent could have a placement advantage over a gelant. That is the case where the capillary entry pressure is less than the limiting capillary pressure in the offending high-permeability zone(s) but is greater than the limiting capillary pressure in the less-permeable hydrocarbon-productive zones. In that case, a low-mobility foam will be generated in the high-permeability zone(s) but not in the less-permeable zones. Since no foam is generated in the less-permeable zones, injected fluids will not be inhibited from entering and displacing oil from these zones. In contrast, as long as the foam persists in the high-permeability zones, it will restrict fluid entry. Of course, exploitation of this concept requires identification of the permeability where the limiting capillary pressure equals the capillary entry pressure. Two other limitations must be recognized. First, the injected foam must not undergo a reaction that forms a blocking agent after placement. For example, the surfactant solution must not include a gelant. A low-mobility foam generated in the high-permeability zone(s) will cause the gelant to penetrate an excessive distance into the less-permeable zones. Second, if water or gas is injected after placement of a foam bank, the foam may eventually be washed out or diminished in effectiveness. One possible method to maintain the integrity of the foam bank was suggested by C. J. Radke (private communication, Berkeley, CA, December 10, 1993). This method involves continuous injection of a dilute surfactant solution (with or without gas) after placement of the foam bank. The surfactant concentration in the foam bank must be sustained at a level high enough to prevent collapse of the foam.

Khatib's experimental support of the limiting-capillary-pressure concept was confined to results from studies in high-permeability beadpacks (72 to 8,950 darcys).⁸ Additional support for the theory is needed in both low- and high-permeability rock. The data of Lee *et al.*⁹ could be viewed as supportive of the limiting-capillary-pressure concept. Their work used cores with permeabilities ranging from 0.4 to 302 md. Fig. 6 replots data from Fig. 2 of Lee *et al.* in a form that is comparable with Fig. 5. The solid curves show the forms predicted by the limiting-capillary-pressure model. Of course, the model would appear to be more valid if more data were available in low- and high-permeability rock. Several other researchers have examined foam mobility as a function of permeability, but that work is not sufficient to confirm or contradict Khatib's prediction of the permeability dependence of foam mobility.^{2,3,10-12}

Minimum Pressure Gradient for Foam Generation

Researchers reported that a minimum pressure gradient or fluid velocity is required for foam generation in porous media.^{13,14} Using a composition that contained 95% nitrogen and 5% surfactant solution, Friedmann *et al.*¹³ found that the minimum pressure gradient for foam generation decreases with increased permeability, as shown in Fig. 7 (which is based on Fig. 8 of Ref. 13). For a given pressure gradient, this result means that foam is more likely to be generated in high-permeability zones than in low-permeability zones. This property promotes the use of foam as a mobility control agent. If a low-mobility foam is generated in the high-permeability zones but no foam is generated in the less-permeable zones, a greater fraction of the injected fluids will enter the less-permeable zones. If the foam is to be used as a blocking agent, the restrictions mentioned above apply. In particular, the surfactant formulation must not undergo a reaction that forms a blocking agent after placement (e.g., it must not contain a gelant). Also, some means must be available to prevent the foam from deteriorating in the high-permeability channels. In addition, a formulation must be identified that will behave properly (i.e., generate foam in the high-permeability channels but not in the low-permeability zones) for the specific near-wellbore pressure gradients and reservoir conditions in the intended application. Kovscek feels that the minimum pressure gradient for foam generation is a phenomenon that will be found primarily for foams with very low liquid saturations (A. R. Kovscek private communication, June 20, 1994).

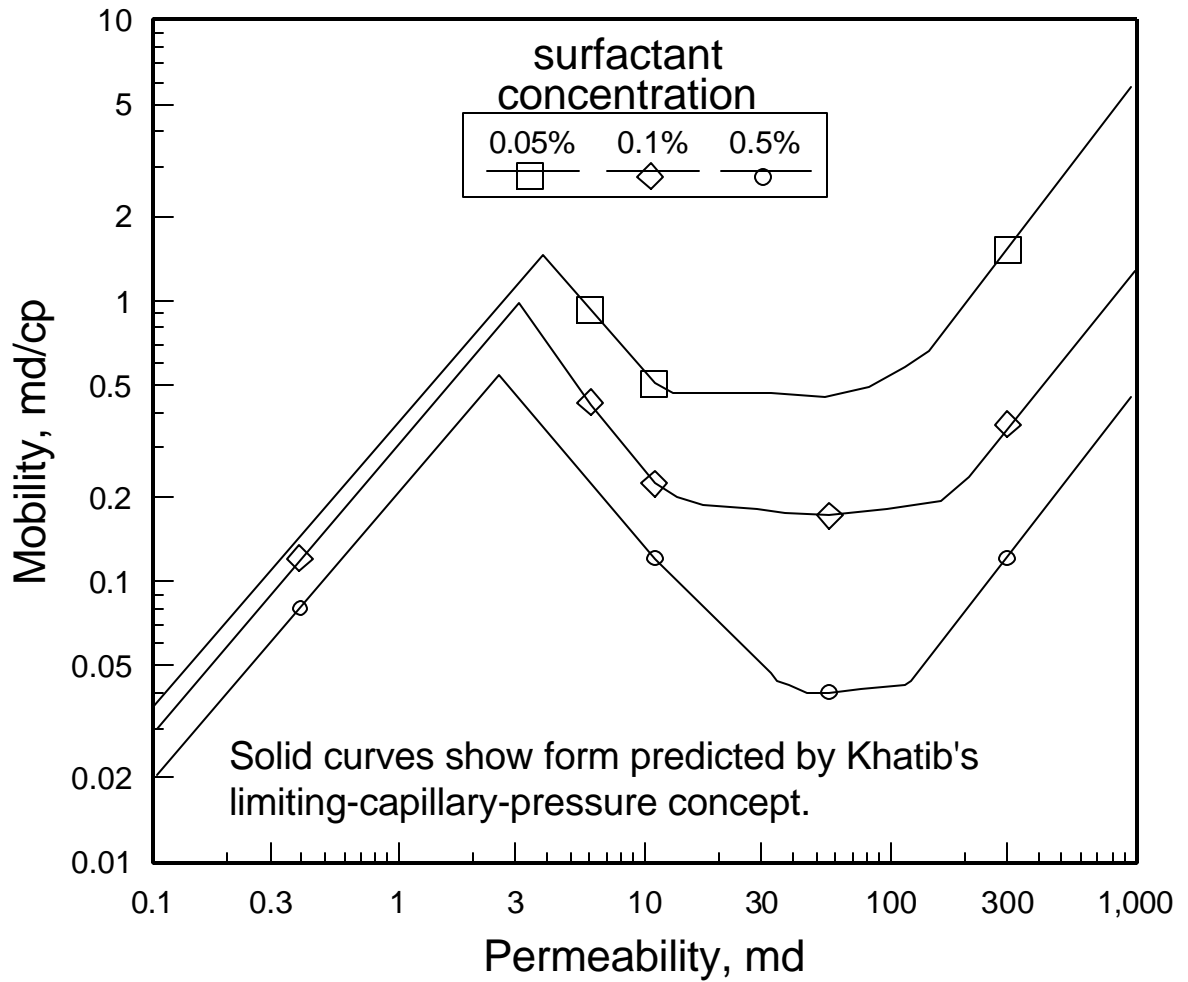


Fig. 6. Replotted data from Lee, Heller & Hoefer.⁹

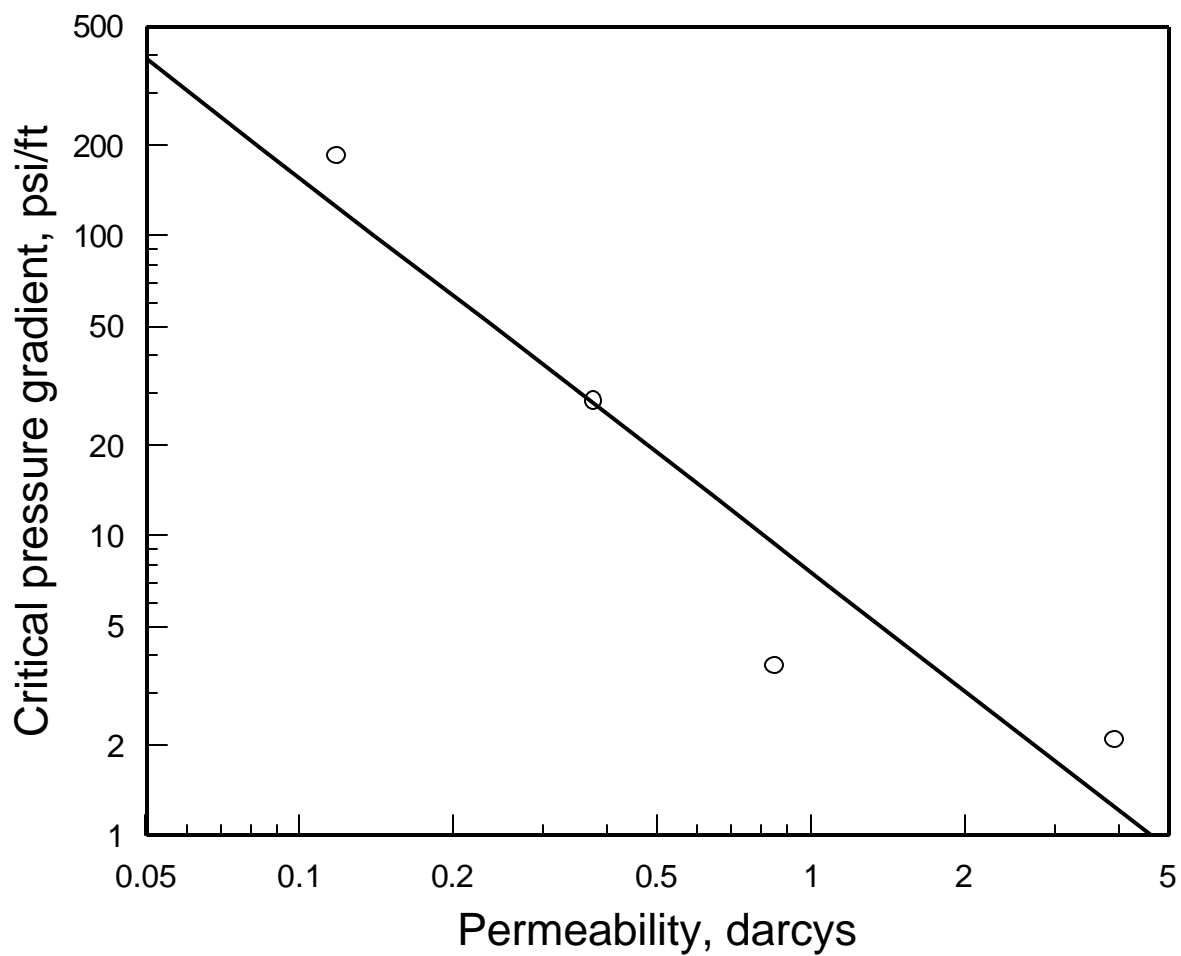


Fig. 7. Minimum pressure gradient for foam generation (replotted data from Friedmann et al.¹³).

Minimum Pressure Gradient for Foam Mobilization

Albrecht and Marsden¹⁵ and Rossen¹⁶ examined the concept of a minimum pressure gradient for foam mobilization (or more correctly, gas mobilization). For foam of a given texture, gas flow will stop if the pressure gradient is reduced below a certain minimum value. (Rossen points out that there are limitations to when this phenomenon will occur.¹⁷) In circumstances where the phenomenon will occur, Rossen suggests that the minimum pressure gradient for foam mobilization, $(dp/dl)_{\min}$, should be inversely proportional to the square root of permeability, k , as indicated in Eq. 1 (C_1 is a constant).

$$\left(\frac{dp}{dl}\right)_{\min} = \frac{C_1}{\sqrt{k}} \quad (1)$$

If the pressure drop between an injection well and a production well is fixed and if the pressure drop is not sufficient to keep the foam mobilized throughout the reservoir, Eq. 1 predicts that the foam will stop flowing in low-permeability zones before they stop flowing in high-permeability zones. Hypothetically, this phenomenon might be exploited to maximize penetration of a blocking agent in the high-permeability zones and minimize penetration in low-permeability zones.

Linear Flow. We wish to quantify whether this effect could be exploited to achieve a placement for foam blocking agents that is superior to that for gelants. First, consider linear flow in a reservoir with two non-communicating zones (Fig. 8). Assume that the foam has flowed until it achieves the minimum pressure gradient for mobilization in the low-permeability zone (Zone 2) and in the high-permeability zone (Zone 1). Because flow is linear, the pressure drops across the foam banks in the low- and high-permeability zones are given by Eqs. 2 and 3, respectively.

$$\Delta p_2 = L_{p2} \left(\frac{dp}{dl}\right)_{\min 2} \quad (2)$$

$$\Delta p_1 = L_{p1} \left(\frac{dp}{dl}\right)_{\min 1} \quad (3)$$

When the foam stops flow in both zones, Δp_1 is necessarily equal to Δp_2 . Therefore, Eqs. 1, 2, and 3 can be combined to give Eq. 4.

$$(4)$$

For comparison, a gelant with a water-like viscosity (Newtonian, unit-mobility displacement) will provide gelant frontal positions in linear flow as described by Eq. 5.¹⁸

$$(5)$$

For realistic values of porosity (ϕ), the expression given by Eq. 5 will always be less than that given by Eq. 4. Therefore, in linear flow in reservoirs without crossflow, the minimum pressure gradient for foam mobilization will not provide a placement for a foam blocking agent that is superior to that for placement of a gelant with a water-like viscosity.

Radial Flow. Next, consider radial flow in a reservoir with two non-communicating zones. Because flow is radial, the foam will flow away from the wellbore until a radius is reached where the pressure gradient falls below the minimum pressure gradient for foam mobilization. At that time, the pressure drop across the foam bank in the low-permeability zone, Δp_2 , is given by Eq. 6.

$$\Delta p_2 = \int_{r_w}^{r_{p2}} \frac{dp}{dr} dr \quad (6)$$

Since

$$\frac{dp}{dr} = \frac{r_{p2}}{r} \frac{dp}{dr}_{\min 2} = \frac{r_{p2} C_1}{r \sqrt{k_2}}, \quad (7)$$

Eq. 6 can be modified to give Eq. 8.

$$\Delta p_2 = \frac{r_{p2} C_1}{\sqrt{k_2}} \ln \left\{ \frac{r_{p2}^2}{r_w} \right\} \quad (8)$$

A similar equation applies to the high-permeability zone.

$$\Delta p_1 = \frac{r_{p1} C_1}{\sqrt{k_1}} \ln \left\{ \frac{r_{p1}^2}{r_w} \right\} \quad (9)$$

When the foam stops flow in both zones, Δp_1 is necessarily equal to Δp_2 . Therefore, Eqs. 8 and 9 can be combined to give Eq. 10.

$$(10)$$

For comparison, a gelant with a water-like viscosity (Newtonian, unit-mobility displacement) will provide gelant frontal positions in radial flow as described by Eq. 11.¹⁸

$$(11)$$

Since r_{p1} (the radius of penetration of blocking agent in the high-permeability zone) is greater than r_{p2} , the ratio of r_{p2}/r_{p1} given by Eq. 10 will be greater than that determined by Eq. 11 (for realistic values of porosity). Therefore, in radial flow in reservoirs without crossflow, the minimum pressure gradient for foam mobilization will not provide a placement for a foam blocking agent that is superior to that for placement of a gelant with a water-like viscosity.

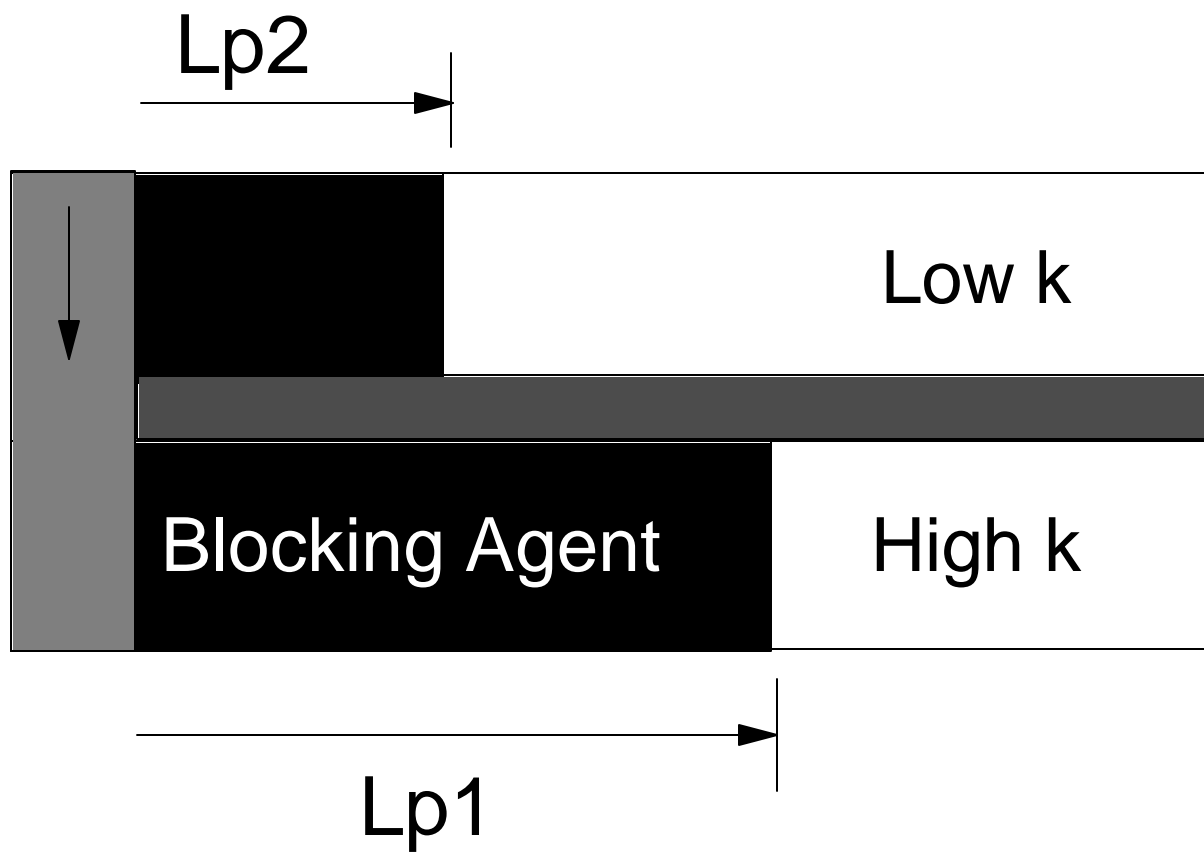


Fig. 8. Blocking agent entering two non-communicating zones.

Reservoir Simulation Using the Limiting-Capillary-Pressure Concept

Rossen^{17,19} and Kovscek *et al.*²⁰ incorporated the limiting-capillary-pressure concept in modeling foam flow in stratified reservoirs. In most circumstances, these modeling efforts predict that gas and surfactant solution (i.e., foam) will penetrate to a greater extent into less-permeable zones than if foams do not form or are not present. However, if two communicating zones are in capillary equilibrium, Rossen argues that the limiting-capillary-pressure phenomenon can increase channeling of gas (but **not** surfactant solution) through high-permeability zones.^{17,19} Kovscek *et al.* predict that the situation described by Rossen will rarely occur because the approach to capillary equilibrium is too long to be of practical importance.

If practical circumstances can be identified where foams maximize gas penetration into high-permeability zones (and minimize gas penetration into low-permeability zones), a gas-based blocking agent may have potential. For example, Irani²¹ describes a composition containing 17.4% polydimethylsiloxane polymer, 5.8% toluene, and 76.8% CO₂ that forms one phase at 8,000 psi and 32°C. Upon dropping the pressure to 2,800 psi, the solution splits into two phases. This phase transition was proposed as a means to form an effective blocking agent. More work is needed to determine whether gas-based blocking agents can have placement advantages over water-based blocking agents.

The analyses of Rossen and Kovscek *et al.* do not suggest a benefit associated with incorporating aqueous gelants into the foam. Both analyses indicate that foam injection increases the tendency for the aqueous phase (surfactant/gelant solution) to penetrate into the less-permeable zones.

Foams as Blocking Agents to Reduce Gas Coning

Foams have been proposed as blocking agents to reduce gas coning.^{4,22-25} Hanssen²³ suggests that some foams can withstand passage of substantial volumes of gas before deteriorating—thereby resisting washout during applications to reduce gas coning. Ideally, gravity could be exploited to place low-density foams above oil zones without damaging oil productivity. Unfortunately, for commonly used injection rates, viscous forces usually dominate over gravity forces near the wellbore.^{1,24,26} Therefore, viscous foams usually penetrate a significant distance into all zones that are open to flow near the wellbore. To minimize this potential problem, researchers from Rogaland Research Institute^{24,27} proposed injecting a nonaqueous surfactant solution (without gas) with a density intermediate between that of gas and oil. Little or no viscous foam is formed while injecting the nonaqueous surfactant solution. During a shut-in period after surfactant injection, gravity will position the low-viscosity surfactant solution between the gas and oil columns in the reservoir. (Depending on the formation permeability and fluid densities and viscosities, this equilibration time may take weeks or months to complete.¹) When the well is returned to production, gas will cone through the surfactant solution and form a gas-blocking foam that will resist further gas coning.

Of course, a similar concept could be applied using gelants. To reduce gas coning, the gelant density should be intermediate between that of oil and gas. To reduce water coning, the gelant density should be intermediate between that of water and the hydrocarbon phase. In both cases, the gelation time must be long enough to allow gravity to position the gelant properly. Often, gelation and shut-in times of many weeks or months will be required to achieve proper placement.¹

No matter what type of blocking agent is used (foam, gel, cement, etc.), practical limitations exist concerning how much the critical rate for water or gas coning can be increased and how long water or gas breakthrough can be delayed by man-made barriers.^{24,28-30} In three-dimensional coning problems, the critical rate for water or gas coning is typically predicted to increase by a factor between 1.5 and 5,

depending on the coning model used.²⁹ Unless the desired production rate is fairly close (i.e., within a factor of 1.5 to 5) to the pretreatment critical rate, man-made barriers of any type will be of limited value in mitigating three-dimensional coning problems. Substantially greater effects on the critical rates are predicted for blocking agents in vertically fractured systems (i.e., two-dimensional "coning" problems).^{29,30}

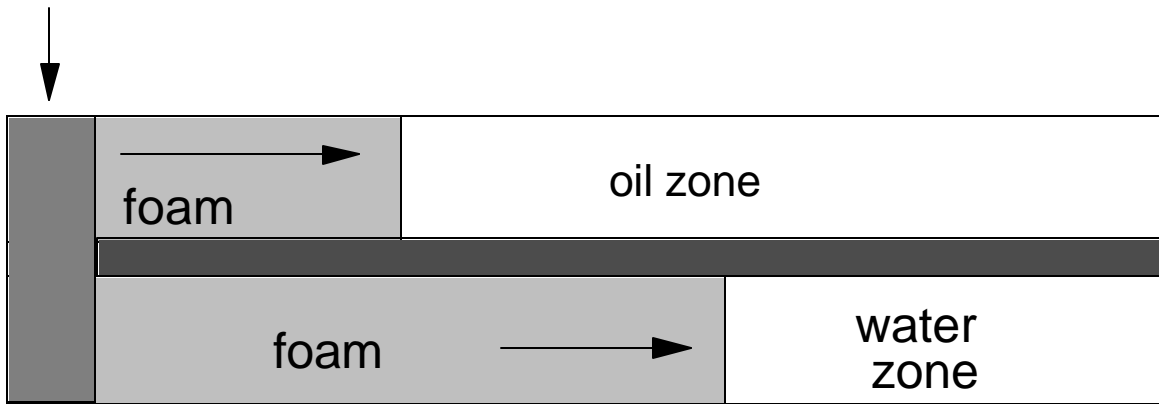
Permeability Reduction Provided by Foams

For applications in injection wells, the ideal blocking agent would reduce permeability in high-permeability zones by a much greater factor than that in low-permeability zones. In other words, ideally, the residual resistance factor of the blocking agent should increase significantly with increased permeability. We note that residual resistance factors for "weak" gels (i.e, gels providing low to moderate residual resistance factors ranging from 1 to 100) generally remain the same or decrease with increased permeability.³¹ "Strong" gels tend to reduce the permeability of any given porous medium to a low value (in the microdarcy range) regardless of the initial permeability of the rock.³¹

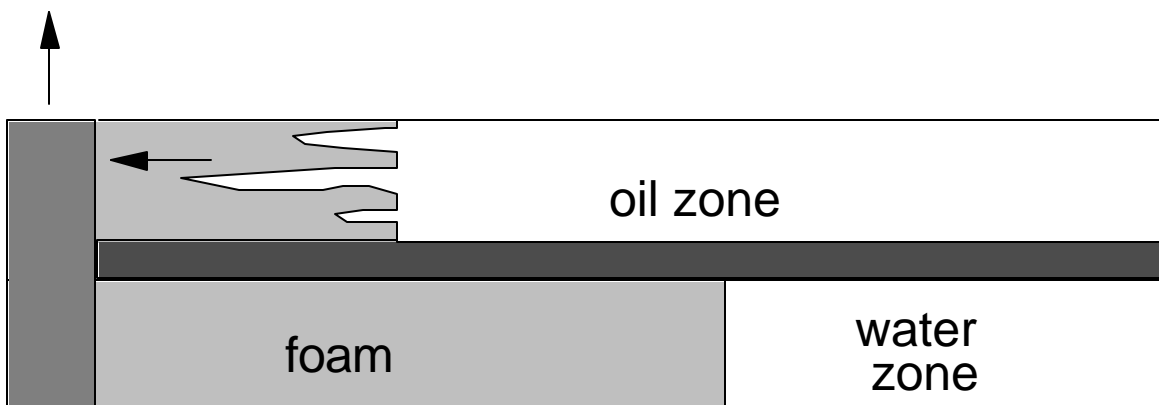
Bernard *et al.*³ reported that during water injection after foam placement, residual resistance factors at a given trapped gas saturation were independent of permeability for sandpacks between 1 and 200 darcys. In contrast, during gas injection after foam placement, gas permeabilities have been reported to decrease with increased initial permeability of the porous medium.^{2,25} This behavior represents a potential advantage of foam blocking agents over gel blocking agents when injecting gas into injection wells.

Many researchers found that foam stability is significantly reduced in the presence of oil.^{2,3,23,32-36} In concept, this phenomenon could be exploited to optimize placement of a foam blocking agent in oil production wells. During foam injection, the foam would penetrate a substantial distance into all open zones.^{17,20,24,30} When the well is returned to production, the foam could provide a large resistance to water flow—thereby restricting production from zones with high water saturations. Initially, the foam block would also restrict flow from zones with high oil saturations. However, produced oil could collapse the foam much more rapidly than the produced water. Therefore, the foam block may collapse or wash out from oil-productive zones much more rapidly than from zones with high water-saturations (Fig. 9). Foam washout from the water zones could be reduced by incorporating a polymer or gel into the foam. If a gelant is used, the foam must be produced from the oil zones before gelation occurs. Otherwise, the oil zones could be damaged.

Note that the above concept is not likely to aid placement of foams in injection wells. Because of its low mobility, injected foam will usually drive the oil saturation to low values in locations upstream of the foam front. Because the residual oil saturation upstream of the foam front will not usually be much different from zone to zone, the residual oil has about the same probability of collapsing the foam in all zones.



foam injection



return to production

Fig. 9. In production wells, foams may collapse in oil zones more rapidly than in water zones.

Foamed Polymers and Gels

An important deficiency of foams is that they often collapse or wash out too easily, especially when in contact with oil.^{14,32-36} A method that has been shown to slow or prevent this collapse is to incorporate polymers or gels with the aqueous portion of the foam.^{32,33,37-50} (Ref. 45 mentions several examples of foamed polymers or gels that were described in the literature.) An important advantage cited for using foamed polymers or foamed gels instead of gels is that the gas in foams significantly reduces the cost per volume for the blocking agent.^{39,45} Another advantage given is that the low density of foamed polymers and foamed gels allows more efficient sweep of the upper portions of fracture systems (because of gravity effects).⁴³

Although some of the literature cited above makes unsubstantiated claims about the ability of foamed polymers and gels to selectively enter or block high-permeability or high-water saturation zones, no supporting evidence is given. Therefore, two important questions that remain are:

1. Will the presence of polymer or gel in the foam aid placement?
2. How will the presence of polymer or gel affect the permeability-reduction properties of foam?

One circumstance where the presence of a preformed gel could aid placement of a foam can be inferred from the work of Craighead *et al.*⁵¹ During hydraulic fracturing, foamed gels show significantly lower leakoff rates than foams or foamed polymers.⁵¹ Logically, preformed foamed gels may propagate substantial distances along fractures with minimum leakoff. This argument parallels that given for injecting preformed gels into fractured systems.²⁶ However, a potential advantage of foamed gels over ordinary gels is that the foamed gels may be more likely to extrude through fractures without developing excessive pressure gradients. This concept needs to be tested experimentally.

Another potential advantage of foamed gels is that they may allow more control in achieving low or intermediate residual resistance factors.⁴⁷ To explain, "strong" gels (without foam) can provide predictable and reproducible residual resistance factors because gelation in the porous medium is fairly complete and the gel fills almost all of the aqueous pore space.^{31,52} These residual resistance factors are usually very high (10^3 - 10^6). However, we sometimes desire lower residual resistance factors (e.g., 1-100), that are commonly associated with "weak" or "thin" gels. Unfortunately, "weak" gels usually result from incomplete gelation and the uncontrolled formation of a small, unpredictable volume and concentration of gel aggregates. Thus, weak gels provide low to intermediate residual resistance factors that are often difficult to reproduce from one experiment to the next.^{31,52} If a foamed gel is used that incorporates a "strong" gel in the aqueous phase, the thin gel films that separate the gas bubbles should be formed reproducibly, and they may allow intermediate residual resistance factors to be attained more reliably. This concept also needs to be tested experimentally.

Gels and foams are known to show different permeability reductions for different phases.^{2,3,53,54} Experimental work is needed to establish the disproportionate permeability reduction properties of foamed polymers and foamed gels.

Field Applications of Foam Blocking Agents

Field results support some of the important laboratory findings concerning foam behavior—especially its performance as a mobility control agent. For example, in cases where vertical injection profiles were measured before, during, and after foam injection, the profiles were consistently improved during foam injection—demonstrating the ability of the low-mobility foams to shift flow from high-permeability zones into less-permeable zones.^{13,55-58} Also, when gas or water injection was resumed after foam injection, the profiles quickly deteriorated and reverted to the profiles that were the same or worse than those observed before foam injection.^{13,55-59} This behavior is consistent with expectations for injection of a high-mobility fluid following a bank of low-mobility fluid in a heterogeneous system.^{60,61} This behavior is opposite to the performance desired for a blocking agent.

For cyclic steam injection projects where the foam was intended to act as a blocking agent, a common observation for successful field applications was that steam and oil flow after the foam treatment was diverted away from upper zones in favor of the middle or lower zones.⁶²⁻⁶⁴ These results suggest that gravity effects (coupled with the viscous character of the resident oil) aided placement of the foam in the upper zones. The results do not suggest an unexpected or extraordinary preference for foams to enter high-permeability zones or zones with high water saturations.

Many field projects report problems with foam propagation and foam stability.^{62,65-69} These problems present challenges for foam applications both as mobility-control agents and as blocking agents.

Conclusions

In concept, several phenomena could allow foams to be superior to gels as blocking agents, however, only in certain circumstances. At present, these circumstances are hypothetical; very few conditions have been verified experimentally or in field applications. Two phenomena (the limiting capillary pressure and the minimum pressure gradient for foam generation) could allow low-mobility foams to form in high-permeability zones but not in low-permeability zones. Exploiting these phenomena during foam placement requires that (1) under given reservoir conditions, a gas/liquid composition must be identified that will foam in high-permeability zones but not in low-permeability zones, (2) the foam must not easily collapse or wash out from the high-permeability zones, and (3) the aqueous phase must not contain a gelant or other reactive blocking agent.

The following is a list of several other ideas where foams, foamed polymers, or foamed gels could have advantages over gels as blocking agents. However, all of these concepts require further development and experimental verification.

1. When oil wells are returned to production after foam injection, foams could collapse more rapidly in oil zones than in water zones. Foam washout from the water zones could be reduced by incorporating a polymer or gel into the foam. If a gelant is used, the foam must be produced from the oil zones before gelation occurs; otherwise, the oil zones could be damaged.
2. Preformed foamed gels may be effective blocking agents for plugging fractures. Because gelation occurs before injection, leakoff from fractures could be minimized using foamed gels. Because they are foams, foamed gels may propagate through fractures more effectively than preformed gels (i.e., foamed gels may be less likely to screen out or develop excessively high pressure gradients during injection).

3. Because of their high gas content, foamed gels formed using "strong" gels may allow more control in achieving low or intermediate residual resistance factors.
4. In cyclic steam projects, foam placement could be aided by gravity effects combined with very large mobility contrasts between the foam and the displaced oil.
5. For foams, residual resistance factors for gas can increase with increasing permeability. This behavior could be exploited when using foam as a gas blocking agent. A similar phenomenon has not been observed for water residual resistance factors in the presence of foam. Gels and foams are known to show different permeability reductions for different phases. Experimental work is needed to establish the permeability reduction properties of foamed polymers and foamed gels.

3. USE OF EMULSIONS AS BLOCKING AGENTS

In this chapter, we examine the use of emulsions as blocking agents to improve reservoir sweep efficiency. Emulsions are liquid-liquid dispersions; commonly, these dispersions are either oil dispersed in water or water dispersed in oil. The basic question that we address in this analysis is, Can emulsions be made to work better than gels as blocking agents? Thus, we use the performance of gels as a basis of comparison. This analysis uses experimental, theoretical, and field results from the literature.

Some Key Features of Emulsion Flow Through Porous Media

Dilute Oil-in-Water Emulsions. A review of the use of emulsions in the petroleum industry, including emulsion flow through porous media, can be found in Ref. 70. One of the most comprehensive studies of emulsion flow through porous media was performed by Soo and Radke.⁷¹⁻⁷⁵ They focused on dilute oil-in-water emulsions (0.5% oil concentration). Average oil-drop sizes used in their work ranged from 2 to 10 μm . Their porous media were quartz sandpacks with permeabilities of either 0.57 μm^2 (580 md) or 1.15 μm^2 (1,170 md). Average pore-throat sizes for these sandpacks were 17.3 μm and 21.6 μm , respectively.

Soo and Radke demonstrated that the rate of propagation of oil drops through a porous medium decreases with increasing drop size.⁷¹ In a 1,170-md sandpack, 2.1- μm oil drops propagated three to four times more rapidly (on average) than 4.5- μm oil drops. Also, for a given drop size, the rate of drop propagation increases with increasing permeability or pore size of the porous medium. Similar observations were reported by McAuliffe⁷⁶ and Spielman and Su.⁷⁷

During emulsion injection, researchers found that emulsion mobility in a porous medium initially decreased with increased PV throughput and approached a constant value that was between 2% and 90% of the original brine mobility.^{71,76-79} For a given oil-drop size, the mobility loss was generally greater with decreasing permeability or pore size of the porous medium. For example, after injecting 20 PV of emulsion (0.5% oil in water) with an average oil-drop size of 3.3 μm , Soo and Radke noted a 50% mobility loss in a 1,170-md sandpack and a 63% mobility loss in a 580-md sandpack.⁷¹ Also, in a given porous medium, the mobility loss was greater with increasing drop size. For example, after injecting 9 PV of emulsion (0.5% oil in water) into a 1600-md Boise sandstone core, McAuliffe observed a 44% mobility loss using 1- μm oil drops and a 98% mobility loss using 12- μm oil drops.⁷⁶ The mobility losses were shown to be caused by deep-bed filtration of oil drops⁷¹⁻⁷⁵; the effect of increased oil saturation on relative permeabilities was shown to be insignificant.⁷⁶

When water was injected after placing an emulsion, several researchers noted that the emulsion did not wash out from the porous medium, so long as the fluid velocity or pressure gradient was not increased.

During water injection after emulsion placement, very few oil droplets were produced, and the water mobility remained about the same as the mobility of the last emulsion injected.^{71,76-79} This behavior suggests that the permeability reduction is caused by trapped oil droplets.⁷¹⁻⁷⁹ One researcher found several cases where the mobility actually decreased significantly when water was injected after placement of an emulsion.⁷⁹ An explanation for this behavior was not given.

For dilute oil-in-water-emulsions, Soo and Radke found that both the rate of propagation of oil droplets and the mobility reduction were independent of oil viscosity, based on experiments using a 1.5-cp oil and a 23-cp oil.⁷¹ They also noted that the droplet propagation rate and the mobility reduction were independent of superficial fluid velocity between 0.005 and 0.08 cm/s (14 and 227 ft/d).⁷³ In contrast, McAuliffe observed significantly greater mobility reductions when injecting an emulsion at a pressure gradient of 2

psi/ft than at 12 psi/ft.⁷⁶ Soo and Radke⁷³ argue that the apparent shear-thinning behavior reported by McAuliffe can be explained partially by gravity effects. They suggest that flow behavior of dilute emulsions in porous media should not be strongly affected by fluid velocity.

Concentrated Oil-in-Water Emulsions. Alvarado and Marsden⁸⁰ studied the rheology of concentrated oil-in-water emulsions in tubes and in porous media. Their emulsions contained from 10% to 70% oil. They reported that emulsions with less than 50% oil showed Newtonian behavior, while emulsions with more than 50% oil showed pseudoplastic behavior. For a given emulsion concentration, they observed analogous behavior in capillary tubes and in porous media. In contrast to results found using dilute emulsions,⁷¹⁻⁷⁹ Alvarado and Marsden reported only minor permeability reductions associated with injecting concentrated oil-in-water emulsions. Using cores with initial permeabilities ranging from 190 md to 847 md, their emulsions typically reduced permeability between 10% and 25%. No trend was evident between initial core permeability and the degree of permeability reduction.⁸⁰

Concentrated Water-in-Oil Emulsions. Gogarty⁸¹ studied the rheology of concentrated water-in-oil emulsions in viscometers and in porous media. His emulsions contained from 11.7% to 27.3% water. Like Alvarado and Marsden,⁸⁰ Gogarty also observed analogous behavior in viscometers and porous media.⁸¹ Using Berea sandstone cores that ranged in permeability from 77 to 480 md, Gogarty found that his emulsions typically reduced permeability to oil by about 10%, regardless of the initial permeability of the rock.

Models of Emulsion Flow Through Porous Media

Several models have been proposed to describe the flow of emulsions through porous media.^{74-77,80-84} The simplest models⁸⁰⁻⁸³ assume that after a small correction is made for permeability reduction, the rheological characteristics of the emulsion are essentially the same in porous media as they are in a viscometer. Alvarado and Marsden⁸⁰ and Gogarty⁸¹ found this type of model to be adequate for describing results from their experiments with concentrated emulsions. For concentrated emulsions, the literature indicates that droplet coalescence is very important and that the liquid phases propagate through porous media as expected from relative permeability concepts. Pore-blocking effects are of minor importance.^{77,82}

In contrast, pore-blocking effects are very important during flow of dilute emulsions through porous media. For flow of dilute emulsions, a droplet-retardation model was attributed to McAuliffe⁷⁶ and Devereux.⁸³ This model assumes that passage of emulsion drops through pore constrictions reduces the rate of drop propagation and causes a temporary permeability reduction in the porous medium. Although this model accounts for several important features of emulsion flow through porous media, Soo and Radke⁷⁴ point out two deficiencies. First, the model predicts a sharp emulsion front. In reality, the emulsion front is smeared because the injected emulsion contains a distribution of drop sizes and different-sized drops propagate at different rates.^{71,76} Second, the model predicts that the permeability of the porous medium will rise back to its original value during water injection after placement of the emulsion. Several researchers showed that the emulsion does not wash out easily during water injection.^{71,76-79}

Based on concepts from deep-bed filtration theory, Soo and Radke^{74,75} proposed a sophisticated model for flow of dilute emulsions through porous media. They point out two mechanisms for droplet capture—straining (droplets being trapped by unsuccessfully attempting to squeeze through pore throats) and interception (droplets sticking to pore walls). Soo and Radke account for both effects in their model.^{74,75} Three important parameters in their model are (1) the filter coefficient, (2) the flow-diversion parameter,

and (3) the flow-restriction parameter. Soo and Radke^{74,75} describe how to estimate these parameters, given drop size, grain-size distribution, and porosity. They also demonstrate the effectiveness of their model in predicting the important elements of flow of dilute emulsions through porous media. Islam and Farouq Ali⁸⁴ also used the model of Soo and Radke^{74,75} in simulating emulsion flow.

Using Emulsions as Blocking Agents

Can emulsions be made to work better than gels as blocking agents? Analysis of the literature suggests no reason to believe that concentrated emulsions have any placement or permeability-reduction advantages over gels and gels. Since their behavior in porous media can be described using standard relative-permeability concepts,^{77,80-82} the placement properties of concentrated emulsions are similar to those of viscous gels.³⁰ Also, the literature indicates that concentrated emulsions provide very low permeability-reduction values (residual resistance factors less than 1.5).^{80,81} Furthermore, the high oil content of concentrated emulsions presents an economic disadvantage associated with their use.

Do dilute emulsions have superior placement or permeability-reduction properties? To examine this question, we will use the data from Fig. 10 of Ref. 71. This figure compares effluent drop concentrations and mobility-reduction data for injection of a 0.5% oil-in-water emulsion (3.3 μm average drop size) into two sandpacks with permeabilities of 1,170 md and 580 md, respectively. This data indicates that the effluent droplet concentrations reach 50% of the injected concentrations after injecting 7.3 PV and 9.7 PV of emulsion in the 1,170-md and 580-md packs, respectively. The figure also shows that the ultimate mobility losses for the two packs are 50% and 63%, respectively. The resistance factor for emulsion in the 1,170-md pack, F_{r1} , is 2 [i.e., $1/(1-0.5)$], and the resistance factor in the 580-md pack, F_{r2} , is 2.7 [i.e., $1/(1-0.63)$]. To be consistent with literature reports,^{71,76-79} we assume that the residual resistance factors during brine injection after emulsion placement are equal to the emulsion resistance factors (i.e., $F_{r1}=F_{r1}=2$ and $F_{r2}=F_{r2}=2.7$).

Consider a two-layer radial system where the permeabilities of Layer 1 and Layer 2 are 1,170 md and 580 md, respectively. An impermeable barrier separates the two layers, and porosities, ϕ_1 and ϕ_2 , are equal. The inner or wellbore radius, r_w , is 0.33 ft, and the outer radius, r_e , of the reservoir is 100 ft. Initially, this radial reservoir is filled only with water. The emulsion is injected in parallel through the wellbore into both layers of the reservoir. Eqs. 12 through 14 (taken from Eq. 20 of Ref. 18) describe the radius of penetration into the 580-md layer, r_{p2} , when the blocking agent reaches the outer radius (100 ft) of the 1,170-md layer, r_{p1} .

$$f(r_{p2}) = f(r_{p1}) \quad (12)$$

where

$$f(r_{p2}) = \frac{(1 + a_{r2})^2}{k_2} \frac{1}{r_{p2}^2} \left[F_{r2} \ln \frac{r_{p2}}{r_w} + \ln \frac{r_{p1}}{r_{p2}} \right] + \frac{1 - F_{r2}}{2} \frac{1}{r_w^2} \left[\ln \frac{r_{p1}}{r_w} + \frac{1 - F_{r2}}{2} \right] \quad (13)$$

$$(14)$$

In these equations, a_1 and a_2 are the retention or delay factors for the 1,170-md and 580-md layers, respectively. Based on the work of Soo and Radke⁷¹ (mentioned above), their values are 7.3 PV and 9.7 PV, respectively.

Once the radius of penetration into a given layer is known, the injectivity retained after placement of a blocking agent, I/I_o , can be calculated using Eq. 15 (taken from Eq. 13 of Ref. 18).

$$\frac{I}{I_o} = \frac{\ln(r_{pi}/r_w)}{F_{ri} \ln(r_{pi}/r_w) + \ln(r_{pi}/r_{pi})} \quad (15)$$

In this equation, the subscript, i , refers to the layer or zone of interest. I/I_o is the water injectivity after the blocking agent has been placed and set (e.g., the gelant has gelled) divided by water injectivity before placement of the blocking agent.

We used Eqs. 12 through 15 to determine the radii of penetration and the injectivity retained after placement of an emulsion in our two-layer radial reservoir. The results are listed in the first data column of Table 1. Two other data sets are included in Table 1 for comparison. These data sets apply to a gelant that has a water-like viscosity during placement. We also assume that the gelant experienced no retention during placement ($a_{r1}=a_{r2}=0$). This assumption was reasonable for gelants such as resorcinol-formaldehyde or acrylamide monomer.⁵² For the gelant cases, flow was stopped after gelant placement to allow a gel to form.

In all three cases, the blocking agent was injected until it reached a radius of 100 ft in the 1,170-md layer. At that point, the emulsion reached a radius of 55.6 ft in the 580-md layer, while the gelants reached a radius of 70.4 ft. The smaller radius of penetration for the emulsion can be attributed to (1) a larger emulsion resistance factor in the less-permeability layer (2.7 vs. 2 in the 1,170-md layer) and (2) a greater emulsion retention value in the less-permeable layer ($a_{r2}=9.7$ vs. $a_{r1}=7.3$). At first glance, this behavior might appear to be a significant advantage associated with using emulsions. However, the subsequent calculation of injectivity retained after the treatment ultimately reveals no significant advantage over gels. In all three cases, the residual resistance factor in the 1,170-md layer was 2, and the injectivity retained after the treatment was 0.5. In the 580-md layer, the final injectivity after the emulsion treatment was 39.6% of the original value. In other words, the emulsion treatment actually made the injection profile less favorable (because I/I_o is greater in the 1,170-md layer than in the 580-md layer). In contrast, for the gel where $F_{r2}=2$, the final injectivity was 51.6% of the original value. Thus, in this case, the gel treatment improved the injection profile by a very small amount.

One other gelant case is included in Table 1, where $F_{r2}=2.7$. After this treatment, the final injectivity in the 580-md layer was only slightly lower than that for the emulsion case (0.385 vs. 0.396).

Table 1. Radial Flow System

	Emulsion	Gelant	
Resistance factor in 1,170-md layer, F_{r1}	2	1	1
Resistance factor in 580-md layer, F_{r2}	2.7	1	1
Residual resistance factor in 1,170-md layer, F_{r1}	2	2	2

Residual resistance factor in 580-md layer, F_{r2}	2.7	2	2.7
Radius of penetration in 1,170-md layer, r_{p1} , ft	100.0	100.0	100.0
Radius of penetration in 580-md layer, r_{p2} , ft	55.6	70.4	70.4
Injectivity retained in 1,170-md layer, I/I_o	0.50	0.50	0.50
Injectivity retained in 580-md layer, I/I_o	0.396	0.516	0.385

These radial-flow calculations do not suggest any beneficial blocking action associated with the use of an emulsion. Is this result contradictory to literature reports? For example, we note that McAuliffe found a definite improvement in sweep efficiency when injecting a dilute oil-in-water emulsion in parallel into three linear cores of different permeability.⁷⁶ The differences in results are due to the inherent differences between linear flow and radial flow.¹⁸ To demonstrate this fact, we will reuse the emulsion data of Soo and Radke⁷¹ in parallel-linear-flood calculations and compare these results with the above parallel-radial-flood calculations.

In the linear case, we consider two 100-ft-long linear cores that will be flooded in parallel. Except for the flow geometry, all other parameters will be the same as those used in the radial case. The permeabilities of Layers 1 and 2 are 1,170 md and 580 md, respectively, and the cores are initially filled only with water. The blocking agent is injected until it reaches the end of the 1,170-md core. The distance of penetration into the 580-md layer, L_{p2} , can be calculated using Eq. 16 (taken from Eq. 21 of Ref. 18).

$$\frac{L_{p2}}{L_{p1}} = \frac{\frac{k_2}{k_1} \frac{1+a_{r1}}{1+a_{r2}} F_{r2} - 1}{F_{r2} - 1} \left(\frac{F_{r1} + 1}{F_{r1}} \right)^{0.5} - 1 \quad (16)$$

After the blocking agent is placed and set, water is injected to determine the injectivity retained after the treatment. For linear flow, the injectivity retained after the treatment can be calculated using Eq. 17 (taken from Eq. 19 of Ref. 18).

$$\frac{I}{I_o} = \frac{L_{p1}}{F_{r1} - 1 L_{p1} + L_{p1}} \quad (17)$$

The results for the linear floods are shown in Table 2 for the analogous three cases that were described in Table 1. When the blocking agent reached 100 ft into the 1,170-md layer, the distance of penetration into the 580-md layer, L_{p2} , was 42.4 ft for the emulsion and 49.6 ft for the gelant. Thus, again, at first glance, the emulsion appears to have a placement advantage over the gelant. However, the injectivity calculations reveal that the injectivity retained during water injection after the treatment was intermediate between the values from the two gelant cases—as was noted for the radial-flow calculations in Table 1.

Table 2. Linear Flow System

	Emulsion	Gelant	
Resistance factor in 1,170-md layer, F_{r1}	2	1	1
Resistance factor in 580-md layer, F_{r2}	2.7	1	1
Residual resistance factor in 1,170-md layer, F_{rr1}	2	2	2
Residual resistance factor in 580-md layer, F_{rr2}	2.7	2	2.7
Distance of penetration in 1,170-md layer, L_{p1} , ft	100.0	100.0	100.0
Distance of penetration in 580-md layer, L_{p2} , ft	42.4	49.6	49.6
Injectivity retained in 1,170-md layer, I/I_o	0.50	0.50	0.50
Injectivity retained in 580-md layer, I/I_o	0.581	0.669	0.543

Note that all three treatments shown in Table 2 improved the injection profile; injectivity was reduced in the high-permeability zone more than in the low-permeability zone. In contrast, the same treatments in the radial-flow system (Table 1) provided a very small improvement in the injection profile in one case and significantly harmed the profile in the other two cases (including the emulsion case). Thus, positive results obtained in a linear-flow system do not necessarily mean that a blocking agent will be effective in a radial-flow system. There are several other pitfalls associated with parallel linear corefloods that make them an extremely ineffective and misleading experimental method to evaluate blocking agents.³¹ Results from parallel linear corefloods have misled several researchers to conclude that certain emulsions might be effective as blocking agents in field applications.^{76,85-87}

Potential Improvements

Could the performance of the emulsion in the above examples be improved by incorporating gelant into the aqueous phase? The answer is clearly "no," since over 7 PV of emulsion formulation were injected to attain the above results. The gelant that propagates ahead of the emulsion banks would fill both layers of the radial reservoir with gel. In the best case, the emulsion/gelant blocking agent would act simply like a gelant.

Could the performance of the emulsion be improved by incorporating gelant into the oil phase? The answer is "probably not." Because the oil content of the emulsions is very low (e.g., 0.5%), it seems unlikely that an oil-based gel would provide very much additional permeability reduction. If the oil content of the emulsion was increased substantially, then, as mentioned earlier, emulsion flow could be described using conventional relative-permeability concepts,^{80,81} and the emulsions would exhibit the same placement characteristics of gelants.³⁰

Patent Literature. Eddins and Lissant⁸⁸ proposed an interesting concept for treating production wells with emulsions. They proposed injecting oil that contained a surfactant. When this surfactant/oil solution entered zones with high water saturations, hypothetically, a viscous emulsion would form that would block the zone. In contrast, when this solution entered the oil zone, no emulsion would form because of the low water saturation. Eddins and Lissant mentioned three field examples where this concept was tested. Unfortunately, they did not provide enough information to allow an objective assessment of the effectiveness of the technique.

At least three unanswered questions exist about the process that Eddins and Lissant proposed. First, how efficiently will an emulsion be formed at the front of the oil-water bank? Second, will the surfactant/oil solution emulsify connate water in the oil-productive zones as well as in the offending water channels? And third, since a concentrated emulsion will be formed and since concentrated emulsions reportedly show conventional fractional-flow properties,^{80,81} will the emulsion form an effective blocking agent? Also, unless very small banks of blocking agent are used, the process is likely to be expensive because oil is injected.

Tosch⁸⁹ and Son⁹⁰ proposed injecting microemulsions that would experience a phase transition and emulsion formation upon contact with water. No information was given concerning (1) how these microemulsions would behave in oil zones and (2) how effectively the emulsion would resist water production.

Dauben⁹¹ patented the use of emulsions as blocking agents during miscible floods. He speculated that emulsions may preferentially enter high-permeability zones. He suggested that the oil droplets in the emulsion should be sized so that they would easily enter the high-permeability zones but not the low-permeability zones. An important flaw in this argument is if the droplets are small enough to propagate easily through the high-permeability zones, they will not provide any blocking action in that zone. Dauben⁹¹ also speculated that when miscible fluids were injected following the emulsion, they would disperse any blocking agent in the less-permeable zones before destroying the emulsion bank in the high-permeability zone. This concept has been clearly demonstrated to be incorrect.^{60,61}

Wu *et al.*⁹² proposed that emulsions generated in situ could be effective as a blocking agent in steam floods. In concept, an injected surfactant solution enters a steam zone, mixes with residual oil, and forms a low-mobility emulsion. Results from a laboratory experiment and a (hypothetical?) field example were given to support this concept. This concept has merit since placement of the emulsion in the steam zone would be aided by the low-mobility of residual oil (i.e., the viscous oil would resist entry of the surfactant formulation into the oil zones). However, use of a foam blocking agent would be even more advantageous in this application (see Chapter 2).

Morris and Terry⁹³ and Brown *et al.*⁹⁴ also proposed that emulsions generated in situ could selectively plug high-permeability zones. However, they offered no experimental or field data to support this suggestion. We expect emulsion-generating surfactant formulations to penetrate into different zones in the same proportions as observed for gels. Therefore, when generating emulsions in situ, we see no placement advantages over conventional gels, based on emulsion behavior reported to date.

Emulsion/Polymer and Emulsion/Gelant Combinations. Falk⁹⁵ patented the use of an emulsion that contained a melamine-formaldehyde resin. The patent discusses placement of the resin along the interface between a high-permeability watered-out zone and a less-permeable oil-productive zone, where extensive vertical communication can occur between zones. Gravity and fluid density differences were

suggested as a method to control placement of the resin. Although this concept is interesting, no experimental, modeling, or field data were provided to support the feasibility of the idea.

Yeung and Farouq Ali⁹⁶ proposed an interesting combination of polymer and emulsion injection to flood an oil zone that is in direct communication with an aquifer. In this process, called the "Dynamic Blocking Procedure," polymer solution is injected into the oil zone while emulsion is injected simultaneously but separately into the water zone. This procedure is performed to allow the emulsion blocking agent to penetrate deep into the water zone with minimum crossflow into the oil zone. Presumably, this process requires that (1) the mobilities of the emulsion and polymer solution must be similar, (2) the densities of the emulsion and polymer solution must be matched properly to prevent crossflow, and (3) the injection rates and pressures for the two injection streams must be precisely controlled. Although not discussed by Yeung and Farouq Ali,⁹⁶ we suspect that the successful application of this concept requires that the effective permeability of the water zone be less than or equal to that of the oil zone. Otherwise, it may be impossible to prevent emulsion near the displacement front in the water zone from crossflowing into and damaging the oil zone.⁶¹

For those circumstances where the Dynamic Blocking Procedure could work, perhaps, a better application of the above concept would involve simultaneous injection of a polymer solution with a crosslinker in the water zone and the same polymer solution without a crosslinker in the oil zones. In this case, achieving the proper mobility and density match for the two injection streams would be much easier.

Analogy with Foams. One might expect emulsions to show some properties that are analogous to those of foams. In analyzing the use of foams as blocking agents (Chapter 2), we noted several phenomena that might allow foams to show placement characteristics superior to those of gels under some circumstances. For example, two phenomena, the limiting capillary pressure and the minimum pressure gradient for foam generation, could allow low-mobility foams to form in high-permeability zones but not in low-permeability zones. If these phenomena exist for emulsions, perhaps emulsions could be formed in high-permeability zones but not in low-permeability zones. However, to our knowledge, these phenomena have not been reported for emulsions in porous media.

Field Application

McAuliffe reported the only field project to date where emulsions were injected to improve oil recovery.⁹⁷ A 3% PV bank (236,000 bbl) of emulsion was injected into three wells in the Midway-Sunset Field. The emulsion contained 14% oil in water. The choice of emulsion concentration was stated to be arbitrary. Most of McAuliffe's laboratory work focused on an emulsion that contained 0.5% oil in water; no corefloods were performed using an emulsion with 14% oil.⁷⁶ In view of the substantial differences in behavior between dilute and concentrated emulsions,⁷¹⁻⁸² a valid relation between the laboratory work⁷⁶ and field work⁹⁷ is not obvious.

McAuliffe reported three observations that suggested decreased fingering and increased volumetric sweep efficiency during emulsion injection.⁹⁷ First, oil production increased and WOR values decreased in wells surrounding the emulsion-treated injectors. Second, produced water salinity increased in several wells—suggesting reduced channeling of the less-saline injection water. Third, interwell tracer studies suggested that the emulsion altered the flood pattern. Based on the results from this field pilot, it is not clear whether the improvements in reservoir sweep resulted from the emulsion acting as a mobility-control agent or as a blocking agent. The pilot project was not expanded to other parts of the field.

Many authors have proposed or discussed emulsions as mobility-control agents.^{76,96,98-103}

Conclusion

Although several features of emulsion flow through porous media remain unanswered, our analysis of the literature indicates that emulsions or emulsion/gel combinations will not perform significantly better than gels as blocking agents, particularly in the areas of placement characteristics and permeability-reduction properties.

4. USE OF PARTICULATES AS BLOCKING AGENTS

Large scale reservoir heterogeneities, such as fractures or high-permeability streaks, can cause severe channeling of the injected fluid during an oil-recovery process. Early breakthrough of the injected fluid can significantly reduce oil recovery efficiency, leaving a large portion of the reservoir unswept. Fractures can also aggravate water and gas coning resulting in premature abandonment of oil wells.

Several researchers¹⁰⁴⁻¹¹¹ proposed the use of particulates as blocking agents for fluid diversion in oil recovery processes. We performed a literature review to determine from the published information whether particulates can be effective in blocking fractures and high-permeability streaks without damaging the oil-productive zones. A theoretical model was developed to study the feasibility of using particulates to prevent gelant penetration into low-permeability zones during the placement process.

Formation Damage From Particulate Invasion

Several researchers¹¹²⁻¹²³ investigated formation impairment resulting from particle invasion. They concluded that the major factors affecting particulate invasion are: (1) particle/pore size ratio, (2) particle concentration, and (3) injection rate.

Barkman and Davidson¹¹⁴ proposed four possible mechanisms for formation impairment from suspended solids: (1) formation of an external filter cake, (2) formation of an internal filter cake, (3) perforation plugging, and (4) wellbore fillup. Barkman and Davidson used the water-quality ratio to estimate the rate of formation impairment. Water-quality ratio is defined as the suspended solid concentration divided by the filter-cake permeability. They speculated that bridging on the rock face might occur if the mean particle diameter is one-tenth of the mean pore diameter or larger. According to their model, the rate of impairment from the formation of an external filter cake is proportional to the water-quality ratio, the reservoir permeability, and the injection rate per net sand thickness. The authors expect perforation plugging to occur unless the solid particles are small enough to be transported through the porous rock. Their model predicts that the rate of impairment from perforation plugging is at least an order of magnitude higher than plugging in an open-hole completion. The authors suggested that if the suspended solids are small enough to penetrate into the porous rock, an internal filter cake is formed. According to their model, the invasion radius is a function of velocity, pore size, and particle size. The authors asserted that the rate of impairment from the internal filter cake is comparable to that from the formation of an external filter cake.

In studying the formation damage caused by drilling-mud invasion, Abram¹¹⁵ concluded that the mud invasion can be minimized by adding bridging additives with a median particle size equal to or slightly greater than one-third the median pore size of the formation. To achieve best results, Abram suggested that the bridging-additive concentration should be at least five percent by volume.

Van Oort *et al.*¹¹⁶ developed a semiempirical model based on material balance and deep-bed filtration theory to predict wellbore impairment by internal filter-cake formation during water injection. Van Oort's model supports Abram's conclusion¹¹⁵ by predicting the formation of an external filter cake on the rock surface when particles involved are larger than one-third of the pore diameter. For particles smaller than one-third and larger than one-seventh of the pore diameter, the model predicts the formation of an internal filter cake in the porous rock. According to the model, the rate of formation impairment caused by the internal filter cake decreases with increasing flow velocity. The flow-velocity dependency is most pronounced at low flow velocities. For particles smaller than one-fourteenth of the pore diameter, the

model predicts no damage to the porous rock.

Vetter *et al.*¹¹² studied the effect of submicron particles on formation damage. They discovered that even the submicron particles can be trapped in the reservoir and cause severe damage to the formation rock. Their results showed that the depth of particle penetration at a given particle size and concentration is proportional to the superficial velocity.

Eleri and Ursin¹¹³ performed linear coreflood experiments to study the formation damage from the infiltration of fine particles into the reservoir. They concluded that the formation impairment is proportional to the superficial velocity of the suspended solids in the reservoir. Their experimental results showed that the higher the concentration of particles in the injection fluid, the more the damage to the porous medium. However, their experimental results also indicated that even in very dilute solutions, suspended particles can cause significant damage to formation permeability.

The success or failure of particulates as blocking agents is determined in part by how effective the particulates can seal the thief zones. The flow of particulates in porous media is very similar to the deep-bed-filtration process. Tien *et al.*¹²³ conducted an extensive review of deep-bed-filtration theory. The authors presented relationships between the amount of deposition and the changes of pressure gradient for two limiting cases of deposition mechanisms. In the first case, particles form a uniform smooth coating outside filter grains (smooth-coating mode) during the deposition process. In the second case, deposition occurs when particles are trapped by pore constrictions (blocking mode). The equations relating the amount of deposition to changes of pressure gradient are summarized in Appendix A. Due to the complexity of the deep-bed-filtration process, we cannot quantify the degree of permeability reduction after treatment through theoretical analysis. However, we can determine qualitatively the effect of formation permeability on the degree of permeability reduction from the equations in Appendix A. For a given amount of deposition, the degree of permeability reduction by particulates increases with decreasing formation permeability. Please refer to Appendix A for a detailed analysis.

In summary, particulates small enough to penetrate into the formation can cause significant damage to the porous rock. The degree of permeability reduction increases with decreasing formation permeability. Therefore, oil productivity can be severely impaired if the particulates cannot be selectively placed into the high-permeability thief zones.

Selective Plugging Using Preformed Xanthan Gels

Hoefner *et al.*¹²⁴ proposed the use of preformed xanthan gels for selective plugging. They suggested that the preformed xanthan gels may enter preferentially into the high-permeability thief zones—thereby eliminating the need for zone isolation during the placement process. The authors used parallel linear coreflood experiments to demonstrate selectivity. They argued that selectivity occurred during their coreflood experiments because the resistance factor in the low-permeability medium exceeded that in the high-permeability medium. A careful examination of Hoefner's results reveals that the apparent selectivity occurred after both cores in the parallel system were completely filled with gelant. When both cores are completely filled with a shear-thinning fluid, the ratio of flow rates in the two cores can be much greater than the original ratio of core permeabilities.¹²⁵ Thus, these flow ratios give the impression that certain shear-thinning fluids are unusually selective in entering high-permeability zones. Results from these experiments would be relevant if all zones in a reservoir were completely filled with a shear-thinning gelant. However, during gel placement in reservoirs, gelants **displace** reservoir fluids. Results from displacement experiments and calculations demonstrate that shear-thinning fluids are **not** unusually

selective in entering high-permeability zones.^{61,125,126}

Hoefner *et al.*¹²⁴ argued that the selectivity that they observed was not due simply to the fact that both cores were filled with a shear-thinning fluid. To support their position, they noted that the resistance factors in their parallel cores were much higher than would be expected from a viscous xanthan solution by itself. They also noted that resistance factors in a given core decreased significantly with increased distance from the core inlet. Hoefner *et al.* felt that (1) gel (rather than gelant or gelant components) was actually propagating through the rock, (2) gel was retained to a greater extent in the low-permeability cores than in the high-permeability cores, and (3) the higher level of gel retention slowed gel propagation to a greater extent in low-permeability cores than in high-permeability cores.¹²⁴

We agree with most of Hoefner's thoughts about gel retention and gel propagation as a function of permeability. However, these concepts do not preclude the possibility that Hoefner's apparent selectivity occurred at least partially because both cores were filled with a shear-thinning fluid. This rheological effect will be important in the presence or absence of gel-retention effects.

As Hoefner *et al.*¹²⁴ noted, an increase in resistance factor and gel retention with decreasing permeability will decrease the distance of gel penetration into less-permeable rock. However, a large decrease in permeability usually accompanies these effects (i.e., residual resistance factor increases significantly with decreasing permeability).^{31,52,127-131} Analyses conducted using data from the literature^{31,52,127-131} suggest that these phenomena will not improve the effectiveness of gel treatments unless the gel in the low-permeability zones is very close to the wellbore—so that one can perforate through the damage caused to the less-permeable zones.^{18,52,130,131} Hoefner *et al.*¹²⁴ suggest that a Cr(III)-xanthan gel can be formulated to penetrate deep into high-permeability zones but filter out at or near the injection face of low-permeability zones. Further work is needed to prove this concept.

Selective Plugging Using Particulates In Unfractured Wells

Willman¹⁰⁵ proposed using oil-resistant polymeric elastomer latex particles, dispersions, or suspensions (e.g., polyisobutylene, polystyrene, polybutadiene, etc.) to control the water injection profile. To achieve selective plugging, the author recommended the injection of latex particles having an average particle size small enough to penetrate deep into the more-permeable water zones but large enough to form an external filter cake on the rock face of the less-permeable zones. Willman suggested the use of commercially available latex particles with average particle diameters ranging from under 0.1 μm to over 2 μm . The invasion potential of a given latex was determined by subjecting cores of different permeability and porosity combinations to latex invasion tests. During the invasion tests, the depths of latex penetration were measured at a constant injection pressure of 50 psi. The invasion potential was determined by plotting the depths of latex penetration against $\sqrt{k / ?}$. Willman recommended the use of particles having a relatively uniform particle size when treating zones with a permeability contrast of less than ten. For zones with higher permeability contrasts (>10), the author asserted that a relatively broad range of particle diameters can be used without significant loss of selectivity. However, the unanswered question is, For a given permeability contrast, how narrow must the particle size distribution be to achieve selectivity? Willman did not provide any coreflood or field data to demonstrate selective plugging. Therefore, additional work is required to test this idea.

White *et al.*¹⁰⁸ proposed a method to selectively reduce the permeability of water-producing intervals without damaging oil productivity. In their method, a water-swelling clay (e.g., bentonite, sodium montmorillonite, etc.) dispersed in a liquid hydrocarbon (e.g., diesel, naphtha, kerosene, etc.) is introduced into the formation. The clay is in an unhydrated state when introduced into the formation. To allow deep

placement, the authors suggested that the particle size of the unhydrated clay should be less than the average pore size of the formation to be treated. During the placement process, the plugging agent penetrates a significant distance into both the water and oil zones. After a postflush by the same liquid hydrocarbon, the well is shut in to allow the clay to react with the formation water. The reaction between the unhydrated clay and the formation water in the water-source zones causes the clay particles to swell in situ, thereby reducing the flow capacity of the water zones. The authors speculated that because the oil zones contain little or no water, the oil productivity remains undamaged after treatment. However, the oil-productive zones are not water-free. The connate water in the oil-productive zones can cause the clay particles to swell, thereby causing significant damage to the oil productivity. The field data provided by the authors do not contain enough details to support the claim of selective plugging. Additional laboratory core experiments are required to test this concept.

Jennings¹⁰⁹ proposed reinjection of produced formation fines to improve the sweep efficiency in enhanced oil recovery processes. In this method, the produced formation fines are mixed with an aqueous saline solution to make a slurry. To prevent further mobilization of the formation fines during the placement process, the author suggested the use of aqueous saline solutions that are compatible with the formation brine. The author suggested that deep placement can be achieved by maintaining the injection velocity above a critical fluid flow velocity. Jennings defined the critical fluid flow velocity as the smallest velocity of the saline solution that will allow fines or small particles to be carried by the fluid and transported within the formation. When the desired depth of penetration is reached, the flow velocity is reduced below the critical fluid flow velocity. The author speculated that the flow velocity reduction would cause the fines to settle out, thereby plugging the more-permeable zones. However, if zones can not be isolated during the placement process, the fines can also penetrate a significant distance into the less-permeable oil-productive zones.^{112,113} The fine particles in the oil-productive zones can cause significant damage to oil productivity.^{112,113} No laboratory or field data were provided by the author to demonstrate sweep-efficiency improvement.

Snowden *et al.*¹¹⁰ developed temperature-sensitive latex particles for conformance control in high-temperature reservoirs. The authors indicated that the latex particles are bigger, softer, and more dispersed at low temperature and flocculate, shrink, and harden at elevated temperature. Snowden proposed the injection of these latex particles at ambient temperature. When the particles reach the high-temperature part of the formation the particles harden in situ, thereby blocking the flow paths. The authors asserted that the latex solution goes wherever water goes. Therefore, the latex solution could selectively plug the water zones without damaging oil zones. However, without zone isolation, particles small enough to penetrate into the formation will penetrate a significant distance into all open zones, thereby damaging the oil productivity.^{112,113} Hypothetically, Snowden's concept could be used as a blocking agent with a thermal trigger in a manner similar to that used by Fletcher *et al.*¹³² with aluminum-citrate-HPAM gels.

Breston¹⁰⁴ used finely divided solid and semisolid particles dispersed in oil or water to plug high-permeability thief zones and fractures. Breston speculated that selective plugging can be achieved by controlling the particle size so that the solid or semisolid particles are small enough to allow in-depth penetration into the pores of the most-permeable zones (or fractures) and large enough not to penetrate the pores of the less-permeable zones. Before treatment, the author used tracer tests or injection profile logs to determine the source of the excess water production. For low-permeability formations (1-10 md), Breston used a rosin emulsion product with 90% of the particles less than 1 μm . For fractures and high-permeability thief zones, mixtures of organic powders and fibers in a wide range of particle sizes were used. To determine the right particle size for a given case, the author used a trial-and-error process where a small slug of a plugging agent was first injected into the reservoir. Depending on the response of the

well, several small slugs of the plugging agent with different particle sizes were then injected in close succession until the intake rate was reduced to the desired value.

The first field example provided by Breton was a 65-ft thick soft sand formation at depth of about 1000 ft. The formation was relatively homogeneous with a porosity of 21% and an average permeability of 450 md. There was a water zone near the bottom of the wells which was plugged back with lead wool. The treatments were conducted in an irregular five-spot area that consisted of four injection wells and two production wells. Breton used water injection profiles before and after treatments to demonstrate selective plugging. A careful examination of the tracer logs reveals that only one injection well showed an improved injection profile after treatment. Another injection well was fractured during the treatment process. The tracer log shows that a new water pathway was created after treatment. The author's interpretation of two other injection wells was too optimistic. The resolution of the tracer logs was not enough to demonstrate improvement in injection profiles after treatments. In the following six months after treatment, one of the production wells within the five-spot pattern showed a significant increase in oil production (from 55 to 82 BPD). The water production was reduced by 41% over the same period of time. The effect of the treatments on the other production well within the five-spot pattern was not very significant. The field data provided by the author does not contain enough details to demonstrate selective plugging. Also, if crossflow can occur, injection profiles measured at the wellbore are not reliable indicators of the selectivity of a treatment process.¹³¹

In another field example, Breton treated a low-permeability Bradford Third sand reservoir. (Breton did not provide any specific information about the reservoir.) The particulates used had very small sizes (90% smaller than 1 μm). In total, 159 wells were treated. The author speculated that a significant amount of incremental oil was recovered as a result of selective plugging. The incremental oil recovery was determined from a decline-curve analysis. Unless the production increase is very significant, the noise in production data often makes it very difficult to accurately determine the decline curve. In Breton's case, decline-curve analysis was not a very reliable way to determine incremental oil recovery after a treatment. A close examination of the oil production data provided by Breton shows that the oil production increase was observed even before the treatment was implemented.

Exploiting Differences In Transient Times For Selective Placement

Breton¹⁰⁴ speculated that selective placement can be achieved by a sudden reduction in injection pressure when the plugging agents reached the target zones (calculated from pipe dimensions and the injection rate). Conceptually, a sudden decrease in injection pressure would create a transient period during which fluids in the reservoir could flow back into the well. The length of the transient period is inversely proportional to the formation permeability.¹³³ Breton's idea relies on the difference in transient times between the high- and low-permeability zones to achieve selective placement. The author asserted that due to the shorter transient time, enough plugging agents can be placed into high-permeability zones while the less-permeable zones are still backflowing. However, supporting evidence was not provided.

The feasibility of this idea depends on whether the difference in transient times is long enough to allow a realistic amount of the plugging agent to be placed into the high-permeability zone. Consider a reservoir with a 1500-md high-permeability zone and a 10-md low-permeability zone. In this example, the injection pressure at the wellbore is suddenly reduced from p_{w0} to p_{w2} where $(p_{w0}-p_e)=2(p_{w2}-p_e)$. We assume a steady-state flow condition in the reservoir before the injection pressure reduction. The parameters involved in this example are listed in Table 3. From Darcy's radial flow equation, before the injection-pressure reduction, the radial distance into the reservoir, r_2 , where the pressure is equal to p_{w2} can be

determined by

$$r_2 = \sqrt{r_e \times r_w} \quad (18)$$

In this example, r_2 is $\sqrt{372 \times 0.3} = 10.5 \text{ ft}$. This tells us that, before the injection-pressure reduction, reservoir pressure within a 10.5 ft radius from the well is greater than p_{w2} . A sudden reduction in injection pressure from p_{w0} to p_{w2} creates a pressure pulse that travels outward into the reservoir. The pressure in the reservoir would remain greater than the wellbore pressure, p_{w2} , until the pressure pulse reaches r_2 . In order for the reservoir fluid to backflow into the well, pressure in the reservoir must be greater than the wellbore pressure. The transient time is therefore the time required for the pressure pulse to reach r_2 . In pressure-drawdown analysis, the transient time is defined as

$$t_{tr} = \frac{? ? c r_e^2}{0.00264 k}, \quad (19)$$

where f is porosity, μ is fluid viscosity in cp, c is compressibility in psi^{-1} , r_e is drainage radius in ft, and k is formation permeability in md.¹³³ This equation calculates the time required for the pressure pulse to reach the drainage radius. The time required for the pressure pulse to reach r_2 can be estimated by substituting r_e for r_2 in the equation. In our example, the transient time for the high-permeability zone ($k_1=1500 \text{ md}$) is about 0.05 seconds and the transient time for the low-permeability zone ($k_2=10 \text{ md}$) is only about 7 seconds. Breton's concept relies on the difference in transient times between the high- and low-permeability zones to achieve selective placement. Our example demonstrates that the difference in transient times ($7-0.05=6.95 \text{ sec.}$) is obviously too short for this concept to have any practical value.

Table 3. Example Rock and Fluid Properties for Transient Time Calculations

k_1	= 1,500 md	k_2	= 10 md
f	= 0.21	μ_b	= 0.7 cp
c_w	= $3? \times 10^{-6} \text{ psi}^{-1}$	r_w	= 0.3 ft
r_e	= 372 ft (20 acre, 5 spot)		

One other possible way of achieving selective plugging is to exploit the difference in formation pressures between high- and low-permeability zones. This is possible only when the high- and low-permeability zones are separated by an impermeable barrier and the formation pressure in the low-permeability zone is significantly higher than that in the high-permeability zone. Selective placement could be achieved by injecting the plugging agent at an injection pressure which is high enough to place a significant amount of plugging agent into the high-permeability zone in a reasonable period of time and yet low enough not to exceed the formation pressure in the low-permeability zone.

Selective Plugging Using Particulates In Fractured Wells

Breton¹⁰⁴ also used particulates to plug fractures and leaky packers. The author attributed the

increased wellhead pressure and reduced water intake observed after treatments to selective plugging. However, increased wellhead pressure and reduced water intake alone are not enough to support selective plugging. The field data provided by the author do not contain enough details to demonstrate selective plugging.

Smith *et al.*¹⁰⁷ reported the field results of using solid plugging agents (e.g., nutshell flour, bentonite, etc.) to improve the sweep efficiency of fractured reservoirs. The finely ground solids were injected as water slurries at pressures above the fracture-opening pressure. The authors speculated that the injection of a solid plugging agent at a pressure above the fracture-opening pressure would result in the solids being tightly packed in the fracture after treatment. To maintain injectivity after treatment, plugging agents were displaced some distance into the fractures during the placement process. The authors speculated that if during subsequent water injection, the injection pressure exceeded the fracture-opening pressure, the plugging agent would move toward the end of the fracture and reseal the fracture. To achieve selective placement, the authors proposed the use of plugging agents with a particle size large enough not to cause significant matrix invasion and small enough to allow in-depth placement in the fractures. They speculated that a mixture of 90% nutshell flour and 10% bentonite could effectively seal fractures without causing any significant damage to low-permeability oil zones. The nutshell flour had 50% (by weight) of the particles smaller than 36 μm . The other 50% of the particles had a size distribution ranging from 36 μm to 162 μm . The authors suggested backflowing the wells for a short period of time to remove the plugging agents deposited on the rock surface. Their field results showed a slight increase of fracture-opening pressure after treatment. The increase in fracture-opening pressure allowed a thirty percent increase in injection rate. However, the authors did not provide any production data to demonstrate improved sweep efficiency.

Garland¹⁰⁶ performed a field study to examine the feasibility of using plugging materials to modify injection profiles. Commercially available plugging agents of various particle sizes were used in the study. Instead of providing numerical values, the author used fine, medium, and coarse to distinguish particles involved in the study. All of the field cases provided by Garland involved fractured reservoirs. The author used the injection-profile change to demonstrate the selectivity of this process. However, the injection-profile change observed in the wellbore is not a reliable indicator of the selectivity of a treatment process because crossflow can occur in the fractures after the fluids leave the wellbore.¹³¹ Also, the production data provided by the author did not demonstrate selectivity. In most cases, the treatments did not have any noticeable effect on fluid production. In one case, a sustained increase in oil production was observed. However, the oil production increase occurred before the treatment was implemented. The author attributed the oil production increase to the arrival of oil banks from other injection wells. Most of the field cases involved multiple treatments, some had as many as twenty repeated treatments. However, the production data demonstrated that even with multiple treatments, this process was not effective in treating fractured reservoirs.

Exploiting Gravity For Selective Placement. Garland¹⁰⁶ speculated that, depending on the location of the thief zones, selective placement can be achieved by using plugging agents mixed in either oil or water. The author proposed that plugging agents be mixed in oil when the thief zones were in the upper part of the formation. Garland asserted that because the plugging agents mixed in oil are lighter than water, they have a tendency to stay in the upper part of the wells. Therefore, during the placement process, most of the plugging agents would enter the thief zones located in the upper part of the formation. The small amount of plugging agents that failed to enter the thief zones would float to the upper part of the wells before reaching the less-permeable zones in the lower part of the formation. Following similar logic, the author proposed that plugging agents mixed in water be used when the thief zones were in the lower part of the formation. However, the author did not provide any field or coreflood data as support. Garland's

concept is very similar to the idea behind the buoyant-ball-sealer technology used in well stimulation. It is a common practice in well stimulation to include buoyant balls in treating fluids for selective placement. When properly designed, the buoyant balls can seal the undamaged high-permeability zones and divert the treating fluids into the low-permeability zones.¹³⁴

To study the feasibility of exploiting gravity for selective placement, consider a reservoir with two zones. First, we consider the case where the high-permeability zone is in the upper part of the formation and the low-permeability zone is in the lower part of the formation. The fluid properties involved in this example are summarized in Table 4. Since we want to selectively plug the upper zone, particulates lighter than the carrier fluid (brine, in this example) are used. We assume that the particulates have the same density as a light oil ($\rho_p=0.7 \text{ g/cm}^3$). When the particulates flow past the high-permeability zone in the upper part of the formation, a certain fraction of the particulates will immediately enter the high-permeability zone. The remaining particulates will however overshoot the high-permeability zone. If the fluid velocity below the high-permeability zone is lower than the rising velocity of the particulates, the particulates will float upward and eventually enter the high-permeability zone. By assuming the particulates to be spherical in shape, we can use the equations derived for buoyant balls¹³⁴ to estimate the rising or settling velocities of particulates in brine. In the Stoke's Law region where Reynolds Number, $N_{Re} < 1$, the particle velocity, v_p , can be calculated by Eq. 20.

$$v_p = \frac{g |\rho_p - \rho_b| d^2}{18 \mu_b} \quad (20)$$

From this equation, the rising velocity, v_p , of the particulates ($d=50 \text{ }\mu\text{m}$) in this example is about 0.075 ft/min. In other words, to achieve selective placement, the fluid velocity in the well below the high-permeability zone must be less than 0.075 ft/min. This velocity is equivalent to about 0.003 bpm in a 7-in, 32-lb/ft casing (27.7-ft/bbl capacity). At an injection rate of 2 bpm, the high-permeability zone must be at least 700 times ($2/0.003 \approx 700$) more permeable than the low-permeability zone for the fluid velocity below the high-permeability zone to stay below 0.003 bpm (assuming the high- and low-permeability zones have the same dimensions). The required permeability contrast is too high for Garland's concept to have any practical value.

Next, we consider the case where the high-permeability zone is in the lower part of the formation. In this case, particulates heavier than the carrier fluid ($\rho_p=4 \text{ g/cm}^3$) are used. The other parameters involved in this example are the same as those used in the previous example. From the same equation used in the previous example, the settling velocity, v_p , for the particulates in this case is 4 ft/min. This means that the flow velocity of the particulates is always 4 ft/min faster than the velocity of the carrier fluid. This is equivalent to about 0.14 bpm in a 7-in, 32-lb/ft casing (27.7-ft/bbl capacity). The added velocity can only reduce the amount of particulates entering the low-permeability zone. Unless the settling velocity is extremely high, a significant amount of particulates can still enter and damage the low-permeability zone. One possible solution to this problem is to introduce the particulates into the well and allow the particulates to fall freely past the low-permeability zone before pumping. However, at 4 ft/min in a 7-in, 32-lb/ft casing, it would take the particulates more than two hours to fall 500 ft in the wellbore. Therefore, this method would be most practical when the low-permeability zone is fairly shallow.

Table 4. Example Fluid Properties for Exploiting Gravity for Selective Placement Calculations

$\rho_p = 0.7 \text{ g/cm}^3$ (buoyant)

$\rho_p = 4 \text{ g/cm}^3$ (nonbuoyant)	
$\mu_b = 1 \text{ cp}$	$d = 50 \text{ }\mu\text{m}$

Shallow Plugging-Selective Re-Entry Technique. Thomeer *et al.*¹¹¹ used a "shallow plugging-selective re-entry technique" for profile correction. This technique involves first plugging all open zones to a shallow distance with particulates and then re-opening selected zones through perforation. There is no need for zone isolation during the treatment process because selective placement is not required for this technique. The authors first conducted laboratory core experiments to study the validity of the shallow-plugging concept. San Andres dolomite cores were used for the core experiments. The authors observed shallow plugging in all the cores tested under simulated reservoir conditions. Field tests were performed in three injection wells in fractured dolomite reservoirs (Cabin Creek field). Commercial bentonite and micronized silica flour with a size distribution ranging from 0.1 to 10 μm were used for shallow plugging. The size distribution was determined using the 1/3-1/10 rule^{114,115} for internal cake formation. All three cases involved severe channeling behind pipes. After multiple treatments with a larger than expected amount of particulates (based on the amount required to invade 2 inches into the reservoir), the injection profile after the reperforation indicated that all channeling behind casing was stopped. The time requirement for completion of the treatments was 4 to 6 months. In one case, the thief zone at the bottom of the well was also sealed by the particulates after treatment. The authors attributed the larger than expected amount of particulates required to the presence of fractures and voids in the reservoirs. This technique might work if there is no communication between the thief zones and the low-permeability oil-productive zones. The long treatment time involved may limit the concept's practicality in treating fractured reservoirs

In summary, most of the literature surveyed made unsubstantiated claims that particulates can selectively plug the high-permeability thief zones without damaging the oil productivity after treatment. Critical analyses of these claims reveal that most of the proposed schemes suffer from the same placement limitations that gels experience. Particulates small enough to penetrate into the formation can cause significant damage to the formation permeability. The differences in transient times between high- and low-permeability zones are too short to be exploited for selective placement. Selective plugging might be achieved by using particulates large enough not to penetrate into the low-permeability oil zones and yet small enough to achieve in-depth placement in the thief zones. Conceptually, selective plugging could be achieved with any kind of permeability contrast by using particulates with an appropriate monodisperse particle size. However, for economic and technical reasons, particulates used in field applications usually have a size distribution. The relatively small permeability contrasts in unfractured cases might not be enough to prevent particle penetration into the less-permeable oil-productive zones. Also, crossflow can render the treatment ineffective.⁶¹ This idea might be more feasible in fractured reservoirs where permeability contrasts are high enough to allow selective placement of particulates with a realistic size distribution. However, particulates alone might not be effective in sealing the fractures. Field examples in the literatures suggest that multiple treatments with a large amount of particulates is usually required to seal off the fractures. A possible solution to this problem is to use particulates in conjunction with gels. When used in conjunction with gels, particulates with the right particle size distribution could minimize gelant leakoff from the fracture face into the rock matrix during the placement process. The gels could then heal the fractures without damaging the oil productivity. In the next section, a theoretical model is developed to examine the feasibility of using particulates to eliminate the need for zone isolation for a water-like gelant during the placement process.

Theoretical Model

The objective of this theoretical analysis is to study the feasibility of using particulates to eliminate the need for zone isolation for a water-like gelant during the placement process. Darcy's law and basic formation damage concepts are applied to mathematically model the effect of particle size distribution on the degree of gelant penetration into zones of different permeabilities.

Basic Assumptions. The following assumptions were made in developing the theoretical model.

1. All fluids are incompressible and Newtonian.
2. Gelant formulations are miscible with water.
3. The gelation reaction is slow relative to the placement process.
4. Cake deposition is proportional to the volume passed through the rock face.
5. The cake permeability is independent of the thickness of the cake.
6. The flow through the cake obeys Darcy's law.
7. Particles larger than 1/3 of the pore size form an external filter cake on the rock face.
8. Particles smaller than 1/3 of the pore size do not have any effect on formation permeability.
9. Each layer is homogeneous, isotropic, and isothermal.
10. The reservoir consists of a number of horizontal, noncommunicating layers.
11. All layers have the same areal dimensions and share the same injector and producer. (The layers can have different thicknesses.)

From Carman-Kozeny's equation,¹³⁵ van Valzen *et al.*¹³⁶ derived the following equation to calculate the particle/pore size ratio.

$$\text{Particle / Pore Size Ratio} = \frac{d_{50}}{0.95 \sqrt{k_m}}, \quad (21)$$

where d_{50} is the median pore size and k_m is the matrix permeability.

According to assumptions (7) and (8) and Eq. 21, the critical particle size, d_{crit} , for a formation can be estimated by the following equation.

$$d_{crit} = \frac{1}{3} \sqrt{k_m} \quad (22)$$

In this study, we assume that particles greater than the critical particle size of a given formation form an external filter cake on the rock face while particles smaller than the critical particle size flow through the porous medium without causing any formation damage.

In the theoretical model, we use filtration coefficient, α_o , to calculate the efficiency of filter cake formation. The filtration coefficient, α_o , is defined as the total filtration volume, V_t divided by cake volume, V_c .

$$\alpha_o = \frac{V_t}{V_c} \quad (23)$$

According to this definition, the efficiency of filter cake buildup is inversely proportional to α_o .

For particles with a size distribution, the filtration coefficient of a given layer, α_i , is defined as

$$\alpha_i = \frac{\alpha_o}{1 - f_p}, \quad (24)$$

where f_p is the fraction of the particles smaller than the critical particle size of the formation.

For linear flow, the instantaneous pressure drop in Layer i between the producer and the injector with a filter cake on the rock face is

$$\Delta p = \frac{q_i}{A_i} \left[-\frac{\mu_p}{k_c} L_{ci} + \frac{\mu_p}{k_i} L_{pi} + \frac{\mu_w (\Delta p_{Di} + 1)}{k_i} L_{pm} \right], \quad (25)$$

where k_c is the filter-cake permeability, μ_p is the gelant viscosity, L_{ci} is the filter-cake thickness on Layer i , L_{pi} is the distance of gelant penetration into Layer i , and L_{pm} is the maximum distance of gelant penetration into the most-permeable layer (Layer 1). Δp_{Di} is defined as the ratio of the pressure drop between L_{pm} and the end of Layer i to the pressure drop between the beginning of Layer i and L_{pm} prior to gelant injection (see Ref. 18 for a more detailed discussion).

From Eq. 23,

$$V_t = -L_{ci} \alpha_i A_i. \quad (26)$$

According to material balance,

$$V_t = -L_{ci} A_i \alpha_c + L_{pi} A_i \alpha_i, \quad (27)$$

where α_c is the filter-cake porosity.

Comparing Eqs. 26 and 27 yields

$$L_{ci} = \left(\frac{\alpha_i}{\alpha_c - \alpha_i} \right) L_{pi}. \quad (28)$$

Also, according to material balance,

$$q_i = -A_i \alpha_c \frac{dL_{ci}}{dt} + A_i \alpha_i \frac{dL_{pi}}{dt}, \quad (29)$$

where t is time.

Substituting Eqs. 28 and 29 into Eq. 25 and rearranging yield,

$$\Delta p = \alpha_i \left(\frac{\alpha_i}{\alpha_i - \alpha_c} \right) \left\{ \left[\frac{\mu_p - \mu_w}{k_i} - \left(\frac{\alpha_i}{\alpha_c - \alpha_i} \right) \frac{\mu_p}{k_c} \right] L_{pi} + \frac{\mu_w (\Delta p_{Di} + 1)}{k_i} L_{pm} \right\} \frac{dL_{pi}}{dt}. \quad (30)$$

Since Δp is the same across Layer 1 and Layer i ,

$$\alpha_i \left(\frac{\alpha_i}{\alpha_i - \alpha_c} \right) \left\{ \left[\frac{\alpha_p - \alpha_w}{k_i} - \left(\frac{\alpha_i}{\alpha_c - \alpha_i} \right) \frac{\alpha_p}{k_c} \right] L_{pi} + \frac{\alpha_w (\alpha_{Di} + 1)}{k_i} L_{pm} \right\} \frac{dL_{pi}}{dt} = \quad (31)$$

$$\alpha_1 \left(\frac{\alpha_1}{\alpha_1 - \alpha_c} \right) \left\{ \left[\frac{\alpha_p - \alpha_w}{k_1} - \left(\frac{\alpha_1}{\alpha_c - \alpha_1} \right) \frac{\alpha_p}{k_c} \right] L_{p1} + \frac{\alpha_w (\alpha_{D1} + 1)}{k_1} L_{pm} \right\} \frac{dL_{p1}}{dt}.$$

Multiplying both sides of Eq. 31 by dt and integrating the left side of the equation between 0 and L_{pi} while integrating the right side between 0 and L_{p1} yield,

$$\alpha_i \left(\frac{\alpha_i}{\alpha_i - \alpha_c} \right) \left\{ \left[\frac{\alpha_p - \alpha_w}{k_i} - \left(\frac{\alpha_i}{\alpha_c - \alpha_i} \right) \frac{\alpha_p}{k_c} \right] \frac{L_{pi}^2}{2} + \frac{\alpha_w (\alpha_{Di} + 1)}{k_i} L_{pm} L_{pi} \right\} = \quad (32)$$

$$\alpha_1 \left(\frac{\alpha_1}{\alpha_1 - \alpha_c} \right) \left\{ \left[\frac{\alpha_p - \alpha_w}{k_1} - \left(\frac{\alpha_1}{\alpha_c - \alpha_1} \right) \frac{\alpha_p}{k_c} \right] \frac{L_{p1}^2}{2} + \frac{\alpha_w (\alpha_{D1} + 1)}{k_1} L_{pm} L_{p1} \right\}.$$

Let $L_{p1} = L_{pm}$

$$\alpha_i \left(\frac{\alpha_i}{\alpha_i - \alpha_c} \right) \left\{ \left[\frac{\alpha_p - \alpha_w}{k_i} - \left(\frac{\alpha_i}{\alpha_c - \alpha_i} \right) \frac{\alpha_p}{k_c} \right] \frac{L_{pi}^2}{2} + \frac{\alpha_w (\alpha_{Di} + 1)}{k_i} L_{pm} L_{pi} \right\} = \quad (33)$$

$$\alpha_1 \left(\frac{\alpha_1}{\alpha_1 - \alpha_c} \right) \left[\frac{\alpha_p - \alpha_w}{k_1} - \left(\frac{\alpha_1}{\alpha_c - \alpha_1} \right) \frac{\alpha_p}{k_c} + \frac{2 \alpha_w (\alpha_{D1} + 1)}{k_1} \right] \frac{L_{pm}^2}{2}.$$

Solving for L_{pi}/L_{pm} ,

$$\frac{L_{pi}}{L_{pm}} = \frac{-\alpha_i \left(\frac{\alpha_i}{\alpha_i - \alpha_c} \right) \frac{\alpha_w (\alpha_{Di} + 1)}{k_i}}{\frac{\alpha_p - \alpha_w}{k_i} - \frac{\alpha_p}{k_c} \left(\frac{\alpha_i}{\alpha_c - \alpha_i} \right)} + \sqrt{\frac{\alpha_i^2 \left(\frac{\alpha_i}{\alpha_i - \alpha_c} \right)^2 \frac{\alpha_w^2 (\alpha_{Di} + 1)^2}{k_i^2} - \alpha_i \left(\frac{\alpha_i}{\alpha_i - \alpha_c} \right) \left[\frac{\alpha_p - \alpha_w}{k_i} - \frac{\alpha_p}{k_c} \left(\frac{\alpha_i}{\alpha_c - \alpha_i} \right) \right] \frac{\alpha_w (\alpha_{Di} + 1)}{k_i}}{\alpha_i \left(\frac{\alpha_i}{\alpha_i - \alpha_c} \right) \left[\frac{\alpha_p - \alpha_w}{k_i} - \frac{\alpha_p}{k_c} \left(\frac{\alpha_i}{\alpha_c - \alpha_i} \right) \right]} \quad (34)$$

For laboratory linear corefloods, the $\alpha_{Di} = 0$ for all layers and $L_{p1} = L_{pm} = L_t$. Therefore, Eq. 34 can be simplified as

$$\frac{L_{pi}}{L_t} = \frac{-\frac{p_i}{k_i} \left(\frac{p_i}{p_i - p_c} \right) \frac{p_w}{k_i}}{\frac{p_p - p_w}{k_i} - \frac{p_p}{k_c} \left(\frac{p_i}{p_i - p_c} \right)} + \sqrt{\frac{p_i^2 \left(\frac{p_i}{p_i - p_c} \right)^2 \frac{p_w^2}{k_i^2} - \frac{p_i}{k_i} \left(\frac{p_i}{p_i - p_c} \right) \left[\frac{p_p - p_w}{k_i} - \frac{p_p}{k_c} \left(\frac{p_i}{p_i - p_c} \right) \right] p_i \left(\frac{p_i}{p_i - p_c} \right) \left[\frac{p_p}{k_c} \left(\frac{p_i}{p_i - p_c} \right) - \frac{p_p - p_w}{k_i} \right]}{p_i \left(\frac{p_i}{p_i - p_c} \right) \left[\frac{p_p - p_w}{k_i} - \frac{p_p}{k_c} \left(\frac{p_i}{p_i - p_c} \right) \right]} \right. \quad (35)$$

where L_t is the total core length.

Effects of Particulates on Gelant Placement

Our previous studies^{18,30} revealed that during an unrestricted injection, the degree of gelant penetration into the less-permeable layers increases with increasing gelant viscosity. Therefore, a water-like gelant should be the preferred choice when zones cannot be isolated during placement. However, the studies also showed that without zone isolation, a water-like gelant can still penetrate a significant distance into the less-permeable oil zones and damage the oil productivity after treatment. Can particulates eliminate the need for zone isolation for a water-like gelant during placement?

Particulates with a Monodisperse Size. We begin our analysis with the ideal case of particulates with a monodisperse size. To quantify the effect of particulates on the degree of penetration, consider injecting a water-like gelant mixed with particulates into two parallel homogeneous cores of equal length from a common injection port. The cores have different permeabilities and contain no oil. The rock and fluid properties are summarized in Table 5.

Table 5. Rock and Fluid Properties for Degree of Penetration Calculations

S_{w1} = 1.0	S_{wi} = 1.0
μ_w = 1 cp	μ_p = 1 cp
k_1 = 10,000 md	k_i = 100 md
d_{crit1} = 33.3 μm	d_{criti} = 3.33 μm
f_1 = 0.2	f_i = 0.2
a_o = 0.2	f_c = 0.2
L_t = 50 ft	p_D = 0

Fig. 10 shows the degree of gelant penetration into the less-permeable core (Core i) when the gelant reached the outlet of the more-permeable core (Core 1). (Eq. 35 was used to generate the results shown in Figs. 10 and 11.) As shown in Fig. 10, when the particle size is smaller than the critical particle size of the less-permeable core ($d_{criti} = 3.33 \mu\text{m}$), the particulates have no effect on the degree of gelant penetration. The degree of gelant penetration into the less-permeable core in this case is the same as that

with no particulates present (particle size = 0 μm in Fig. 10). Fig. 10 also shows that, when the particle size is greater than the critical particle size of the more-permeable core ($d_{\text{crit1}} = 33.3 \mu\text{m}$), the gelant penetrates roughly the same distance into both cores. This is not surprising because the particulates form filter cakes on the inlet rock faces of both cores. To achieve selective placement, Fig. 10 shows that the size of the particulates used must be smaller than the critical particle size of the more-permeable core and larger than that of the less-permeable core. Since we are using particulates with a monodisperse size, with the right particle size, we could achieve selective placement with any degree of permeability contrast. Fig. 10 shows that the degree of gelant penetration into the less-permeable core increases with increasing filter-cake permeability, k_c . However, the effect of filter-cake permeability on the degree of gelant penetration is not very significant.

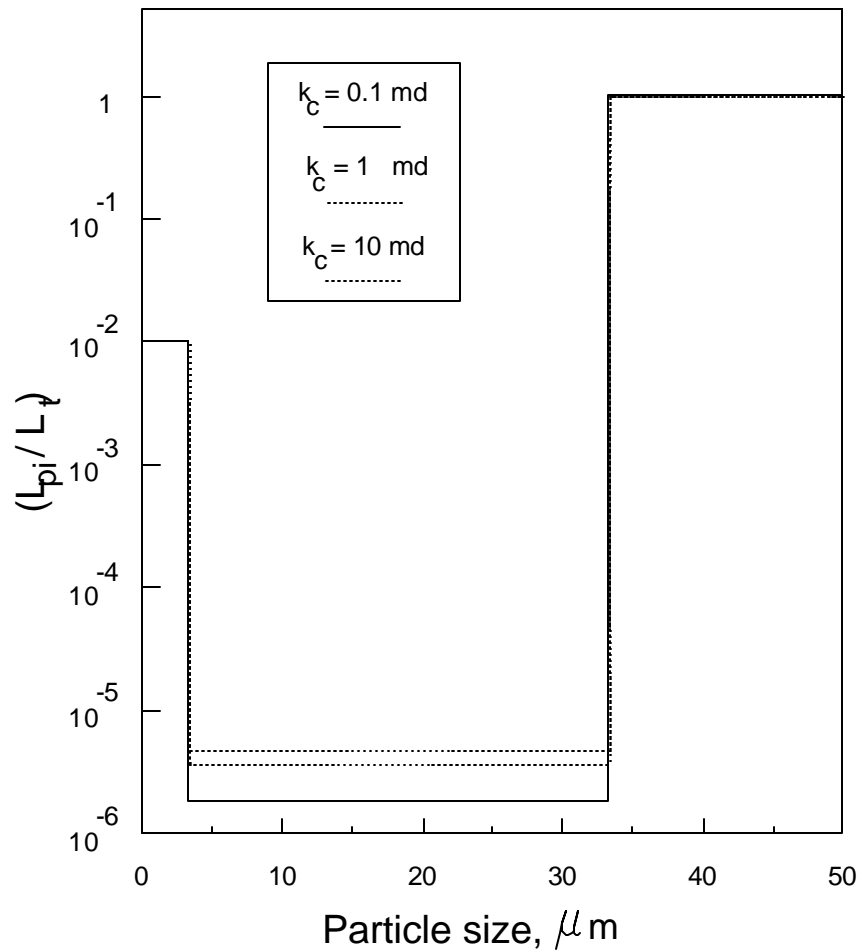


Fig. 10. Effect of particle size and filter-cake permeability (k_c) on the degree of gelant penetration for particulates with a monodisperse size.

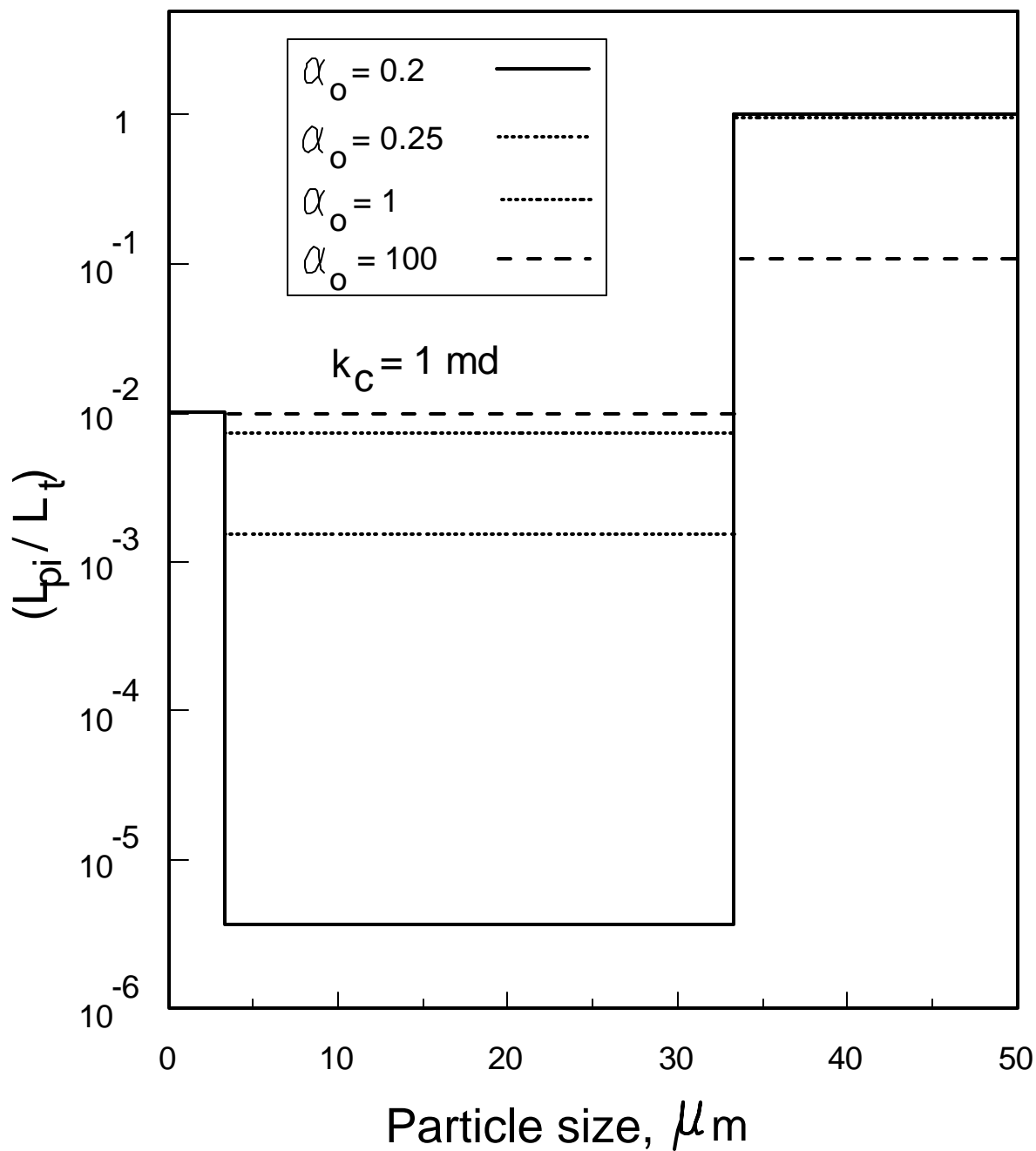


Fig. 11. Effect of filtration coefficient on the degree of gelant penetration for particulates with a monodisperse size.

Fig. 11 shows that the degree of gelant penetration is, however, very sensitive to changes in filtration coefficient, α_0 . The degree of gelant penetration into the less-permeable core increases significantly with increasing α_0 . This is because at higher α_0 more gelant leakoff into the less-permeable core is required to build the filter cake to a given thickness (see Eq. 23). Hence, a high filter-cake-buildup efficiency (i.e., a small α_0) is essential to the success of using particulates to prevent gelant penetration into low-permeability zones during the placement process.

Particulates with a Size Distribution. We demonstrated in the previous section that selective placement of a water-like gelant could be achieved by using particulates with a monodisperse size. However, for economic and technical reasons, particulates used in field applications usually have a size distribution. Can particulates with a size distribution prevent gelant penetration into low-permeability zones during the placement process?

To answer this question, consider injecting a water-like gelant mixed with particulates into two parallel homogeneous cores of equal length from a common injection port. In this case, we assume that the particulates injected with the gelant have a normal size distribution. Fig. 12 illustrates a normal size distribution where the mean particle size, \bar{d}_3 , is 18 μm and the standard deviation, s , is 4 μm . For a normal size distribution, the mean particle size locates the center of the distribution and the standard deviation measures its spread. The cores have different permeabilities and contain no oil. The example rock and fluid properties are summarized in Table 5.

We begin our analysis by arbitrarily assigning the average of the critical particle sizes of the high- and low-permeability cores, $(33.3+3.33)/2 \approx 18 \mu\text{m}$, to be the mean particle size. As shown in Fig. 13, for a given permeability contrast, the degree of gelant penetration into the low-permeability core increases with increasing standard deviation. Fig. 13 shows that, for our example case where $k_1=10,000 \text{ md}$ and $k_2=100 \text{ md}$, the standard deviation must be smaller than 9 μm to achieve better selectivity than a water-like gelant without particulates. To achieve the same degree of selectivity as particulates with a monodisperse size ($\bar{d}_4=18 \mu\text{m}$, $s=0 \mu\text{m}$), Fig. 13 shows that the standard deviation must be smaller than 4 μm . Fig. 14 demonstrates that, for a given standard deviation, maximum selectivity is achieved by choosing the average of the critical particle sizes of the high- and low-permeability cores ($\bar{d}_5=18 \mu\text{m}$ in this case) as the mean particle size.

Next, we examine the effect of permeability contrast on the degree of gelant penetration. In the following example, the particulates have a normal size distribution with a mean particle size of 20 μm and the permeability of the high-permeability core, k_1 , is 10,000 md. We change the permeability contrast by varying the permeability of the low-permeability core, k_2 . To achieve a given degree of selectivity ($L_{pi}/L_t < 10^{-4}$ in this example), Fig. 15 shows that the maximum standard deviation allowed decreases with decreasing permeability contrast. In other words, the maximum standard deviation for selective placement decreases with decreasing permeability contrast. Eqs. 24 and 35 were used to generate the results shown in Figs. 13, 14 and 15.

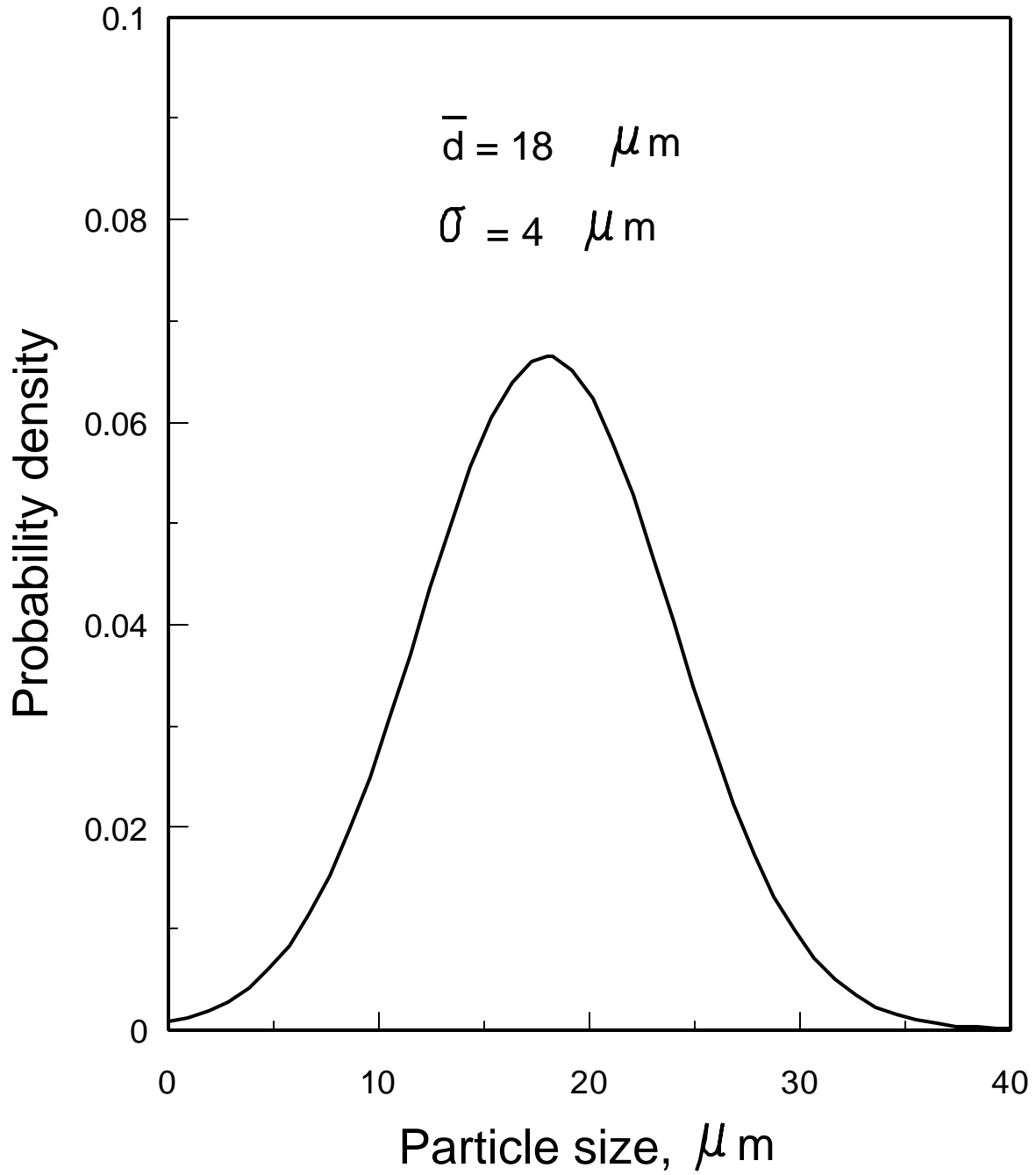


Fig. 12. Particulates with a normal size distribution.

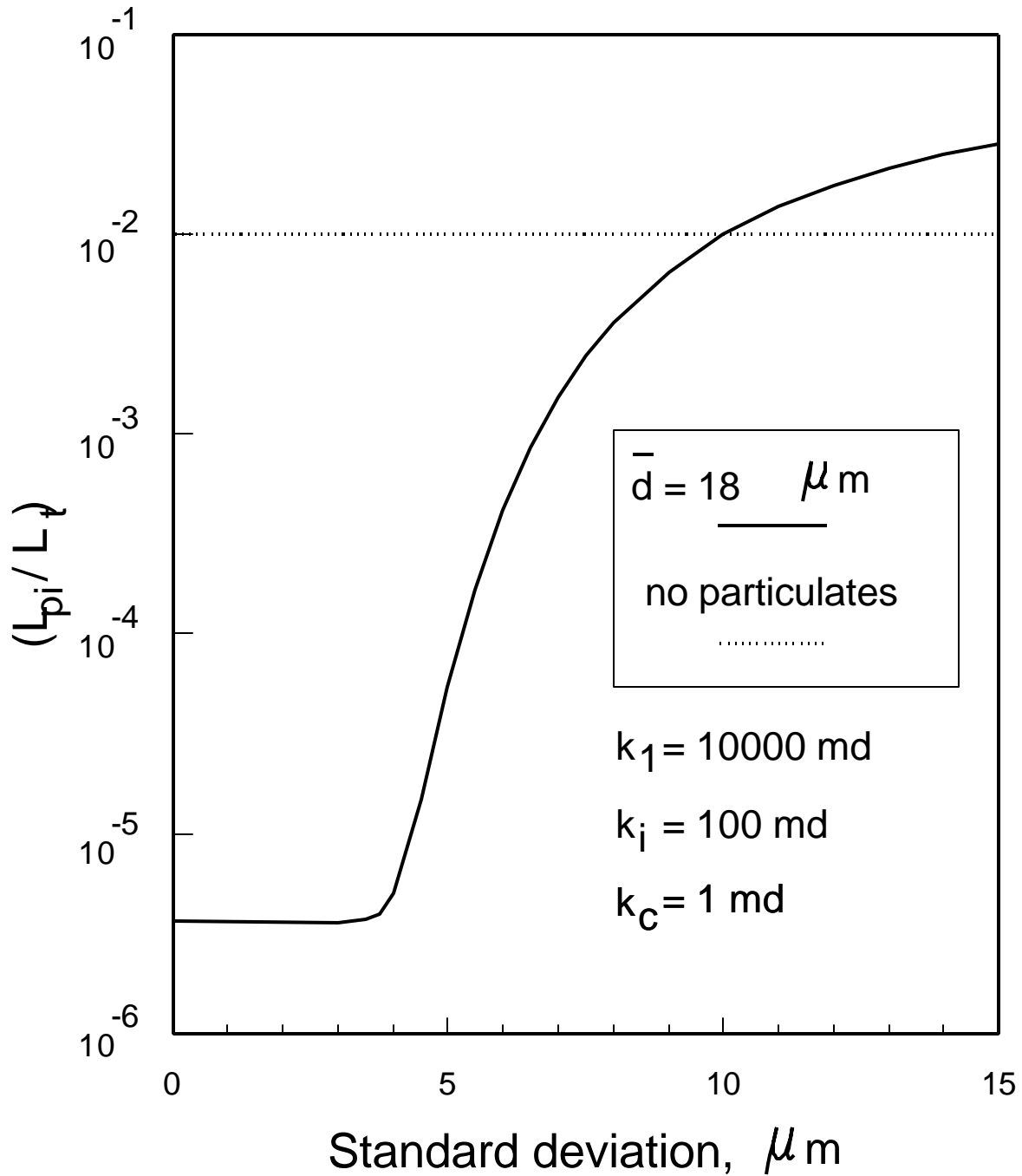


Fig. 13. Effect of standard deviation on the degree of gelant penetration, $(k_1/k_i) = 100$.

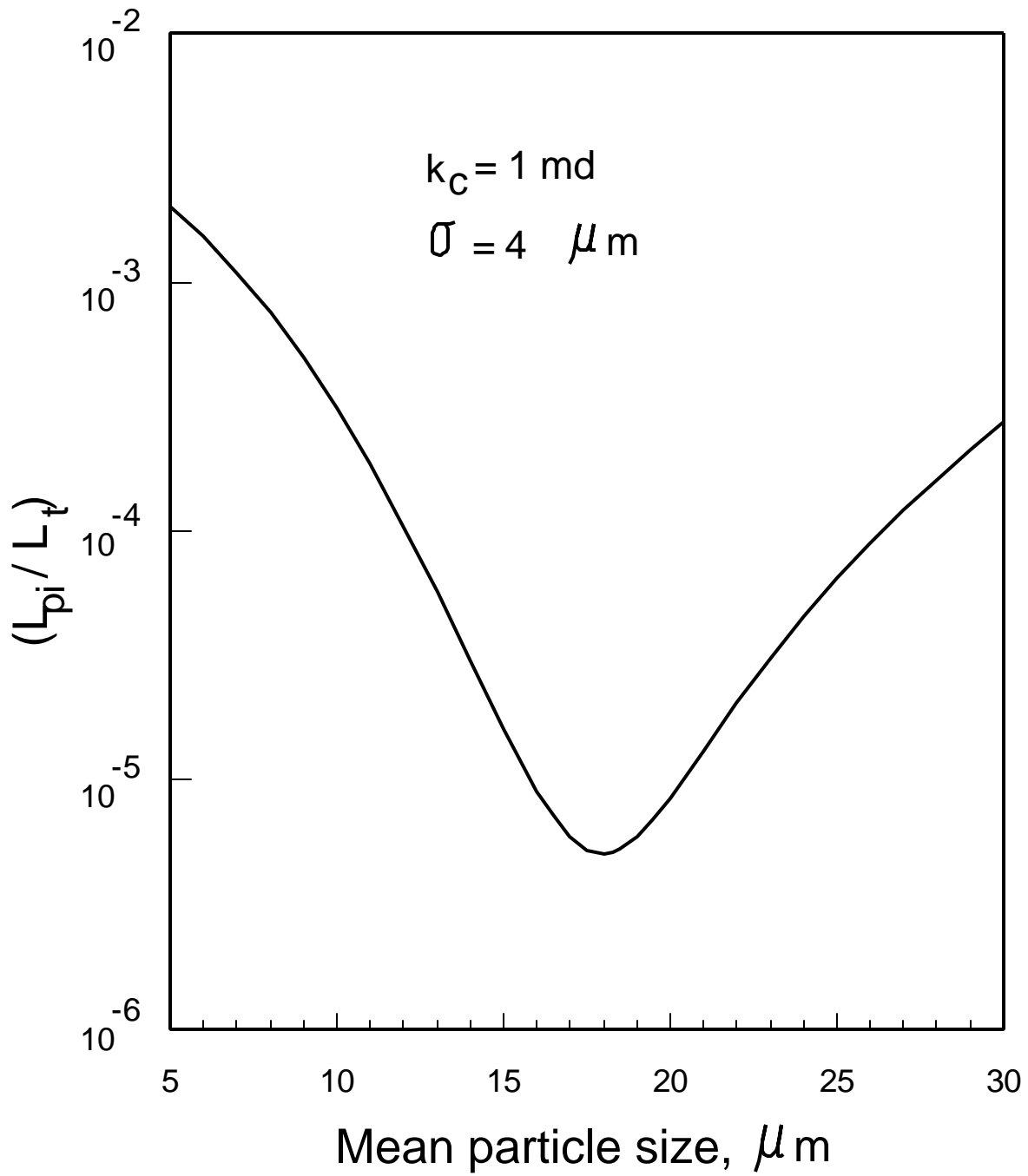


Fig. 14. Effect of mean particle size on degree of gelant penetration.

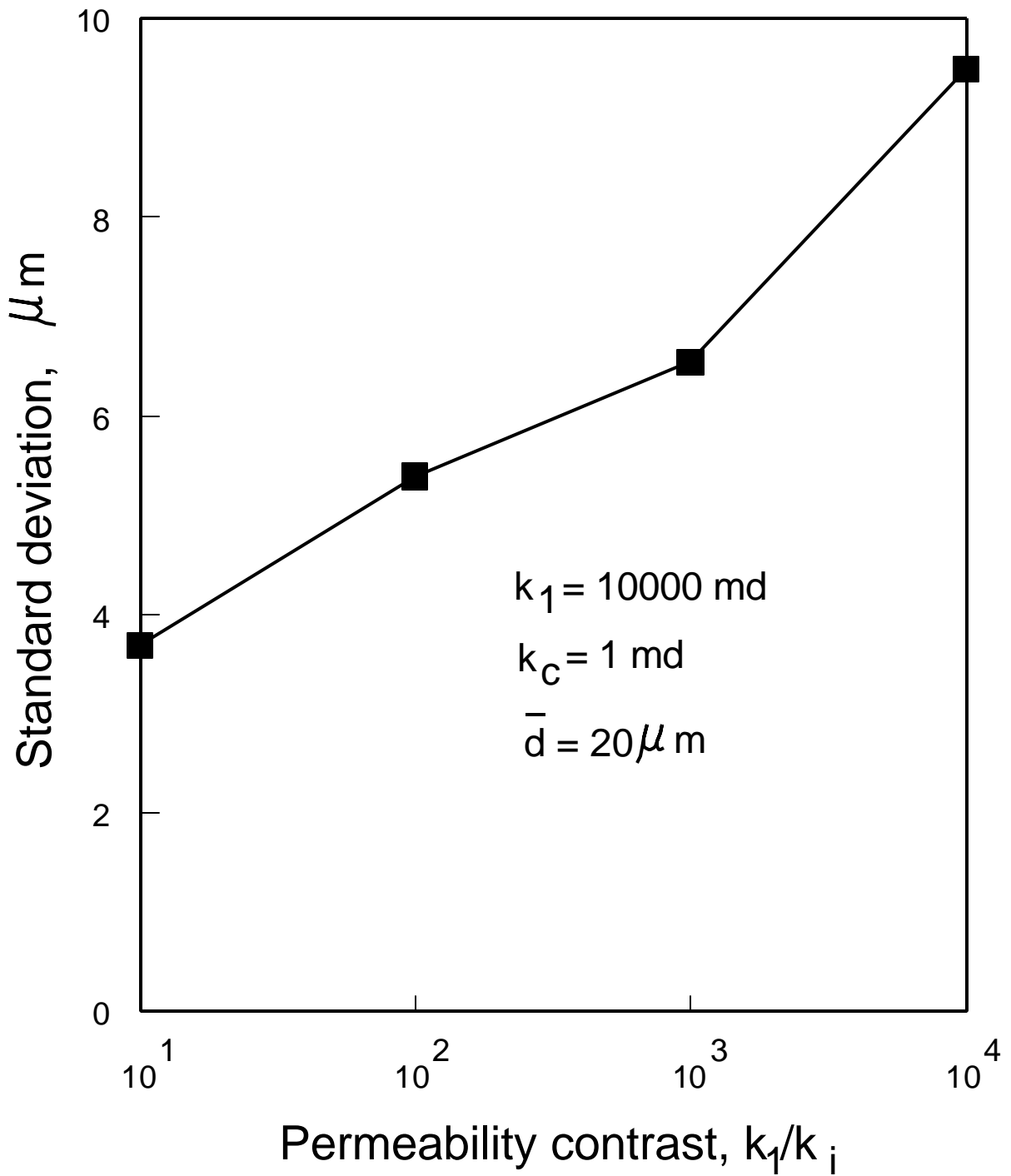


Fig. 15. Effect of permeability contrast on the maximum standard deviation for a given selectivity.

Conclusions

The following conclusions are reached based on our survey of petroleum and patent literature.

1. Most of the literature surveyed made unsubstantiated claims that particulates can selectively plug the high-permeability thief zones without damaging the oil productivity after treatment. Critical analyses of these claims reveal that most of the proposed schemes suffer from the same placement limitations that gels experience.
2. Particulates small enough to penetrate into the formation can cause significant damage to the formation permeability. The degree of permeability reduction increases with decreasing formation permeability.
3. The differences in transient times between high- and low-permeability zones are too short to be exploited for selective placement.

The following conclusions are based on our theoretical analyses using particulates to prevent gelant penetration into low-permeability zones during the placement process.

1. To achieve selective placement using particulates with a monodisperse size, the size of the particulates used must be smaller than the critical particle size of the fracture and larger than that of the formation matrix.
2. The degree of gelant penetration is not sensitive to the filter cake permeability.
3. The degree of gelant penetration is, however, very sensitive to changes in the filtration coefficient, α_o . A high filter-cake-buildup efficiency (i.e., a small α_o) is essential to the success of using particulates to prevent gelant penetration into low-permeability zones during the placement process.
4. To achieve selective placement using particulates with a normal size distribution, there is a maximum standard deviation that should not be exceeded for a given permeability contrast. For our example case where $k_1=10,000$ md and $k_2=100$ md, the standard deviation must be smaller than $9 \mu\text{m}$ ($\bar{d}_c=18 \mu\text{m}$) to achieve better selectivity than a water-like gelant without particulates. To achieve the same degree of selectivity as particulates with a monodisperse size of $18 \mu\text{m}$, the standard deviation must be smaller than $4 \mu\text{m}$.
5. The maximum standard deviation for selective placement decreases with decreasing permeability contrast. For a given standard deviation, maximum selectivity is achieved by choosing the average of the critical particle sizes of the high- and low-permeability zones as the mean particle size.

5. PROPAGATION OF AN ALUMINUM-CITRATE-HPAM "COLLOIDAL-DISPERSION" GEL THROUGH BERE SANDSTONE

This chapter examines the ability of an aluminum-citrate-HPAM "colloidal-dispersion" gel to propagate through Berea sandstone. Recently, incremental oil recovery values as high as 18.2% original oil in place (OOIP) were reported by the vendor applying these gels to improve oil recovery.¹³⁷ These gels were speculated to penetrate deep into non-fractured sandstone formations (e.g., the Minnelusa formation of Northeastern Wyoming).^{137,138}

Importance of the Suggested Behavior

The latter suggestion is of particular interest, since if valid, it represents a potentially major advance in enhanced oil recovery (EOR). To understand why this concept is controversial, consider how other gels perform in porous media.^{26,31,52,130,139,140} Early in the gelation process, most gels behave like clean fluids that do not contain suspended particulate matter.^{26,31,52,130,139} For example, early in the gelation process, the rheology in porous media is the same for a Cr(III)-xanthan gelant as for a xanthan solution without a crosslinker.¹³⁰ However, after gel aggregates form and grow to the size of pore throats, gel filtration can radically increase the resistance to flow.^{139,140} The literature indicates that gelants can penetrate a significant distance into porous rock before gelation, but after gelation, gel propagation is extremely slow or negligible.^{26,31,52,130,139,140}

In contrast to normal gel behavior, the aluminum-citrate-HPAM gels (after gel formation) were speculated to propagate through porous rock like viscous polymer solutions.¹³⁸ Therefore, these gels are purported to act like mobility-control agents. If true, this mechanism of action would be radically different from that for other gels, which act exclusively as blocking agents.

The distinction between a blocking agent and a mobility-control agent is an important concept to understand (see Fig. 1). A mobility-control agent should penetrate as much as possible into the less-permeable zones so that oil can be displaced from poorly swept zones. In contrast, we wish to minimize penetration of blocking agents into the less-permeable, oil-productive zones. Any blocking agent that enters the less-permeable zones can hinder subsequent injected fluids (e.g., water, CO₂, steam) from entering and displacing oil from those zones.

Typically, the aluminum-citrate-HPAM gels contain only 300-ppm HPAM and from 10- to 30-ppm aluminum (as citrate).¹³⁷ In brines, the viscosity of a 300-ppm HPAM solution is very low (e.g., 3 cp at 41°C). Unfortunately, this low viscosity is usually not sufficient to provide a more efficient oil displacement during a polymer flood. However, if a low concentration of aluminum can substantially increase the effective viscosity (resistance factor) of the solution, the formulation could be effective as a mobility-control agent. Also, since the concentrations of polymer and aluminum are very low, one can afford to inject large pore-volume (PV) banks of gel formulation. Thus, polymer floods could be applied much more frequently.

Experimental

Mack and Smith stated that obtaining suitable gels requires the use of certain select polymers and aluminum-citrate chemicals.¹³⁷ Therefore, we obtained the HPAM (Tiorco HiVis 350®), aluminum citrate (Tiorco 677®), and preparation procedures directly from Tiorco. Fig. 16 shows viscosity vs. shear rate and HPAM concentration for solutions without aluminum citrate. We focused our examination on a formulation that contained 300-ppm HPAM, 15-ppm aluminum (as citrate) and 0.5% KCl. All experiments were performed at 41°C. Fig. 17 shows the viscosity of the gelant formulation (at 6 s⁻¹ and 41°C) as a function of time. The viscosity of the freshly prepared gelant was the same as that for the polymer solution without the aluminum (3.3 cp). Over the course of 30 days, the viscosity of the gelant gradually decreased to 2.1 cp (Fig. 17).

A coreflood was performed using a 707-md Berea sandstone core. This core had a length of 14.7 cm and a diameter of 3.56 cm. An internal pressure tap was located 2.3 cm from the inlet sandface. The core was initially saturated with a brine that contained 0.5% KCl.

Injection of Polymer Solution Without Aluminum. The first polymer formulation that was injected into the core contained 300-ppm HPAM (Tiorco HiVis 350®) and 0.5% KCl. This solution contained no aluminum. Fig. 18 shows resistance factors observed while injecting 13 PV of this polymer solution using a superficial velocity of 15.8 ft/d. In this figure, the first core segment refers to the first 2.3 cm of the core, while the second core segment refers to the remaining 12.4 cm of the core. Fig. 18 shows that the resistance factors in both core segments rose rapidly and stabilized at values between 63 and 70. Because the resistance factors were stable during polymer injection and because the resistance factors were about the same in both core segments, the polymer did not appear to cause any plugging of the inlet sandface or the interior part of the core.

The observed resistance factors were about 15 times the values expected based on the viscosity of the polymer solution. Upon first consideration, this polymer might appear to be a remarkable mobility-control agent even without the aluminum. However, previous experience reveals that this type of behavior is common for freshly prepared polyacrylamide solutions.^{128,141} The phenomenon is caused by high-molecular-weight polymer components.^{142,143} Unfortunately, these very high-molecular-weight components are extremely fragile. They are easily destroyed or removed by shear, chemical retention, heating or pH adjustments.¹⁴¹⁻¹⁴⁵ Therefore, we were concerned that the high resistance factors might be a temporary phenomenon that would not occur deep in a reservoir.

To test the permanence of the resistance factors reported in Fig. 18., the core was shut in for six days. Then, injection of polymer solution was continued at the rate of 15.8 ft/d. After injecting two PV of polymer solution, the resistance factors in the two core segments were about 30 (see Fig. 19). Thus, after six days, the resistance factors were substantially less even though the viscosity of the solution had not changed.

After injecting 2 PV of polymer solution at 15.8 ft/d, the injection rates were decreased in stages to determine the resistance factors as a function of superficial velocity. Resistance factors for the second core segment are shown by the solid curve in Fig. 20 (labeled "10/26/93"). The curve shows the apparent shear-thickening behavior that is characteristic of polyacrylamide solutions in porous media.¹⁴²

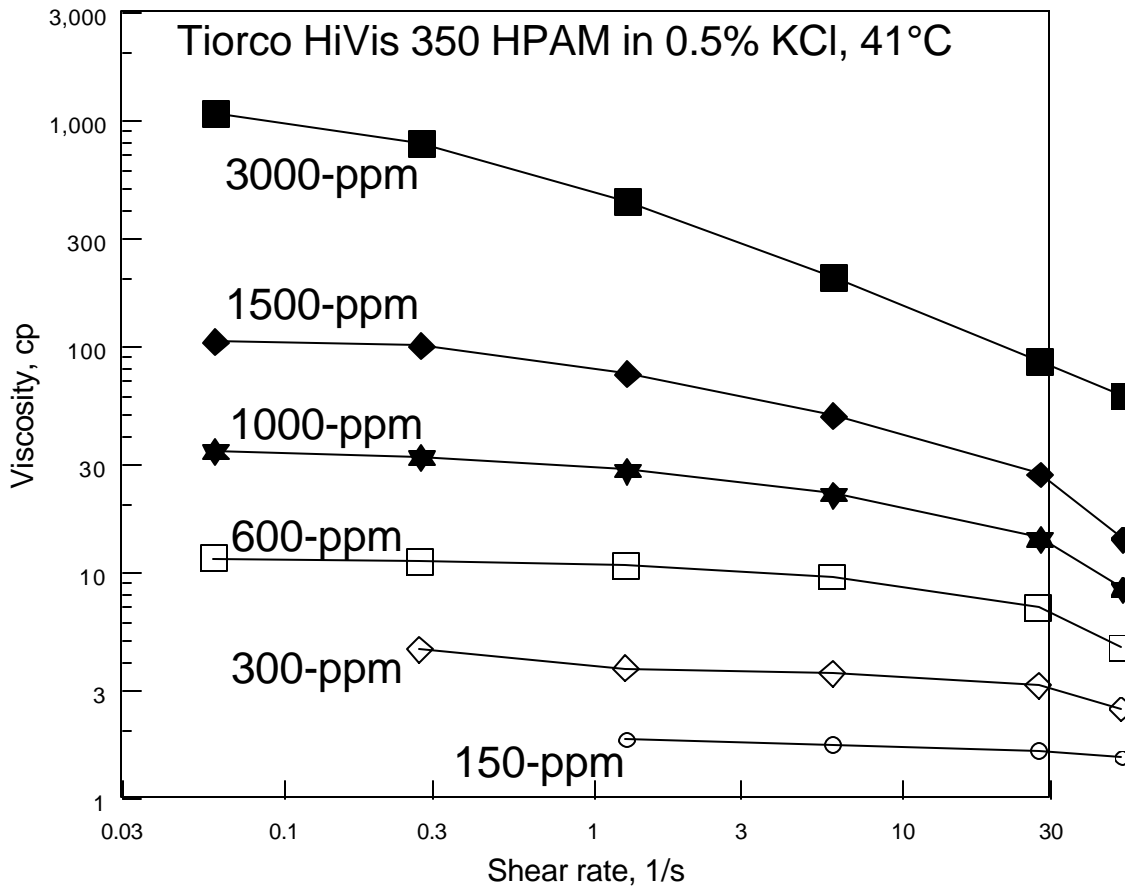


Fig. 16. Viscosity vs. shear rate and HPAM concentration.

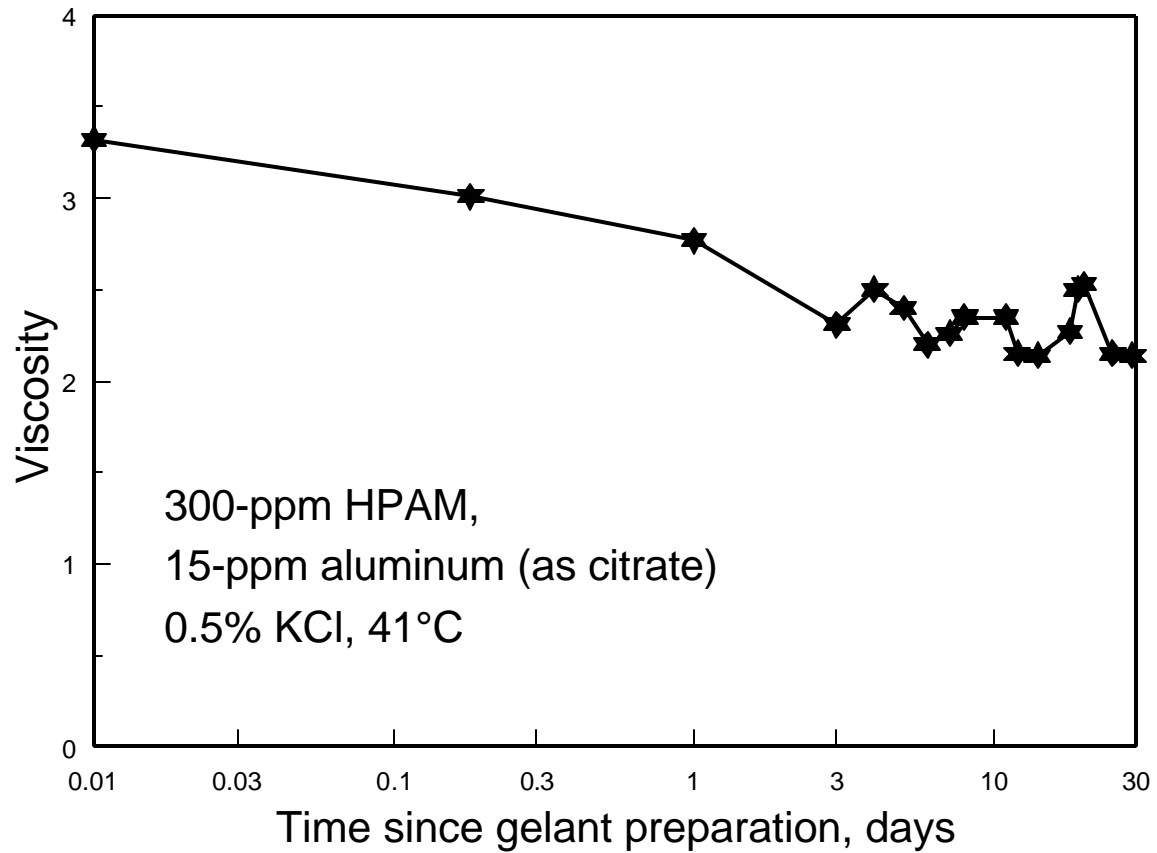


Fig. 17. Viscosity vs. time since gelant preparation.

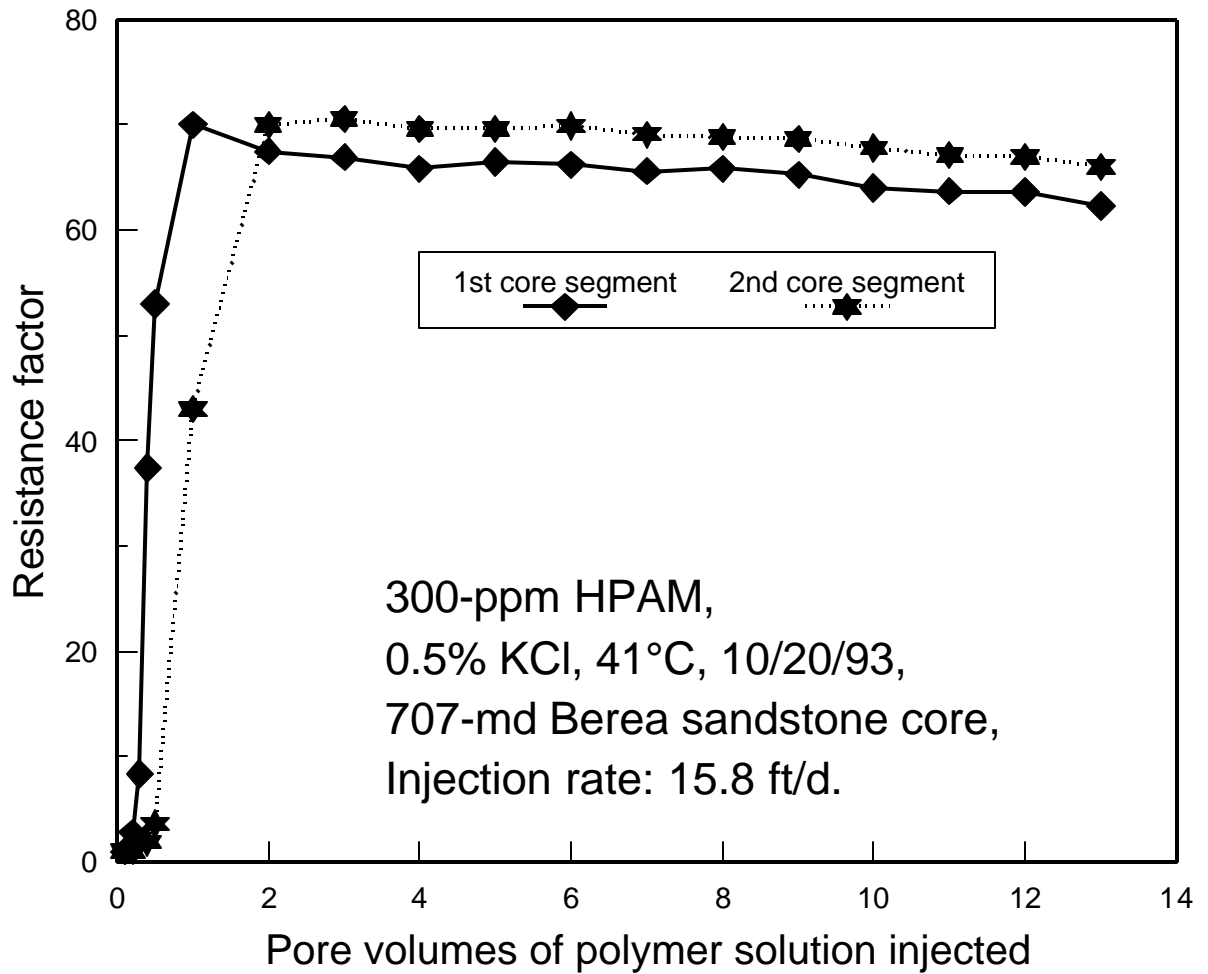


Fig. 18. Resistance factor vs. throughput for HPAM: first 13 PV.

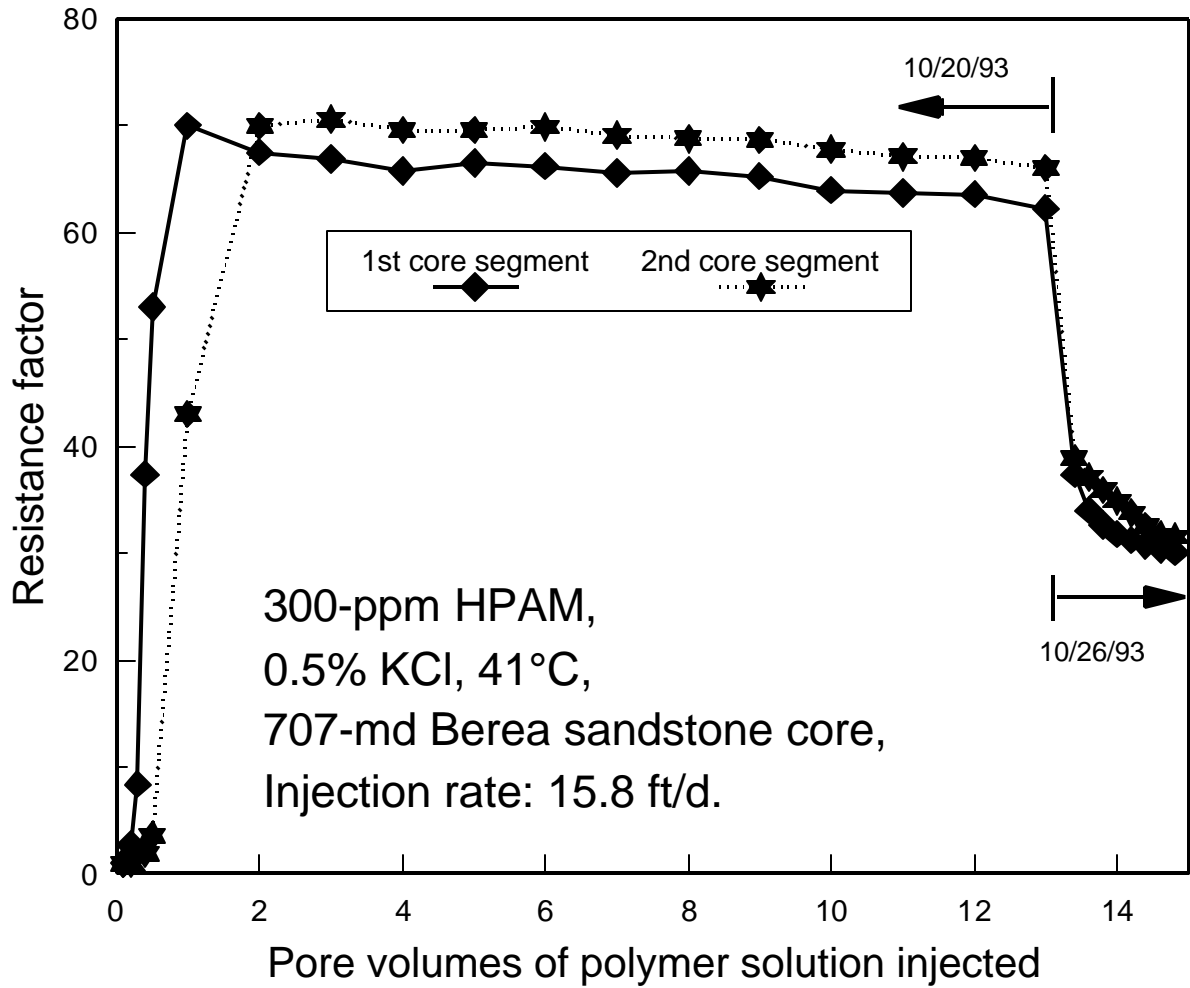


Fig. 19. Resistance factor vs. throughput for HPAM: first 15 PV.

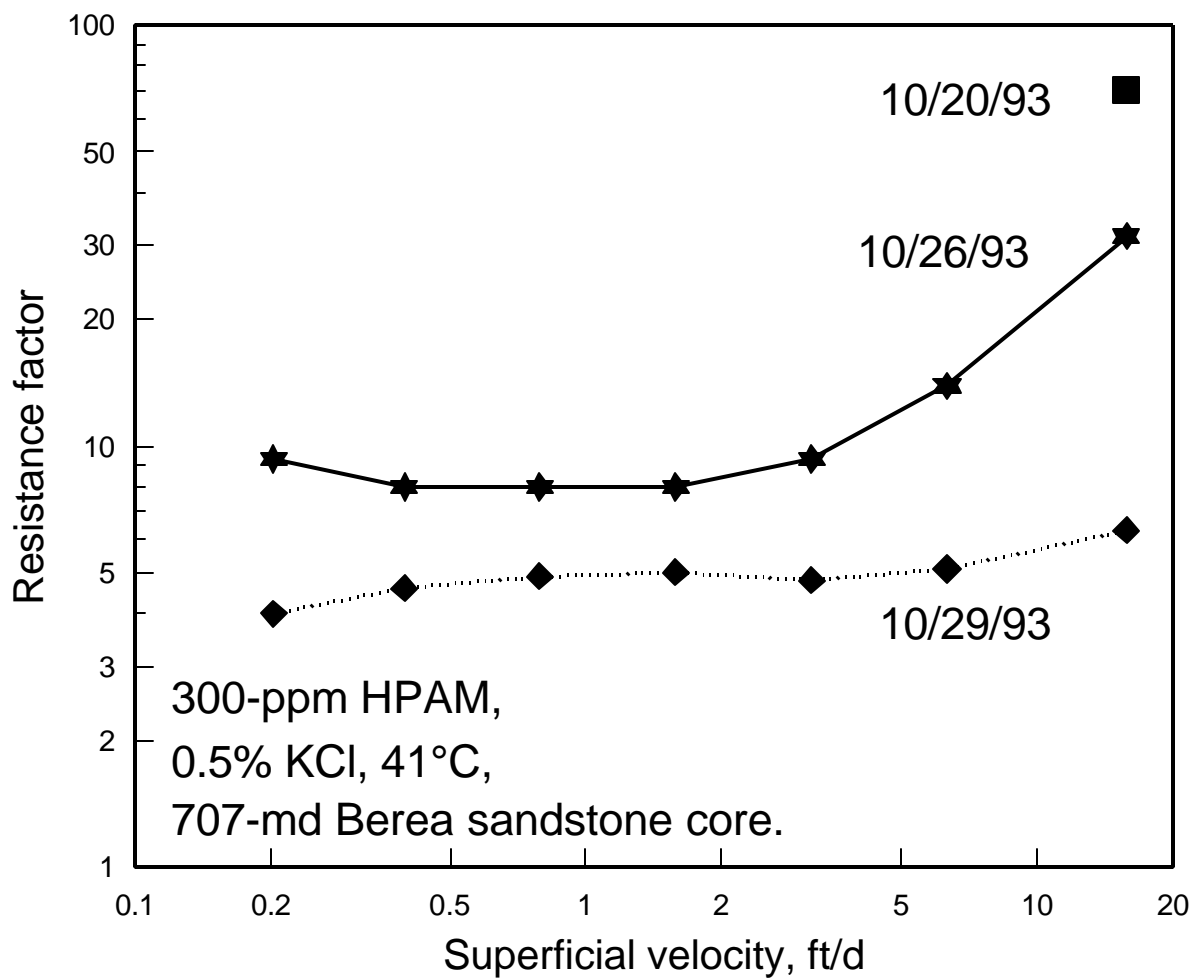


Fig. 20. Resistance factor vs. velocity for HPAM.

After determining resistance factors on October 26, 1993, the core was shut in for three days. Then, polymer injection was resumed, and resistance factors were again determined as a function of superficial velocity. These results are shown by the dashed curve in Fig. 20. At this time, the polymer solution showed near-Newtonian behavior, exhibiting a resistance factor of about 5. Therefore, nine days after preparation, the resistance factor of the polymer solution was similar to the value expected from the viscosity of the solution.

Injection of Polymer Solution With Aluminum. After the above experiments, a freshly prepared aluminum-citrate-HPAM gelant was injected into the core at a superficial velocity of 15.8 ft/d. This gelant had the same composition as the polymer solution except that 15-ppm aluminum (as citrate) was included. Fig. 21 shows resistance factors for the two core segments as a function of pore volumes of gelant injected.

During injection of the first seven PV of gelant, resistance factors in both core segments stabilized at a value of about 30. However, after seven PV (two hours after gelant preparation), the resistance factor in the first segment rose to high values, and the resistance factor in the second segment dropped to low values. This behavior is characteristic of plugging that occurs after gelation.^{26,139,140} After gel aggregates form and grow to the size of pore throats, continued gel injection results in stripping of the polymer and crosslinker from solution (especially at the inlet sandface). The only fluid that continues to propagate is the brine from which the crosslinked polymer has been stripped. This explains why resistance factors are very high in the first core segment and are very low in the second core segment.

After 10 PV of gelant/gel were injected as indicated in Fig. 21, the core was shut in over night. Then, gel injection was resumed. (This time was 24 hours after gelant preparation.) Surprisingly, the resistance factors in both segments approached a value of about 300 (Fig. 22). This behavior was unexpected; we anticipated seeing continued plugging/stripping behavior (i.e., a continuation of the trends shown in the last part of Fig. 21). Perhaps, relaxation of stress on the gel during the evening of November 8 allowed a temporary postponement of the plugging behavior.

After injecting seven PV of gel on November 9, 1993, the core was again shut in over night. When gel injection was resumed on November 10, continued plugging/stripping behavior was observed (Fig. 22). No further behavior like that seen on November 9 was observed with this core.

Fig. 23 shows residual resistance factors vs. PV of brine injected at the end of this experiment. These residual resistance factors, which apply to the second core segment, were very low. These low values were expected because of the polymer-stripping behavior mentioned earlier (i.e., very little "gel" resided in the second core segment).

Summary. Our results indicate that the aluminum-citrate-HPAM formulation basically behaves like other gels and gelants. Early in the gelation process, it propagates through sandstone like a polymer solution without crosslinker. After some point (presumably when gel aggregates grow to the size of pore throats), gel propagation is extremely slow or negligible. Although we observed an unusual behavior during the second day of gelant injection, we do not expect aluminum-citrate-HPAM formulations to propagate through porous rock like a "super polymer" after gel formation.

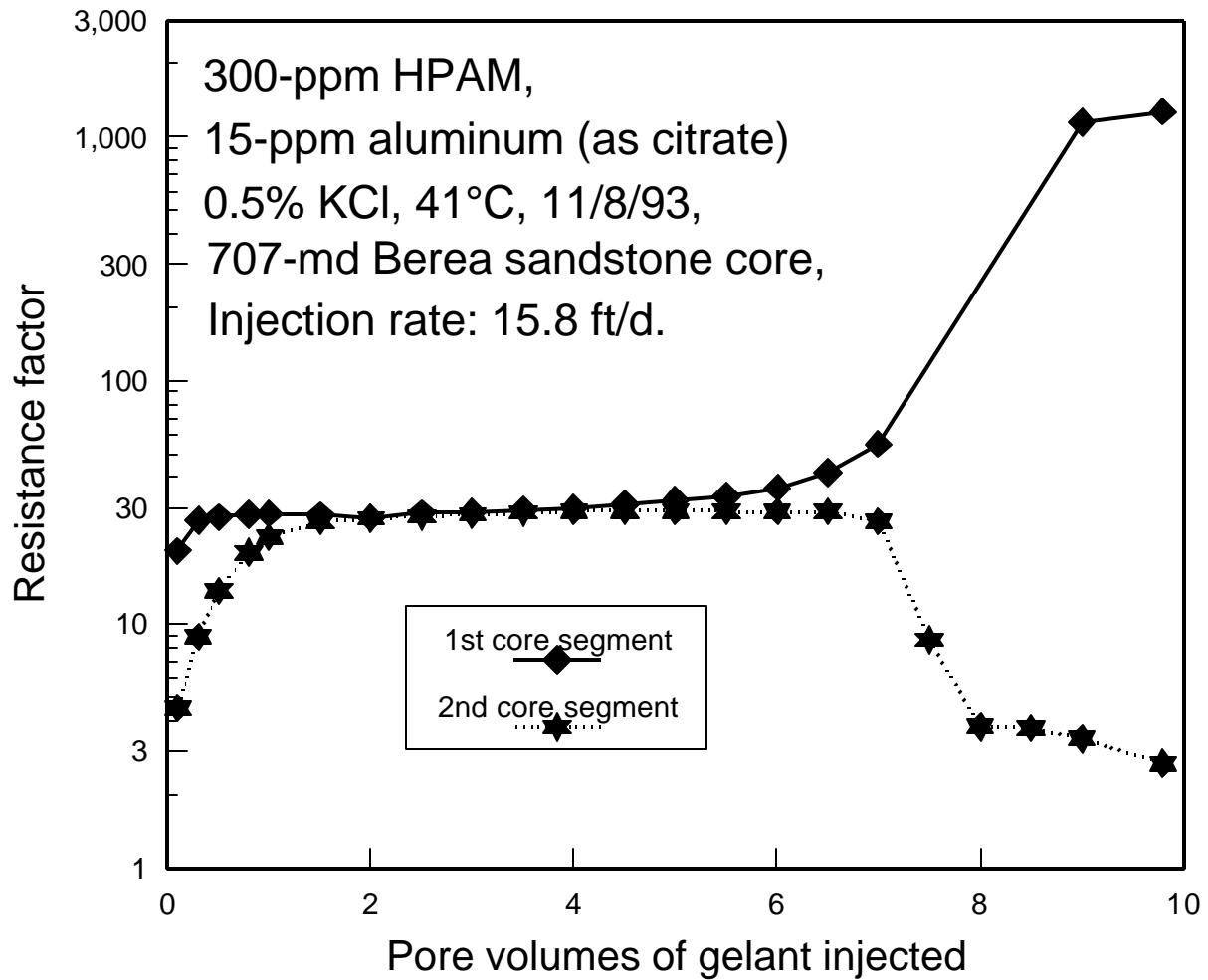


Fig. 21. Resistance factor vs. throughput for first 10 PV of Al-citrate-HPAM injection.

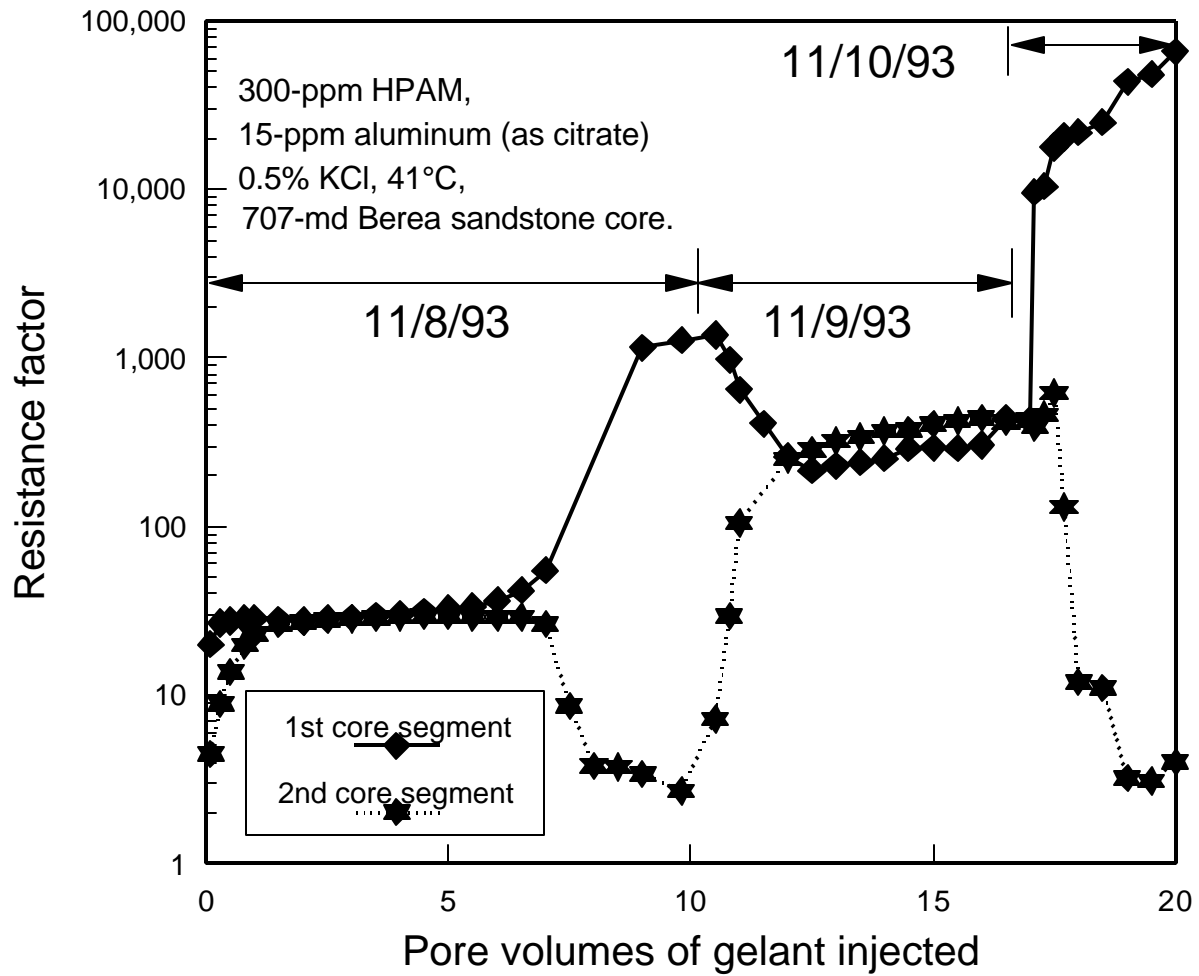


Fig. 22. Resistance factor vs. throughput for first 20 PV of Al-citrate-HPAM injection.

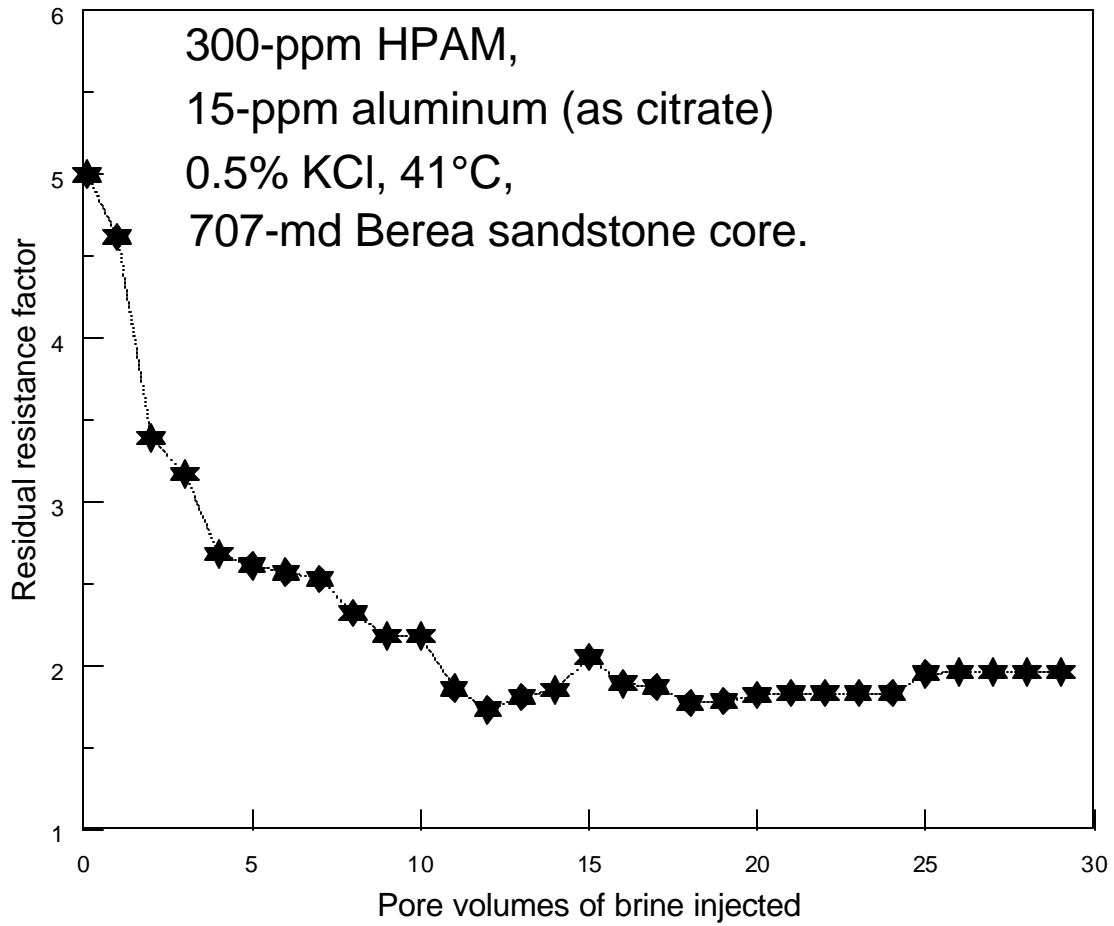


Fig. 23. Residual resistance factor vs. throughput for Al-citrate-HPAM gel.

Consideration of Literature Reports

Our experimental results indicate that aluminum-citrate-HPAM gels (as opposed to gelants) will not propagate through porous sandstone at a practical rate. Certainly, this finding contradicts some of the concepts expressed in Refs. 137 and 138. Therefore, a close examination of the data presented in Refs. 137 and 138 and other literature is appropriate.

Tiorco Laboratory Data. Fielding *et al.*¹³⁸ stated, "CDG gels flow at high-pressure differentials and resist flow at low-pressure differentials." This statement was based on flow of the gels through a screen pack.¹³⁷ No evidence was presented to show that the same behavior would occur in porous rock. In contrast, 48 hours after gelant preparation, we found that the gel showed no significant propagation through 700-md Berea sandstone even with pressure gradients over 1,000 psi/ft.

Using aluminum-citrate-HPAM gels, Mack and Smith reported resistance factors ranging from 200 to 20,000 in a 15-darcy sandpack.¹³⁷ Higher resistance factors can be expected in less-permeable porous media.³¹ Gels with these extremely high resistance factors cannot be expected to propagate through reservoir rock at a practical rate during a polymer flood.

To demonstrate the diversion properties of their gels, Mack and Smith used results from floods of parallel sandpicks.¹³⁷ Permeabilities of the two packs were 19 and 1.7 darcys, respectively. During brine injection after gel placement, Mack and Smith reported that 100% of the flow entered the less-permeable sandpack; no flow occurred in the high-permeability pack.¹³⁷ Previous work has shown that this type of result is an experimental artifact associated with using parallel linear corefloods.³¹ Because their performance and interpretation are fraught with pitfalls, parallel linear corefloods should not be used to evaluate the diversion properties of a blocking agent.³¹

Other Literature Data. Fletcher *et al.*¹³² investigated the propagation of an aluminum-citrate-HPAM gelant through a 190-ft slim tube that contained 5-darcy sand. The temperature was 25°C in the first 150-ft section of the sandpack, while the temperature was 70°C in the last 40 ft of the pack. Fletcher *et al.* demonstrated that the gelant propagated readily through the first 160 ft of the pack, exhibiting a very low resistance factor. Between 160 ft and 170 ft from the pack inlet, the resistance factor rose to high values, indicating thermally induced gelation. Resistance factors were very low in the final 20 ft of the pack, indicating that the gel did not propagate once gelation occurred. This behavior for the aluminum-citrate-HPAM gel is consistent with that of other gels (i.e., once formed, the gel does not propagate through the porous medium) and is inconsistent with the claims made in Refs. 137 and 138.

Walsh *et al.*¹⁴⁶ and Rocha *et al.*¹⁴⁷ demonstrated that propagation of aluminum-citrate through porous media can be very slow depending on pH, aluminum-to-citrate ratio, and other factors.

Tiorco Field Data. Fielding *et al.*¹³⁸ described the injection of aluminum-citrate-HPAM gels in the North Rainbow Ranch Unit in Northeast Wyoming. The formation (Minnelusa Upper "A" sand) contained 5.7 million bbl OOIP, and the average formation thickness was 8.6 ft. Average reservoir permeability was 155 md (from core analysis), the estimated residual oil saturation was 30%, and the estimated average reservoir pressure was 3732 psi (R.C. Fielding, private communication, June 27, 1994). Oil viscosity was 3.94 cp at the reservoir temperature of 94.4°C (202°F). The reservoir had two active injection wells and three active production wells.¹³⁸ The Dykstra-Parsons coefficient of permeability variation was stated to be 0.74.¹³⁷

Gel was injected into only one well that was located near the edge of the field (Carter Well #1-24A). The following aqueous fluids were injected:

1. 81,000 bbl with 775-ppm cationic polyacrylamide,
2. 46,000 bbl with 1,400-ppm HPAM (anionic polyacrylamide),
3. 198,000 bbl with 1,200-ppm HPAM and 1,000-ppm Al-citrate (?75-ppm as Al³⁺),
4. 654,000 bbl with 300-ppm HPAM and 330-ppm Al-citrate (?25-ppm as Al³⁺).

The total volume of aluminum-citrate-HPAM gel amounted to slightly more than 10% PV, and this gel was injected over a 2.5-year period.¹³⁸ This volume included 174,250 lbs of HPAM and 182,000 lbs of aluminum citrate. This mass of chemical could not have been removed by filtration at the sandface of an unfractured injection well without noticing severe plugging in the well. Therefore, either the well was fractured or the gel flowed through the porous rock.

Fielding *et al.*¹³⁸ indicated that the well was not fractured, but they presented no evidence to support this position. In apparent contradiction, injection rates of 1,500 BPD and 2,890 BPD (with the well on vacuum) were reported for Carter Well #1-24A in July 1987 and March 1993, respectively.¹³⁸ Since the formation thickness was about 14 ft in the injection well,¹³⁸ as much as 206 BPD were injected per ft of pay with the well on vacuum. Based on experience with other unfractured wells in formations with permeabilities averaging 100-md, injection rates per ft of pay are commonly 10 times less than the values for the Carter Well #1-24A.

The Darcy equation for radial flow (Eq. 36) can be used to assess the fracture status of the well.¹⁴⁸

$$\frac{q}{?p} = \frac{? kh}{141.2 ? \ln(r_e/r_w)} \quad (36)$$

If the injectivity calculated by the right side of Eq. 36 was substantially less than the actual $q/?p$, then a fracture or formation part was probably present. Formation thickness, h , for this well was about 14 ft, the injection rate in July 1987 was 1,500 BPD, the estimated reservoir pressure was 3,732 psi, water viscosity at 94°C is about 0.3 cp, and the term, $\ln(r_e/r_w)$, is about 7. In this case, two parameters in Eq. 36 must be estimated. First, the effective permeability was less than the absolute permeability of 155 md. Here, we assumed that the endpoint permeability to water was 31 md—one-fifth the absolute permeability. Second, since the well was on vacuum during water injection, the wellbore pressure was unknown. To be conservative, we assumed that the wellbore was full of water, so the downhole pressure was 4,113 psi (9,500 ft x 0.433 psi/ft). Using these numbers, the actual injectivity, $q/?p$, was 4 BPD/psi, while the injectivity calculated by the right side of Eq. 36 was 1.4 BPD/psi. Thus, the actual injectivity was about 3 times greater than the injectivity expected from the Darcy equation. This number is conservative. If the gelant was more viscous than water, if the fluid level in the well was not very close to the surface, or if the end-point water relative permeability was less than 0.2, the discrepancy between the real and calculated injectivities would be greater. Therefore, Carter Well #1-24A was probably fractured.

Given the formation temperature (94.4°C) and the injection rate, we suspect that the gel had formed before leaving the wellbore of Carter Well #1-24A. In our experiments, plugging in 700-md sandstone (at 41°C) was noted 2 hours after gelant preparation. Since reaction rates proceed more rapidly at higher temperatures and since the gels used at the North Rainbow Ranch Unit contained at least as much HPAM and aluminum citrate as we used in our experiments, gel formation should have occurred before 2 hours. Assuming a 4-inch diameter casing and 9,500-ft formation depth, an approximate wellbore volume was 830 ft³. Given an injection rate of 1500 BPD, the residence time in the wellbore was more than 2 hours. Therefore, the gel had time to form before reaching the formation. If the well was not fractured, severe

plugging of the formation would be expected.

Using field results, Mack and Smith¹³⁷ stated that a steady increase of pressure with increased injection volume (in a Hall plot) demonstrated deep propagation of the gels into a formation. However, the observed pressure response could also be obtained by the dilute gel being removed by filtration as the injection water leaks off from fracture faces into the formation. To rationalize in-depth penetration of the gel, Mack and Smith¹³⁷ also reported results from "pressure fall-off" tests. However, no analysis was presented to distinguish whether the gel actually penetrated into the porous rock or simply filtered out on the sandface.

Since over 800,000 bbl of gelant or polymer formulation was injected, this volume seems much too large to be accommodated by a single fracture. This large volume would probably require the presence of natural fractures in the formation if no polymer was produced. However, the fracture volume need not total 800,000 bbl. Because gel can be dehydrated (by squeezing water into the rock while leaving the polymer and crosslinker at the fracture face), a fracture system with a volume of 10,000 bbl or less could account for the result. However, even this volume would probably require the presence of a natural fracture system.

If no fractures (natural or induced) exist in the field, another explanation for the results could be that gelation simply never occurred. Several researchers have argued that the aluminum crosslinker may not propagate very far into a reservoir.^{146,147} Therefore, the benefits from the 800,000 bbl of polymer solution may simply be the normal benefits expected from a polymer flood that used ~300-ppm HPAM solution. Perhaps, the aluminum had no effect on the displacement.

Conclusions

Our experimental results indicate that an aluminum-citrate-HPAM formulation basically behaves like other gels and gelants. Early in the gelation process, it propagates through sandstone like a polymer solution without crosslinker. After some point (presumably when gel aggregates grow to the size of pore throats), gel propagation is extremely slow or negligible. Although we observed an unusual behavior during the second day of gelant injection, we do not expect aluminum-citrate-HPAM formulations to propagate through porous rock like a "super polymer" after gel formation.

An objective analysis of the literature supports these findings. Claims to the contrary were based largely on field results that assumed the wells were not fractured. The field and laboratory results can be explained if the reservoir is assumed to be naturally fractured. Alternatively, the results could be explained by assuming that gelation never occurred because the aluminum crosslinker did not propagate through the formation.

6. FLOW OF ONE-DAY-OLD GELS THROUGH FRACTURES

This chapter documents results of experiments in which preformed gels were forced through fractured cores. Using several different types of gels, the objectives of these experiments were to (1) determine whether excessive pressure gradients would develop during gel injection, (2) assess how effectively the gels "heal" fractures, and (3) determine whether the gels wash out easily during brine injection after gel placement.

Core Properties

These experiments were conducted using fractured Berea sandstone cores. All experiments were performed at 41°C. The nominal permeability for the cores was 650 md before fracturing. Core porosities were typically 0.21. The cylindrical cores were 14-cm long with a cross-sectional area of 10 cm². These cores were fractured lengthwise using a core splitter (Park Industries Hydrasplit®). The two halves of the core were repositioned as shown in Fig. 24 and cast in epoxy. Two internal pressure taps were drilled 2 cm from the inlet sandface. One tap was located 90° from the fracture to measure pressure in the rock matrix, while the other tap was drilled to measure pressure in the fracture. During our corefloods, the fracture was always oriented vertically.

After casting the core in epoxy and saturating with brine, the permeability to brine was determined. The third column in Table 6 lists brine permeabilities, k_{av} , for several fractured cores. These permeabilities average the effects of flow through the fracture and the porous rock. The fourth column in Table 6 lists calculated fracture conductivities, k_{fw} . The flow capacity of the fracture relative to that of the porous rock is given by the ratio, $k_{fw}h_f/Ak_m$ (fifth column in Table 6). The fracture flow capacities ranged from 13 to 108 times greater than the flow capacities of the porous rock.

Table 6. Core and Fracture Permeabilities

Core	Nominal k_m , darcys	k_{av} , darcys	k_{fw} , darcy-cm	Relative flow capacity, $k_{fw}h_f/Ak_m$
7	0.65	19.9	53.8	29.6
9	0.65	70.6	196	108
10	0.65	13.6	36.2	13.0
12	0.65	24.1	65.5	36.1
13	0.65	18.3	49.2	27.1
14	0.65	28.8	78.5	43.2

We routinely performed water-tracer studies before and after gel placement during our experiments. These tracer studies were used to characterize pore volumes and dispersivities of the cores. These studies involved injecting a brine bank that contained potassium iodide as a tracer. The tracer concentration in the effluent was monitored at a wavelength of 230 nm. In Fig. 25, the curve with the solid circles illustrates the results from a tracer study for an unfractured Berea core that was saturated with brine. Dispersivities of unfractured Berea sandstone cores were typically 0.1 cm, and the effluent tracer concentration reached 50% of the injected concentration after injecting 1 PV of tracer solution.

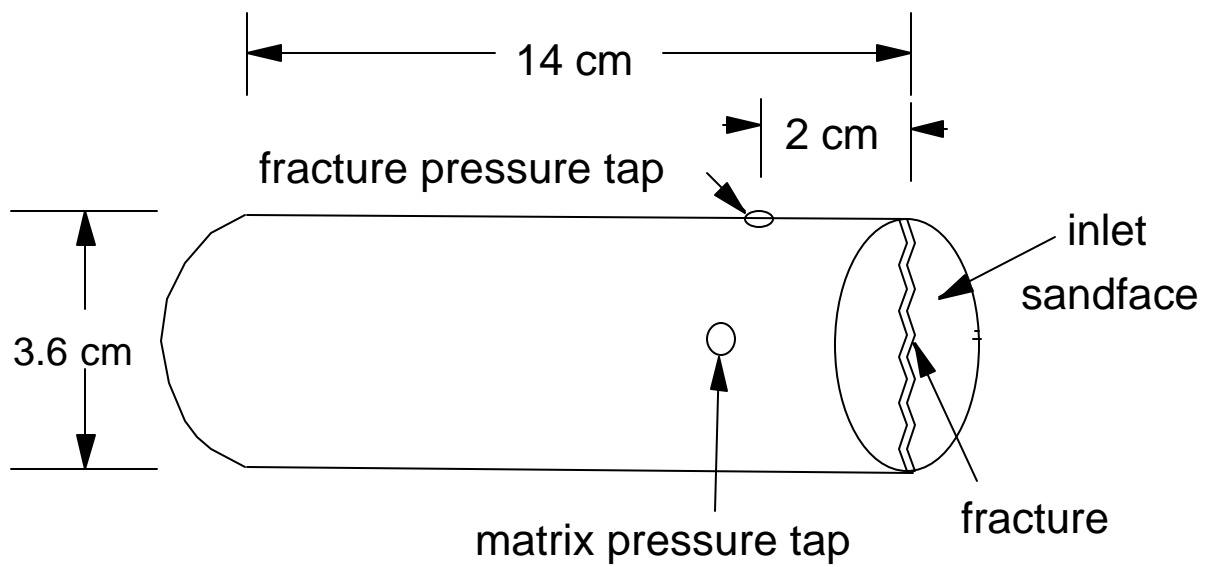


Fig. 24. Schematic of a fractured core.

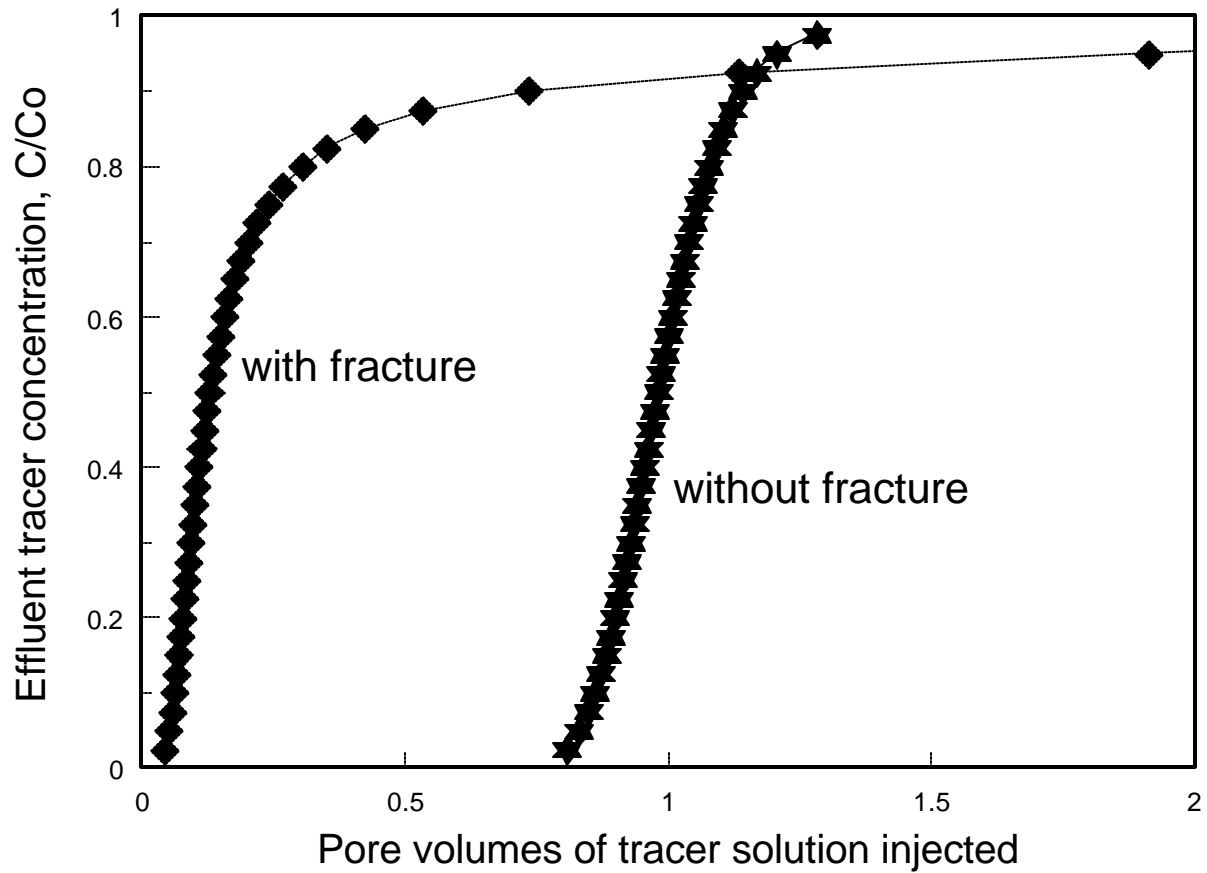


Fig. 25. Tracer results in fractured vs. unfractured Berea sandstone cores.

The solid triangles in Fig. 25 show the tracer results from a fractured Berea core. For this fractured core, the first tracer was detected in the effluent after injecting 0.04 PV of tracer solution. In contrast, for the unfractured core, the first tracer was detected after injecting 0.8 PV.

Gels Examined

Table 7 lists compositions for the gels used in this study. In all cases, one day elapsed between gelant preparation and gel injection into the cores. For all but two compositions listed in Table 7, the gelation times were less than 10 hours at 41°C. The two exceptions, Cr(III)-acetate-PAM/AMPS and Al-citrate-HPAM, did not show signs of gelation during visual observation of the fluids over the course of several weeks.

Table 7. Gel Compositions

Gel abbreviation	Composition	pH
Cr(III)-acetate-HPAM	0.5% HPAM (Allied Colloids Alcoflood 935®), 0.0417% chromium acetate, 1% NaCl	6
resorcinol-formaldehyde	3% resorcinol, 3% formaldehyde, 0.5% KCl, 0.42% NaHCO ₃	9
Cr(III)-xanthan	0.4% xanthan (Pfizer Flocon 4800®), 0.047% CrCl ₃ , 0.5% KCl	4
Cr(III)-acetate-PAM/AMPS	0.3% PAM/AMPS (Drilling Specialties HE-100®), 0.044% chromium acetate, 2% KCl	5
Al-citrate-HPAM	0.03% HPAM (Tiorco HiVis 350®), 0.0015% aluminum (as citrate, Tiorco 677®), 0.5% KCl	8
Cr(VI)-redox-PAM/AMPS	0.3% PAM/AMPS (Drilling Specialties HE-100®), 0.05% Na ₂ Cr ₂ O ₇ , 0.15% Na ₂ S ₂ O ₄ , 2% KCl	5

Coreflood Sequence

For each of the gel compositions listed in Table 7, we used a new fractured Berea sandstone core. After casting in epoxy, the fractured cores were saturated with brine, and porosities and permeabilities were determined. Next, tracer studies were performed. Then, typically, 10 to 17 PV of gel were injected into a fractured core at a rate of 200 ml/hr. (Note that the fracture volume was less than 0.05 PV.) After gel injection, the cores were shut in for several days, followed by brine injection. Finally, another tracer study was performed. Figs. 26 through 41 show detailed results from these studies for the various gels, while Table 8 summarizes the results.

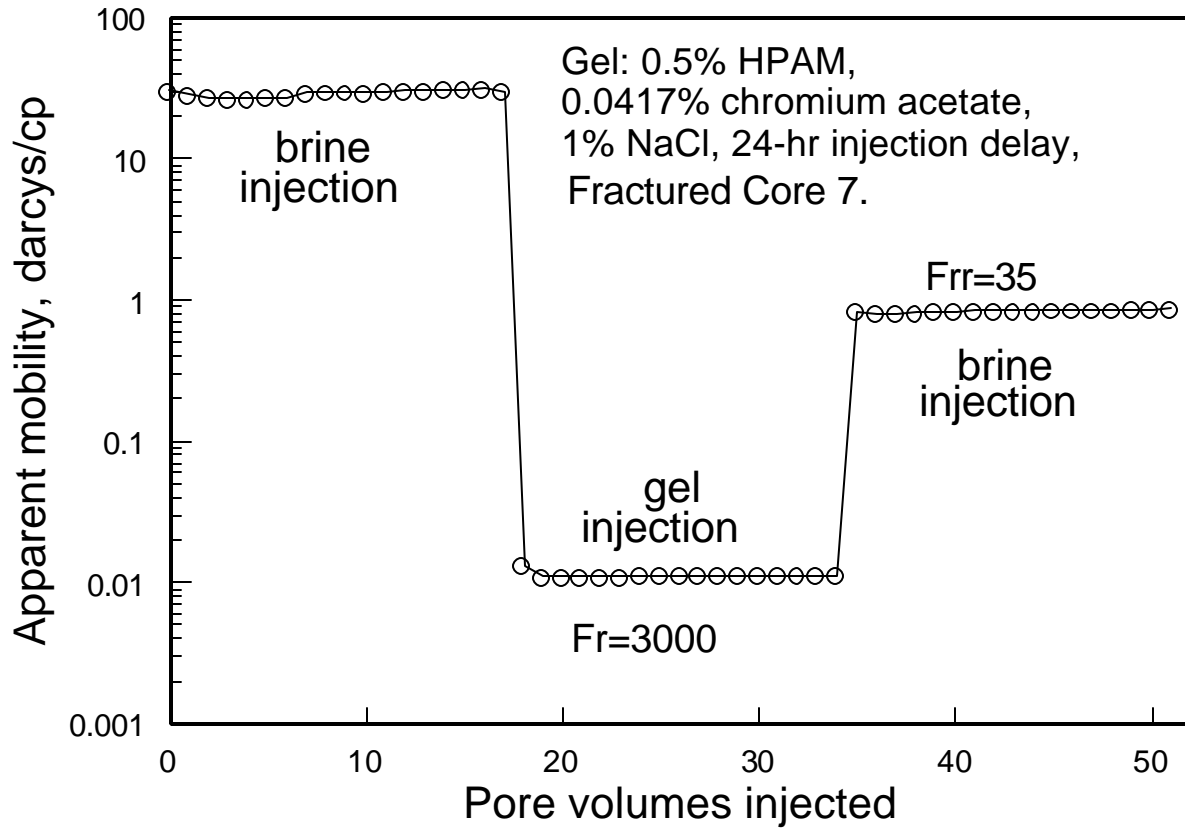


Fig. 26. Apparent mobility before, during, and after placement of a Cr(III)-acetate-HPAM gel.

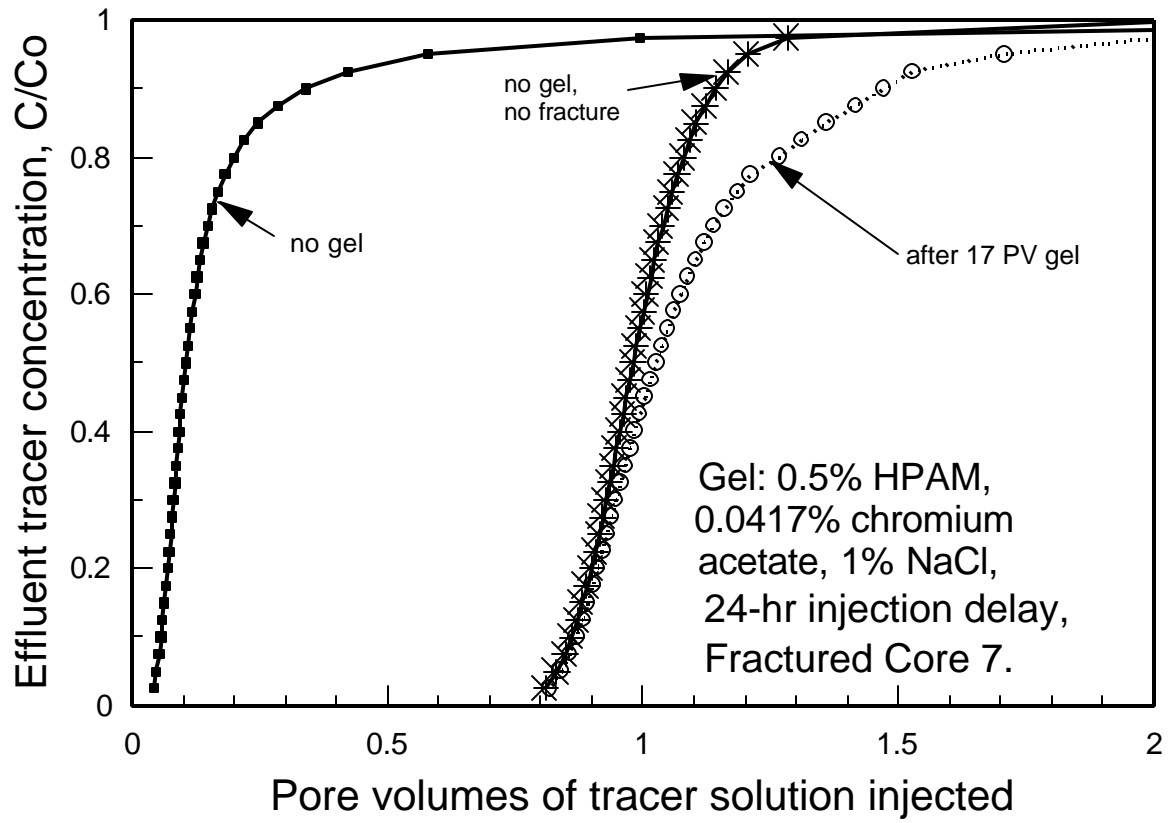


Fig. 27. Tracer results before vs. after placement of a Cr(III)-acetate-HPAM gel.

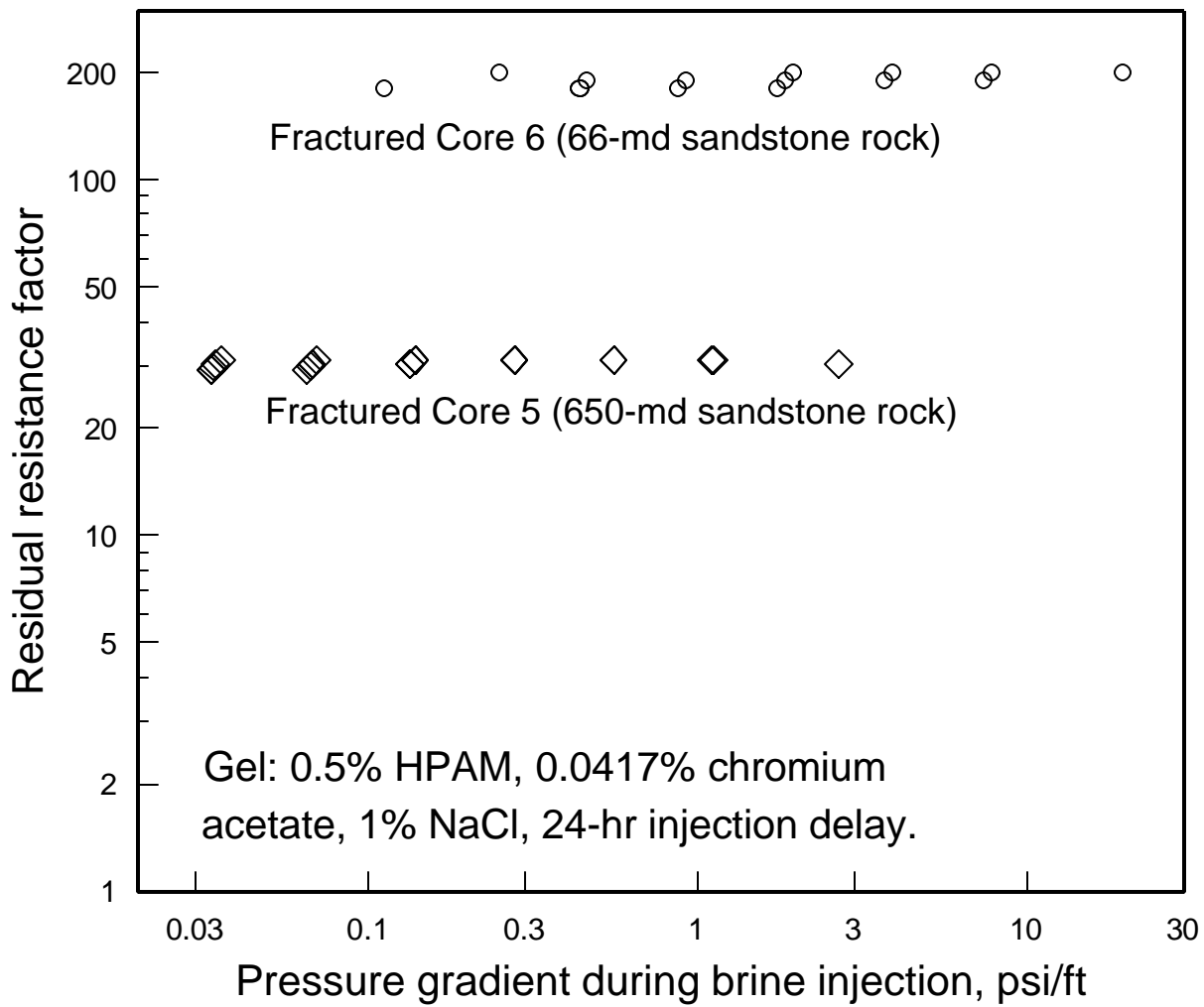


Fig. 28. Permeability reduction vs. pressure gradient after placement of a Cr(III)-acetate-HPAM gel.

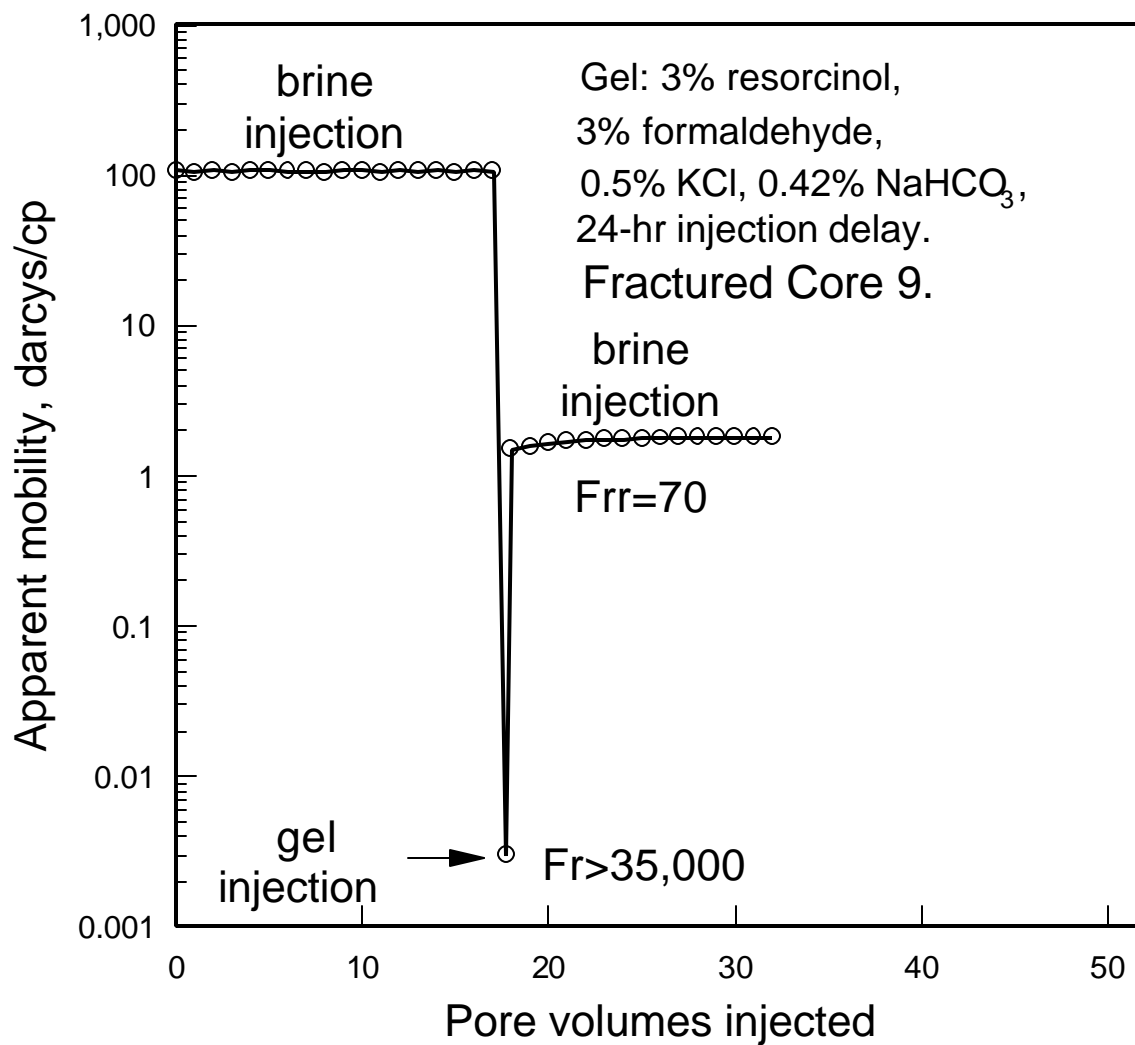


Fig. 29. Apparent mobility before, during, and after placement of a resorcinol-formaldehyde gel.

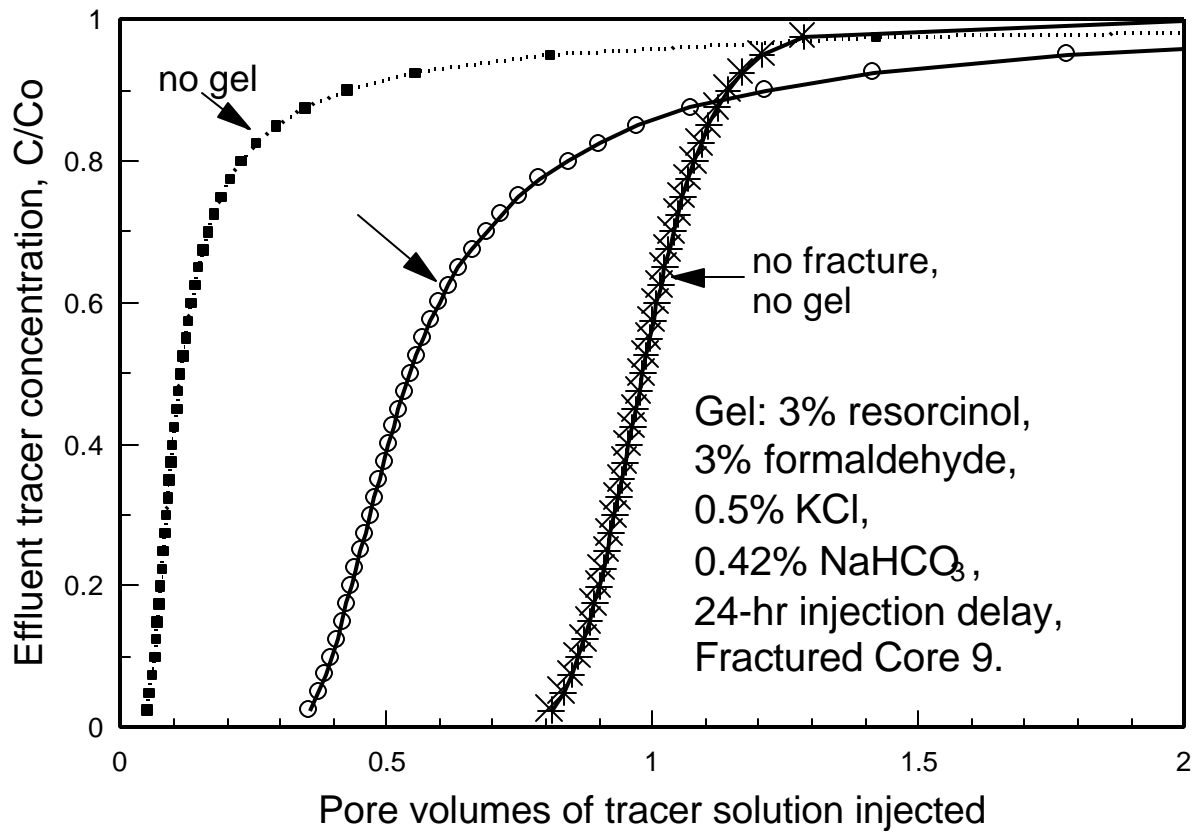


Fig. 30. Tracer results before vs. after placement of a resorcinol-formaldehyde gel.

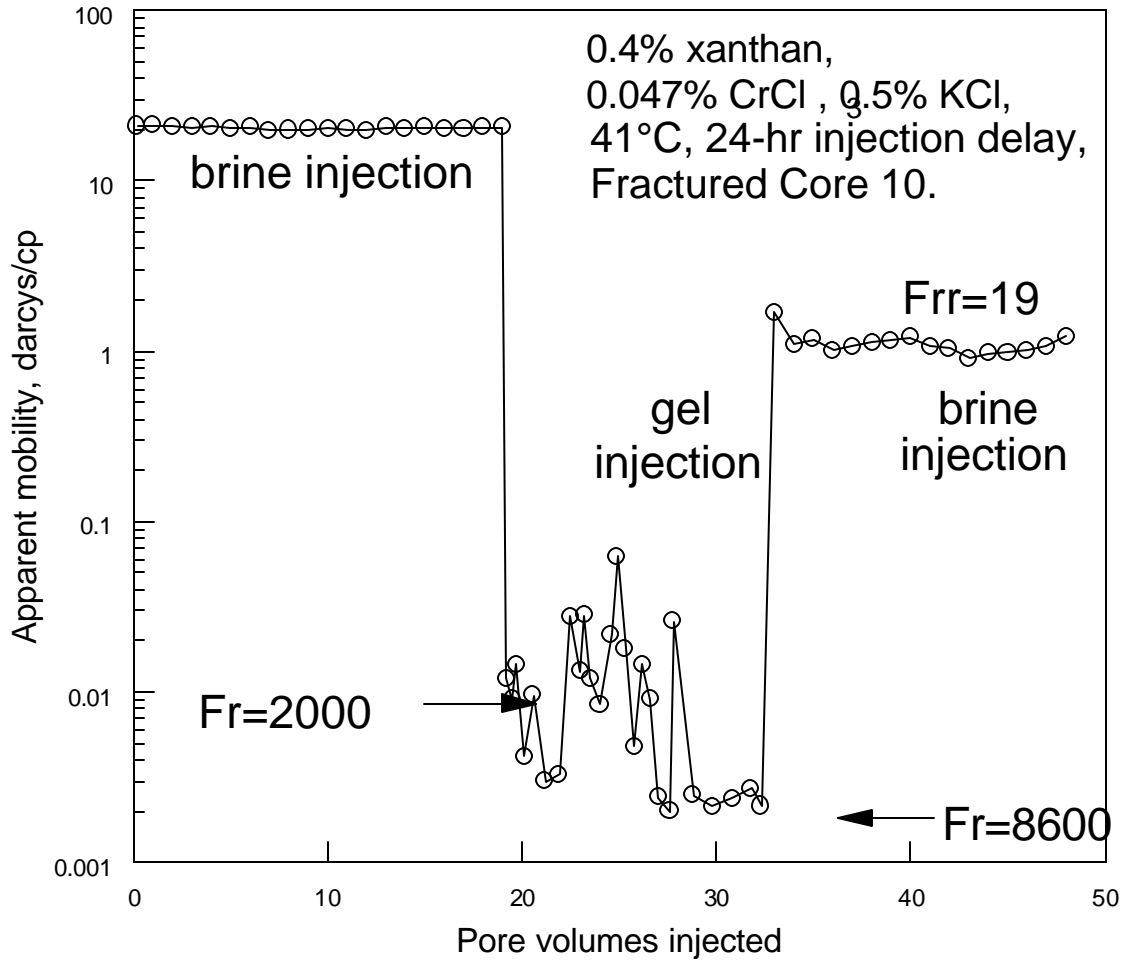


Fig. 31. Apparent mobility before, during, and after placement of a Cr(III)-xanthan gel.

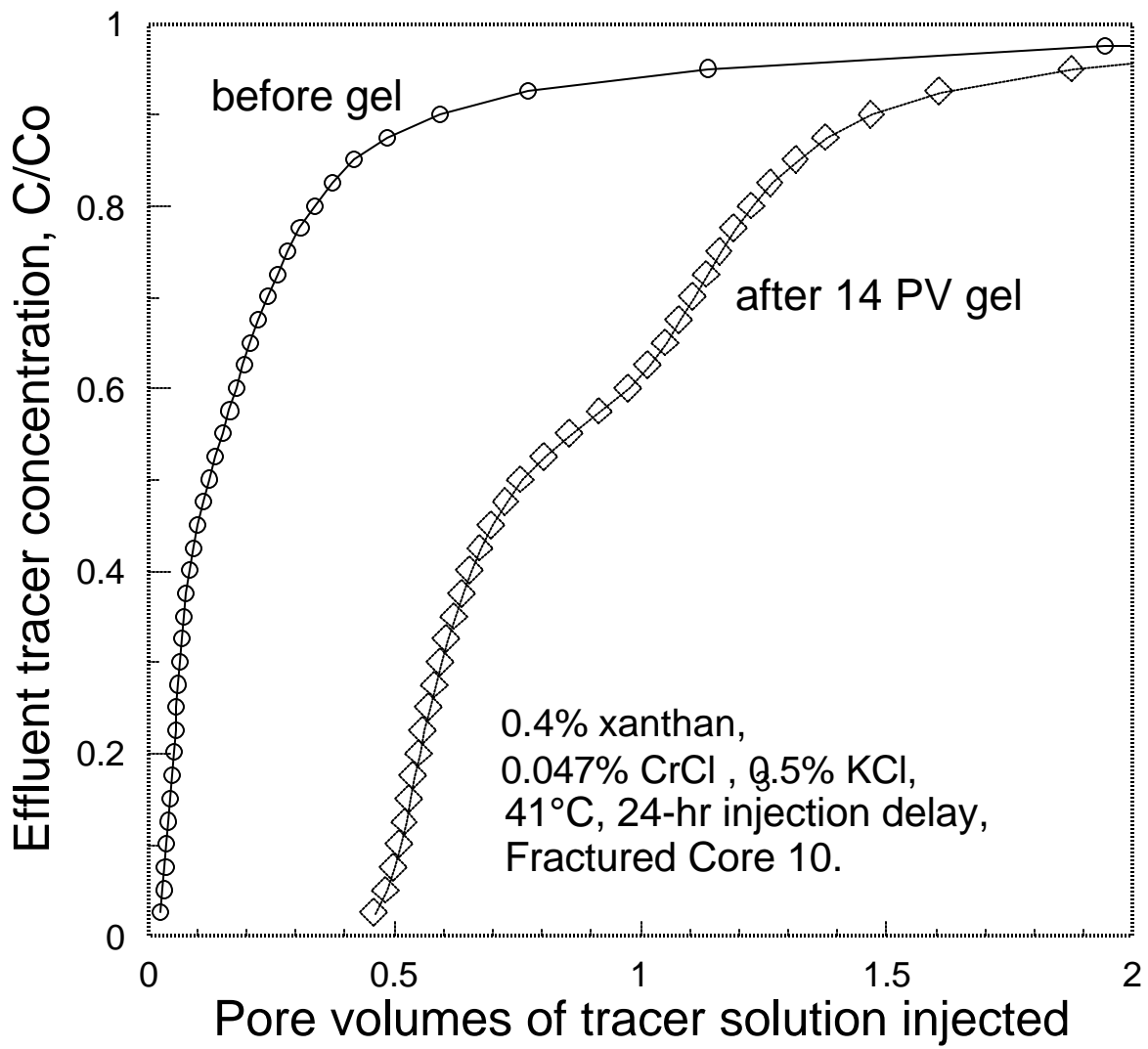


Fig. 32. Tracer results before vs. after placement of a Cr(III)-xanthan gel.

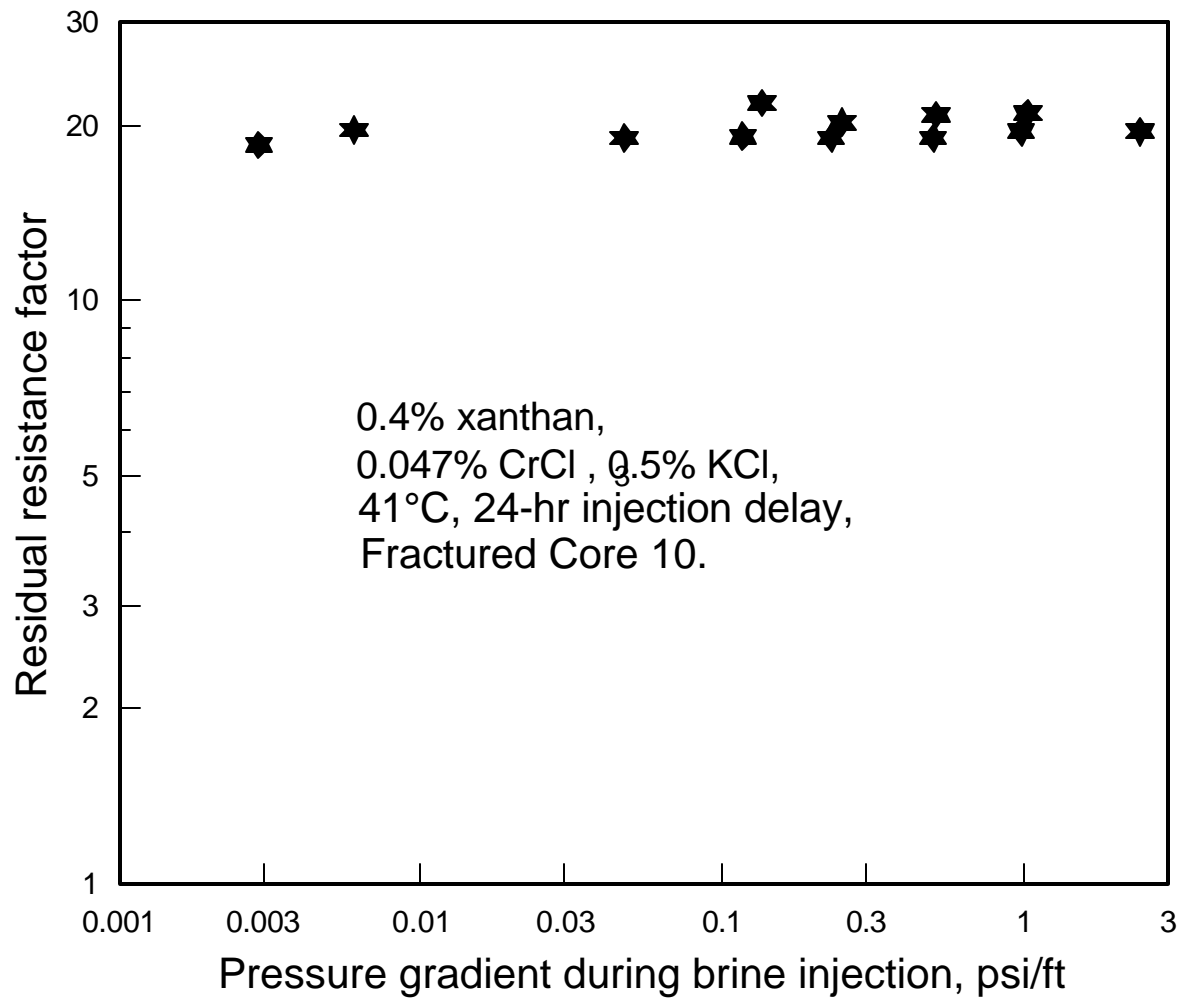


Fig. 33. Permeability reduction vs. pressure gradient after placement of a Cr(III)-xanthan gel.

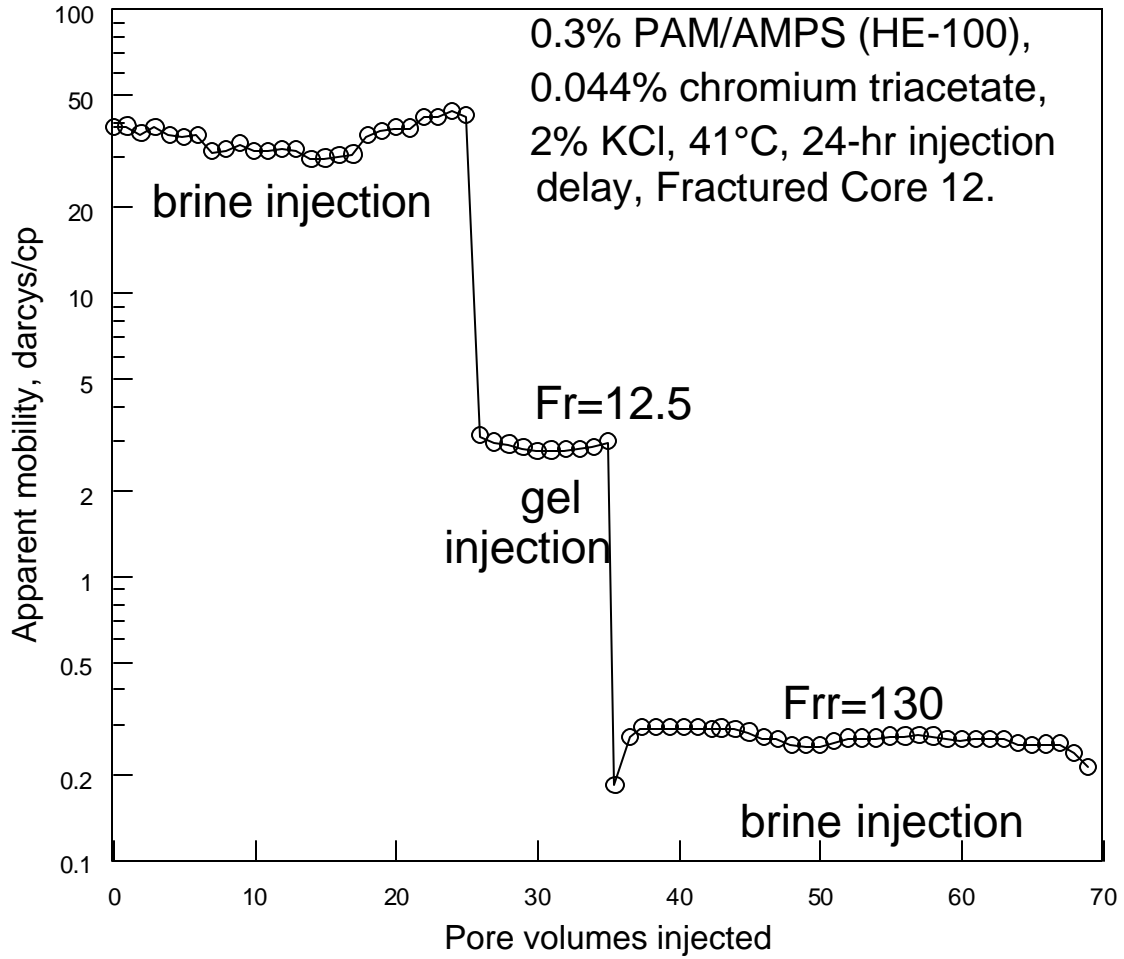


Fig. 34. Apparent mobility before, during, and after placement of a Cr(III)-acetate-PAM/AMPS gel.

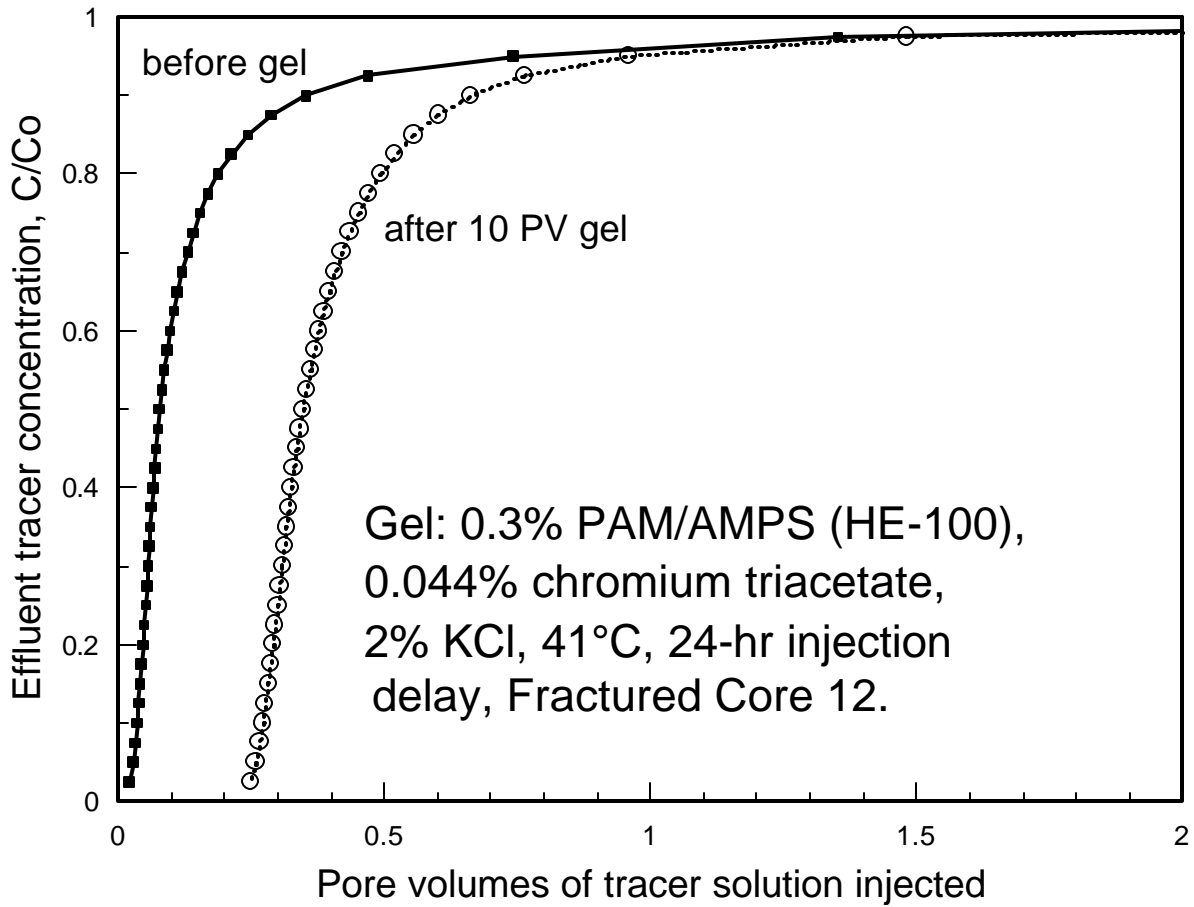


Fig. 35. Tracer results before vs. after placement of a Cr(III)-acetate-PAM/AMPS gel.

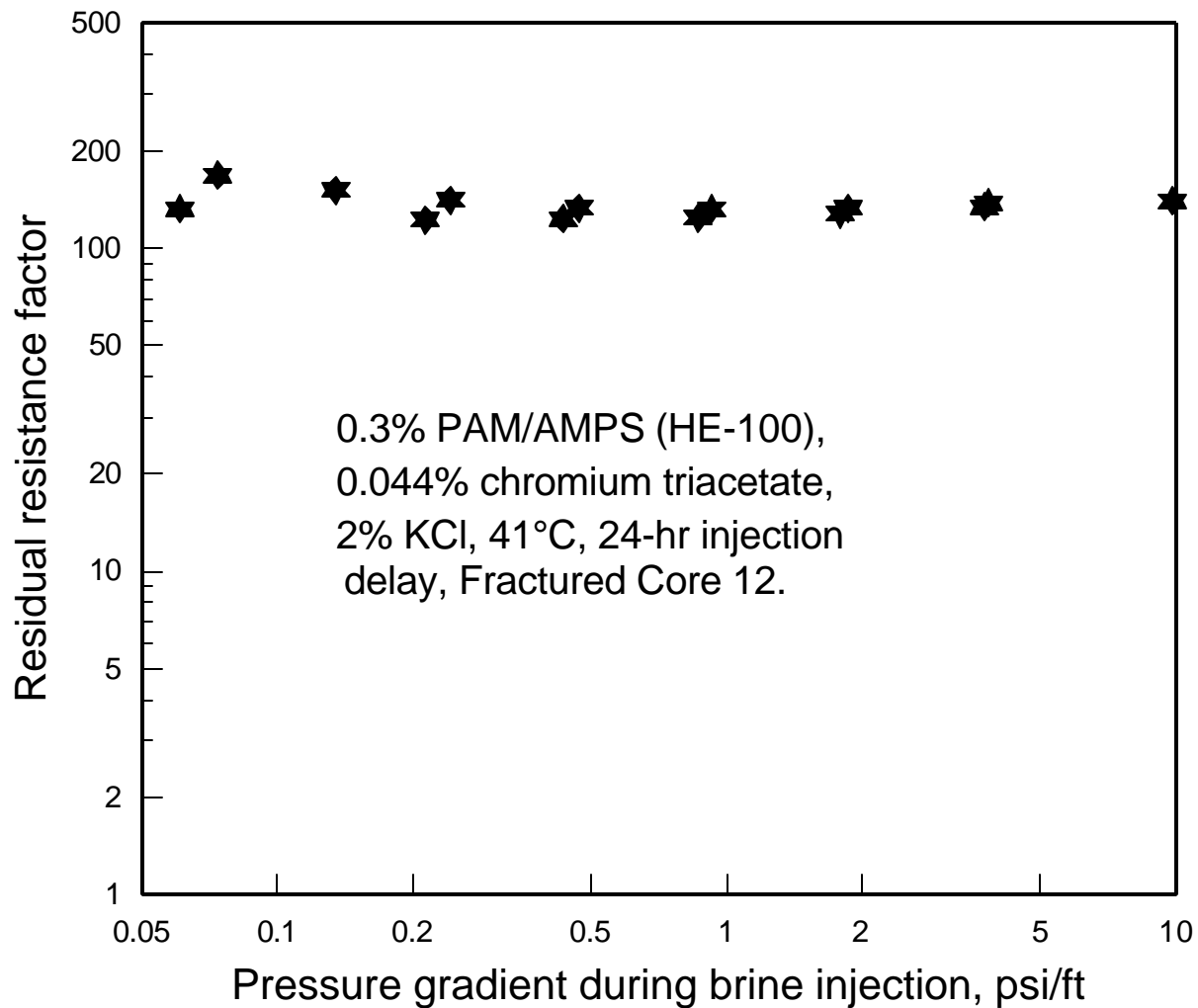


Fig. 36. Permeability reduction vs. pressure gradient after placement of a Cr(III)-acetate-PAM/AMPS gel.

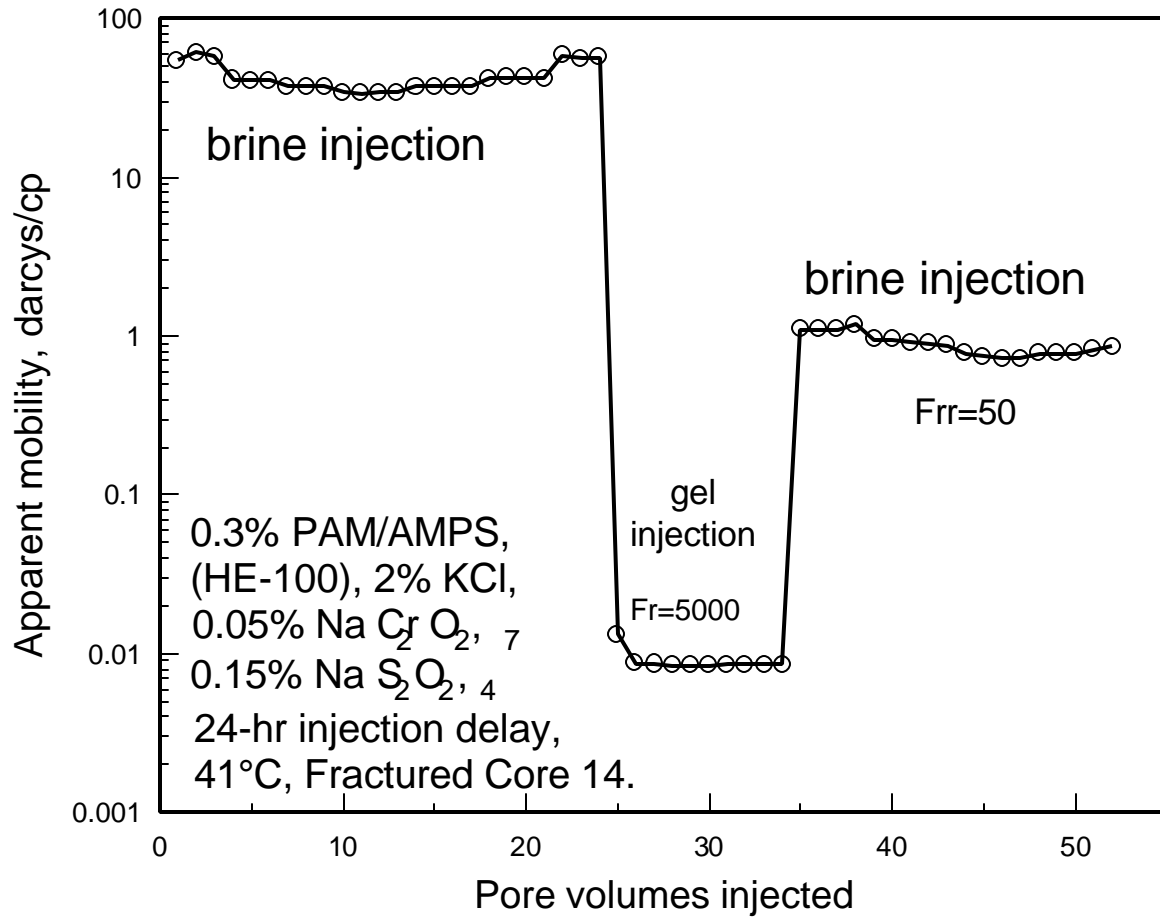


Fig. 37. Apparent mobility before, during, and after placement of a Cr(VI)-redox-PAM/AMPS gel.

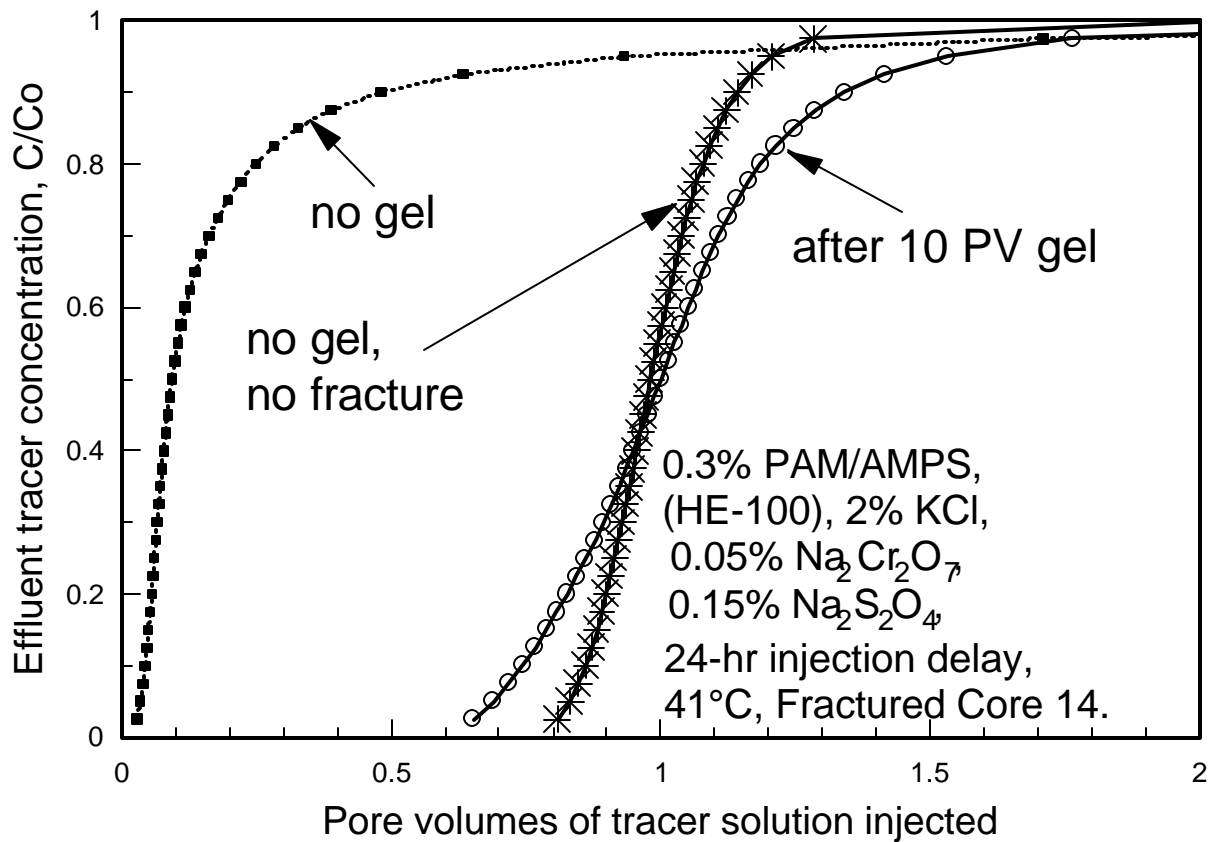


Fig. 38. Tracer results before vs. after placement of a Cr(VI)-redox-PAM/AMPS gel.

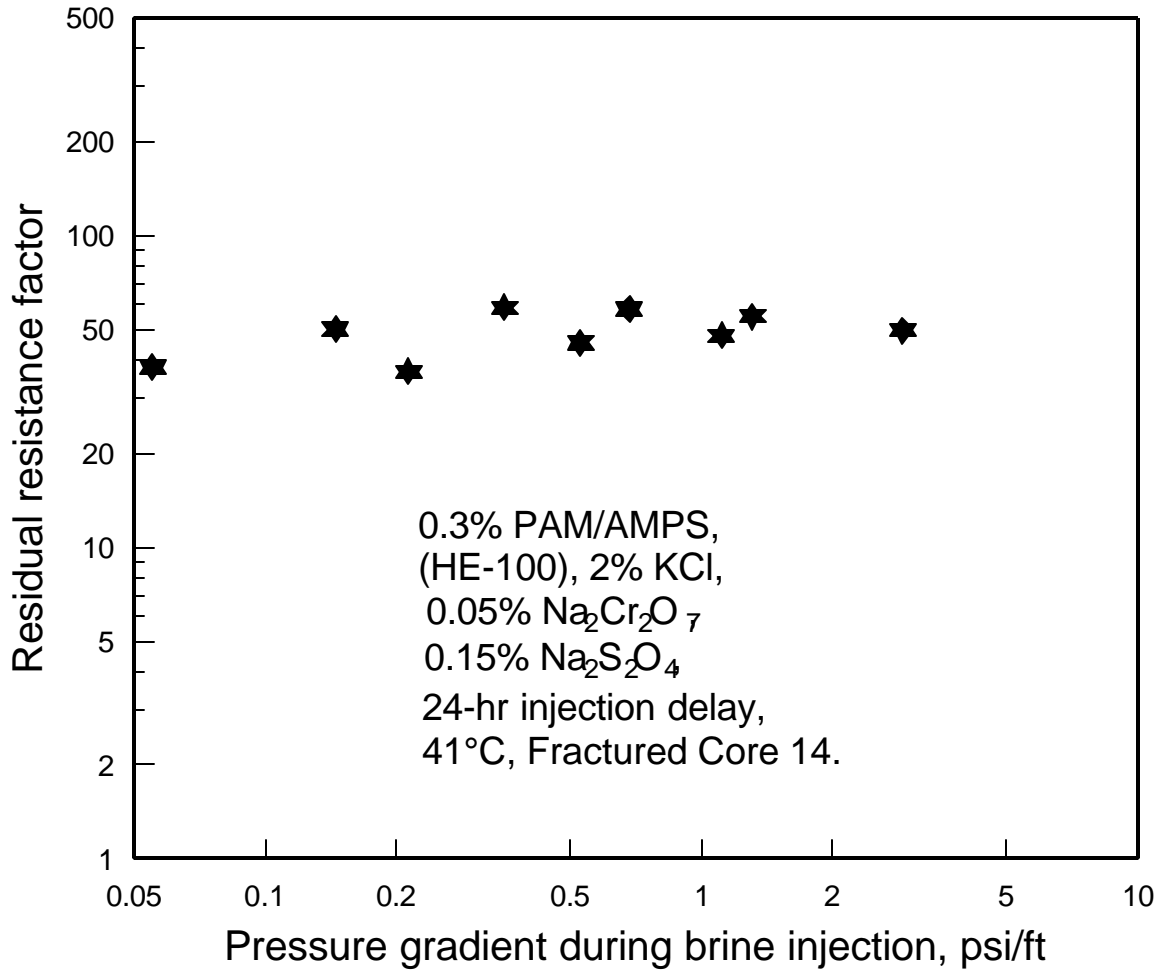


Fig. 39. Permeability reduction vs. pressure gradient after placement of a Cr(VI)-redox-PAM/AMPS gel.

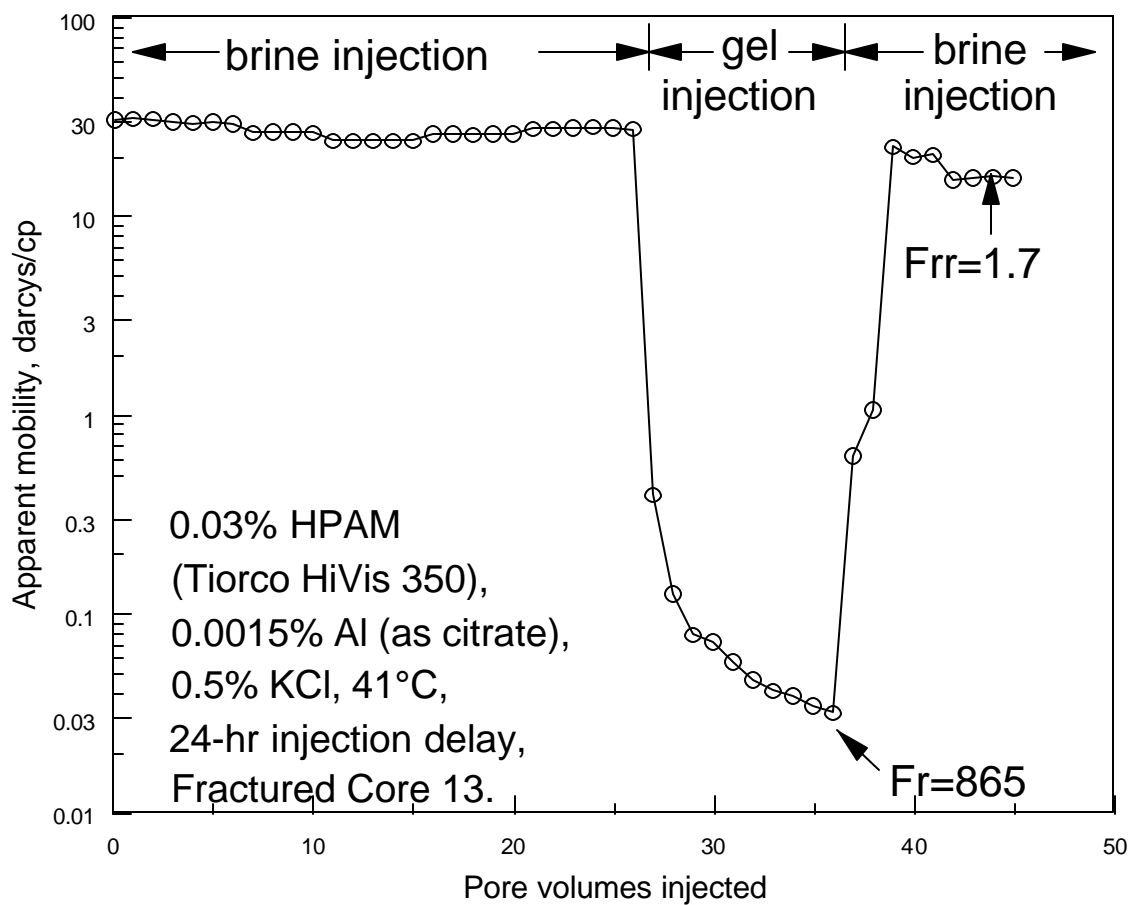


Fig. 40. Apparent mobility before, during, and after placement of an Al-citrate-HPAM gel.

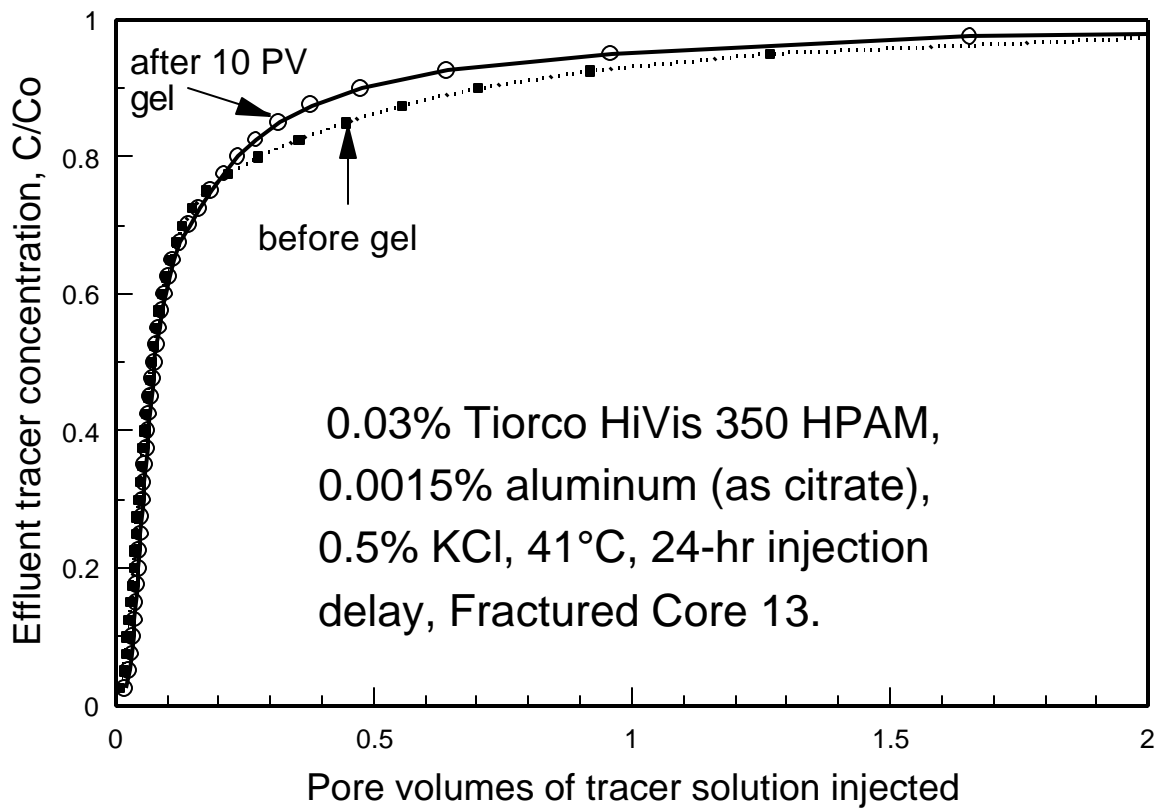


Fig. 41. Tracer results before vs. after placement of an Al-citrate-HPAM gel.

Table 8. Properties in Fractured Cores with One-Day-Old Gels

Core	Gel	Resistance Factor	Residual Resistance Factor	Tracer Results, PV at	
				Breakthrough	C/C ₀ =0.5
no fracture 7	none none	— 1	— 1	0.81 0.05	1.00 0.12
7	Cr(III)-acetate-HPAM	3,000	35	0.82	1.03
9	resorcinol-formaldehyde	plugged	70	0.36	0.54
10	Cr(III)-xanthan	8,600*	19	0.46	0.76
12	Cr(III)-acetate-PAM/AMPS	12.5	130	0.25	0.35
13	Al-citrate-HPAM	865**	1.7	0.02	0.08
14	Cr(VI)-redox-PAM/AMPS	5,000	50	0.65	1.00

* erratic

** still increasing after 10 PV

Discussion of Results

The first two listings in Table 8 provide data for unfractured and fractured cores without gel. The ideal gel treatment would heal the fracture so that tracer results matched those associated with the unfractured core. The ideal gel would also exhibit low resistance factors so that the gel could be placed without developing excessive pressure gradients. It would also provide a residual resistance factor that was approximately equal to the corresponding relative flow capacity value given in Table 6. (The latter property would indicate that the gel had plugged the fracture but not the porous rock.)

Cr(III)-Acetate-HPAM. Using fractured Core 7, we injected 17 PV of brine, followed by 17 PV of Cr(III)-acetate-HPAM gel (24 hrs after preparation), followed by 17 PV of brine (see Fig. 26). During these steps, the injection rate was 200 ml/hr. During the first brine injection, the apparent brine mobility was 30 darcys/cp. During the subsequent injection of gel, the apparent gel mobility stabilized at 0.01 darcys/cp. Thus, the gel was injected without plugging or "screening out" in the fracture. Since the apparent brine and gel mobilities were known (30 and 0.01 darcys/cp, respectively) and since these values were associated almost exclusively with flow in the fracture, we can calculate a resistance factor (F_r) for gel in the fracture. This value was 3,000. Thus, the effective viscosity of gel in the fracture was 3,000 times greater than that of water.

After injecting the gel, the core was shut in for several days. Gel was removed from the flow lines and the inlet and outlet core faces. Then, 17 PV of brine were injected (Fig. 26). The apparent brine mobility was stable at 0.85 darcys/cp (residual resistance factor, F_{rr} , was 35). This value was close to that expected for an unfractured core.

Tracer results confirmed that the gel effectively healed the fracture. For the tracer curve that was obtained after gel placement (circles in Fig. 27), the first half of the curve was virtually identical with that for an unfractured core (with no gel). The top half of the tracer curve (circles in Fig. 27) deviated significantly from that associated with the unfractured core. This result suggests that the tracer (potassium iodide) was retained or that a problem occurred with tracer detection during this part of the

experiment. This anomalous result was reproduced during four replicate tracer studies using two injection rates (differing by a factor of five). Further work is needed to understand the cause of this deviation from expected behavior. (I thank Stan McCool of the University of Kansas for pointing out this anomalous effect.)

During brine injection after gel placement, we routinely determined residual resistance factors (permeability reduction values) as a function of pressure gradient or fluid velocity. Fig. 28 (taken from Fig. 57 of Ref. 1) shows that residual resistance factors for the Cr(III)-acetate-HPAM gel in fractures were insensitive to pressure gradient over the range examined (0.03 to 20 psi/ft). In contrast, our previous work demonstrated that Cr(III)-acetate-HPAM gels in porous rock (i.e., in unfractured cores) exhibited a strong apparent shear-thinning behavior during brine injection.³¹

Resorcinol-Formaldehyde. Using fractured Core 9, a set of experiments was performed using a resorcinol-formaldehyde gel (aged 24 hrs before injection). During the first brine injection, the apparent brine mobility was stable at 105 darcys/cp (see Fig. 29). During the subsequent injection of gel (at a rate of 200 ml/hr), the apparent gel mobility dropped sharply to 0.003 darcys/cp after injecting less than 1 PV of gel. The resistance factor in the fracture was greater than 35,000 at this point, and no stabilization was evident. Thus, severe plugging was apparent during gel injection. (We note that the fracture in this experiment had the highest conductivity of any that we used.) After a shut-in period, 17 PV of brine were injected. The apparent brine mobility was stable at 1.5 darcys/cp ($F_r=70$). After completion of the experiment, the core was disassembled to reveal that the gel had only penetrated 7 cm into the fracture (total length was 14 cm). This observation confirmed that the gel was "screening out" during injection into the fracture. Fig. 30 shows tracer results before and after injection of the gel. The small amount of gel that was placed provided a moderate increase in sweep efficiency.

Cr(III)-Xanthan. For the Cr(III)-xanthan gel, the resistance factors were erratic during gel injection—possibly a result of intermittent screen-outs of gel aggregates in the fracture (see Fig. 31). Resistance factors averaged about 2,000 during injection of the first 9 PV of gel. During the last 5 PV of gel injection, resistance factors were more stable, averaging 8,600. During subsequent brine injection, stable residual resistance factors were observed (values averaging 19). Tracer studies revealed that this Cr(III)-xanthan treatment provided a moderate improvement in sweep efficiency (Fig. 32). During brine injection after gel placement, residual resistance factors were independent of pressure gradient between 0.003 and 3 psi/ft (Fig. 33).

Cr(III)-Acetate-PAM/AMPS. As shown in Fig. 34, the Cr(III)-acetate-PAM/AMPS formulation exhibited a low resistance factor in the fracture during placement ($F_r=12.5$ and apparent mobility was 3 darcys/cp). Upon first consideration, this result seems very favorable during gel placement. However, the tracer results did not indicate much improvement in sweep efficiency for the core (Fig. 35). Also, because the residual resistance factor (130) was much greater than the corresponding relative flow capacity (36.1) in Table 6, we suspect that the gel was not sufficiently formed before injection to prevent substantial leakoff into the porous rock (i.e., the gel plugged the porous rock at least as much as the fracture). During brine injection after gel placement, residual resistance factors were independent of pressure gradient between 0.05 and 10 psi/ft (Fig. 36).

Cr(VI)-Redox-PAM/AMPS. Using fractured Core 14, a second experiment was performed with a gel that contained 0.3% PAM/AMPS (HE-100®). However, the polymer was crosslinked using the Cr(VI)-redox system rather than using Cr(III)-acetate. The chromium concentration in this formulation was about twice that for the Cr(III)-acetate-PAM/AMPS gel. Results from this experiment were similar to those using the Cr(III)-acetate-HPAM gel (compare Figs. 26 and 37). During injection of 10 PV of Cr(VI)-

redox-PAM/AMPS gel, resistance factors were stable at 5,000 (see Fig. 37). During brine injection after gel placement, the apparent mobility was stable at about 0.8 darcy/cp ($F_{rr}=50$). The residual resistance factors and the tracer results (Fig. 38) indicated that this gel treatment effectively healed the fracture. During brine injection after gel placement, residual resistance factors were independent of pressure gradient between 0.05 and 4 psi/ft (Fig. 39).

Al-Citrate-HPAM. For Al-citrate-HPAM, resistance factors steadily increased (apparent mobilities steadily decreased) throughout injection of 10 PV of formulation, suggesting a slow but continuous plugging effect (Fig. 40). During brine injection after gel placement, the residual resistance factor was very low (1.7) and the tracer results (Fig. 41) indicated no improvement in sweep. As was the case for the Cr(III)-acetate-PAM/AMPS formulation, gel formation was not evident when viewing the Al-citrate-HPAM composition in a bottle.

The tracer results and residual resistance factors suggest that for the gels examined, the Cr(III)-acetate-HPAM and Cr(VI)-redox-PAM/AMPS gels most effectively healed the fractures. In both cases, the tracer results after gel placement approached those seen for the unfractured core. Also, the residual resistance factors were similar to the corresponding relative flow capacities for the cores, as listed in Table 6. However, the high resistance factors (3,000 to 5,000) raise concern about our ability to propagate these gels deep into fractured systems. This concern also applies to most of the other gels. As mentioned earlier, severe plugging was apparent during injection of the resorcinol-formaldehyde gel (resistance factors exceeded 35,000 after injecting less than one pore volume of gel).

For most gels listed in Table 8, residual resistance factors in the fractured cores were stable and independent of injection rate. As an exception, residual resistance factors for the Al-citrate-HPAM gel decreased with increased injection rate. Also, washout of gel from the fractures appeared to be significant only for the Al-citrate-HPAM gel.

Conclusions

Our data indicates both hope and caution concerning the injection of gels into fractured systems. Our tracer studies indicated that some gels can effectively heal fractures under the right circumstances. However, the high resistance factors and pressure gradients exhibited during placement raises concern about our ability to propagate these gels deep into a fracture system. We suspect that the ability of a given gel to propagate effectively through a fracture depends on (1) the composition of the gelant, (2) the degree of gelation or gel curing, (3) the fluid velocity (or pressure gradient) in the fracture, and (4) the width, conductivity and tortuosity of the fracture. Thus, at this point, we are not suggesting that one gel is necessarily better than other gels for fracture applications. More work will be needed to establish the best circumstances for propagation of gels in fractures.

7. EFFECTS OF GEL CURING AND MECHANICAL BREAKDOWN ON GEL PROPAGATION THROUGH FRACTURED CORES

Our previous work²⁶ suggested that under some circumstances, improved fluid diversion in fractured systems might be obtained by injecting preformed gels rather than gelants that form gels in situ. However, for this approach to be successful, the injected gel must be able to propagate through the fractures without "screening out" or developing excessive pressure gradients. We suspect that the ability of a given gel to propagate effectively through a fracture depends on (1) the composition of the gelant, (2) the degree of gelation or gel curing, (3) the fluid velocity (or pressure gradient) in the fracture, and (4) the width, conductivity, and tortuosity of the fracture.

In this chapter, we describe several experiments that probe how the degree of gel curing affects the flow of gels through fractured Berea sandstone cores. In these experiments, the sandstone cores had nominal permeabilities to brine of 650 md before fracturing. The cores were 14.7 cm in length and 3.6 cm in diameter. Preparation of the fractured cores was described earlier.²⁶ In this work, we report results from studies involving two gels, including a Cr(III)-acetate-HPAM gel and a hydroquinone-hexamethylenetetramine-HPAM gel. An interesting feature of the latter gel is that a high temperature (e.g., 110°C) is required for the gelation reaction to proceed at a rapid rate. At the temperature of our core experiments (41°C), the gelation rate is negligible. Therefore, the gelation reaction can be allowed to proceed to a desired point at 110°C and then be quenched and studied at 41°C. We also investigate the performance of a mechanically blended (sheared) Cr(III)-acetate-HPAM gel in a fractured core.

Finally, we examine the effects of recycling a Cr(III)-acetate-HPAM gel through a single fractured core and through a series of fractured cores.

Curing Effects for a Cr(III)-Acetate-HPAM Gel

We studied the effect of gel aging or curing on the flow of Cr(III)-acetate-HPAM gels through fractured cores. For each experiment, we prepared a formulation that contained 0.5% HPAM (Allied Colloids Alcoflood 935®, $M_w \approx 5 \times 10^6$ daltons, degree of hydrolysis: 5-10%), 0.0417% chromium triacetate (Sargent-Welch), and 1% NaCl (pH=6). The gelation time for this composition was roughly 5 hours at 41°C. We injected this gel into our fractured cores after allowing different time periods to elapse. These delay times ranged from 5 to 72 hours (see Column 1 of Table 9). During gel injection, the injection rate was fixed at 200 ml/hr. All experiments were performed at 41°C.

The third, fourth, and fifth columns of Table 9 list average core permeability (k_{av}), fracture conductivity (k_{fw}), and relative fracture/rock flow capacity ($k_{fw}h_f/Ak_m$), respectively, for each core. Properties of Cores 7, 11, 20, and 25 were fairly similar, with fracture conductivities ranging from 44.4 to 70.2 darcy-cm. In contrast, the conductivities of the fractures in Cores A, 28, 8, and 30 were 122.2, 163.4, 187, and 1,560 darcy-cm, respectively.

The fourth and sixth columns in Table 9 illustrate the effect of fracture conductivity on gel propagation. For a gel that was aged 24 hours before injection, the resistance factor was about the same ($\approx 3,000$) in fractures with k_{fw} values ranging from 53.8 to 1,560 darcy-cm. However, the pressure gradient in the 1,560-darcy-cm fracture was about 5% of that in the 53.8-darcy-cm fracture. Additional work should be performed to establish how resistance factors and pressure gradients vary over a wider range of fracture widths, conductivities, and tortuosities.

Table 9. Injection of a Cr(III)-Acetate-HPAM Gel into Fractured Cores

Injection delay, hours	Core	k_{av} darcys	k_{fwf} darcy-cm	k_{fwf}/Ak_m	Resistance factor	dp/dl, psi/ft
5	28	59.1	163.4	89.9	137	4
10	20	23.7	64.3	35.4	500	35
24	7	19.9	53.8	29.6	3,000	250
24	25	25.8	70.2	38.7	3,560	232
24	A	44.4	122.2	67.3	2,280	85
24	30	559	1,560	859	4,024	12
24	8	67.7	187.0	103	2,750	68
32	8	67.7	187.0	103	14,500	357
72	11	16.5	44.4	15.9	340	34

Column 6 in Table 9 suggests that gel resistance factors (apparent gel viscosities in the fractures) increased dramatically with increased curing time up to 32 hours. However, between 32 and 72 hours, the gel resistance factors decreased substantially. An explanation for this decrease must await further research. The pressure gradients in the cores during gel injection are listed in Column 7 of Table 9. For most cases shown, the pressure gradients raise concern about the practicality of injecting these preformed gels unless the fractures have very high conductivities. However, for the 5-hr gel, the pressure gradient was acceptably low (4 psi/ft) after injecting 10 PV of gel. For this gel, resistance factors steadily increased from 59 after 1 PV to 137 after 10 PV. In contrast, resistance factors for the other gels were stable during the gel injection process.

Fig. 42 compares tracer results during brine injection after placement for four Cr(III)-acetate-HPAM gels (aged 5, 10, 24, and 72 hours). The tracer curves for the 10-hr, 24-hr, and 72-hr gels approach the results associated with an unfractured core. Therefore, these three gels effectively healed the fractures without damaging the porous rock of the core. In contrast, the 5-hr gel washed out from the fracture during brine injection—resulting in a tracer curve that was very similar to that for the fractured core before gel injection.

Curing Effects for a Hydroquinone-Hexamethylenetetramine-HPAM Gel

A concern during our study of the Cr(III)-acetate-HPAM gel (and most other commercial gels) was that gel curing and resistance factors increased with time and distance of propagation in the fractures. Ideally, gelation should be allowed to proceed enough to prevent leakoff but not enough to cause a large resistance to flow during gel placement in the fracture. However, conventional gelants that are exposed to a fixed temperature will react continually until reaction completion. Therefore, properties of these gels can change continually during core studies and during injection into fractured reservoirs.

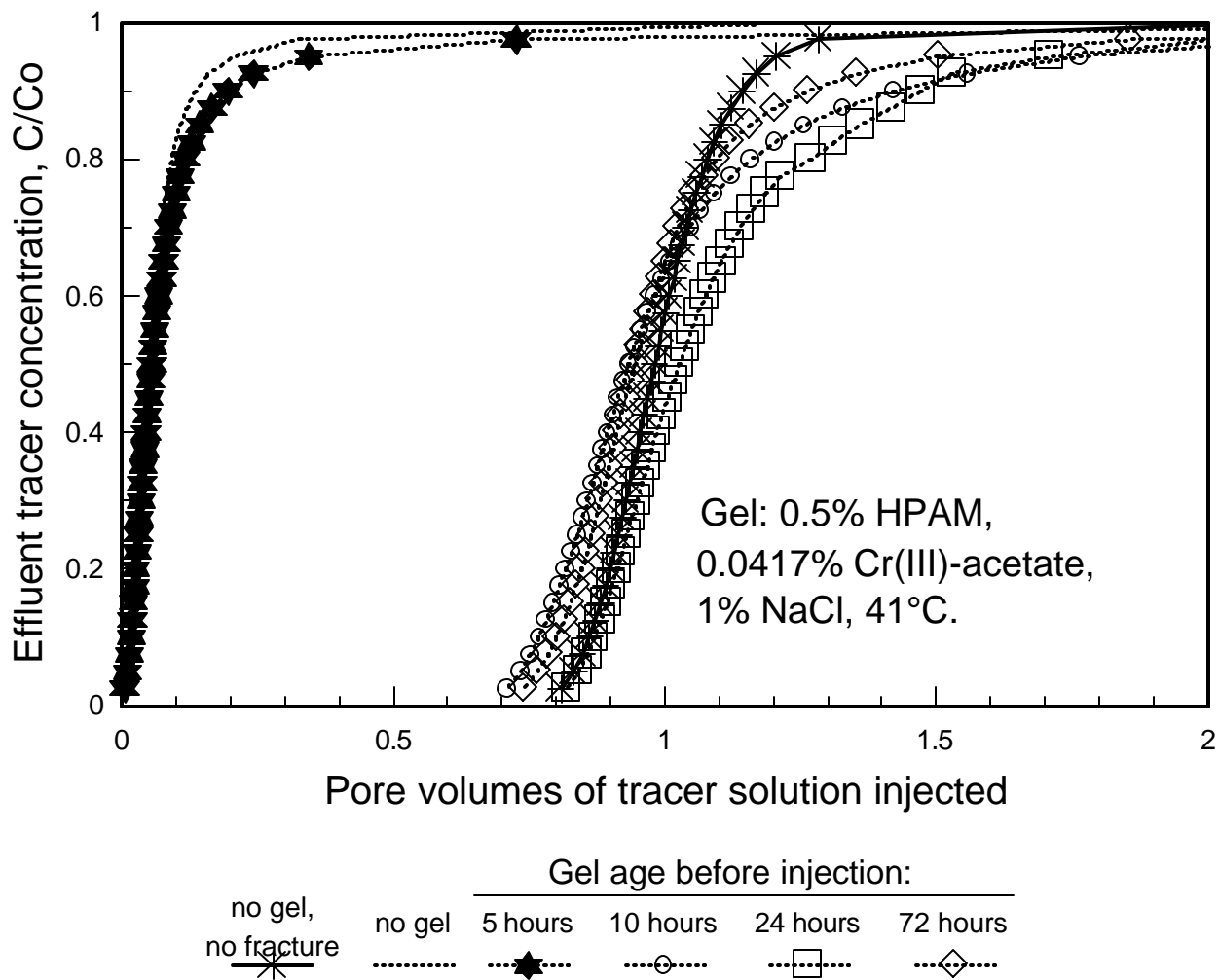


Fig. 42. Tracer results before vs. after placement of Cr(III)-acetate-HPAM gels in fractured cores.

In an attempt to study a gel with a fixed level of reaction or curing, we investigated a hydroquinone-hexamethylenetetramine-HPAM gel. This gel contained 0.5445% HPAM (Allied Colloids Alcoflood 935®), 0.25% hydroquinone (Sigma), 0.1% hexamethylenetetramine (Sigma), and 1% NaHCO₃ at pH=8.2. An interesting feature of this gel is that a high temperature (e.g., 110°C) is required for the gelation reaction to proceed at a rapid rate. At the temperature of our core experiments (41°C), the gelation rate is negligible. Therefore, the gelation reaction can proceed to a desired point at 110°C and then be quenched and studied at 41°C. (We thank Rick Hutchins of Unocal for suggesting this gel.)

After preparation, the gelant was exposed to 110°C (230°F) for time periods ranging from 0.5 to 8 days. After the desired time had elapsed, the formulation was rapidly cooled to 41°C. The first row in Table 10 lists gel-strength codes exhibited by the gels after various times of exposure to 110°C. The gels used in these studies were more or less fluid, with gel codes that range from "highly flowing" gels (Sydansk gel code B¹⁴⁹) to "barely flowing" gels (Sydansk gel code E¹⁴⁹). As expected, gel strengths increased with increased time of exposure at 110°C.

Table 10. Injection of a Hydroquinone-Hexamethylenetetramine-HPAM Gel into Fractured Cores

Days at 110°C Sydansk gel code ¹⁴⁹	0.5 B	0.75 C	1 C	2 C	4 D	8 D-E
Fractured Core #	27	29	26	23	22	24
k _{av} , darcys	53.5	71.7	75.3	15.6	20.3	34.3
k _f w _f , darcy-cm	148	199	209	43.6	55.0	94.1
k _f w _h /Ak _m	81.3	109	115	24.0	30.3	51.8
F _r pressure gradient, psi/ft	63 2	140 3	2,580 48	3,200 351	707 63	4,700 238
F _{rr} pressure gradient, psi/ft PV of brine injected	1.3 0.04 20	26 0.6 20	130 2.9 26	9.2 1.0 16	130 10.7 23	66 3.2 29
PV at tracer breakthrough PV when C/C ₀ =0.5	0.031 0.083	0.034 0.084	0.687 0.858	0.673 0.895	0.584 0.831	0.709 0.894

After quenching to 41°C, 10 PV of a given gel (315 ml) was injected into a fresh, fractured core using an injection rate of 200 ml/hr to determine resistance factors (F_r) in the fracture. Properties of the fracture cores (Cores 22, 23, 24, 26, 27, and 29) are listed in the second row of Table 10. Fracture conductivities ranged from 43.6 to 209 darcy-cm. After gel placement, the inlet and outlet endcaps were removed, and gel was scraped from flow lines and the inlet and outlet rock faces. The endcaps were then repositioned, and brine injection commenced at 200 ml/hr. Between 16 and 29 PV of brine were injected to determine residual resistance factors (F_{rr}). Finally, tracer studies were performed to assess how effectively the gel treatments healed the fractures.

Resistance factors and pressure gradients observed during gel injection are listed in the third row of Table 10. For gels that were exposed for 1 day, 2 days, and 8 days at 110°C, resistance factors ranged from 2,580 to 4,700. For these gels, the resistance factors increased with increased time of exposure at 110°C; however, the increase was not as large as we expected. Surprisingly, the resistance factor was only 707 for the gel that was exposed for 4 days at 110°C. At present, we cannot explain why this result

deviated from the trend found from the other resistance factors. We understand that several reaction processes may be occurring with this gel formulation at 110°C. In addition to the gelation reaction, hydrolysis of amide groups can occur on the polymer,^{150,151} and polymer and gel degradation reactions can occur (e.g., oxidation/reduction, etc.). These multiple reactions could cause a complex variation of gel resistance factor with time.

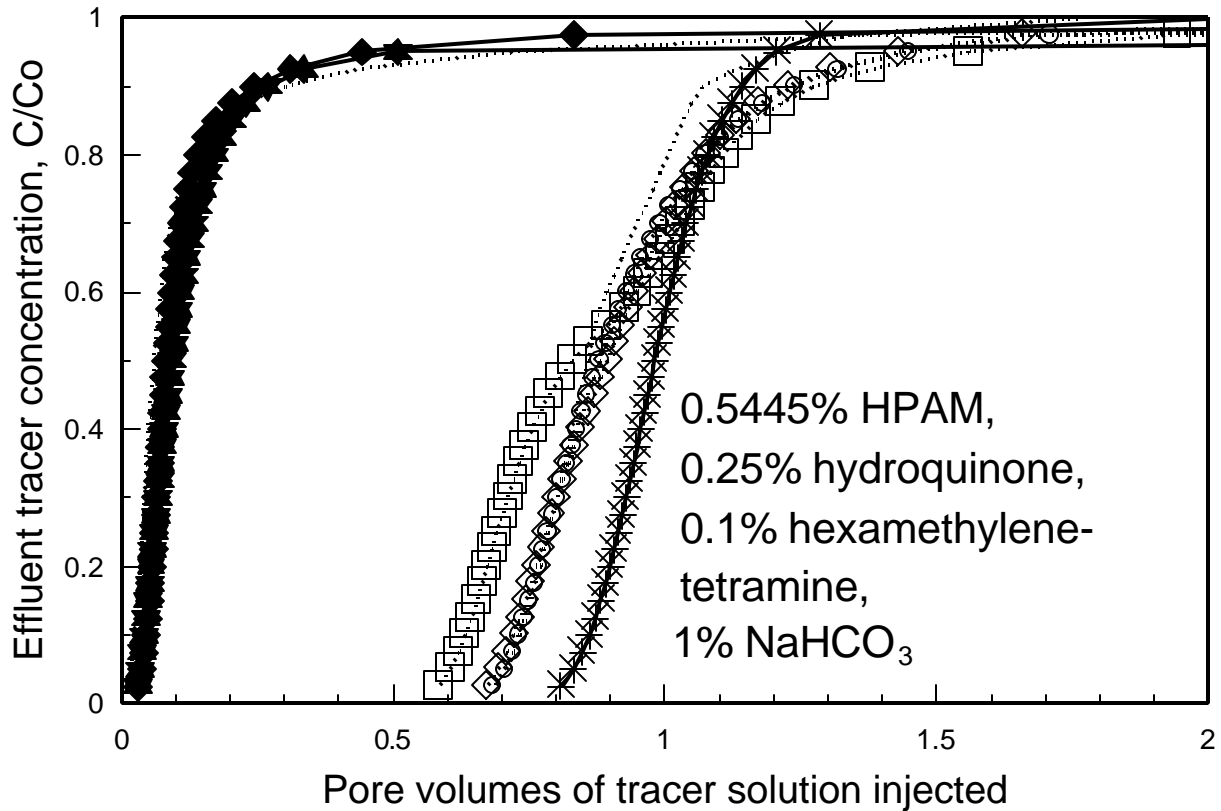
For the gels that were exposed to 110°C for 1 day or more, the high resistance factors and pressure gradients raise concern about the ability of these gels to propagate through fractures unless the fractures have a high conductivity. In contrast, the gels that experienced 110°C for 0.5 to 0.75 days exhibited relatively low resistance factors (63-140) and pressure gradients (2-3 psi/ft). However, the latter gels apparently did not undergo sufficient gelation to prevent them from washing out from the fractures during brine injection after gel placement. This conclusion is evident from the tracer results (Fig. 43 and fifth row of Table 10). The rapid tracer breakthrough values (0.031-0.034 PV) are very similar to results associated with the fractured cores before gel placement (tracer breakthrough = 0.027 PV).

For the four gels that were exposed to 110°C for 1 day or more, the gel treatments healed the fractures to about the same extent. This conclusion can be reached by examining the tracer results in Fig. 43. In all four cases, the tracer first arrived at the outlet of the core after injecting between 0.58 and 0.71 PV of tracer solution. Also, the tracer concentration in the effluent reached 50% of the injected concentration after injecting between 0.83 and 0.90 PV. For comparison, perfect healing of the fractures would be indicated by tracer breakthrough at 0.8 PV and PV=1.0 when the tracer $C/C_o=0.5$.

Residual resistance factors can complement tracer results when assessing gel treatments in fractures. If the gel treatment heals the fracture without damaging the porous rock, the residual resistance factor (F_{tr} , determined during brine injection after gel placement) should be approximately equal to the flow capacity of the fracture relative to that of the porous rock ($k_{fw}h_f/Ak_m$, determined before gel placement). For the gels that experienced 1 day and 8 days at 110°C, the residual resistance factors were fairly consistent with the tracer results in that they indicated that the gel treatments healed the fractures without damaging the porous rock in Cores 24 and 26 (see Table 10). The values for F_{tr} and $k_{fw}h_f/Ak_m$ were 130 and 115, respectively, for Core 26 and were 66 and 51.8, respectively, for Core 24.

For Cores 22 and 23, the residual resistance factors were less consistent with the tracer results. In Core 23 (where the gel was exposed to 110°C for 2 days), the F_{tr} value (9.2) was significantly less than the $k_{fw}h_f/Ak_m$ value (24.0). The residual resistance factor suggested that the fracture was not healed very effectively, while the tracer results (Fig. 43) indicated that the fracture was healed as well in Core 23 as it was in Cores 24 and 26. At present, we cannot explain this result. In Core 22 (where the gel was exposed to 110°C for 4 days), the F_{tr} value (130) was significantly greater than the $k_{fw}h_f/Ak_m$ value (30.3). This result suggests either that the gel (or gelant) penetrated into (i.e., leaked off from the fracture) and damaged the porous rock or that we were not thorough enough in removing gel from the flow lines and inlet core face before brine injection.

Our results to date with the hydroquinone-hexamethylenetetramine-HPAM gels indicate that additional experiments should be performed with the gels aged between 0.75 and 1 days at 110°C. A gel aged for only 0.75 days at 110°C washed too easily from the fracture, while gels aged for 1 day or more at 110°C exhibited resistance factors and pressure gradients that were too high during gel placement.



Time gel was exposed to 110°C:

no gel, no fracture	no gel	8 days	4 days	2 days	1 day	0.75 days	0.5 days
*○.....□.....◇.....★.....◆.....

Fig. 43. Tracer results before vs. after placement of hydroquinone-hexamethylenetetramine-HPAM gels in fractured cores.

Performance of a Sheared Cr(III)-Acetate-HPAM Gel

Another approach to achieving a gel with a fixed level of curing is to allow the gelation reaction for a conventional gel to proceed to completion and then mechanically degrade the gel to a desired fluidity. In this section, we examine the performance of a 5-day-old Cr(III)-acetate-HPAM gel that was sheared in a blender. Our objective was to determine whether this mechanical degradation could reduce gel resistance factors while still providing effective fluid diversion in a fractured core. In this work, we used the same composition of Cr(III)-acetate-HPAM gel that was described earlier. After preparation, the gel was allowed to set for 5 days at 41°C. Then, it was sheared for 1 minute in a Waring blender at 75% of full power. After shearing, the product had a smooth consistency (no chunks).

We injected 10 PV (315 ml) of sheared Cr(III)-acetate-HPAM gel through a fractured Berea sandstone core (Core 21). As with other cores, Core 21 had a nominal permeability to brine of 650 md before fracturing, and the core was 14.7 cm in length and 3.6 cm in diameter. After fracturing, the average core permeability was 8.81 darcys, the fracture conductivity was 22.8 darcy-cm, and the $k_{wf}h_f/Ak_m$ value was 12.6.

Fig. 44 shows resistance factors and pressure gradients during gel injection at a rate of 200 ml/hr. During injection of 10 PV of gel, the resistance factor steadily increased from 45 to 200, while the pressure gradient increased from 9 to 38 psi/ft. These values are lower (and therefore more desirable) than most previous values that we observed. These low values are especially encouraging because Core 21 had one of the least conductive fractures that we have studied (22.8 darcy-cm). However, the steady increase in these values still raises a concern that unacceptably high pressure gradients could develop unless the fractures are very conductive.

After gel placement, the inlet and outlet endcaps were removed, and gel was scraped from flow lines and the inlet and outlet rock faces. The endcaps were then repositioned, and 25 PV of brine were injected. Fig. 45 shows residual resistance factors and pressure gradients that were observed during brine injection. In this experiment, measurements were first at a brine injection rate of 2.6 ml/hr. Then, measurements were obtained at successively higher injection rates up to 200 ml/hr. Finally, the measurements were repeated at successively lower rates down to 2.6 ml/hr. Fig. 45 shows that residual resistance factors exhibited an apparent shear-thinning behavior. The pressure gradient was more or less independent of injection rate, with an average value of 2.5 psi/ft. In contrast, we observed Newtonian behavior (i.e., residual resistance factors were independent of injection rate and pressure gradient) during similar experiments with gels that were not sheared (see Chapter 6). At present, we cannot explain the difference in results.

The open circles in Fig. 46 show tracer results that were obtained during brine injection after gel placement. In this study, tracer breakthrough occurred at 0.345 PV and $C/C_o=50\%$ at 0.505 PV. Thus, the treatment improved sweep efficiency somewhat in the core, but the fracture was not healed.

In summary, this sheared gel did exhibit lower than usual resistance factors and pressure gradients during gel injection. This result offers hope that mechanical degradation could be used to control resistance factors for a given gel in a fracture. More work is needed to identify conditions and compositions that will (a) during placement, flow readily through fractures without penetrating significantly into porous rock and without "screening out" or developing excessive pressure gradients and (b) at a predictable and controllable time, become immobile and resist breakdown upon exposure to moderate to high pressure gradients.

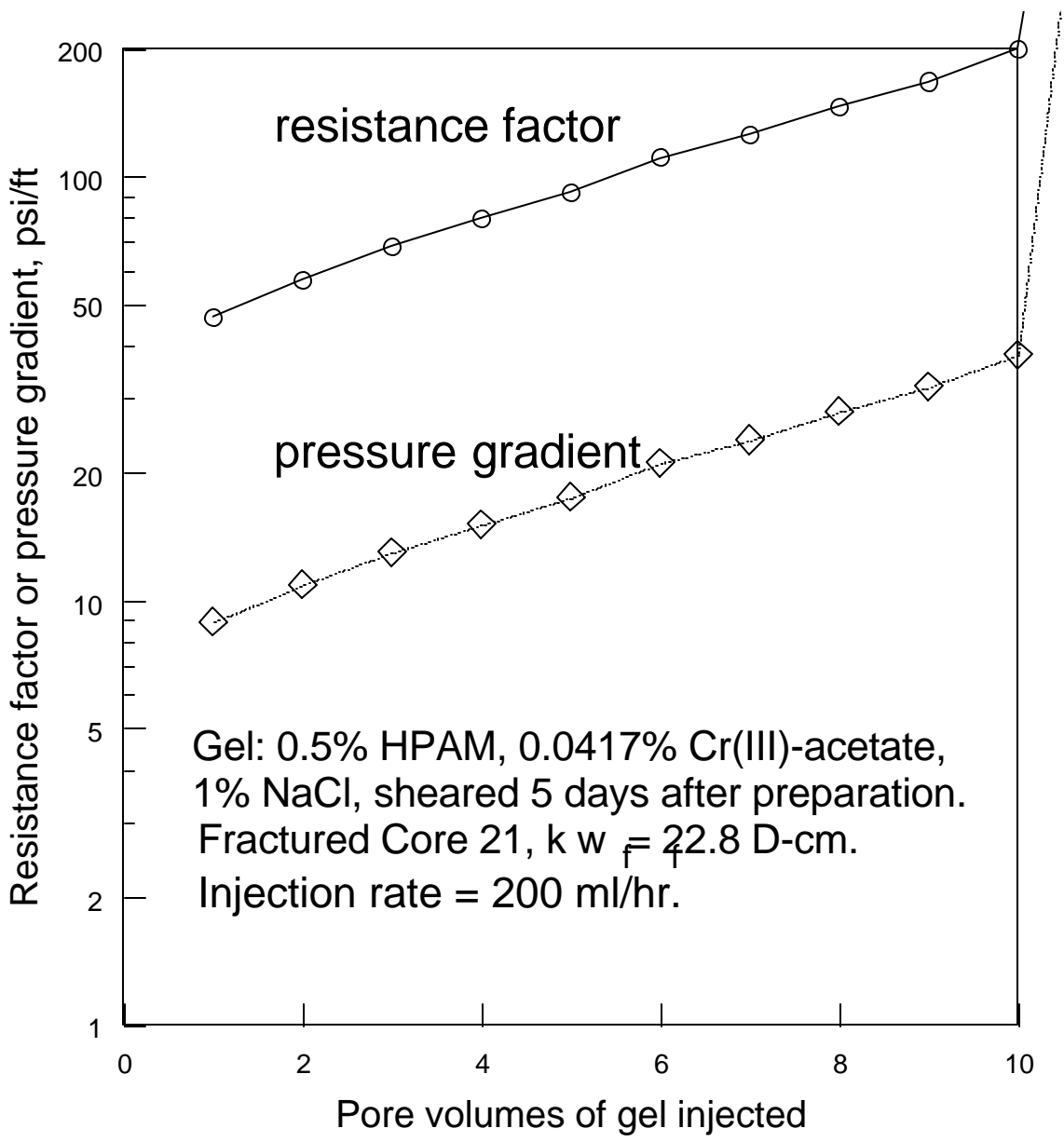


Fig. 44. Resistance factors and pressure gradients during placement of a sheared Cr(III)-acetate-HPAM gel.

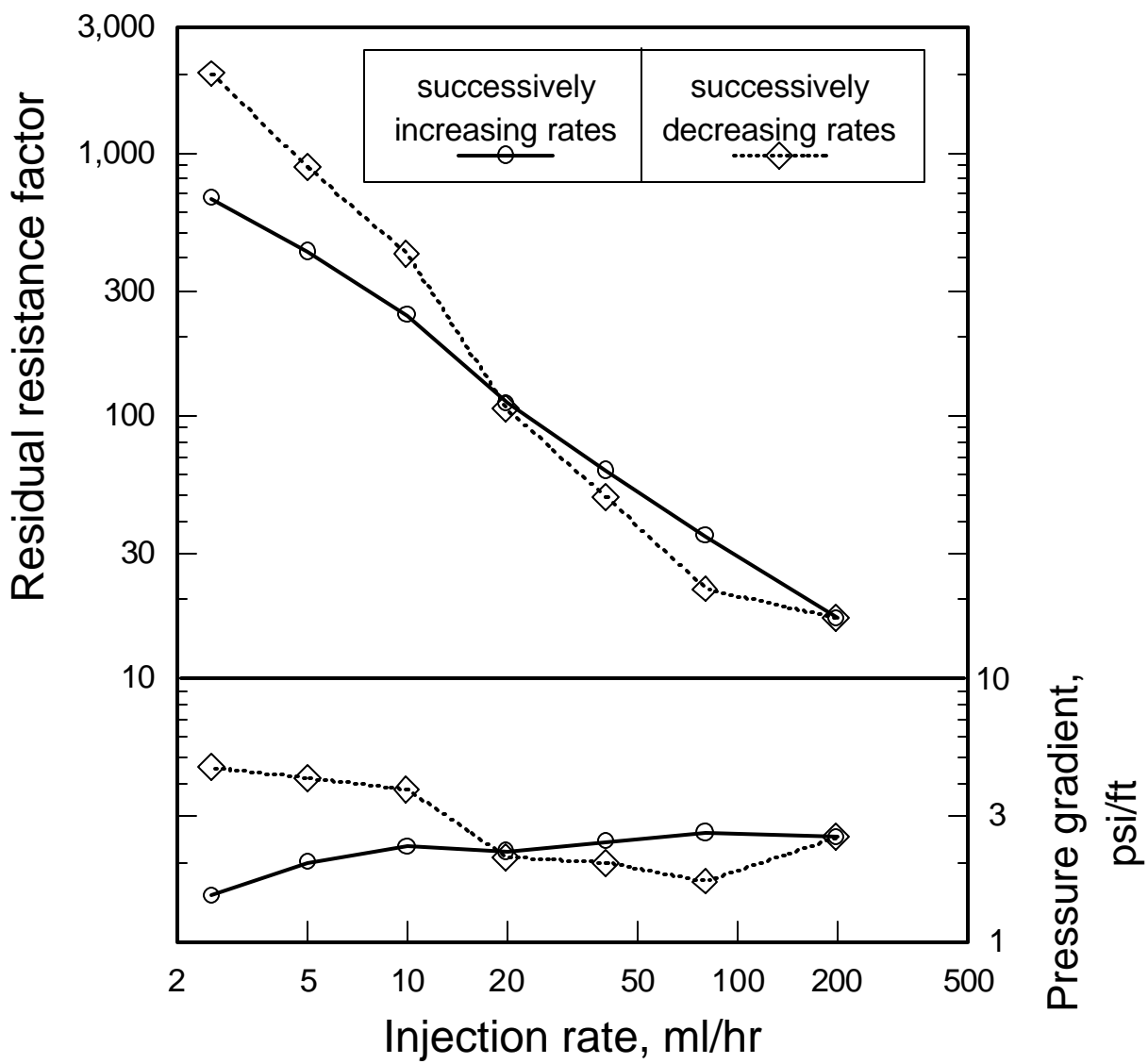


Fig. 45. Residual resistance factors and pressure gradients during brine injection after placement of a sheared Cr(III)-acetate-HPAM gel.

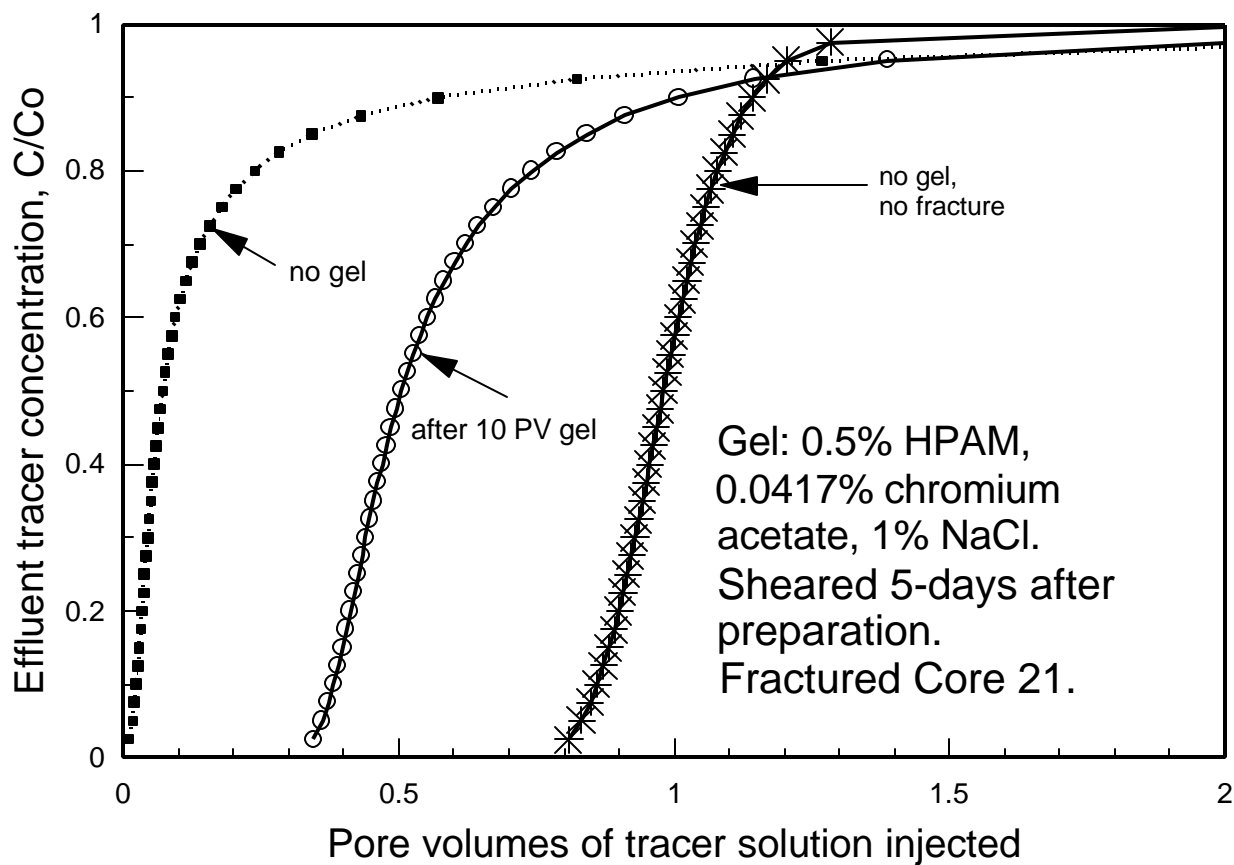


Fig. 46. Tracer results before vs. after placement of a sheared Cr(III)-acetate-HPAM gel.

Recycling of a Cr(III)-Acetate-HPAM Gel Through a Fractured Core

During gel injection into our short (14.7 cm) fractured cores, mechanical degradation of the gel was probably small. In contrast, mechanical degradation may be significant after extrusion through a long fracture in a reservoir. Of course, mechanical breakdown can change the resistance factor and residual resistance factor for a gel in a fracture. Therefore, we are interested in assessing the effects of gel breakdown as a function of distance along a fracture.

In our first attempt to characterize mechanical breakdown of gels, we recycled 14 PV (440 ml) of Cr(III)-acetate-HPAM gel eight times through a fractured Berea sandstone core (Core 25). As with other cores, Core 25 had a nominal permeability to brine of 650 md before fracturing, and the core was 14.7 cm in length and 3.6 cm in diameter. After fracturing, the average core permeability was 25.8 darcys, the fracture conductivity was 70.2 darcy-cm, and the $k_{fw}h_f/Ak_m$ value was 38.7.

The composition of the Cr(III)-acetate-HPAM gel was the same as that mentioned earlier: 0.5% HPAM (Allied Colloids Alcoflood 935®), 0.0417% chromium triacetate, and 1% NaCl (pH=6). One day after this gelant was prepared, it was injected into the fractured core using a rate of 200 ml/hr. Fig. 47 shows resistance factors during the first two cycles of gel injection. During the first injection cycle, the resistance factor in the fracture was stable at 3,560 and the pressure gradient was 232 psi/ft. The injection process required about 2 hours for the first cycle.

The effluent from the first cycle was fairly homogeneous, but some free water was seen with the gel. This free water was found in the effluent during all subsequent cycles. There are two possible sources of this free water. First, since the core was initially saturated with brine, some of this water may have been displaced from the core during gel injection. Second, the water may have resulted from syneresis or breakdown of the gel.

The effluent from the first cycle (including the free water) was reinjected into the same core, beginning 27 hours after the gelant was prepared. During the second cycle, resistance factors were lower than expected during the first and last two PV of gel injection (see Fig. 47). We suspect that the free water with the gel was responsible for the lower resistance factors (i.e., gravity segregation in the ISCO injection pump may have resulted in different fractions of gel and free water being injected at different times). For the intermediate data points of the second injection cycle, the resistance factors decreased steadily from 3,500 to 1,900.

Resistance factors during the third through fifth cycles of gel injection are shown in Fig. 48. These cycles began 47, 50, and 53 hours after gelant preparation, respectively. Through these cycles, the resistance factors generally followed a steady decline—from 4,100 at the beginning of the third cycle to 700 at the end of the fifth cycle. Of course, notable deviations from the trend were found at the end of the third cycle and the beginning of the fifth cycle. As mentioned above, we suspect that these deviations resulted from free water with the gel.

For the first through fifth cycles of gel injection, the average resistance factor per cycle decreased substantially—from 3,560 during the first cycle to 800 during the fifth cycle. Therefore, mechanical degradation was evident after each of these cycles. The total fracture distance represented by the first five cycles of gel injection was about 2.4 ft.

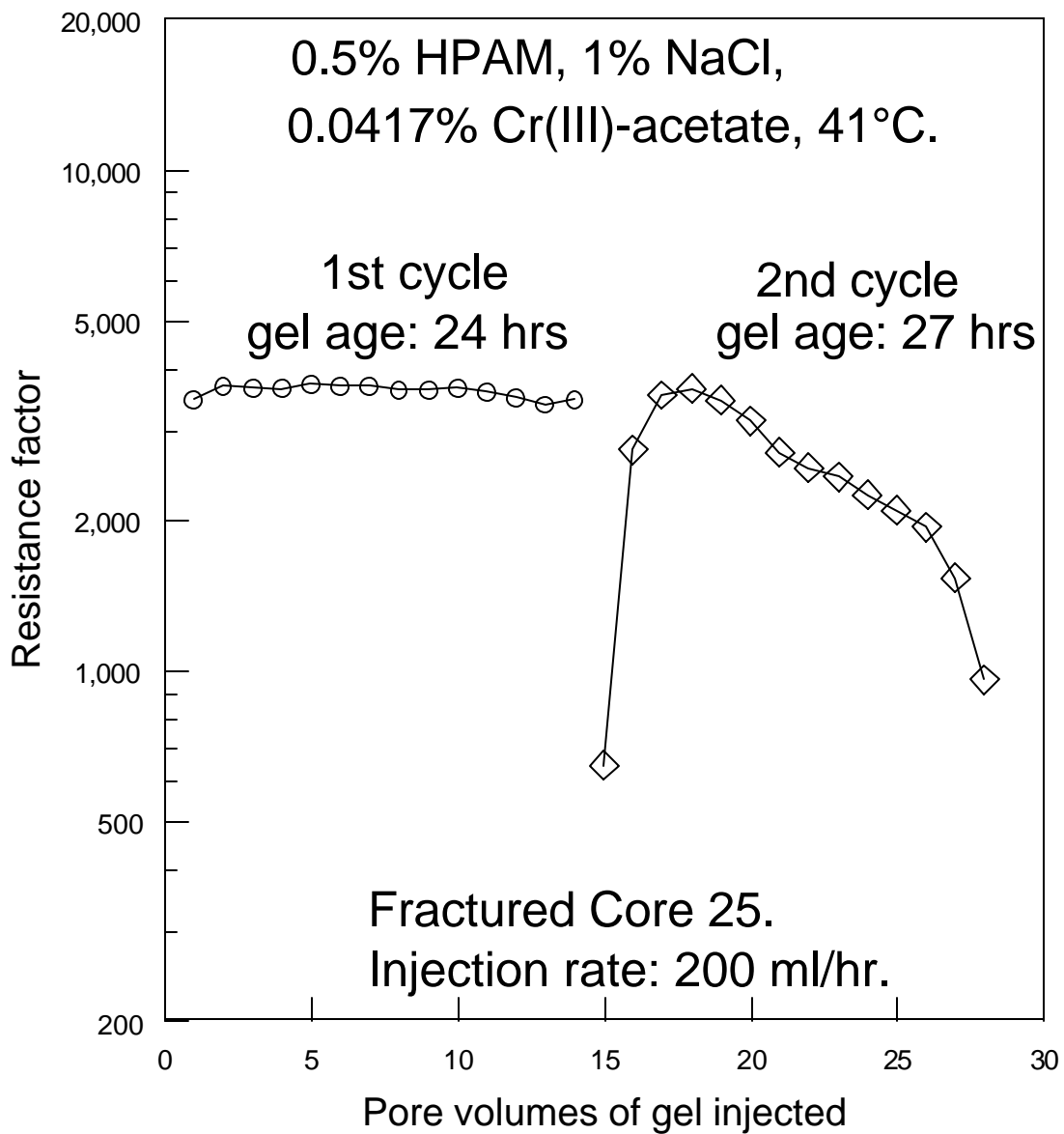


Fig. 47. Resistance factors during the first and second cycles of gel injection.

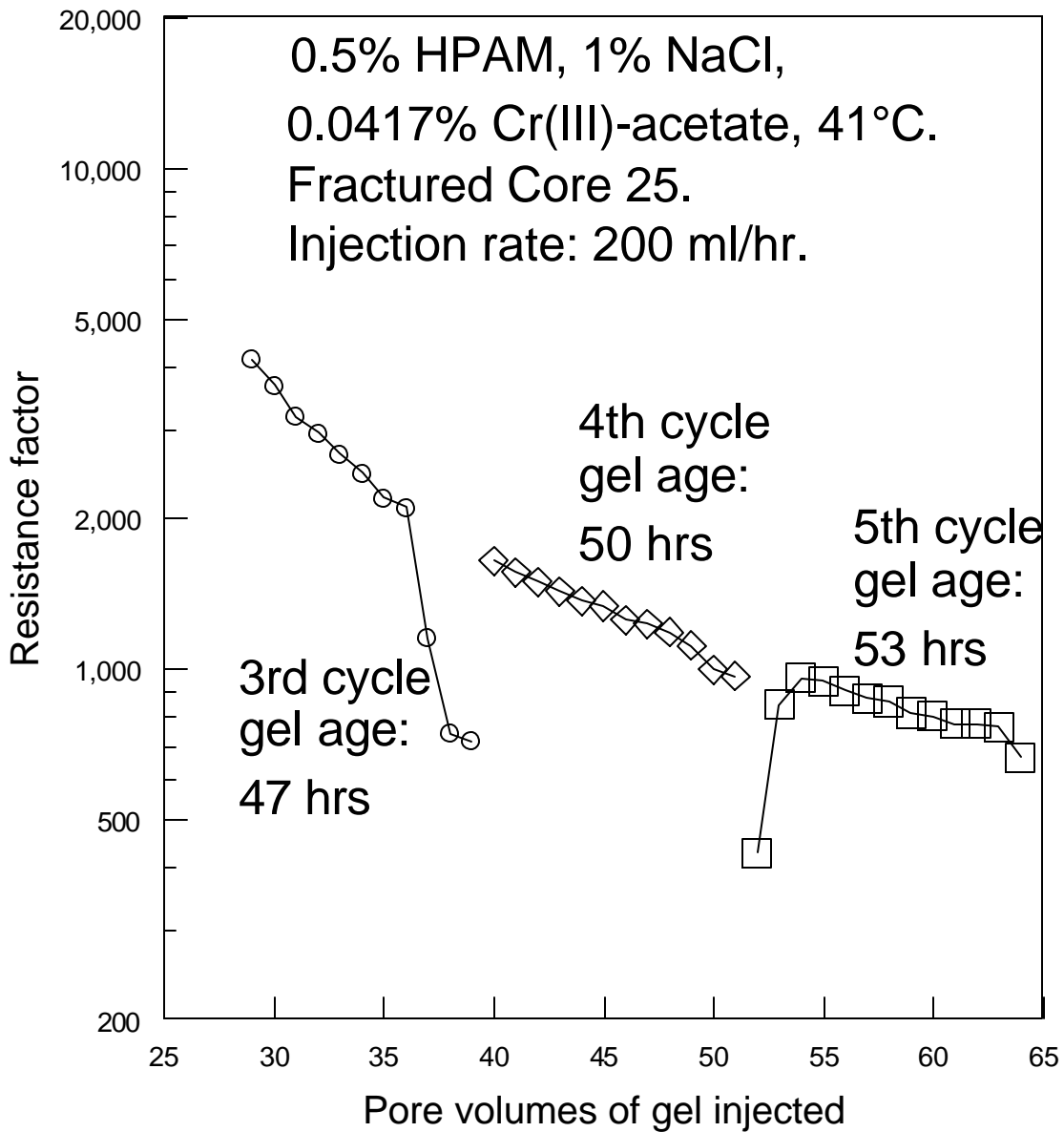


Fig. 48. Resistance factors during the third, fourth, and fifth cycles of gel injection.

Resistance factors during the sixth through eighth cycles of gel injection are shown in Fig. 49. These cycles began 71, 74, and 76 hours after gelant preparation, respectively. Surprisingly, resistance factors during the sixth through eighth cycles were significantly higher (typically having values from 8,000 to 14,000) than those observed in the first through fifth cycles. Based on the resistance factors, degradation was not evident during the last three cycles. Further work is required to explain these results.

The final throughput value associated with recycling the gel through the core was 92 PV. Obviously, some fluid losses occurred during each cycle (mostly while refilling the pump between cycles).

After injecting the gel, the core was shut in for 5 days. Then, the inlet and outlet endcaps were removed, and gel was scraped from flow lines and the inlet and outlet rock faces. The endcaps were then repositioned, and brine was injected. The residual resistance factor was about 1,250 after injecting 8 PV of brine. Finally, a tracer study was performed. Results from this tracer study are shown by the open circles in Fig. 50. For comparison, tracer results are also shown for the fractured core (dashed curve) before gel injection and for an unfractured core (asterisks). Interestingly, the tracer curve after gel injection suggests that the fracture was largely still open after the gel treatment (because tracer breakthrough occurred very early). Also, the long "tail" on this tracer curve indicates that the gel reduced the flow capacity of the rock as much or more than it reduced the flow capacity of the fracture.

In summary, the results reported in this section indicate that injected gels can experience significant mechanical degradation during extrusion through fractures. However, additional work is needed to understand the amount of degradation as a function of time and distance in the fracture. Work is also needed to understand how degraded gels damage porous rock.

Recycling of a Cr(III)-Acetate-HPAM Gel Through a Series of Fractured Cores

During the experiments that were reported in the previous section, we were concerned that results obtained using a short fracture might be different than those using longer fractures. Therefore, we repeated the above experiment using five fractured cores that were connected in series. The dimensions and composition of these cores were the same as those described in the previous section. Properties of these fractured cores are listed in Table 11. These five cores were connected by short tubing, and pressure drops were monitored continuously across each core. Fracture conductivities ranged from 45.9 to 122.2 darcy-cm. The two cores with the most similar fracture conductivities (Cores A and E) were placed first and last in the sequence, respectively. Coincidentally, these fractures were the most conductive of the group. The core with the least conductive fracture (Core D) was placed fourth in the sequence.

The composition of the Cr(III)-acetate-HPAM gel was the same as that described earlier. A 24-hr delay occurred between gelant preparation and the first gel injection. Throughout this experiment, an injection rate of 200 ml/hr was used. Fig. 51 shows resistance factors vs. PV of gel injected for each of the five cores during the first injection cycle. In this cycle, 14 PV or 440 ml of gel were injected. In the figures in this section, a PV refers to the pore volume of one of the five cores (?31 ml). This value was used instead of the combined pore volume of the cores (157 ml) so that comparison with our other results would be easier. Note that the volume associated with a fracture in a given core was less than 0.05 PV or 1.5 ml.

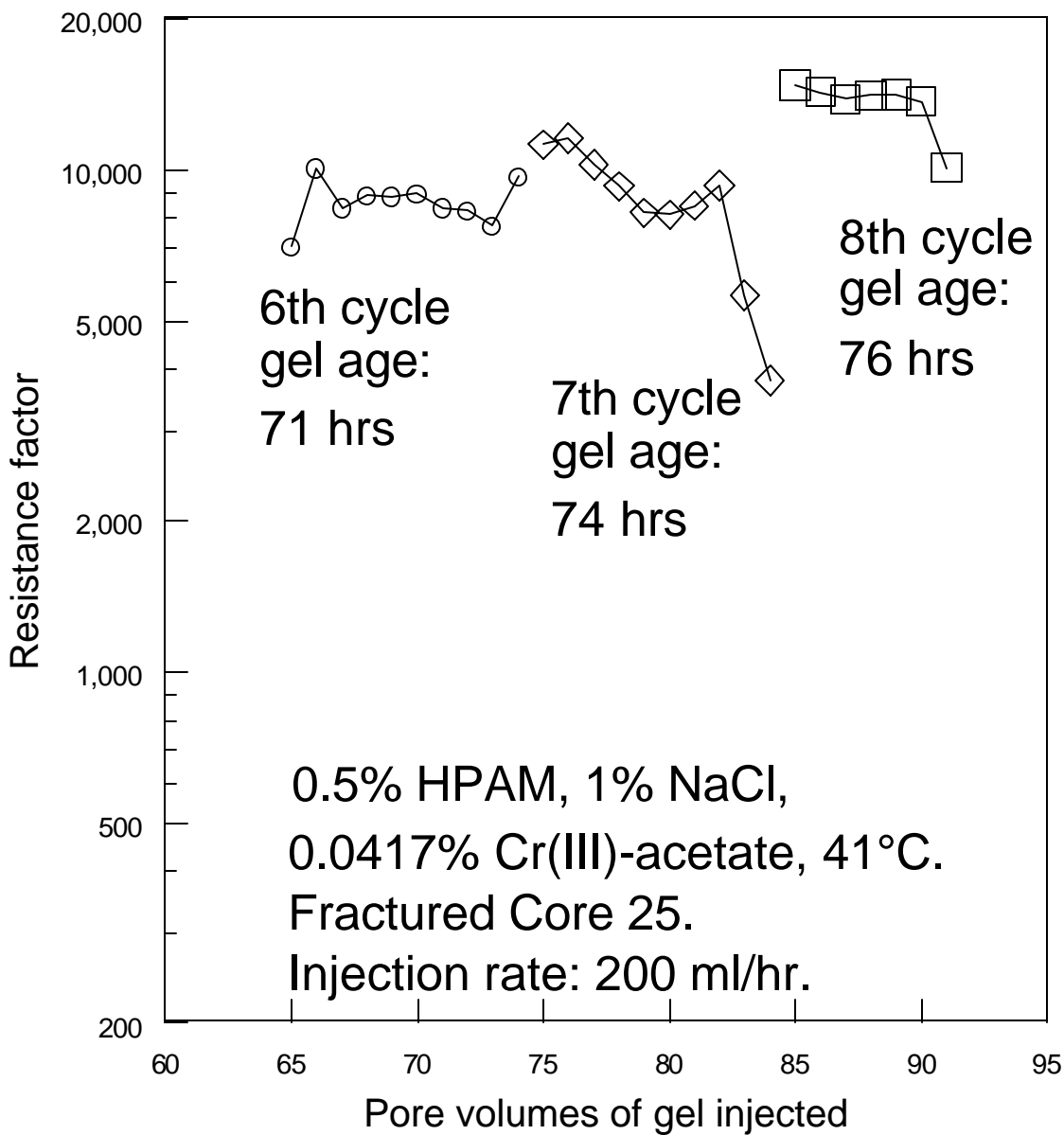


Fig. 49. Resistance factors during the sixth, seventh, and eighth cycles of gel injection.

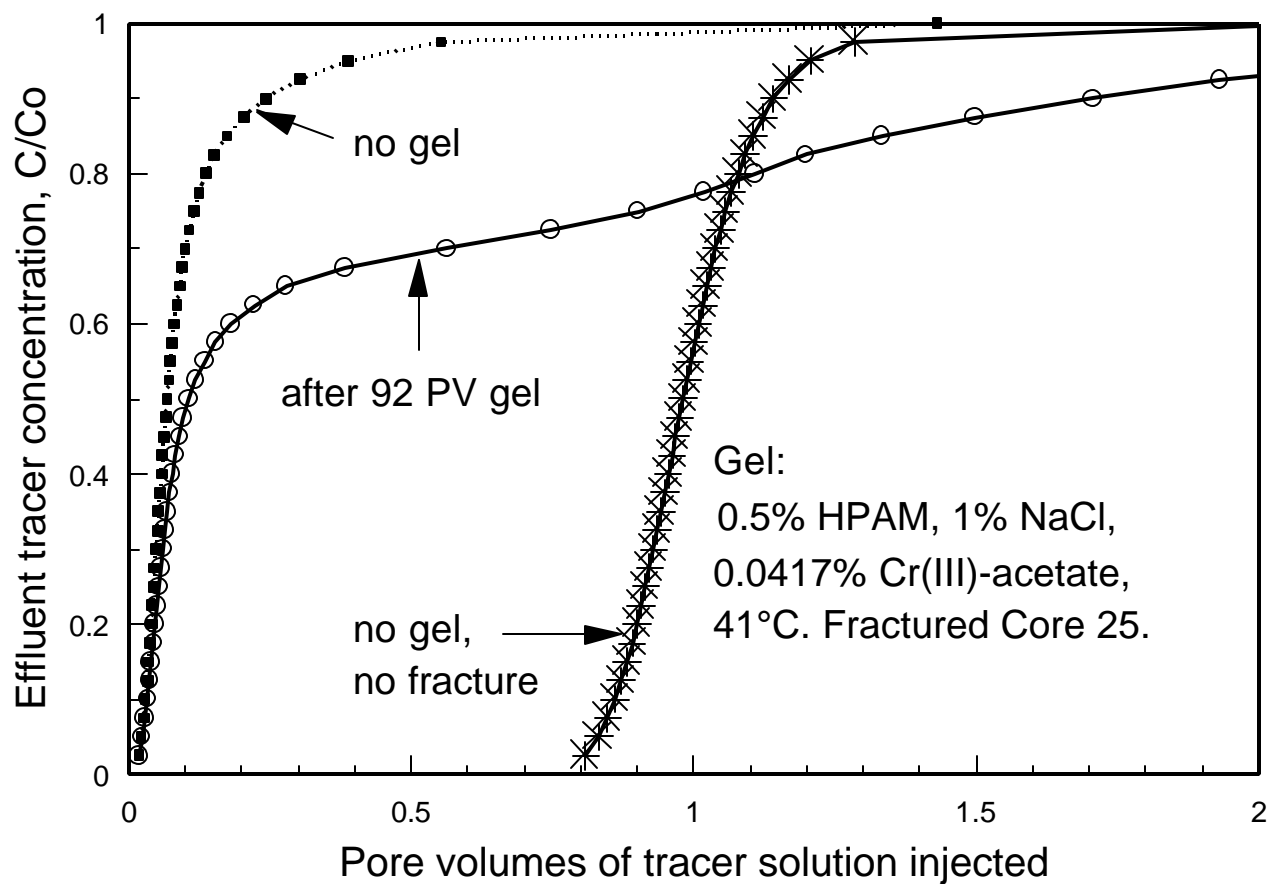


Fig. 50. Tracer results before vs. after placement of a Cr(III)-acetate-HPAM gel in Fractured Core 25.

Table 11. Properties of Fractured Cores Mounted in Series

Position in the sequence	Core	k_{av} darcys	k_{fwf} darcy-cm	$k_{fwf}h_f/Ak_m$
1	A	44.4	122.2	67.3
2	B	31.0	84.7	46.6
3	C	27.4	74.7	41.1
4	D	17.1	45.9	25.3
5	E	43.7	120.2	66.2

After injecting 14 PV of gel, resistance factors were fairly stable in each of the five cores (Fig. 51). This result indicates that fracture plugging was not significant during the first injection cycle. After 14 PV, the highest resistance factor (2,188) occurred in the first core (Core A), while the lowest resistance factor (1,468) was observed in the last core (Core E). The ordering of the curves in Fig. 51 suggests that mechanical degradation may have caused the decrease in resistance factors through the sequence of cores.

We discarded the first 150 ml (5 PV) of effluent from the first cycle since the gel in this effluent was diluted with water that originally saturated the flow lines, cores, and fractures. The remaining 9 PV of gel effluent were recycled through the cores 11 more times.

Resistance factors during the first and second cycles of gel injection are shown in Fig. 52. During the second cycle, resistance factors were typically 20% to 40% less than those at the end of the first cycle. Resistance factors in the second, fourth, and fifth cores (Cores B, D and E) were stable at about 1,000 through injection of 9 PV of gel in Cycle 2. Resistance factors in the first and third cores (Cores A and C) were typically 70% to 80% greater than those in the other three cores.

Table 12 lists resistance factors for each core at the end of each of the 12 cycles. Table 12 also lists the total PV throughput at the end of each cycle, the gel age at the beginning of each cycle, and the equivalent feet of fracture traversed by the gel at the end of each cycle. Through 12 cycles, the total gel throughput was equivalent to 110 PV or 3,450 ml. The equivalent length of fracture was 28.9 ft. Injection of the twelve cycles of gel required approximately 24 hrs.

In Table 12, six data values are missing. During Cycle 9, three values were missed because they were not downloaded from the data acquisition system. One value was missed during each of Cycles 10, 11 and 12 because the pressures exceeded the scale of the transducers.

Resistance factors through the 12 cycles are plotted in Figs. 53 and 54. Fig. 53 plots resistance factors for the first, third, and fifth cores (Cores A, C, and E), while Fig. 54 plots resistance factors for the second and fourth cores (Cores B and D). Frequently, resistance factors in a given core were greatest at the beginning of a cycle and decreased throughout the cycle. We noted this behavior in some of our previous work (see Figs. 47 and 48). Additional work will be needed to determine why this decrease occurs.

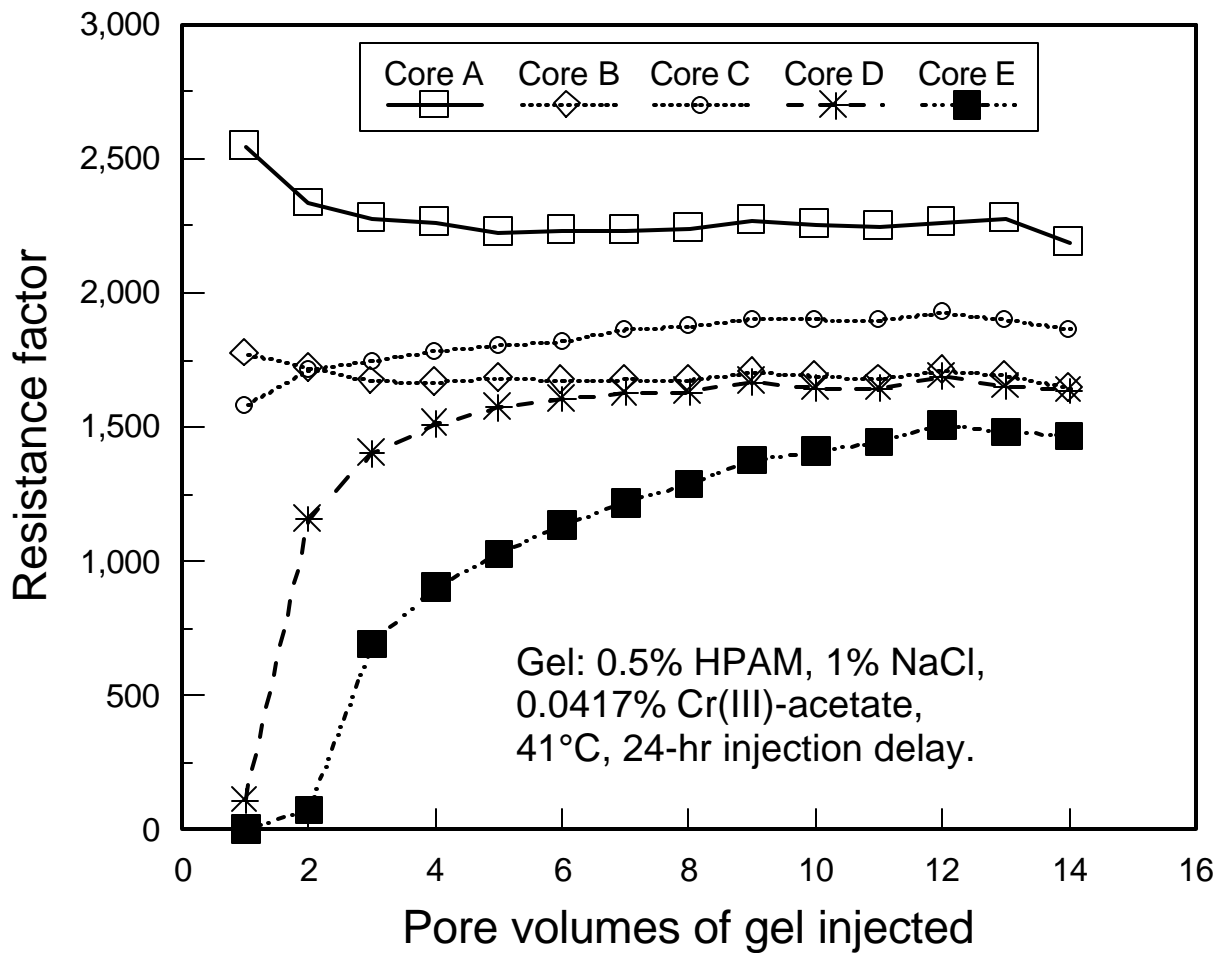


Fig. 51. Resistance factors during the first cycle of gel injection into a series of five fractured cores.

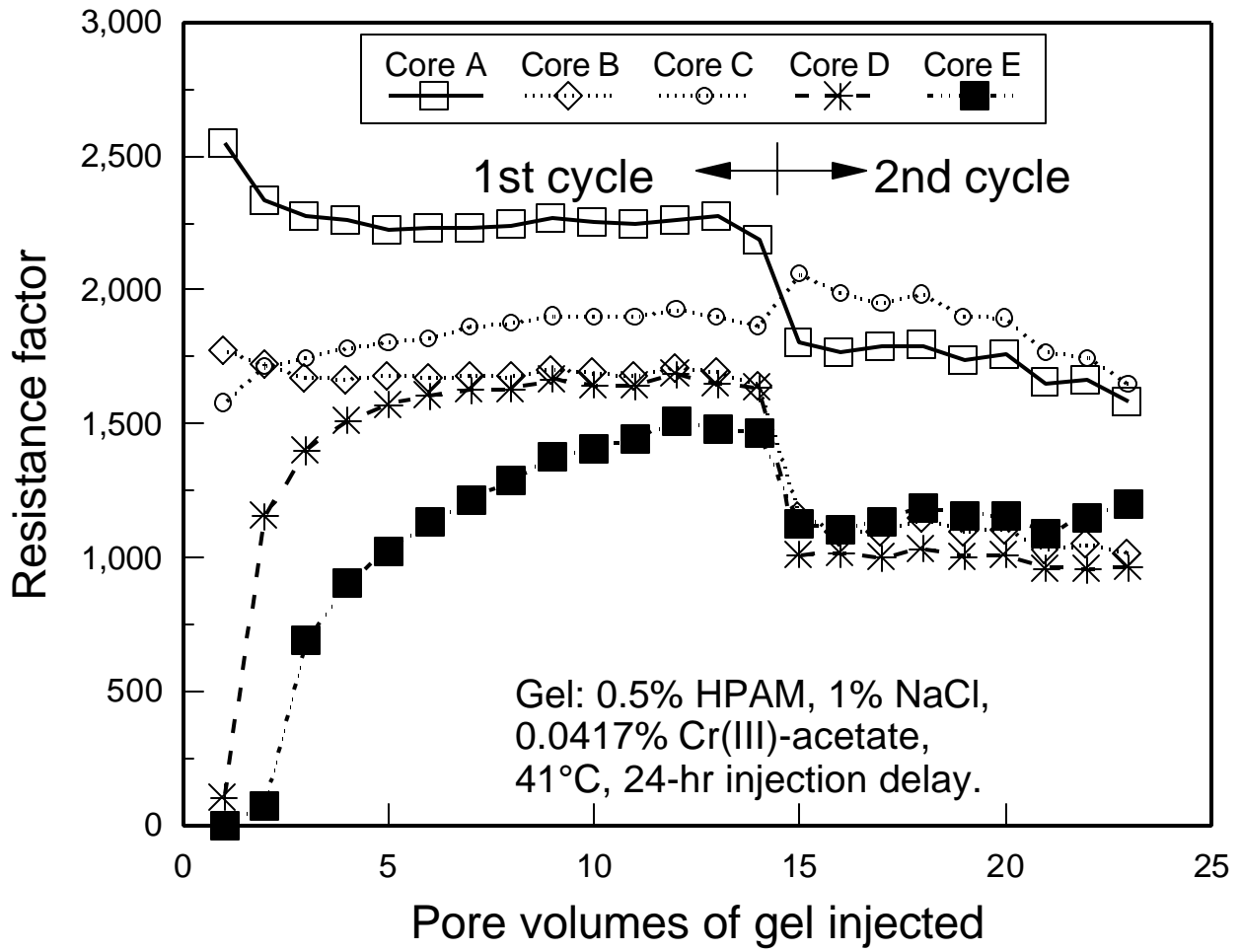


Fig. 52. Resistance factors during the first two cycles of gel injection into five fractured cores.

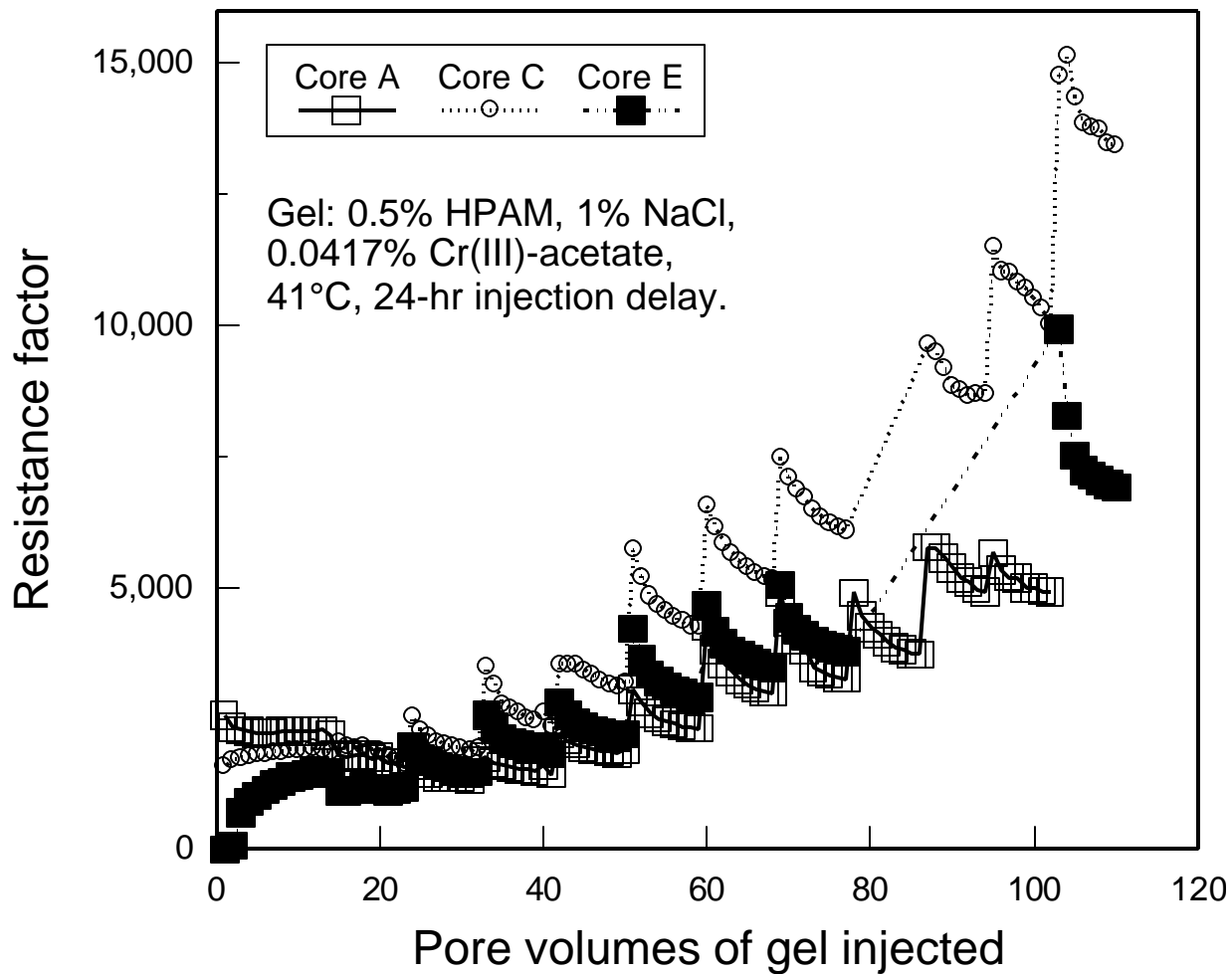


Fig. 53. Resistance factors in the first, third, and fifth fractured cores through 12 cycles (110 PV or 3450 ml) of gel injection.

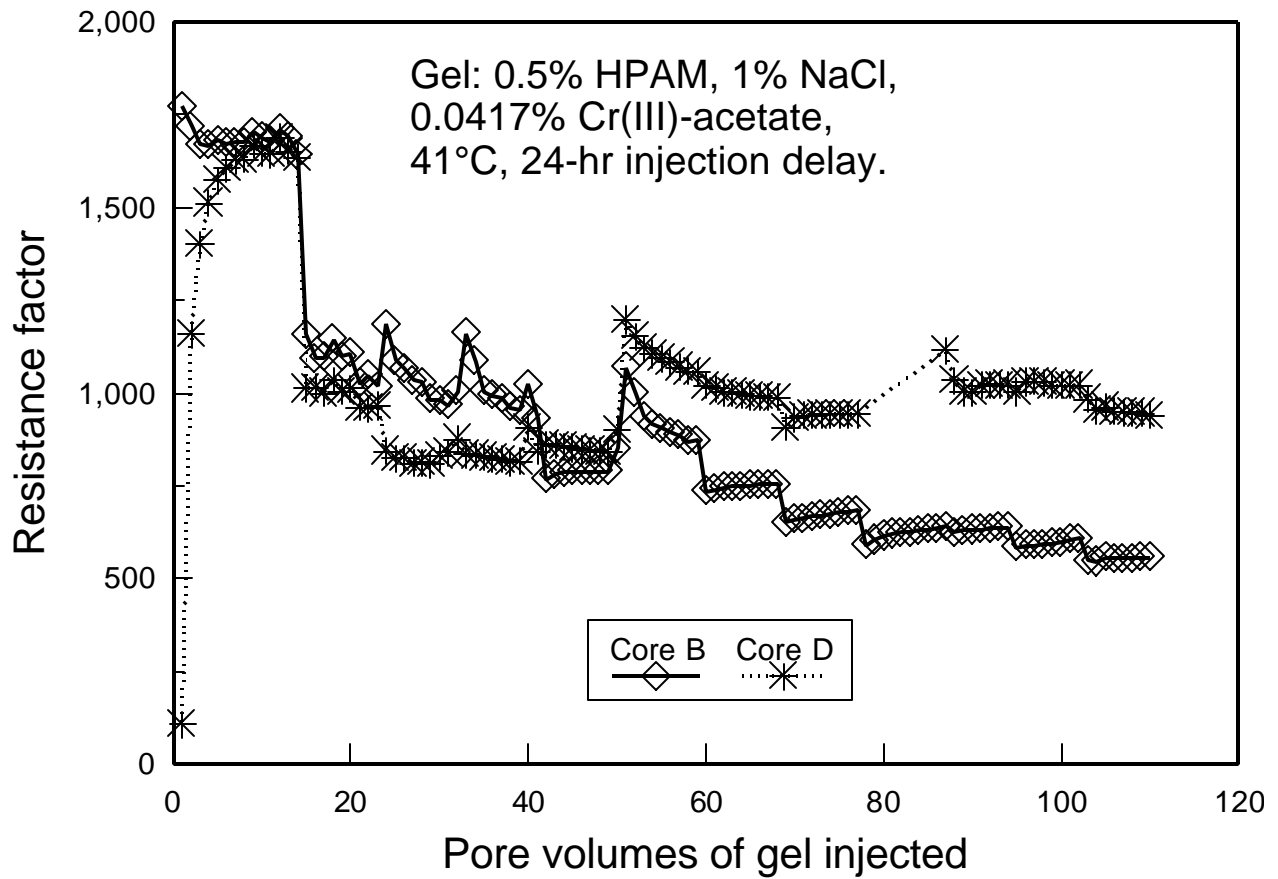


Fig. 54. Resistance factors in the second and fourth fractured cores through 12 cycles (110 PV or 3450 ml) of gel injection.

Table 12. Resistance Factors During Gel Injection into a Series of Five Fractured Cores

				Core A	Core B	Core C	Core D	Core E
$k_f w_b$, darcy-cm				122	85	75	46	120
Cycle	PV	Gel age, hrs	Equivalent feet of fracture	Resistance factor at the end of the cycle				
1	14	24	2.4	2,188	1,644	1,865	1,635	1,468
2	23	27	4.8	1,582	1,017	1,646	965	1,205
3	32	29	7.2	1,674	1,004	1,919	876	1,479
4	41	31	9.6	1,435	931	2,349	843	1,823
5	50	33	12.0	1,900	850	3,203	900	2,197
6	59	35	14.4	2,302	871	4,233	1,055	2,897
7	68	37	16.8	2,993	754	5,142	988	3,459
8	77	39	19.2	3,256	682	6,089	943	3,780
9	86	41	21.7	3,717	636			
10	94	43	24.1	4,906	638	8,701	1,022	
11	102	45	26.5	4,919	609	10,013	1,022	
12	110	47	28.9		556	13,440	940	6,908

In Cores A, C, and E, the average resistance factor generally increased with each cycle (Fig. 53 and Table 12). The increase was most dramatic for the third core in the sequence (Core C)—from 1,646 after Cycle 2 to 13,440 after Cycle 12. The second most dramatic increase was associated with the last core (Core E)—from 1,205 after Cycle 2 to 6,908 after Cycle 12. Ironically, the first core (Core A) experienced a smaller increase than those for Cores C and E. One might expect the first core in the sequence to experience the greatest degree of plugging. Alternatively, one might expect the least conductive fracture (in Core D) to exhibit the most plugging. A comparison of Figs. 53 and 54 reveals behavior contrary to these expectations. Table 12 and Fig. 54 show that resistance factors in Core D were more or less the same from Cycle 2 through Cycle 12. Resistance factors in Core B decreased from 1,017 after Cycle 2 to 556 after Cycle 12.

After gel injection, the core was shut in for 4 days. Then, the inlet and outlet endcaps were removed, and gel was scraped from flow lines and the inlet and outlet rock faces. On the inlet face of each core, we found a rigid layer of gel about 1/16-inch thick. For Cores B through E, no differences were apparent among the gel layers on the core; they all appeared to have a Sydansk gel strength code¹⁴⁹ of I. The gel layer on the inlet face of Core A appeared more densely packed and rigid than those for the other four gels. In all five cases, the gel layer was significantly more rigid than the final gel effluent from the cores (Sydansk gel code B), and it was more rigid than a 5-day-old gel that remained quiescent in a bottle at 41°C (Sydansk gel code E). This result suggests that during gel injection, polymer or gel filtration occurred at the inlet sandface of each of the five cores.

After removing gel from the flow lines, the endcaps were repositioned, and brine injection commenced

at 200 ml/hr. Fig. 55 shows residual resistance factors for the five cores during injection of 56 PV (1,760 ml) of brine. The residual resistance factors were fairly stable for Cores B, D, and E—averaging 84, 78, and 120, respectively. For Cores A and C, residual resistance factors exhibited a small, steady decrease. During injection of 56 PV of brine, values averaged 2,800 and 9,700 for Cores A and C, respectively.

In all five cores, the residual resistance factors were significantly higher than the corresponding $k_{wf}h_f/Ak_m$ values before gel injection (compare Fig. 55 and Table 11). For Cores B, D, and E, residual resistance factors were roughly 2 to 3 times greater than the corresponding $k_{wf}h_f/Ak_m$ values. This result suggests mild damage to the flow capacity of the porous rock (probably primarily at the injection sand faces). In contrast, for Cores A and C, the resistance factors were 42 and 236 times greater than the corresponding $k_{wf}h_f/Ak_m$ values. This result suggests severe damage to the flow capacity of the porous rock in these cores.

Finally, tracer results were performed for all five cores. These results are shown in Fig. 56. For comparison, tracer results are also shown for an unfractured core (asterisks) and for a fractured core before gel injection (dashed curve). The tracer results indicated that Cores B, D, and E were healed fairly effectively by the gel treatment. We note that these three cores showed the lowest residual resistance factors during brine injection after gel placement (Fig. 55). In contrast, the gel treatment provided the least improvement in sweep efficiency (open squares and circles in Fig. 56) and the highest residual resistance factors (Fig. 55) in Cores A and C. We noted that gel accumulation and plugging at the inlet faces of Cores A and C resulted in extremely high pressure gradients in these cores during gel injection. These high pressure gradients may have forced gel a short distance into the porous rock of the cores, so that gel damage could not be effectively removed by simply scraping gel from the sandfaces. Consequently, the porous rock was permanently damaged by the gel treatment.

After the experiments were completed, all five cores were dismantled. Gel was not observed on any of the inlet or outlet rock faces, except at the fracture. Gel protruded about 1 mm from the fracture on the inlet rock face of all five cores. No gel protrusion was seen at the fracture outlet.

Next, the fractured cores were pulled apart to examine the fracture faces. In all cases, the gel adhered to the fracture faces. No obvious differences occurred among the fractures that would explain why some of the fractures experienced plugging while others did not. All five sets of fracture faces had about the same degree of surface roughness, and the density of iron specs were the same in all cases. The core with the least conductive fracture (Core D) had a small streak with a high density of iron specs crossing the width of the fracture faces.

The gel in the fracture generally had the same width and texture in all five fractures. The gel (Sydansk gel code I) was generally slightly thicker in the inlet half of a given fracture than at the outlet half of the fracture. In Cores C and E, streaks of slightly thicker gel (with a more gray or purple-gray color than the normal clear color) were noted in some parts of the core, but these generally corresponded to small regions where the fracture was locally wider than normal. The outlet half of the fracture in Core B contained gel that was less rigid than in other fractures. Additional work is needed to determine why the gel heals some fractures more effectively than others.

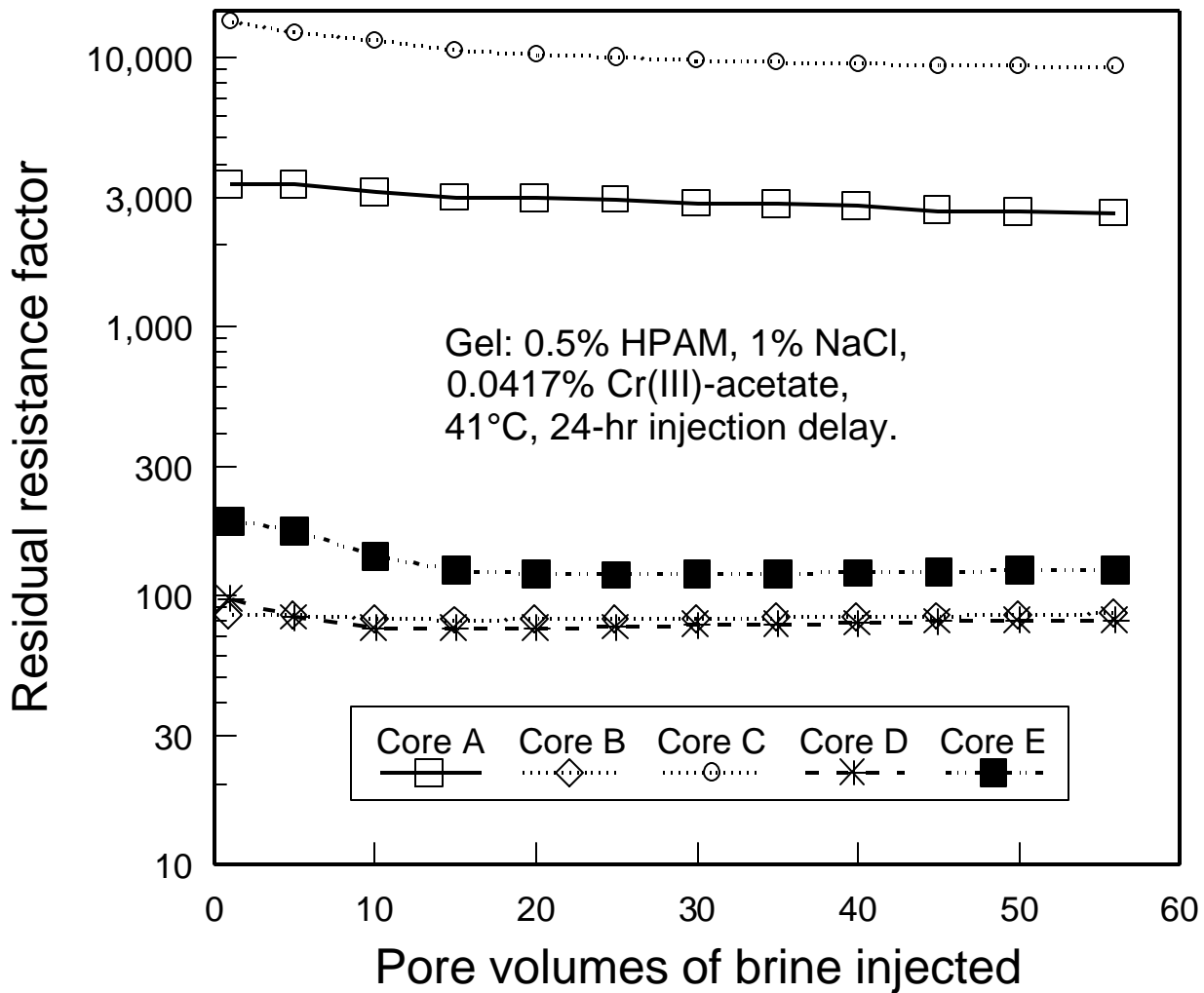


Fig. 55. Residual resistance factors during brine injection into five fractured cores.

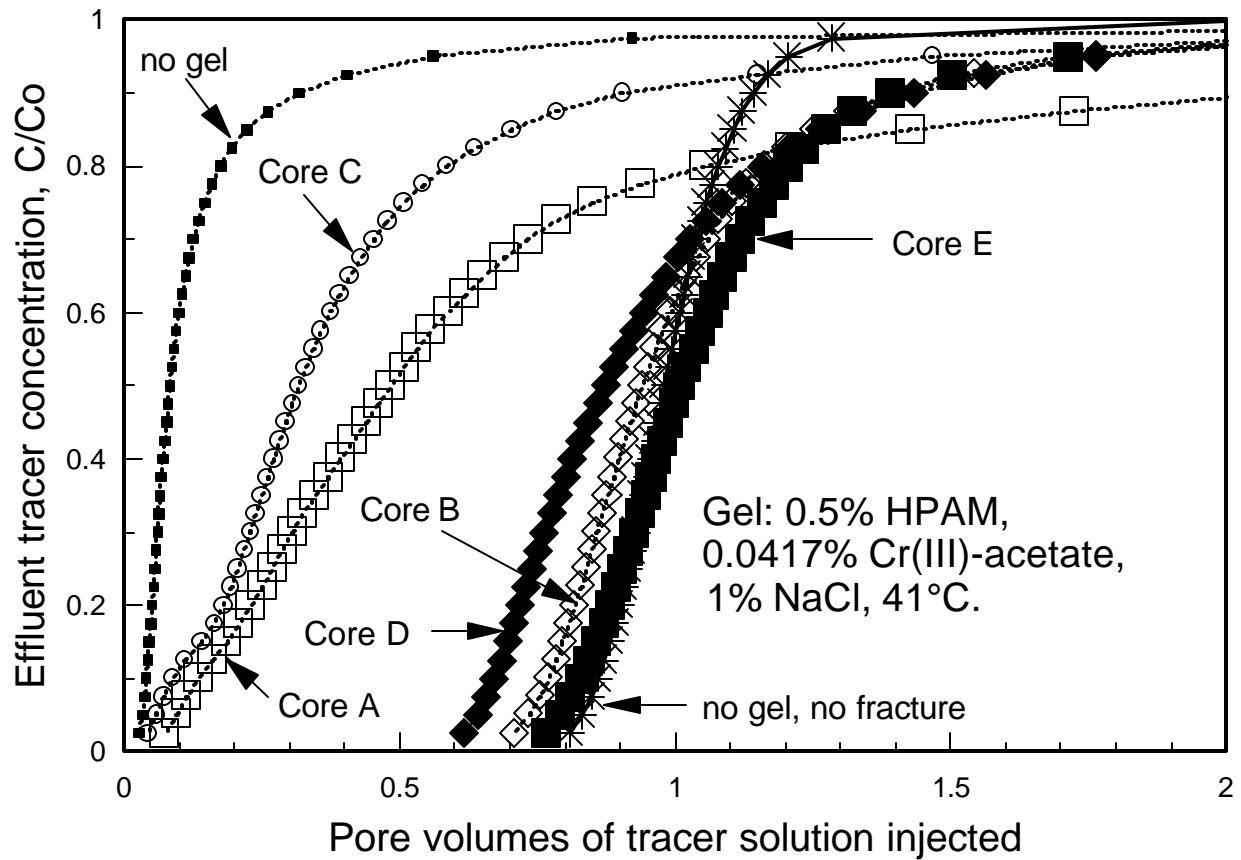


Fig. 56. Tracer results after gel placement for Fractured Cores A, B, C, D, and E.

Conclusions

1. For Cr(III)-acetate-HPAM gels that were aged 10, 24 and 72 hrs before injection into short fractured cores, gel treatments effectively healed the fractures without damaging porous rock. However, using a gel that was aged only 5 hrs (the gelation time for the gelant), a gel treatment had no significant effect on a fracture. For the latter case, the gel apparently washed out from the core during brine injection after gel placement.
2. For Cr(III)-acetate-HPAM gels that were aged 24 hrs before injection (at 200 ml/hr), gel resistance factors were typically about 3,000 in fractures with conductivities ranging from 53.8 to 1,560 darcy-cm. This result suggests that resistance factors may be independent of fracture conductivity for a gel with a fixed velocity and a fixed degree of gelation or curing. Also, during gel injection, the pressure gradient may be inversely proportional to the fracture conductivity.
3. For hydroquinone-hexamethylenetetramine-HPAM gels that were aged for 1 day or more at 110°C, these gels effectively healed fractures at 41°C, but they exhibited high resistance factors and pressure gradients during injection. For gels that were aged for 0.5 to 0.75 days at 110°C, low resistance factors and pressure gradients were observed during injection, but the gel treatments did not improve sweep efficiency in the fractured cores.
4. A 5-day-old mechanically blended (sheared) Cr(III)-acetate-HPAM gel exhibited lower than usual resistance factors and pressure gradients in a fractured core. Although this gel treatment did not heal the fracture, it did significantly improve sweep efficiency.
5. Experiments were performed where Cr(III)-acetate-HPAM gels were recycled through a single fractured core and through a series of fractured cores. In these experiments, the gel showed plugging behavior in some cores but not in others. The plugging behavior did not correlate with fracture conductivity or with fracture position in a series of fractured cores. Additional work is needed to determine why the gel heals some fractures more effectively than others.

8. GEL PLACEMENT IN ANISOTROPIC FLOW SYSTEMS

In Ref. 18, mathematical models were used to examine the degree of gelant penetration and injectivity loss in zones with different permeabilities. Equations were derived for the distance of gelant penetration into a less-permeable layer when the fluid penetrated a given distance in the most-permeable layer. In that paper, two cases were considered: one for a linear flow geometry (e.g., fractured wells) and the other for a radial flow geometry (e.g., unfractured wells). The paper concluded that if zones are not isolated during gelant injection, a satisfactory placement for the blocking agent is far more likely to occur in a linear flow geometry than in a radial flow geometry.

In the mathematical models described in Ref. 18, permeability within a given layer was assumed to be homogeneous. In a real reservoir, the distribution of rock properties may be heterogeneous areally as well as vertically. For example, a reservoir may have a larger permeability in one direction than in another direction (i.e., the reservoir may be anisotropic).

Anisotropic reservoirs can be viewed as flow geometries that are intermediate cases between linear and radial flow. In fact, a linear flow geometry can represent the extreme case of an anisotropic reservoir. The question arises, How anisotropic must an unfractured reservoir be to allow gelant placement to approximate that for the linear flow case? Asked another way, How anisotropic must an unfractured reservoir be to achieve an acceptable gel placement during unrestricted gelant injection? These questions will be addressed here by developing two models of simple anisotropic flow systems and by performing sensitivity studies with these models.

Models Used

To illustrate how areal flow profiles in an anisotropic reservoir are modified by a gel treatment, two circular theoretical reservoir models were used. Model 1 was established in a Cartesian coordinate system by aligning the x -axis with the most-permeable direction while aligning the y -axis with the least-permeable direction. The origin coincided with the center of the reservoir. An injection well was located in the center of the reservoir, and flow was produced at the outer boundary of the reservoir. Both the injection well and the outer boundary of the reservoir were assigned a constant pressure.

In Model 2, an isotropic reservoir having the same dimensions was considered. The pressure distribution was symmetrical about both the x -axis and the y -axis, and only the injection well was assigned a constant pressure. The reservoir experienced the largest pressure drop in the x -direction while the smallest pressure drop occurred in the y -direction.

Analysis Using Model 1

Streamlines. In Model 1, both the inner boundary (injection wellbore) and the outer drainage boundary are circular equipotential lines. Therefore the equipotential curves in the drainage area should also be concentric circles. Since streamlines are always perpendicular to the equipotential curves, the streamlines in the drainage area must be radial. Therefore, the key to the solution of this problem is to determine an expression for the permeability distribution and the relationship between the distance of gelant penetration and the fluid and reservoir properties.

Permeability Distribution. Permeabilities in any radial direction between the x -axis and the y -axis are

given by the following equation:

$$k_i = \frac{1}{\frac{\cos^2 \theta_i}{k_x} + \frac{\sin^2 \theta_i}{k_y}} \quad (37)$$

where

- k_x = permeability in the most-permeable direction (x-direction), md
- k_y = permeability in the least-permeable direction (y-direction), md
- k_i = permeability in a given radial direction, md
- θ_i = the angle between the considered radial direction and the x-axis

Eq. 37 is derived in Appendix B.

Areal Flow Profile During Gelant Injection. Eq. 38 can be used to find the distance of gelant penetration in any radial direction.

$$\frac{\theta_i}{k_i} \frac{1}{r_{pi}^2} F_r \ln \frac{r_{pi}}{r_w} + \ln \frac{r_e}{r_{pi}} + \frac{1-F_r}{2} \frac{1}{r_w^2} \ln \frac{r_e}{r_w} + \frac{1-F_r}{2} \frac{1}{r_w^2} = \text{constant} \quad (38)$$

where

- r_w = radius of the injection wellbore, ft
- r_e = radius of the outer boundary, ft
- r_{pi} = distance of gelant penetration in a given radial direction i , ft
- F_r = resistance factor (brine mobility before gelant placement divided by gelant mobility)
- f_i = effective porosity in radial direction i

The derivation of Eq. 38 is given in Appendix C and is based on the following assumptions:

1. Fluids are incompressible and Newtonian.
2. The displacement is miscible and piston-like.
3. Dispersion and adsorption are negligible.
4. The pressure drop between the injection well and the outer boundary is constant.
5. Only aqueous fluids are mobile in the reservoir.
6. The drainage area is circular.
7. The resistance factor is independent of permeability.
8. The displacing fluid and the displaced fluid have the same effective permeability.
9. Gravity effects are negligible.

The areal flow profiles of the gelant front when gelant reaches the outer boundary in the x-direction are shown in Fig. 57, which was generated using the following parameters: (1) $r_w=1/3$ ft, (2) $r_e=50$ ft, (3) $f_i=0.2$, and (4) $F_r=1$. Fig. 57 shows that, as expected, the areal flow profile in this anisotropic reservoir becomes less favorable as k_x/k_y increases.

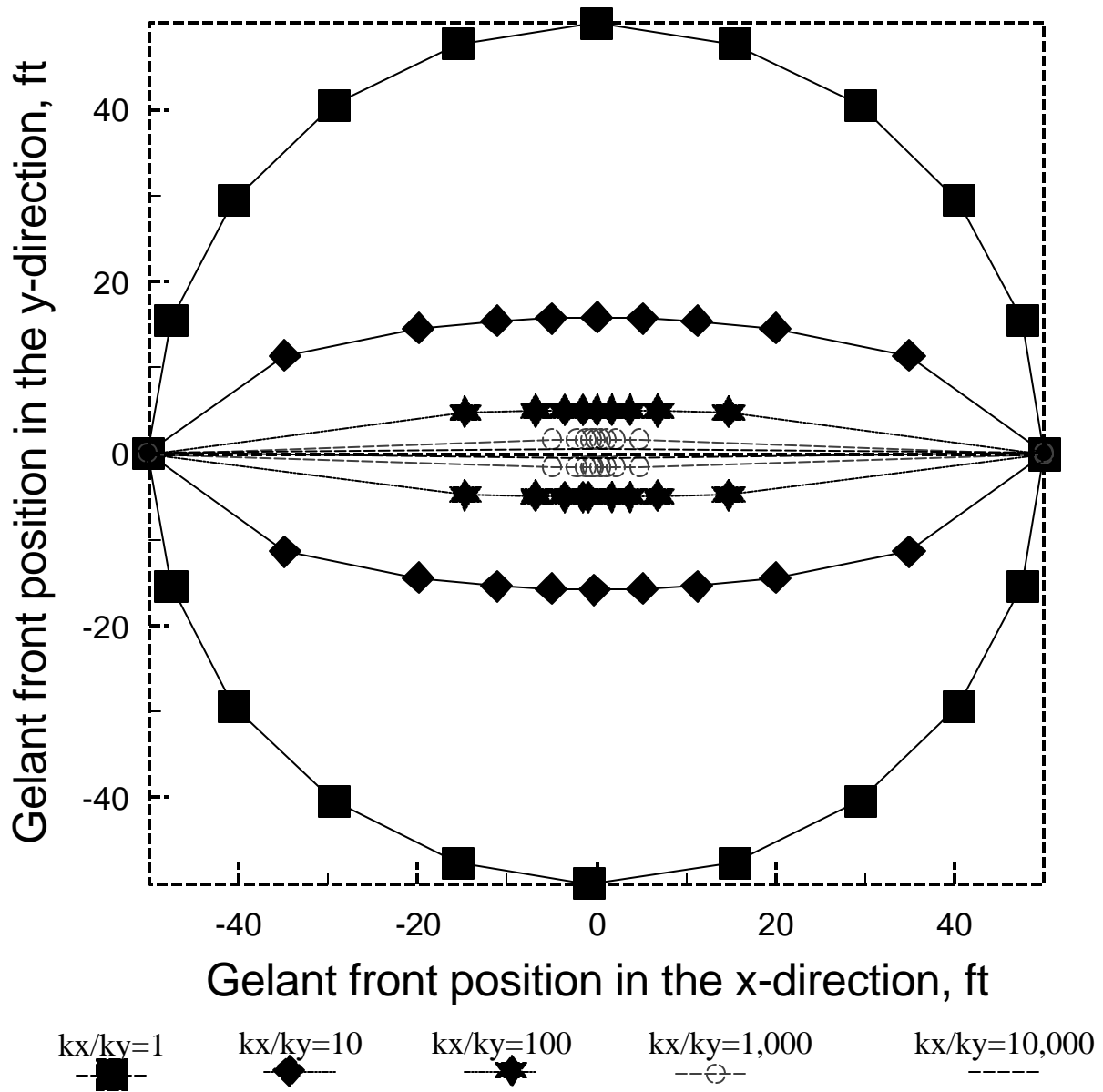


Fig. 57. Plan view of the gelant front. $F_r = 1$.

Effect of Resistance Factor. Fig. 58 plots the degree of gelant penetration (the distance of gelant penetration in direction i divided by the distance of gelant penetration in the x-direction) against permeability ratio (k_x/k_i) when gelant reaches the outer boundary in the x-direction. Fig. 57 shows that:

1. For a given permeability ratio, the degree of gelant penetration, $(r_{pi}-r_w)/(r_{px}-r_w)$, increases with increased resistance factor.
2. For the range of permeability variations investigated ($k_x/k_y \cdot 10^6$), the degree of gelant penetration becomes insensitive to resistance factor for F_r values greater than 100.
3. For a given permeability ratio, the degree of gelant penetration is greater in anisotropic radial flow than in linear flow.

These observations are consistent with those reported in Ref. 18.

Injectivity Expressions. Injectivity loss in a well is a common measure used to judge the success of a "profile modification" treatment. For convenience in the following study, we assume that the resistance factor for gelant is equal to one.

The fluid injectivity, I_{io} , in direction i prior to gelant injection can be found by Eq. 39.

$$I_{io} = \frac{q_{io}}{p_w - p_e} = \frac{?_i h k_i}{141.2 ?_w \ln \frac{?_e}{?_w}} \quad (39)$$

where

- q_{io} = total injection rate before gelant placement, B/D
- p_w = pressure at the injection well, psi
- p_e = pressure at the outer boundary, psi
- h = thickness of the net pay, ft
- μ_w = water viscosity, cp

The fluid injectivity, I_i , in direction i after gelation can be found by Eq. 40.

$$I_i = \frac{q_i}{p_w - p_e} = \frac{?_i h k_i}{141.2 ?_w F_{rr} \ln \frac{?_{rpi}}{?_{rw}} + \ln \frac{?_e}{?_{rpi}}} \quad (40)$$

where

- q_i = total brine injection rate after gel forms, B/D
- F_{rr} = residual resistance factor (brine mobility before gelant injection divided by brine mobility after gelation)

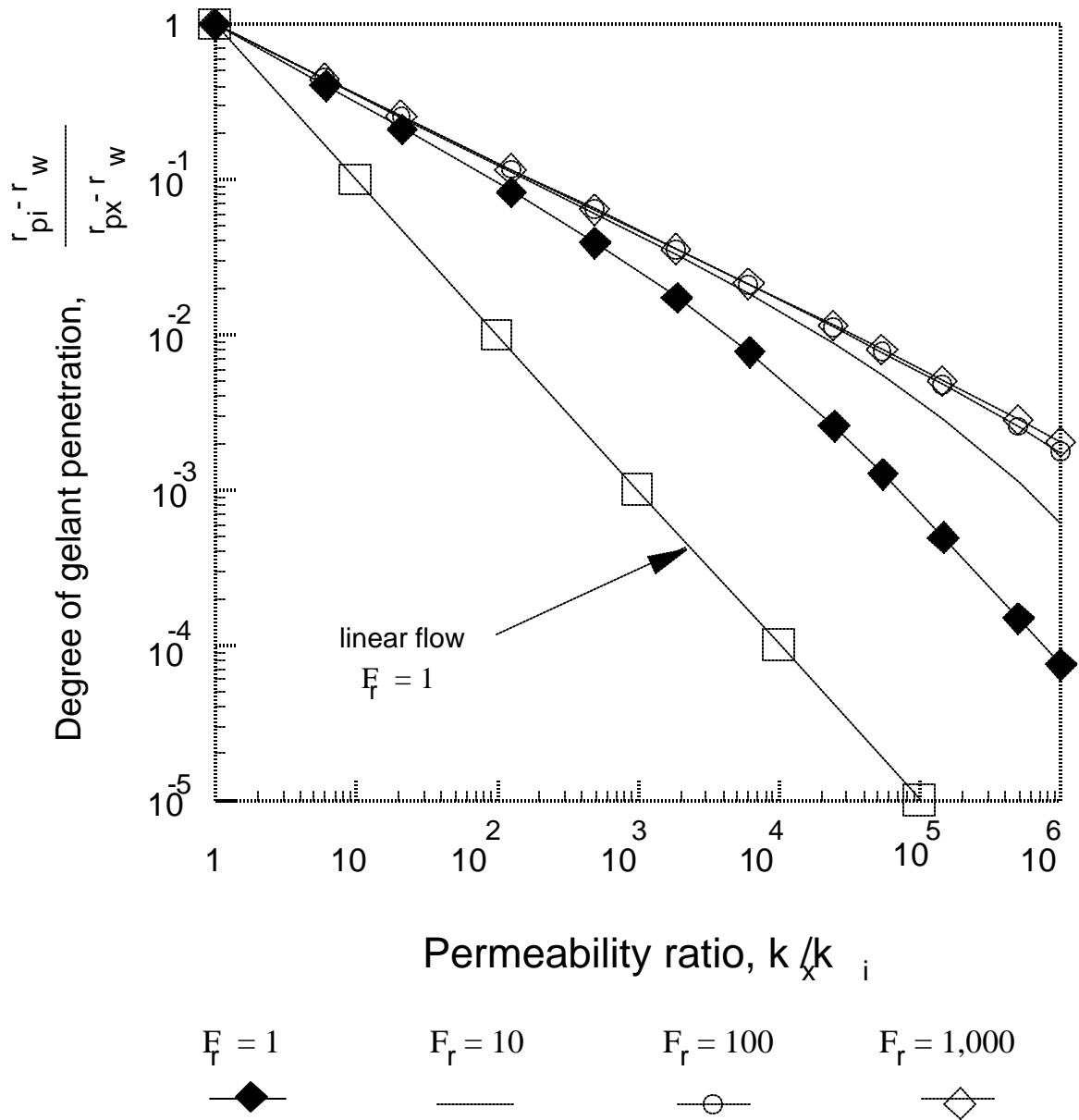


Fig. 58. Degree of gelant penetration in direction i vs. permeability ratio when gelant reaches the outer boundary in the most-permeable direction.

The overall injectivity ratio, I/I_o , or the ratio of the total brine injection rate after gel forms to the total brine injection rate before gelant injection is given by Eq. 41.

(41)

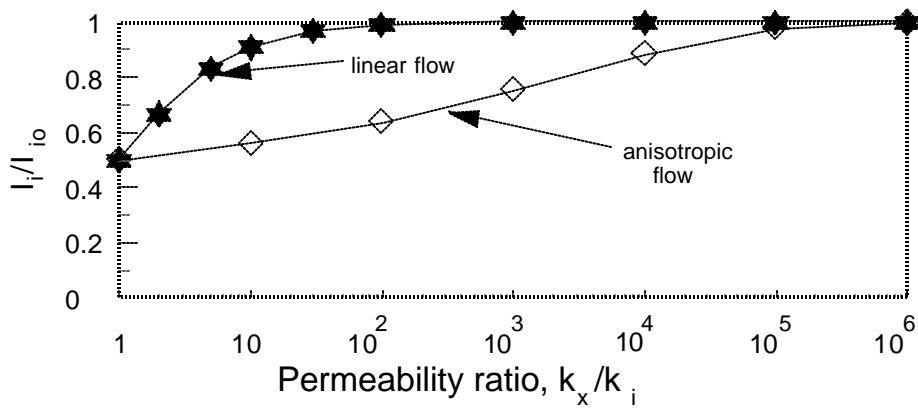
For the derivation of Eqs. 39, 40 and 41, please refer to Appendix D.

Comparison of Linear Flow with Anisotropic Radial Flow. The primary question to be answered in this work is, how anisotropic must an unfractured reservoir be to allow gelant placement and profile modification to approach that associated with a linear flow geometry? Fig. 59 can be used to answer this question. Figs. 59a through 59c plot injectivity ratio vs. permeability ratio for three cases of gel residual resistance factor. The case where $F_r=2$ corresponds to a "weak" gel; the $F_r=100$ case represents a fairly "strong" gel; while the $F_r=10$ case can be associated with a gel of intermediate strength.

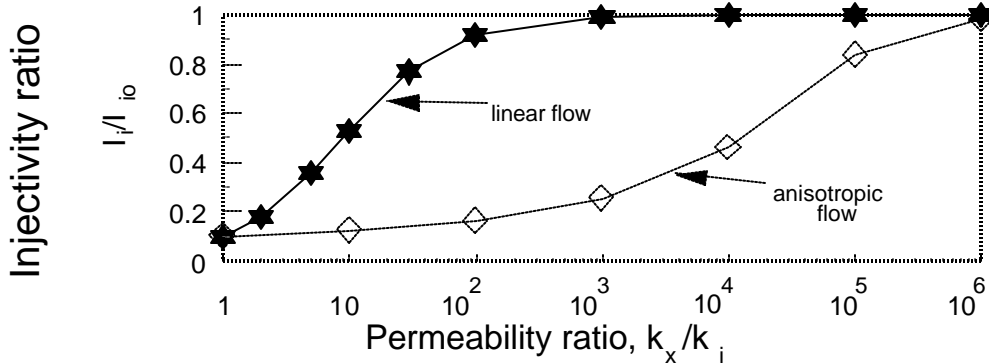
Because linear flow has been shown to provide the most desirable profile modification results,¹ this case will be used as a base case for comparison with profile modification in anisotropic systems. In these comparisons, we assume that the gelant resistance factor is equal to 1 during gelant placement. In Fig. 58 and Ref. 18, the case where $F_r=1$ was shown to provide the best result during gelant placement (i.e., minimum gelant penetration into low-permeability zones and maximum gelant penetration into high-permeability zones).

After gel placement, profile modification can be assessed using the injectivity ratios, I_i/I_{io} , in Fig. 59. This ratio is the brine injectivity in direction i after gel placement divided by that before gel placement. To illustrate the utility of Fig. 59, consider an anisotropic zone that is 10 times more permeable in the x direction than in the i direction (i.e., $k_x/k_i=10$). For a gel with $F_r=2$, Fig. 59a indicates that in the x direction, 50% of the original injectivity will remain after the gel treatment. In the i direction (where $k_x/k_i=10$), 56.5% of the original injectivity will remain after the gel treatment. Ideally, we want the gel treatment to reduce injectivity in the x -direction by a large factor, while having little effect on injectivity in the i -direction. Unfortunately, in our example, the gel treatment improved the flow profile only slightly while reducing injectivity by about 50% in both the x -direction and the i -direction. The benefit from this minor redistribution of fluid flow is unlikely to offset the loss of driving force (injectivity) for displacing oil in the i -direction.

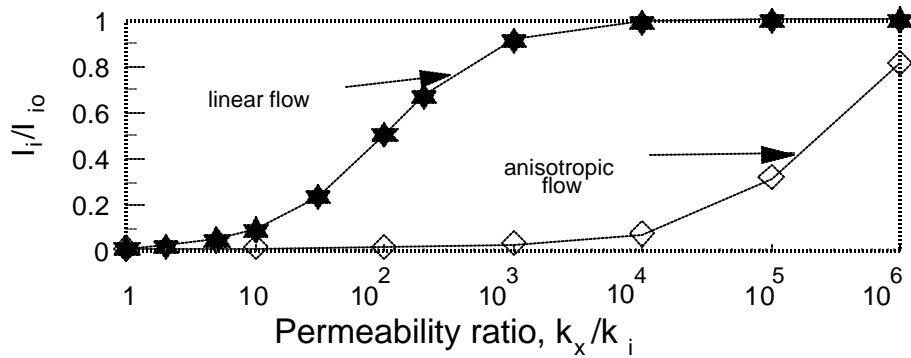
For comparison, consider a similar gel treatment in linear flow (e.g., a fractured well) instead of anisotropic radial flow. Again, we assume that $k_x/k_i=10$ and $F_r=2$. The linear-flow case could be a fracture that cuts through two zones—Zone x with permeability k_x , and Zone i with permeability k_i . From the solid curve in Fig. 59a, in Zone x (where $k_x/k_i=1$), 50% of the original injectivity will remain after the gel treatment. However, in Zone i (where $k_x/k_i=10$), 91% of the original injectivity will remain after the gel treatment. Thus, in linear flow, the gel treatment results in a substantial improvement in the flow profile and a relatively small amount of damage (9% injectivity loss) in Zone i . In contrast, to achieve this same result in anisotropic radial flow, k_x/k_i must be 10,000.



a. $F_{rr} = 2$.



b. $F_{rr} = 10$.



c. $F_{rr} = 100$.

Fig. 59. Comparison of injectivity ratio for linear flow and anisotropic radial flow when $r_{px} = 50$ ft.

Using Figs. 59a through 59c, similar analyses can be performed for different gel residual resistance factors. These analyses show that k_x/k_i must be greater than 1,000 (and usually greater than 10,000) before anisotropy can be exploited to achieve a satisfactory gel placement in unfractured wells. We doubt that any unfractured wells or reservoirs exist with this degree of anisotropy. In contrast, in wells and reservoirs where anisotropic flow is due to fractures, the linear flow geometry and the extreme permeability contrast between the fracture and the porous rock can aid gel placement substantially.^{18,26}

Effect of Distance of Gelant Penetration. In the previous section, the gelant penetrated 50 ft in the x -direction. Using Fig. 60, we examined the sensitivity of profile modification to the distance of gelant penetration. Figs. 60a through 60c plot injectivity ratio vs. permeability ratio for different radii of gelant penetration in the x -direction (r_{px}). Analysis of these figures reveals that for r_{px} values greater than 5 ft, very large k_x/k_i values (typically greater than 1,000) are needed to attain a satisfactory profile modification. Figs. 60b and 60c suggest that in some circumstances, an acceptable profile modification could be attained if $r_{px} \geq 1$ ft, $k_x/k_i \geq 10$, and $10 \geq F_r \geq 100$. Of course, these treatments would involve very small gelant volumes and their effects would be confined to the region very near the wellbore.

Careful consideration of Ref. 18 and Eqs. 38 through 40 reveals that the conclusions reached in the preceding sections and figures apply to areal anisotropy in vertically stratified reservoirs with noncommunicating layers as well as to individual strata.

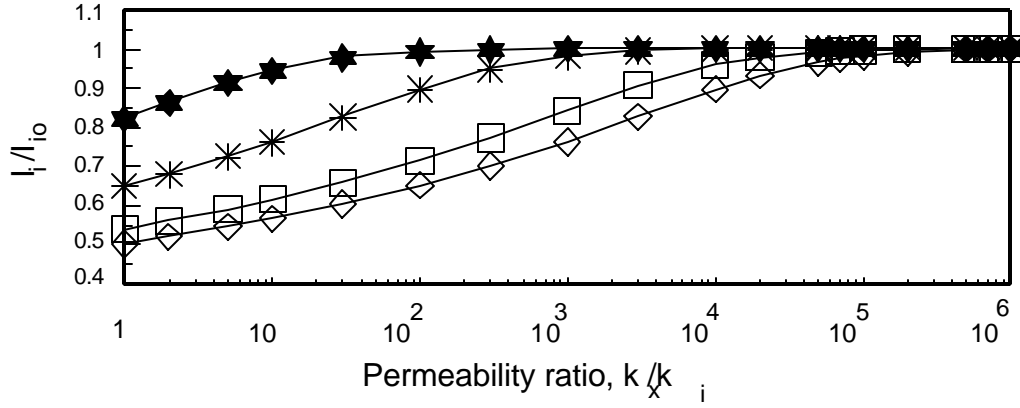
Conclusions for Model 1.

1. During unconfined gelant injection, a satisfactory placement for the gelant is far more likely to occur in a linear flow geometry than in an anisotropic radial flow geometry.
2. As we expected, the injectivity after gelation decreases as the value of residual resistance factor and the distance of gelant penetration increase.
3. For a given permeability ratio, the degree of gelant penetration, $(r_{pi}-r_w)/(r_{px}-r_w)$, increases with increased resistance factor.
4. For the range of permeability variations investigated ($k_x/k_i \geq 10^6$), the degree of gelant penetration becomes insensitive to resistance factor for F_r values greater than 100.
5. The above conclusions also apply to heterogeneous reservoirs with multiple noncommunicating layers.

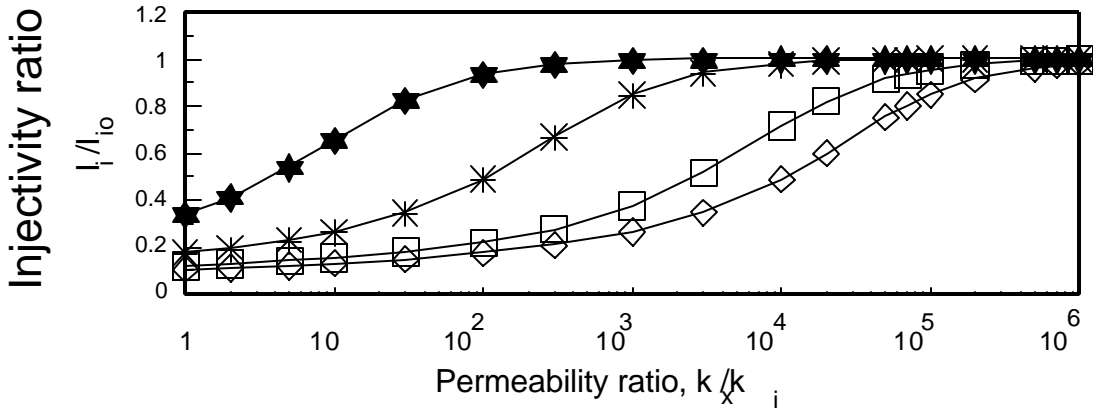
Analysis Using Model 2

In Model 1, a uniform pressure drop was applied across a radial reservoir that was areally anisotropic with respect to permeability. In Model 2, the radial reservoir was isotropic with respect to permeability, but the pressure drop across the reservoir varied with direction. The pressure distribution was symmetrical about both the x -axis and the y -axis, and only the injection well was assigned a constant pressure. The reservoir experienced the largest pressure drop in the x -direction while the smallest pressure drop occurred in the y -direction. For many of the results shown in this section, the pressure at the injection wellbore was 3,000 psi, the pressure at the outer boundary in the x -direction was 1,000 psi, and the pressure at the outer boundary in the y -direction was 2,800 psi.

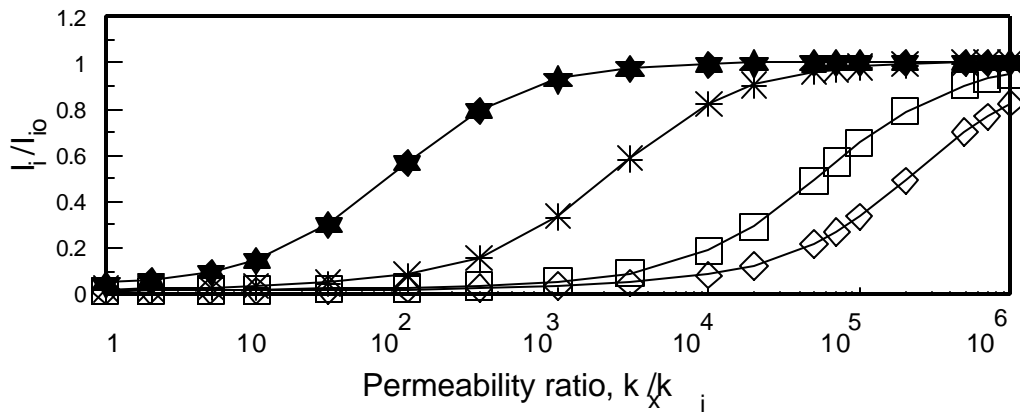
Model Description. Because of the symmetrical pressure distribution, only the first quadrant was considered. To quantitatively describe this model, a pressure distribution was assigned so that the pressure value at any point of the outer boundary was proportional to the angle between the x -axis and the line passing through the injection well (i.e., the origin) and the point considered.



a. $F_r = 2$.



b. $F_r = 10$.



c. $F_r = 100$.

$r_{px} = 1 \text{ ft}$



$r_{px} = 5 \text{ ft}$



$r_{px} = 25 \text{ ft}$



$r_{px} = 50 \text{ ft}$



Fig. 60. Injectivity ratios in anisotropic radial flow for different radii of gelant penetration.

In Model 2, both analytical and numerical methods were used to attack the problem. Since we hoped to perform a reliable sensitivity study, we needed an accurate description of the profile for the gelant front and the pressure distribution. Finite element and finite difference methods, which are widely used in large-scale reservoir problems, may not be optimal for this purpose. A finite mesh system may not represent the shape of the gelant front accurately enough, and the superposition technique, which is often incorporated in finite element and finite difference methods, also seems awkward for handling the pressure values along the outer boundary. Therefore, for this problem, we used another numerical method—the Fourier series approximation.¹⁵²

Pressure Profile Before Gel Placement. During brine injection before gel placement or during injection of a gelant with $F=1$, the pressure at any point within the drainage area can be expressed by Eq. 42. (Eq. 42 is derived in Appendix E.)

$$\begin{aligned}
 p = & \frac{\frac{m}{4} + n - p_w}{\log \frac{r_e}{r_w}} \log(r) + p_w - \log(r_w) - \frac{\frac{m}{4} + n - p_w}{\log \frac{r_e}{r_w}} \\
 & + \sum_{k=1,3,5,\dots} \frac{2m}{k^2 (r_w^{4k} r_e^{-2k} - r_e^{2k})} r^{2k} + \frac{2m}{k^2 (r_w^{-4k} r_e^{2k} - r_e^{-2k})} r^{-2k} \cos(2k\theta)
 \end{aligned}
 \tag{42}$$

where

- n = the pressure at the intersecting point of the x-axis and the outer boundary, psi
- m = slope of the pressure distribution at the outer boundary

Using Eq. 42, pressure profiles were generated for the case where the pressure drop was 10 times greater in the x-direction than in the y-direction ($p_x/p_y=10$). The results (Fig. 61) show that radial flow only existed close to the injection wellbore. The streamlines from the injection well quickly turned to parallel the x-axis as they penetrated deeper into the reservoir. Fluid was forced to flow away from the y-axis. Thus, the region at the outer boundary near the y-axis was not swept by the injected fluid.

Fig. 62 shows gelant-front profiles for different pressure-drop ratios when gelant reached the outer boundary in the x-direction. Fig. 62 was generated by following several streamlines from the injection well using an appropriate time step. As shown in Appendix F, a Fortran program was used to execute this procedure. The program also solves for the mathematical expression of the gelant front using a least-squares fit.

In Fig. 62, the gelant-front profiles appear to be insensitive to pressure-drop ratio for p_x/p_y values greater than 100. This result is intuitively incorrect and contrasts with the results shown in Fig. 57. These incorrect profiles probably resulted from numerical limitations associated with Model 2. Since we assigned a constant pressure drop in the x-direction (1,000 psi), as the p_x/p_y increased, the change of pressure at any point at the outer boundary decreased to small values. Consequently, the profiles for the gelant fronts appear to be insensitive to the higher values of pressure-drop ratio. (We will elaborate on the numerical limitations of our methods later.) We feel that our results using p_x/p_y values of 10 or less are probably reliable. However, the results for p_x/p_y values greater than 100 are undoubtedly unreliable.

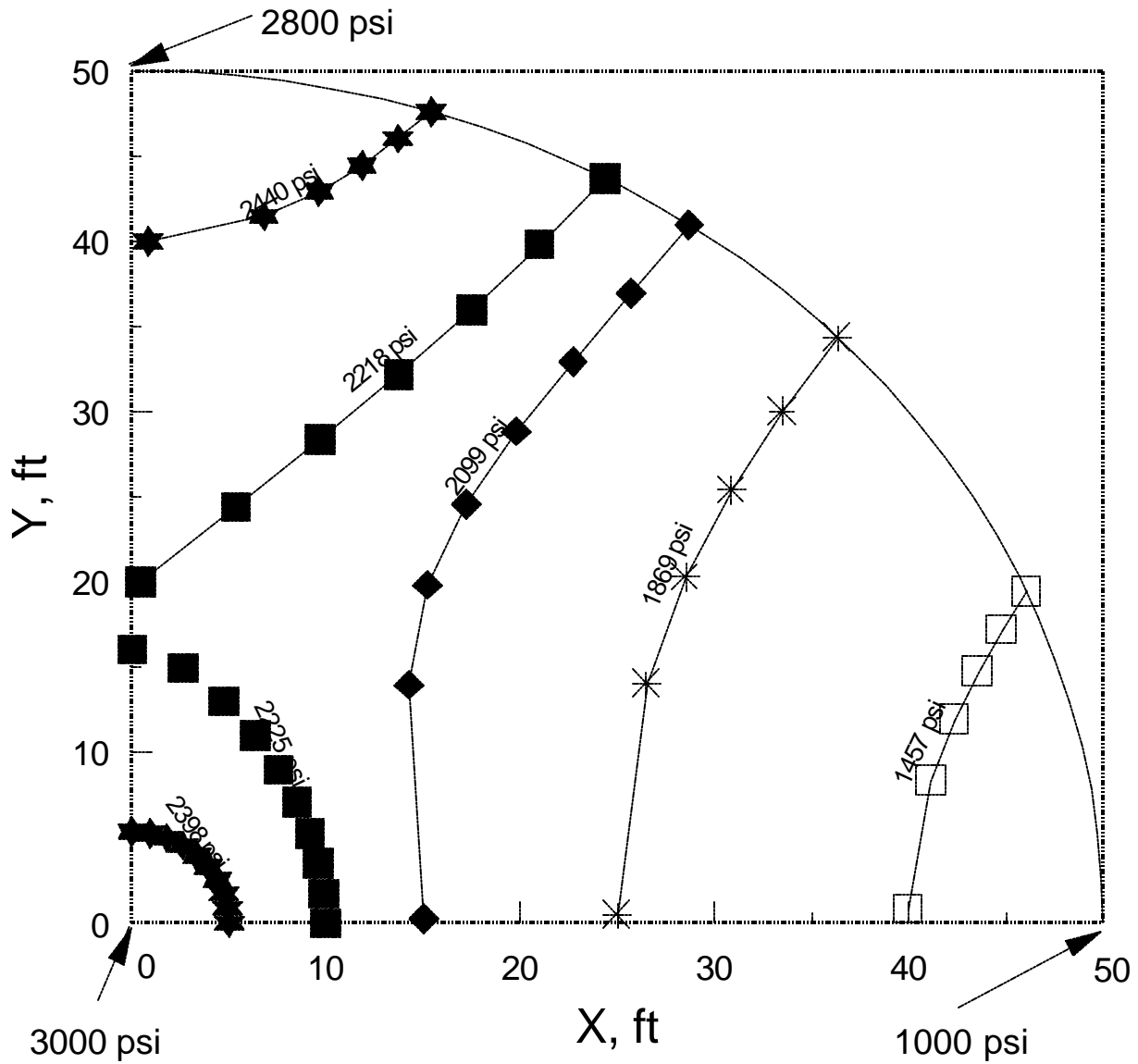


Fig. 61. Pressure profile during brine injection before gel placement when $p_x/p_y = 10$.

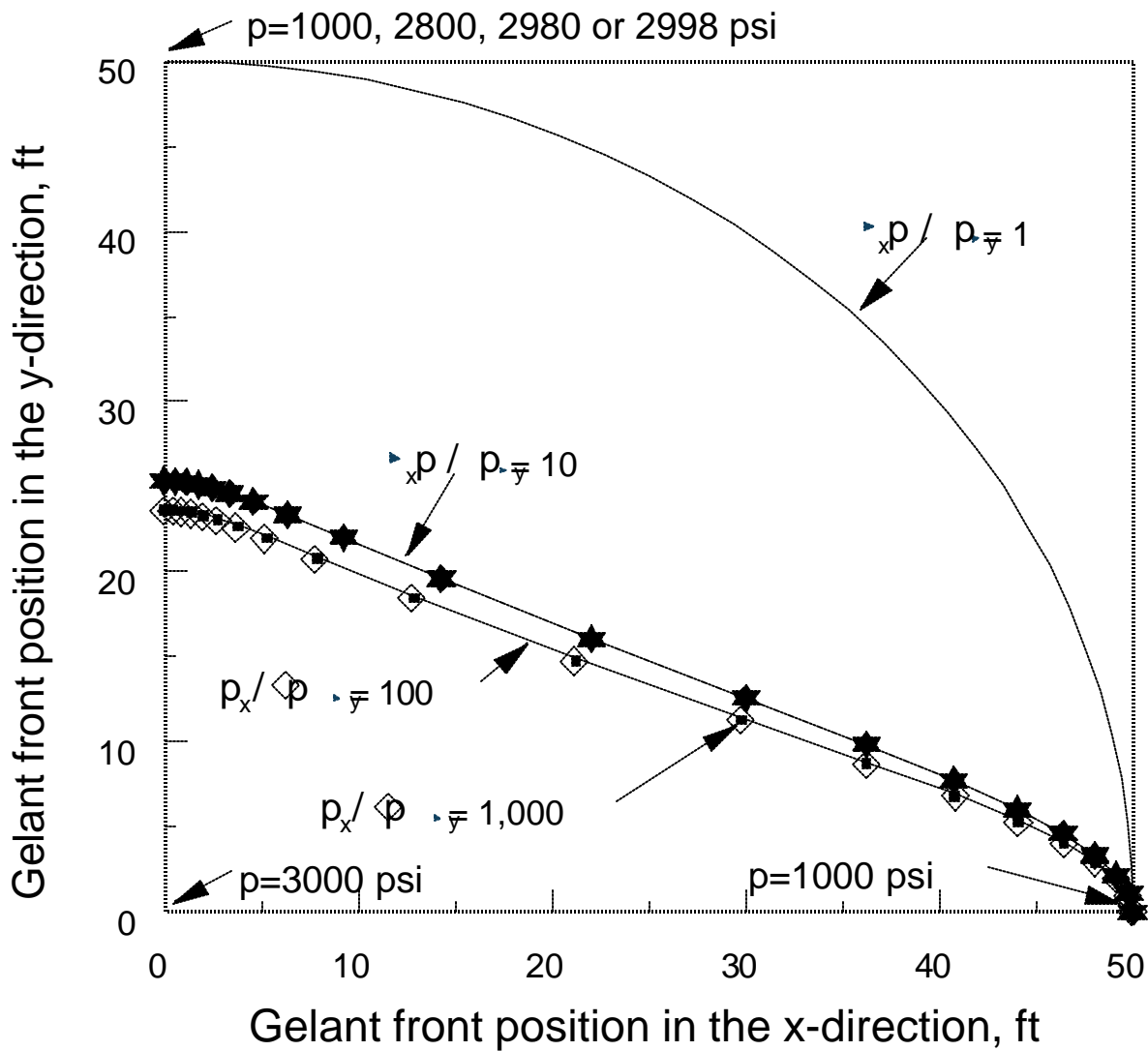


Fig. 62. Plan view of the gelant front in the first quadrant when gelant reached the outer boundary—in the x-direction.

Pressure Profile After Gel Forms. Pressure profiles during brine injection after gelation were determined for different distances of gelant penetration. We focused on the case where the pressure drop in the x-direction was 10 times that in the y-direction.

Fig. 63 shows the pressure profiles for three values of residual resistance factor ($F_r=2$, $F_r=10$, and $F_r=100$). In these cases, the gel extended 5 ft from the wellbore in the x-direction. An analytical method (described in Appendix G) was used to determine the pressure profiles. A comparison of the equipotential lines before (the thin dashed lines in Fig. 63) and after (the solid lines) gel placement reveals that the gel treatments (with $F_r=2$, $F_r=10$, or $F_r=100$) did not improve the areal flow profiles.

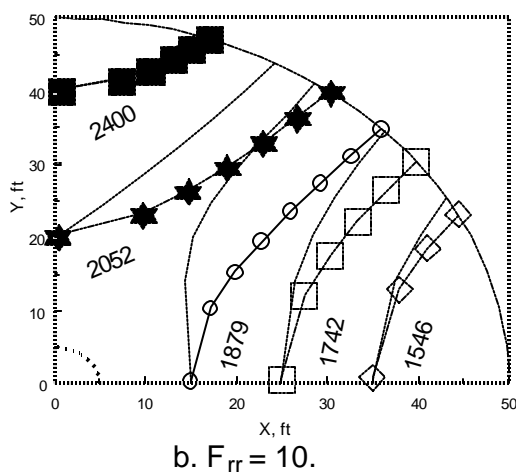
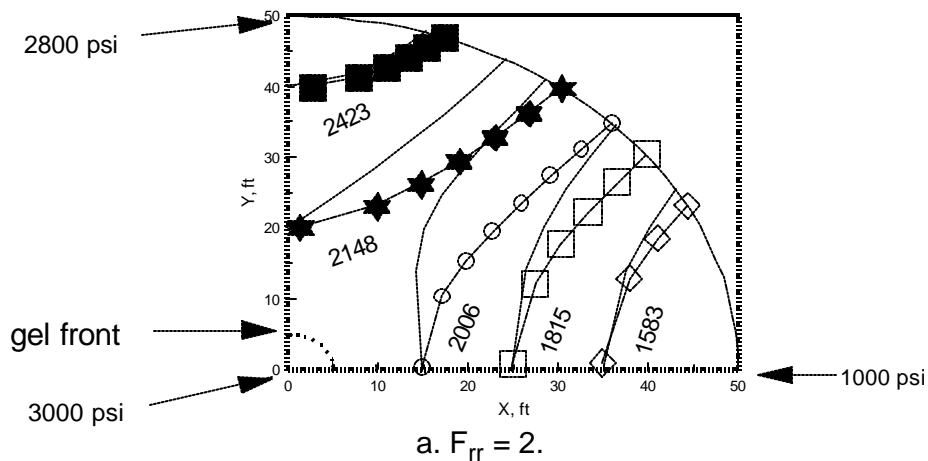
For comparison, Fig. 64 shows the pressure profiles for the three typical values of residual resistance factor when gelant extended to the outer boundary in the x-direction. A Fourier-approximation method was used to establish the pressure profiles, and a Gaussian elimination technique was used to solve the simultaneous linear equation set. Details of the solution can be found in Appendix H. In Fig. 64, as F_r increases, the equipotential lines bend toward the y-axis in the zone swept by the gelant while bending toward the x-axis in the zone not swept by the gelant. In this case, the injected fluid is diverted to the y-axis in the zone swept by the gelant. However, outside of the gel-treated region, Fig. 64 indicates no significant improvement in the areal flow profile.

Based on the above analysis, a satisfactory placement for the gelant did not occur for the case where the pressure drop ratio, $\frac{\Delta p_x}{\Delta p_y}$, was 10.

Limitations Associated with Using Numerical Methods in Model 2. Theoretically, Fourier approximation can describe pressure distributions very well. However, in practice, this method experiences many problems that are associated with most numerical methods. First, using finite terms to approximate the infinite series results in a truncation error. Second, underflow or overflow problems during computations also reduce the accuracy of the calculation. The combined errors may propagate and distort the results. We also found that the mathematical expression for the gelant-front profile that was generated by the least-square fit did not match the actual profile exactly. We also noted that injectivity losses were difficult to evaluate quantitatively using numerical methods with Model 2. Finally, numerical limitations precluded our investigation of cases where $\frac{\Delta p_x}{\Delta p_y}$ values were greater than 100.

Conclusions

1. During unconfined gelant injection, a satisfactory placement for the gelant is far more likely to occur in a linear flow geometry than in an anisotropic radial flow geometry.
2. As we expected, the injectivity after gelation decreases as the value of residual resistance factor and the distance of gelant penetration increase.
3. For a given permeability ratio, the degree of gelant penetration, $(r_{pi}-r_w)/(r_{px}-r_w)$, increases with increased resistance factor.
4. For the range of permeability variations investigated ($k_x/k_i \approx 10^6$), the degree of gelant penetration becomes insensitive to resistance factor for F_r values greater than 100.
5. The above conclusions also apply to heterogeneous reservoirs with multiple noncommunicating layers.
6. In an isotropic radial reservoir where the pressure drop was 10 times greater in the x-direction than in the y-direction ($\frac{\Delta p_x}{\Delta p_y}=10$), the anisotropy induced did not allow a gel treatment to significantly improve the areal flow profile in the reservoir.



thin dashed lines:
before gel placement

thin solid lines:
after gel placement

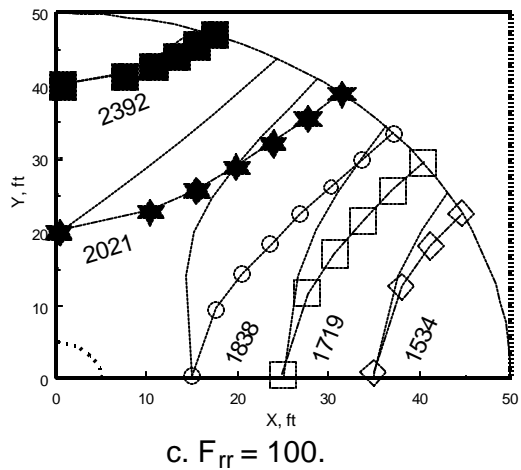


Fig. 63. Pressure profiles during brine injection after gel placement when $r_{px} = 5$ ft and $p_x/p_y = 10$. Pressures (in psi) are given for each solid equipotential curve.

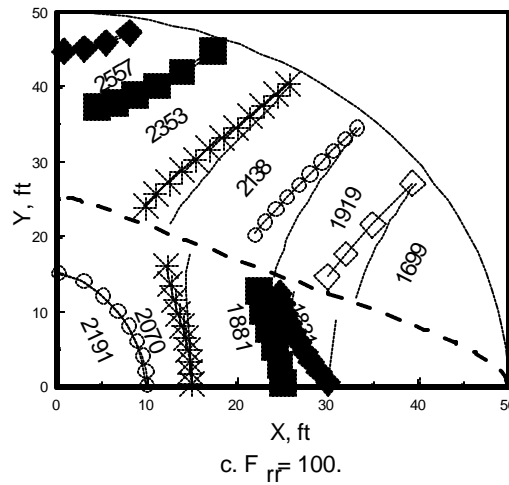
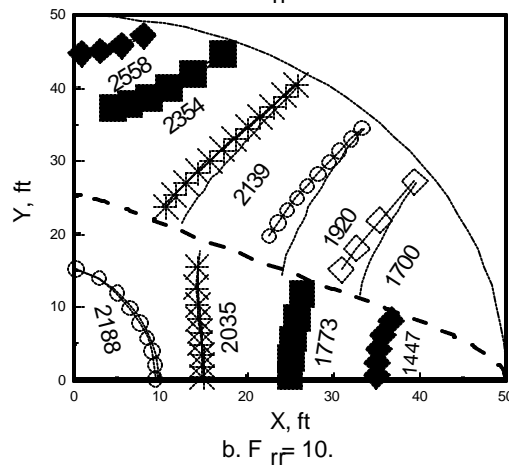
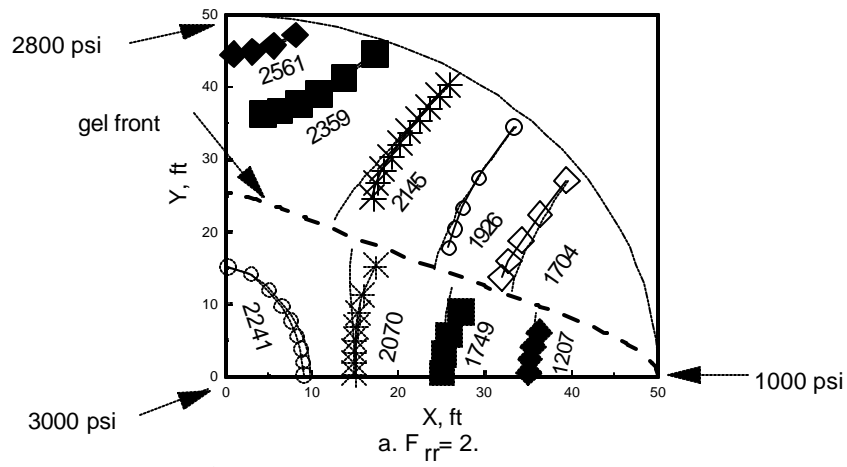


Fig. 64. Pressure profiles during brine injection after gel placement when $r_{px} = 50$ ft and $p_x/p_y = 10$. Pressures (in psi) are given for each solid equipotential curve.

9. DISPROPORTIONATE PERMEABILITY REDUCTION

Several researchers¹⁵³⁻¹⁶¹ reported that polymers or gels can reduce permeability to water much more than to oil. This property is critical to the success of gel treatments in production wells if zones cannot be isolated during gel placement.^{29,30} However, a plausible explanation for the phenomenon was unclear. We have demonstrated that the disproportionate permeability reduction is not caused by gravity or lubrication effects.¹⁶² Our experimental results also indicated that gel shrinking and swelling are unlikely to be responsible for the phenomenon.¹⁶² In this chapter, we continue our study of the disproportionate permeability reduction by examining three more possible mechanisms, including (1) water and oil pathway constrictions, (2) wettability effects, and (3) segregated oil and water pathways. We also examine the effects of lithology and permeability on the disproportionate permeability reduction. The ultimate objectives of our research in this area are to determine why this phenomenon occurs and to identify conditions that maximize this phenomenon.

Experimental Procedures

Gelants Studied. Three types of gels were used in this study: (1) Cr(III)-acetate-HPAM (using HPAM from Marathon), (2) Cr(III)-acetate-HPAM (using Alcoflood 935® HPAM from Allied Colloids), and (3) 12-hydroxystearic acid—Soltrol 130® (an oil-based gel). Table 13 lists the compositions of these gelants. Two partially-hydrolyzed polyacrylamide (HPAM) polymers were used in this study. The HPAM provided by Marathon had a molecular weight of about 2 million daltons and a degree of hydrolysis of 2%. Allied Colloids Alcoflood 935® HPAM had a molecular weight of about 5 million daltons and a degree of hydrolysis between 5% and 10%. The 12-hydroxystearic acid used in the lowest concentration oil-based gel (2%) was obtained from Johnson Wax. The other chemicals used in this study were reagent grade.

Table 13. Gelant Compositions and Viscosities (at 41°C)

Gelant Composition	pH	μ at 11 s ⁻¹ , cp
1.39% HPAM (from Marathon), 0.0212% Cr(III)-acetate, 1% NaCl	6.0	33
0.5% HPAM (Alcoflood 935®), 0.0417% Cr(III)-acetate, 1% NaCl	5.6	20
0.75% HPAM (Alcoflood 935®), 0.0625% Cr(III)-acetate, 1% NaCl	5.6	60
1% HPAM (Alcoflood 935®), 0.0834% Cr(III)-acetate, 1% NaCl	5.6	81
2% 12-hydroxystearic acid (from Johnson Wax) in Oil A (Soltrol-130®)		1.05
4% 12-hydroxystearic acid in Oil A		1.05
18% 12-hydroxystearic acid in Oil A		1.05

Rock and Fluids Used. Three types of rock were used during our core experiments, including (1) high-permeability Berea sandstone, (2) low-permeability Berea sandstone, and (3) Indiana limestone. Table 14 summarizes the lithology and permeabilities of the cores. Typically, each core was about 14-cm long and 3.6 cm in diameter. All cores had two internal pressure taps located approximately 2 cm from the inlet and outlet rock faces. The first core segment was treated as a filter; whereas, the middle core segment was used to measure mobilities and residual resistance factors. The cores were not fired. A refined oil,

Soltrol-130® (hereafter called "Oil A") was used as the oil phase. This oil had a viscosity of 1.05 cp and a density of 0.76 g/cm³ at 41°C. All brines contained 1% NaCl and had viscosities of 0.67 cp at 41°C. For the water-based gels, the brine used to saturate the cores had the same composition as that used for gelant preparation. Table 14 also lists the gelants used in each core experiment.

Table 14. Rock and Fluid Properties

Core ID	Lithology	k _w , md	Gelant Injected
SSH-64	Berea Sandstone	565	2% 12-hydroxystearic acid in Oil A
LSH-67	Indiana Limestone	32	1.39% HPAM (Marathon), 0.0212% Cr(III)-acetate
SSL-68	Berea Sandstone	123	1.39% HPAM (Marathon), 0.0212% Cr(III)-acetate
SSH-69	Berea Sandstone	684	4% 12-hydroxystearic acid in Oil A
SSH-71	Berea Sandstone	820	0.5% HPAM (Alcoflood 935®), 0.0417% Cr(III)-acetate
SSH-75	Berea Sandstone	818	1% HPAM (Alcoflood 935®), 0.0834% Cr(III)-acetate
SSH-77	Berea Sandstone	797	0.75% HPAM (Alcoflood 935®), 0.0625% Cr(III)-acetate
SSH-78	Berea Sandstone	773	0.75% HPAM (Alcoflood 935®), 0.0625% Cr(III)-acetate
SSH-85	Berea Sandstone	599	18% 12-hydroxystearic acid in Oil A
SSH-86	Berea Sandstone	586	18% 12-hydroxystearic acid in Oil A
SSH-S2	Berea Sandstone	667	0.5% HPAM (Alcoflood 935®), 0.0417% Cr(III)-acetate

Coreflood Sequence. Table 15 summarizes our general coreflood sequence. Unless otherwise indicated, the sequence listed in Table 15 was followed during core experiments. Water- and oil-tracer studies were routinely performed to characterize pore volumes and dispersivities. Effluent samples were routinely monitored and material balance calculations were performed to determine residual saturations. All experiments were performed at 41°C. A more detailed description of the coreflood sequence can be found in our first annual report.¹⁶²

Table 15. Sequence Followed During Oil/Water Core Experiments

Step

1. Saturate core with brine and determine porosity.
2. Determine absolute brine permeability and mobility.
3. Perform water-tracer study to confirm the pore volume (V_{po}) and to determine core dispersivity (a_o).
4. Inject oil (flow direction #1) to displace brine at a constant pressure drop of 100 psi across the core and determine oil mobility at residual water saturation, S_{wr} .
5. Perform oil-tracer study (flow direction #1) to determine the fraction of the original pore volume remaining (V_p/V_{po}) and the relative dispersivity (a/a_o).
6. Inject brine (flow direction #1) to displace oil at a constant pressure drop of 100 psi across the core and determine brine mobility at residual oil saturation, S_{or} .
7. Perform water-tracer study (flow direction #1) to determine V_p/V_{po} and a/a_o .
8. Inject gelant using the highest possible injection rate without exceeding the pressure constraint (flow direction #1).
9. Shut in core to allow gelation.
10. Reverse the flow direction (flow direction #2) and inject brine to determine the water residual resistance factors (F_{rw}).
11. Perform water-tracer study to determine V_p/V_{po} and a/a_o (flow direction #2).
12. Inject oil (flow direction #2) to determine the oil residual resistance factor (F_{ro}).
13. Perform oil-tracer study to determine V_p/V_{po} and a/a_o (flow direction #2).
14. Repeat Steps 10 through 13 (second water-oil injection cycle after shut-in).
15. Repeat Steps 10 through 13 (third water-oil injection cycle after shut-in).

Endpoint Permeabilities Before Gel Treatments

Before gelant injection, endpoint water and oil permeabilities were measured to establish baselines for residual-resistance-factor measurements. The residual resistance factor (F_{rw} or F_{ro}) is defined as the fluid (brine or oil, respectively) mobility before gel placement divided by fluid mobility during brine or oil injection after gelation. For high-permeability Berea sandstone cores, our previous study established that the endpoint permeabilities (either for water or oil) are not sensitive to flow-direction reversal and multiple imbibition and drainage cycles.¹⁶³ Therefore, only one set of endpoint water- and oil-permeability measurements was performed (Steps 4 through 7 in Table 15) for most high-permeability Berea sandstone cores. For the low-permeability Berea sandstone core (SSL-68) and the Indiana limestone core (LSH-67), Steps 4 through 7 in Table 15 were repeated with the flow direction reversed (flow direction #2). During the process, each step was also repeated to verify that the results were reproducible. Table 16 shows that, for the low-permeability Berea sandstone core (Core SSL-68), no hysteresis of endpoint permeabilities (either for water or oil) was observed as a result of flow-direction reversal and multiple imbibition and drainage cycles. However, for the Indiana limestone core (Core LSH-67), a steady increase for both endpoint water and oil permeabilities was observed during the multiple imbibition and drainage cycles (Table 17). In the limestone core, the endpoint oil permeabilities averaged 1.7 times greater than the endpoint water permeabilities. In contrast, in Berea cores (Table 16), the endpoint oil permeabilities averaged 6.7 times greater than the endpoint water permeabilities. To some researchers,

this result might indicate that the limestone core was less water-wet than the sandstone cores. The endpoint permeabilities and residual saturations for other high-permeability Berea sandstone cores are summarized in Tables I-1a through I-1f in Appendix I. The residual saturations (S_{wr} , S_{or}) in Tables 16, 17 and I-1a through I-1f are from material balance calculations.

Table 16. Summary of Residual Saturations (S_{wr} , S_{or}) and Endpoint Permeabilities (k , k) Obtained Before Gel Treatment
Core: Strongly Water-Wet Berea Sandstone (SSL-68), 41°C

Stage	S_{wr}	k
After 1st oilflood	0.28	119
After 2nd oilflood	0.27	118
After 3rd oilflood*	0.27	125
After 4th oilflood*	0.28	125
Stage	S_{or}	k
After 1st waterflood	0.42	19
After 2nd waterflood	0.43	17
After 3rd waterflood*	0.43	18
After 4th waterflood*	0.41	17

* Flow-direction reversed.

Table 17. Summary of Residual Saturations (S_{wr} , S_{or}) and Endpoint Permeabilities (k , k) Obtained Before Gel Treatment
Core: Indiana Limestone (LSH-67), 41°C

Stage	S_{wr}	k
After 1st oilflood	0.36	23
After 2nd oilflood	0.37	34
After 3rd oilflood*	0.40	42
After 4th oilflood*	0.38	48
Stage	S_{or}	k
After 1st waterflood	0.30	15
After 2nd waterflood	0.31	18
After 3rd waterflood*	0.34	24
After 4th waterflood*	0.36	29

* Flow-direction reversed.

Gelant Placement in Cores

To simulate the "pump-in, pump-out" sequence during gel treatments in production wells, the gelant was injected into a core from one direction (flow direction #1 in Table 15) and residual resistance factors were measured in the opposite direction (flow direction #2 in Table 15). During a given gelant-injection process, a constant pressure drop (100 psi across the core) was maintained. (The pressure constraint was imposed to avoid mobilizing the residual phase during gelant injection.) Effluent samples were collected continuously throughout the gelant-injection process at 1-PV intervals. The samples were allowed to gel, and the final gel strength was compared with gelant that had not been injected into the core. The gelant placement data are summarized in Table 18, including gel code¹⁴⁹ and the number of pore volumes injected.

Table 18. Gelant Placement Data (41°C)

Core ID	Gelant	Gel code ¹⁴⁹	PV injected
SSH-64	2% 12-hydroxystearic acid in Oil A	I	10
LSH-67	1.39% HPAM (Marathon), 0.0212% Cr(III)-acetate, 1% NaCl	H	1.8
SSL-68	1.39% HPAM (Marathon), 0.0212% Cr(III)-acetate, 1% NaCl	H	0.9
SSH-69	4% 12-hydroxystearic acid in Oil A	I	10
SSH-71	0.5% HPAM (Alcoflood 935®), 0.0417% Cr(III)-acetate, 1% NaCl	E	10
SSH-75	1% HPAM (Alcoflood 935®), 0.0834% Cr(III)-acetate, 1% NaCl	H	2
SSH-77	0.75% HPAM (Alcoflood 935®), 0.0625% Cr(III)-acetate, 1% NaCl	D/E	10
SSH-78	0.75% HPAM (Alcoflood 935®), 0.0625% Cr(III)-acetate, 1% NaCl	D/E	4
SSH-85	18% 12-hydroxystearic acid in Oil A	I	8
SSH-86	18% 12-hydroxystearic acid in Oil A*	I	5
SSH-S2	0.5% HPAM (Alcoflood 935®), 0.0417% Cr(III)-acetate, 1% NaCl	E	10

* Injected in 50/50 volume ratio with brine.

For each case, we tried to inject 10 PV of gelant. However, in some cases, pressure increases during

the placement process limited injection to less than 10 PV. For Core SSH-86, an oil-based gelant was injected with brine using a 50/50 volume ratio. This change in gelant injection strategy was designed to study the theory that the disproportionate permeability reduction is caused by segregated oil and water pathways. The details of the concept will be discussed in a later section.

Permeability Reduction Using Cr(III)-Acetate-HPAM Gels

Using a solution that contained 0.5% HPAM (Alcoflood 935®), 0.0417% Cr(III)-acetate, and 1% NaCl, 10 PV of gelant were injected into a high-permeability Berea sandstone core with $S_{or}=0.28$. After injecting the gelant, the core was shut in for 5 days (at 41°C). After shut-in, brine was injected from the opposite direction (flow direction #2) to determine residual resistance factors for water (F_{rw}). To determine the apparent rheology of the gel in porous media and whether gel mobilization occurred at a given flow rate, residual resistance factors were determined as a function of injection rate. Measurements of residual resistance factors were first made at a very low injection rate. After stabilization, the measurements were repeated at a higher injection rate. Then, the rate of brine injection was lowered to the previous injection rate to determine whether the F_{rw} value had changed. This cycle was repeated several times using successively higher injection rates until the pressure drop across the core approached the pressure constraint used in the process of establishing residual saturations (100 psi across the core). Table 19 shows that the residual resistance factors for water measured immediately after shut-in exhibited a shear-thinning behavior and could be described by a power-law equation ($F_{rw}= 1,016 u^{-0.34}$). After the F_{rw} measurements, oil was injected at a pressure equal to the pressure constraint (100 psi across the core) until no more water was produced. F_{ro} values were then determined at a number of fluid velocities. These values were measured at successively decreasing flow rates. As shown in Table 19, the flow behavior of oil in this case was also non-Newtonian. However, severe gel breakdown occurred during the oil-water injection cycles. Table 19 shows that the residual resistance factors for both oil and water were reduced to about 5 after two oil-water cycles. More detailed results from the residual-resistance-factor measurements are listed in Table I-2a in Appendix I.

Table 19. Summary of Residual Resistance Factors
Core: High-Permeability Berea Sandstone (SSH-S2)
Gel: 0.5% HPAM (Alcoflood 935®), 0.0417% Cr(III)-Acetate, 1% NaCl

F_{rw} (1st waterflood)	F_{ro} (1st oilflood)	F_{rw} (2nd waterflood)	F_{ro} (2nd oilflood)	F_{rw} (3rd waterflood)
$1,016 u^{-0.34}$	$15 u^{-0.37}$	4.5	4.6	5.2

To verify that the gel breakdown was not an experimental artifact, the same gelant was injected into a high-permeability Berea sandstone core with no residual oil present ($S_w=1$). In total, 10 PV of gelant were injected into the core. Water was injected immediately after shut-in to determine the residual resistance factor for water. Continuous gel breakdown occurred during the F_{rw} measurements. As shown in Table 20, the residual resistance factor for water stabilized at about 1. This implied that the gel completely washed out during the process. The water-tracer results summarized in Table 20 confirm that the gel completely washed out ($V_p/V_{po}=1$). Interestingly, the appearance and gel strength of the effluent samples collected during the gelant injection process were very similar to those of gelant that had not been injected. (The gel code for this gel was E¹⁴⁹ and the gelation time was about 5 hrs.) Detailed results from tracer studies are summarized in Tables I-3a through I-4p in Appendix I.

Table 20. Summary of Residual Resistance Factor and Tracer Results
 Core: High-Permeability Berea Sandstone (SSH-71)
 Gel: 0.5% HPAM (Alcoflood 935®), 0.0417% Cr(III)-Acetate, 1% NaCl

S_w	PV of Gelant Injected	F_{rrw}	V_p/V_{po}	a/a_o
1.0	10	~1	~ 1	~ 20

Next, using a new core with $S_w=1$, we doubled the concentrations of HPAM (Alcoflood 935®) and Cr(III)-acetate in the gelant to 1% and 0.0834%, respectively. Only two pore volumes of the gelant were injected before the pressure constraint (100 psi across the core) was reached. During the residual-resistance-factor measurements after shut-in, the pressure drop was so high that F_{rrw} could only be measured at a very low flow velocity (0.025 ft/d). As shown in Table 21, the residual resistance factor for water measured at 0.025 ft/d was 42,000.

Table 21. Summary of Residual Resistance Factors
 Core: High-Permeability Berea Sandstone (SSH-75)
 Gel: 1% HPAM (Alcoflood 935®), 0.0834% Cr(III)-Acetate, 1% NaCl

S_w	PV of Gelant Injected	Flux, ft/d	F_{rrw}
1.0	2	0.025	42,000

Since the injection of multiple pore volumes of gelant through the core is required to insure complete saturation, the concentrations of HPAM (Alcoflood 935®) and Cr(III)-acetate in the gelant were reduced to 0.75% and 0.0625%, respectively. The gelant was first injected into a new high-permeability Berea sandstone core with no residual oil present ($S_w=1$). Ten PV of gelant were forced through the core without exceeding the pressure constraint (100 psi across the core). After shut-in, residual resistance factors were measured at a single velocity of 0.025 ft/d. Table 22 shows that the core was much more permeable to oil than to water after treatment. Also, no gel breakdown was observed during the oil and water injection cycle.

An oil-water experiment was then performed in a new high-permeability Berea sandstone core using the same gelant. The gelant was injected into the core at residual oil saturation ($S_{or}=0.33$). Four PV of gelant were forced through the core before reaching the pressure constraint (100 psi across the core). As shown in Table 23, the residual resistance factors for water exhibited an apparent shear-thinning behavior while the flow of oil remained Newtonian. Table 23 also shows that gel breakdown occurred during the oil-water injection cycles and no significant disproportionate permeability reduction was observed after the first oil-water injection cycle. As in the previous cases, the appearance and gel strength of the effluent samples were very similar to those of gelant that had not been injected. The results seem to imply that Cr(III) ions propagated through the porous medium without any problem during injection. However, during the shut-in period, the rock may have depleted a significant portion of the dissolved Cr(III) through ion exchange and adsorption. Additional core experiments with higher Cr(III)-acetate concentrations in the gelant are being performed to resolve the issue. More detailed results from the residual-resistance-factor measurements can be found in Tables I-2a through I-2f in Appendix I.

Table 22. Summary of Residual Resistance Factors
 Core: High-Permeability Berea Sandstone (SSH-77)
 Gel: 0.75% HPAM (Alcoflood 935®), 0.0625% Cr(III)-Acetate, 1% NaCl

Fluid Injected	Flux, ft/d	F_{rr}
Brine	0.025	32,000
Oil	0.025	4,200
Brine	0.025	38,000

Table 23. Summary of Residual Resistance Factors
 Core: High-Permeability Berea Sandstone (SSH-78)
 Gel: 0.75% HPAM (Alcoflood 935®), 0.0625% Cr(III)-Acetate, 1% NaCl

F_{rw} (1st waterflood)	F_{ro} (1st oilflood)	F_{rw} (2nd waterflood)	F_{ro} (2nd oilflood)	F_{rw} (3rd waterflood)
$300 u^{-0.35}$	23	$30 u^{-0.18}$	17	$23 u^{-0.10}$

Effects of Permeability and Lithology on the Disproportionate Permeability Reduction

To examine the effect of permeability and lithology on the disproportionate permeability reduction by gels, oil/water experiments were conducted in a low-permeability Berea sandstone core and an Indiana limestone core. The strongly water-wet low-permeability Berea sandstone core (SSL-68) had a nominal absolute permeability to brine of 123 md. The limestone core (LSH-67) had a nominal absolute permeability to brine of 32 md. The gel had a composition of 1.39% HPAM (from Marathon), 0.0212% Cr(III) as acetate and 1% NaCl. Immediately before gelant injection, the residual oil saturations for the low-permeability sandstone core and the limestone core were 0.41 and 0.36, respectively.

During a given gelant injection process, the gelant was injected into the core using the maximum possible injection rate without exceeding the pressure constraint (100 psi across the core). For the low-permeability Berea sandstone core, we only managed to inject about 0.9 PV of gelant before the injection rate became unacceptably low. The core was then shut in for about 5 days. After shut-in, water was injected first and residual resistance factors for water (F_{rw}) were measured at different flow velocities. As shown in Table 24, the residual resistance factors for water exhibited a shear-thinning behavior and could be described by a power-law equation ($F_{rw} = 12 u^{-0.26}$). In order to minimize gel breakdown, the subsequent residual resistance factor measurements were performed using a single injection velocity (1.575 ft/d). Table 24 shows that the permeability reduction for water was only about twice that for oil after treatment. In contrast, the gel in a high-permeability Berea sandstone core reduced water permeability 30 times more than oil permeability.¹⁶² The low F_{rw} and F_{ro} values were probably caused by poor gelant propagation and insufficient gelant saturation in the porous medium.

For the limestone core, we were able to inject about 1.8 pore volumes of the gelant before the injection rate became too low under the pressure constraint (100 psi across the core). As shown in Table 24, the residual resistance factors for water were non-Newtonian and could be described by a power-law

equation. In contrast, the flow behavior of oil in the porous medium after treatment was more or less Newtonian. Table 24 shows that water permeability was reduced significantly more than oil permeability after treatment.

Because we were not able to force multiple pore volumes of gelant into the low-permeability Berea sandstone core and the Indiana limestone core, we have not yet established the effects that permeability and lithology have on the disproportionate permeability reduction. Additional work will be required to address this issue.

Table 24. Effects of Permeability and Lithology on the Disproportionate Permeability Reduction
Gel: 1.39% Marathon HPAM, 0.0212% Cr(III), and 1% NaCl

Core	PV of Gelant Injected	F_{rw} (1st waterflood)	F_{ro} (1st oilflood)	F_{rw} (2nd waterflood)
617-md Berea sandstone	6	> 35,300	50	$1,430 u^{-0.44}$
123-md Berea sandstone	0.9	$12 u^{-0.26}$	4*	9*
32-md Indiana limestone	1.8	$47 u^{-0.51}$	4	$18 u^{-0.52}$

* Measured at a single flow rate (1.575 ft/d).

Possible Mechanisms For Disproportionate Permeability Reduction

In our first annual report, we demonstrated that the disproportionate permeability reduction is not caused by gravity or lubrication effects.¹⁶² Our experimental results also indicated that gel shrinking and swelling are unlikely to be responsible for the phenomenon.¹⁶² In this report, we examine three more possible mechanisms for the disproportionate permeability reduction, including (1) water and oil pathway constrictions, (2) wettability effects, and (3) segregated oil and water pathways.

Water and Oil Pathway Constrictions and Wettability Effects. Zaitoun and Kohler proposed the following equation to estimate the permeability reduction after a polymer or gel treatment:¹⁶⁴ where F_r is the permeability reduction, d is the thickness of polymer or gel adsorbed on pore walls, and r

$$F_r = 1 - \frac{d^2}{r^2} \quad (43)$$

is the pore radius. According to Eq. 43, increasing the thickness of the adsorbed layer, d , and/or reducing the pore radius, r , should increase the permeability reduction. Zaitoun and Kohler proposed that in a strongly water-wet system, the presence of residual oil droplets at the center of the pores can significantly reduce the effective pore radius, r , during waterflooding. In contrast, no such constriction exists during oilflooding. Therefore, for a given d , the permeability reduction for water during waterflooding is greater than that for oil during oilflooding.

Using the above reasoning, we expect the disproportionate permeability reduction to be most evident in strongly water-wet cores (if hydrophilic polymers or gels are used). For less water-wet cores, polymers

and gels should adsorb on pore walls to a lesser extent, and consequently, should be less likely to restrict water flow. Thus, we expect the disproportionate permeability reduction to be less apparent in cores of intermediate wettability.

In an earlier study, we performed core experiments with both strongly water-wet cores and cores of intermediate wettability.¹⁶¹ Table 25 shows that the disproportionate permeability reduction was observed in systems of intermediate wettability as well as in strongly water-wet systems. Surprisingly, for a resorcinol-formaldehyde gel, the disproportionate permeability reduction was actually more evident in a core of intermediate wettability than in a strongly water-wet core. For a Cr(III)-xanthan gel, the impact of wettability on disproportionate permeability reduction was not evident. Obviously, the impact of wettability on gel performance varied with the gel. Although wettability may play a role that affects the disproportionate permeability reduction, it does not appear to be the root cause for water permeability being reduced more than oil permeability.

Table 25. Impact of Wettability on Gel Performance

Gelant	Wettability	F_{rw}	F_{ro}	F_{rw}/F_{ro}
3% resorcinol, 3% formaldehyde	strongly water-wet	49	11	4.5
	intermediate	510	26	20
0.4% xanthan, 0.0154% Cr(III)	strongly water-wet	8	5	1.6
	intermediate	22	14	1.6

Zaitoun and Kohler¹⁶⁰ speculated that the stretching of coiled macromolecules in the adsorbed polymer or gel layer under elongational flow could make the pore throats more constricted at higher water rates. They also speculated that higher oil rates might reduce the apparent thickness of the polymer or gel layer, thereby reducing the resistance to oil flow. In our standard coreflood procedure, residual resistance factors are determined as a function of injection rate to determine the apparent rheology of gels in porous media. As shown in Fig. 65, for a Cr(III)-acetate-HPAM gel, the flow of brine in a strongly water-wet Berea sandstone core after treatment exhibited a strong apparent "shear-thinning" behavior, where the F_{rw} values actually decreased with increasing superficial velocity. The residual resistance factors for water, in this case, can be described by a power-law equation, $F_{rw} = 105 u^{-0.55}$. In contrast, the flow behavior of oil in the porous medium after treatment was Newtonian.

Segregated Oil and Water Pathways. White *et al.*¹⁵⁸ proposed that the disproportionate permeability reduction might be caused by water and oil following segregated pathways. As illustrated in Fig. 66, during high water fractional flow, water flows through most of the open pathways while some of the open pathways remain connected by oil and inaccessible to water. If on a microscopic level, a water-based gelant follows primarily the pathways available to water, then many of the oil pathways could remain

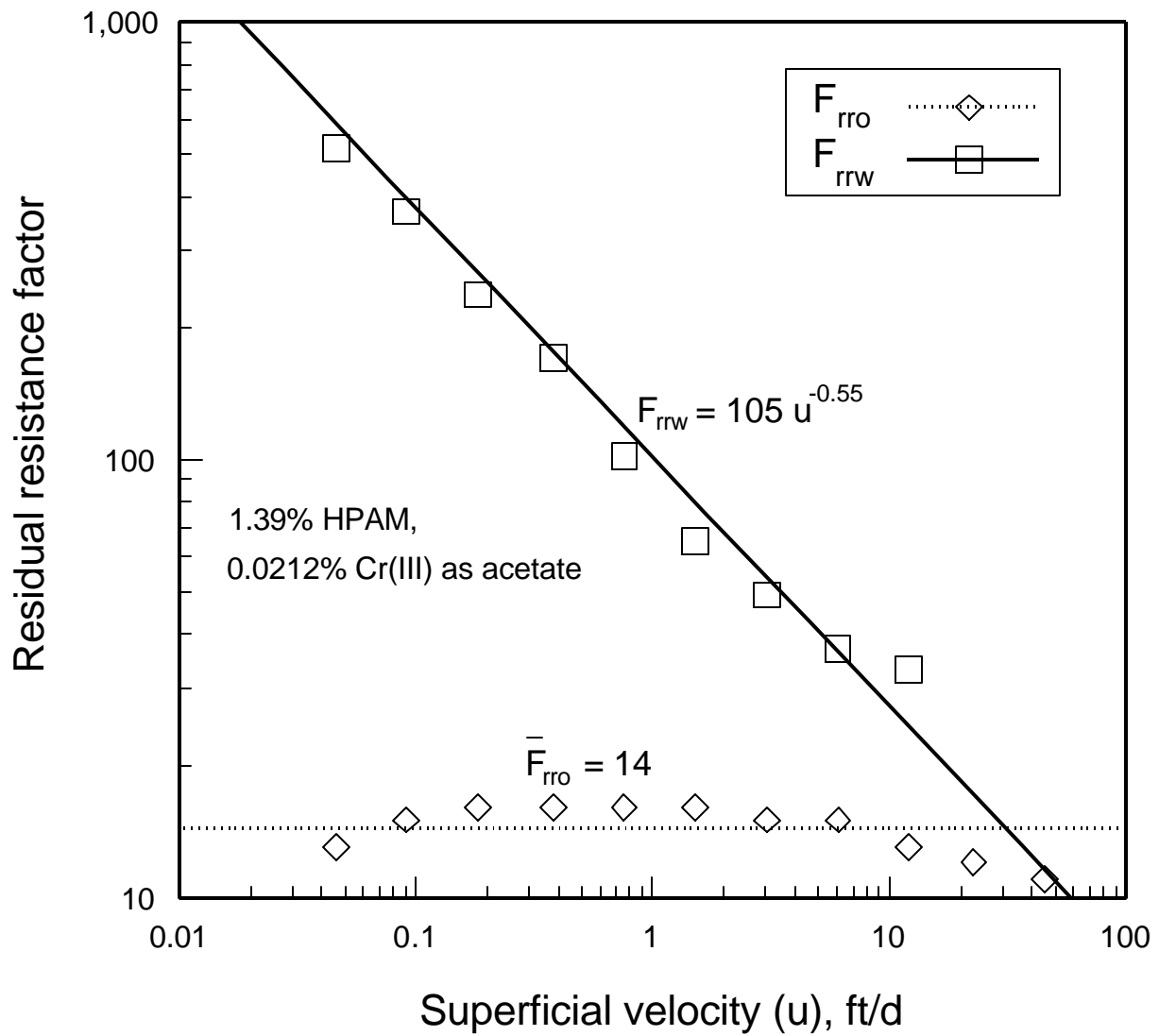
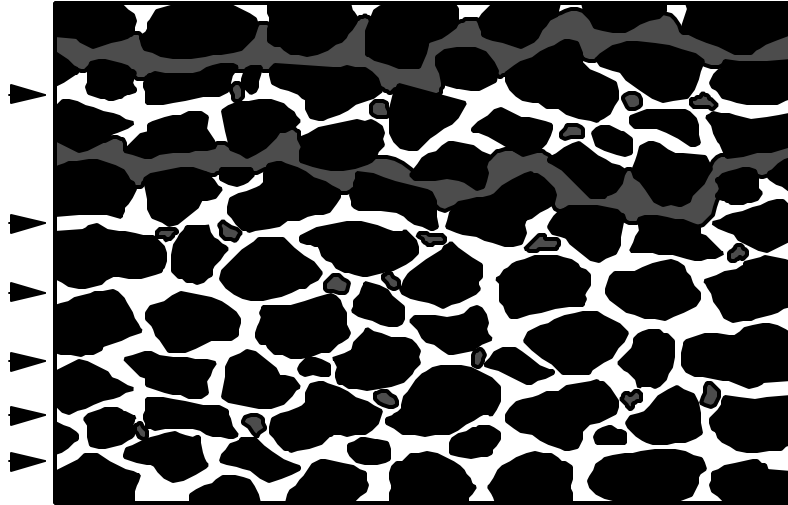
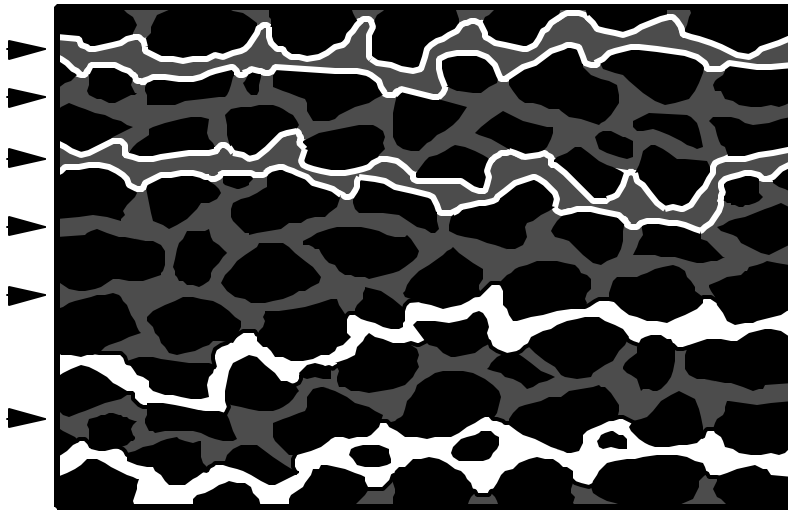


Fig. 65. Apparent rheology during oil and water injection.



a. High Water Fractional Flow



b. High Oil Fractional Flow

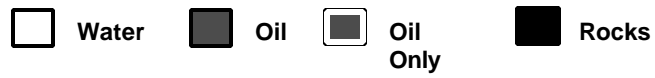


Fig. 66. Segregated water and oil pathways.

connected and gel-free after treatment. In this way, the water-based gel could reduce water permeability more than oil permeability. Following the same logic, if an oil-based gelant follows primarily the pathways available to oil, then many of the water pathways could remain connected and gel-free after treatment. Therefore, if this concept is valid, an oil-based gel should reduce oil permeability more than water permeability.

To investigate this concept, an oil-based gel consisting of 12-hydroxystearic acid and Oil A (Soltrol-130®) was used in this study. In this case, the gelation reaction is triggered by lowering the temperature. Above 65°C, 12-hydroxystearic acid is soluble in Oil A. However, if the temperature is lowered below 60°C, an opaque gel forms. The gelation reaction can be reversed by raising the temperature above the gelation temperature. For the oil-based gel, three formulations of different final gel strength were used in the core experiments. During each core experiment, 10 PV of gelant were injected into a high-permeability Berea sandstone core at residual water saturation. Gelant injection occurred at 80°C. After gelant injection, the core was shut in at 41°C for about 3 days. After shut-in, for the gelant that contained 2% 12-hydroxystearic acid in Oil A, residual resistance factors were determined at different flow rates. The flow behavior was Newtonian for both water and oil. Table 26 shows that the gel reduced oil permeability more than water permeability. However, severe gel breakdown occurred during the oil-water injection cycles. The core experiment was repeated (in a new core) with a stronger gel containing 4% 12-hydroxystearic acid in Oil A. In order to minimize gel breakdown, residual resistance factors were determined at a single flow rate (0.787 ft/d). The oil residual resistance factor was determined immediately after shut-in. Brine was then injected at the same flow rate (0.787 ft/d) until a steady state was reached. After brine injection, oil was reinjected again to verify that the disproportionate permeability reduction was not caused by gel breakdown. As shown in the last row of Table 26, the gel reduced oil permeability significantly more than water permeability. This result suggests that a significant portion of the water pathways remained open to water flow after treatment. The number of oil pathways open to oil flow was, however, reduced by the gel after treatment.

Table 26. Summary of F_{ro} and F_{rw} Values for Dilute Oil-Based Gels
Core: High-Permeability Berea Sandstone, 41°C

Gelant	F_{ro} (1st oilflood)	F_{rw} (1st waterflood)	F_{ro} (2nd oilflood)
2% 12-hydroxystearic acid, Oil A	26	1	3
4% 12-hydroxystearic acid, Oil A	36*	2*	18*

* Measured at a single flow rate (0.787 ft/d).

If water and oil follow segregated pathways, we should be able to obtain lower F_{ro} values by increasing the number of open pathways that remains gel-free and connected by oil after treatment. One possible way of achieving that is to inject a water-based gelant with oil during placement. By the same argument, the permeability reduction to water by an oil-based gel could be reduced by injecting the gelant with brine during gelant placement.

An oil-based gel containing 18% 12-hydroxystearic acid in Oil A was used to verify this idea. Ten PV of gelant were injected into a high-permeability Berea sandstone core at residual oil saturation. In this

case, water was injected (instead of oil) into the core immediately after shut-in to determine F_{rw} . To minimize gel breakdown, the F_{rw} and F_{ro} values were measured at a single rate of 0.025 ft/d. Table 27 shows that the gel reduced oil permeability significantly more than water permeability ($F_{rw}=30$, $F_{ro}=300$).

Table 27. Summary of F_{ro} and F_{rw} Values for a Concentrated Oil-Based Gel
Core: High-Permeability Berea Sandstone, 41°C

Gelant	F_{rw} (1st waterflood)	F_{ro} (1st oilflood)	F_{rw} (2nd waterflood)
18% 12-hydroxystearic acid, Oil A	34*	300*	30*
18% 12-hydroxystearic acid, Oil A**	5*	225*	14

* Measured at a single flow rate (0.025 ft/d).

** Gelant injected with brine (1% NaCl) using a 50/50 volume ratio.

The core experiment was repeated with the same gelant except that this time, the gelant was injected with brine (1% NaCl) using a 50/50 volume ratio during the placement process. As shown in Table 27, the residual resistance factor for water measured immediately after shut-in was 5 (at 0.025 ft/d). This number was significantly lower than that in the previous experiment ($F_{rw}=34$ at 0.025 ft/d). Next, oil was injected into the core at 0.025 ft/d to determine the F_{ro} . Table 27 shows that the residual resistance factor for oil was 225. Interestingly, the gel treatment provided an F_{ro} value that was comparable to that for the previous experiment (where no brine was injected with the gelant). Finally, water was injected into the core again at various injection rates. The flow of water in the porous medium was Newtonian and the F_{rw} was 14. These findings suggest that the number of open water pathways after treatment can be increased by injecting an oil-based gelant with brine during placement. The increase in water pathways could reduce the permeability reduction to water after treatment. Similar core experiments using a water-based gel are being conducted to confirm the validity of this theory. Of course, these concepts could also be applied by substituting gas for oil.

Results from our experiments suggest that segregation of oil and water pathways through a porous medium may play the dominant role in causing the disproportionate permeability reduction. Experiments are continuing to verify this concept.

Conclusions

Based on our experimental results, we conclude the following:

1. Some water-based gels reduced water permeability more than oil permeability in both intermediate-wet and strongly water-wet systems. The impact of wettability varied with the gel. Although wettability effects may play a role that affects the disproportionate permeability reduction, they do not appear to be the root cause for water permeability being reduced more than oil permeability.
2. In contrast, an oil-based gel reduced oil permeability significantly more than water permeability. Injecting the oil-based gelant with brine during placement reduced the permeability reduction to water while still maintaining a significant permeability reduction to oil.

3. Results from our experiments suggest that segregation of oil and water pathways through a porous medium may play the dominant role in causing the disproportionate permeability reduction. Experiments are continuing to verify this concept.
4. Disproportionate permeability reduction was observed in a low-permeability Berea sandstone core and in an Indiana limestone core with a water-based gel. Because we were not able to force multiple pore volumes of gelant into the low-permeability Berea sandstone core and the Indiana limestone core, we have not yet established the effects that permeability and lithology have on the disproportionate permeability reduction. Additional work will be required to address this issue.

Future Work

1. Perform core experiments using water-based gels to study the feasibility of reducing the permeability reduction to oil or gas after treatment by simultaneously injecting gelant and an oil phase or by simultaneously injecting gelant and a gas phase.
2. Use NMR imaging technique to observe the disproportionate permeability reduction on a microscopic level.
3. Continue oil/water experiments in cores with different permeabilities, lithologies, and wettabilities.

NOMENCLATURE

A	= core cross-sectional area, cm ²
A _i	= cross-sectional area of Zone i, m ²
a _{ri}	= retention or delay factor, PV
C	= tracer concentration in the effluent, g/cm ³
C _o	= injected tracer concentration, g/cm ³
C ₁	= constant in Eq. 1, ft-md ^{1/2} /psi [m ² /Pa]
c	= compressibility, psi ⁻¹ [Pa ⁻¹]
c _w	= water compressibility, psi ⁻¹ [Pa ⁻¹]
d	= size of particulates, μm
d _{criti}	= critical particle size of Zone i, μm
d _{crit1}	= critical particle size of Zone 1, μm
\bar{d}	= mean particle size, μm
d ₅₀	= median pore size, μm
F _r	= resistance factor (brine mobility before placement of blocking agent divided by blocking-agent mobility before setting or gelation)
F _{ri}	= resistance factor in Zone i
F _{rr}	= residual resistance factor (mobility before placement of blocking agent divided by mobility after placement of blocking agent)
F _{ri}	= residual resistance factor in Zone i
F _{ro}	= oil residual resistance factor
F _{rw}	= water residual resistance factor
f _p	= fraction of the particles smaller than the critical particle size of the formation
?(r _{pi})	= function defined by Eqs. 13 and 14
g	= acceleration of gravity, ft/s ² [m/s ²]
h	= formation thickness, ft [m]
h _f	= fracture height, cm
I	= injectivity, bbl/D-psi [m ³ /s-Pa]
I _i	= injectivity in direction i, bbl/D-psi [m ³ /s-Pa]
I _{io}	= initial injectivity in direction i, bbl/D-psi [m ³ /s-Pa]
I _o	= initial injectivity, bbl/D-psi [m ³ /s-Pa]
k	= permeability, md [μm ²]
k _{av}	= average permeability of a fractured core, md [μm ²]
k _c	= permeability of the filter cake, md [μm ²]
k _f	= effective fracture permeability, md [μm ²]
k _i	= permeability in Zone i or direction i, md [μm ²]
k _m	= effective rock permeability, md [μm ²]
k	= endpoint oil permeability, md [μm ²]
k _{rw}	= relative permeability to water, md [μm ²]
k	= endpoint water permeability, md [μm ²]
k _x	= permeability in the most-permeable direction (x-direction), md [μm ²]
k _y	= permeability in the least-permeable direction (y-direction), md [μm ²]
k ₁	= permeability in Zone 1, md [μm ²]
k ₂	= permeability in Zone 2, md [μm ²]
L _{ci}	= filter-cake thickness on Zone i, ft [m]
L _{pi}	= distance of gelant penetration into Zone i, ft [m]
L _{pm}	= maximum distance of gelant penetration into the most-permeable layer (Zone 1), ft [m]
L _{p1}	= distance of gelant penetration into Zone 1, ft [m]

L_t	= total core length, ft [m]
m	= slope of the linear pressure distribution for the outer boundary
n	= pressure at the intersection point of the outer boundary and the x-axis, psi [Pa]
p_e	= reservoir pressure, psi [Pa]
p_w	= pressure at the injection well, psi [Pa]
p_{wo}	= original wellbore pressure, psi [Pa]
p_{w2}	= wellbore pressure after injection-pressure reduction, psi [Pa]
p_1	= pressure in the zone swept by the gelant, psi [Pa]
p_2	= pressure in the zone not swept by the gelant, psi [Pa]
$?p$	= pressure drop or difference between flowing and static bottomhole pressures, psi [Pa]
$?p_{Di}$	= ratio of the pressure drop between L_{pm} and the end of Zone i to the pressure drop between the beginning of Zone i and L_{pm} prior to gelant injection (see Ref. 18 for a more detailed discussion)
$?p_{D1}$	= ratio of the pressure drop between L_{pm} and the end of Zone 1 to the pressure drop between the beginning of Zone 1 and L_{pm} prior to gelant injection (see Ref. 18 for a more detailed discussion)
$?p_i$	= pressure drop in Zone i, psi [Pa]
$(dp/dl)_{mini}$	= minimum pressure gradient for foam mobilization in Zone i, psi/ft [Pa/m]
q	= volumetric injection or production rate, bbl/D [m^3/s]
q_i	= injection rate in Zone i, bbl/D [m^3/d]
q_{io}	= total brine injection rate before gelant placement, B/D
r	= pore radius, ft [m]
r_e	= external drainage radius, ft [m]
r_{pi}	= radius of penetration into Zone i or in direction i, ft [m]
r_{px}	= distance of gelant penetration in the x-direction, ft [m]
r_w	= wellbore radius, ft [m]
r_2	= radial distance into the reservoir where the pressure is p_{w2} , ft [m]
S_{gel}	= gel saturation (fraction of PV occupied by gel)
S_{or}	= residual oil saturation
S_w	= irreducible water saturation
S_{wi}	= water saturation in Zone i
S_{wr}	= irreducible water saturation
S_{w1}	= water saturation in Zone 1
t	= time, seconds
t_{tr}	= transient time, seconds
u	= superficial or Darcy velocity or flux, cm/s
u_i	= superficial velocity, ft/s [cm/s]
u_x	= the component of u_i in the x-direction, ft/s [cm/s]
u_y	= the component of u_i in the y-direction, ft/s [cm/s]
v_i	= velocity of the gelant front, ft/s [cm/s]
v_p	= particle velocity, ft/s [m/s]
V_c	= cake volume, ft^3 [m^3]
V_p	= apparent remaining pore volume, cm^3
V_{po}	= initial pore volume of the core, cm^3
V_t	= total filtration volume, ft^3 [m^3]
w_f	= fracture width, cm
a	= dispersivity, cm
a_i	= filtration coefficient of Zone i
a_o	= initial dispersivity of the core, cm

a_1	=	filtration coefficient of Zone 1
d	=	thickness of polymer or gel adsorbed on pore walls, μm
θ	=	the angle between the x-direction and the line passing through the origin and the considered point
θ_i	=	the angle between radial direction and the x-direction
μ	=	fluid viscosity, cp [mPa-s]
μ_b	=	brine viscosity, cp [mPa-s]
μ_o	=	oil viscosity, cp [mPa-s]
μ_p	=	gelant viscosity, cp [mPa-s]
μ_w	=	water viscosity, cp [mPa-s]
ρ_b	=	brine density, g/cm^3
ρ_p	=	particle density, g/cm^3
s	=	standard deviation, μm
f	=	porosity
f_c	=	porosity of filter cake
f_i	=	effective aqueous-phase porosity in Zone i or direction i
f_1	=	porosity of Zone 1
f_2	=	porosity of Zone 2

REFERENCES

1. Seright, R.S.: "Improved Techniques for Fluid Diversion in Oil Recovery Processes," first annual report (DOE/BC/14880-5), Contract No. DE-AC22-92BC14880, U.S. DOE (Dec. 1993).
2. Bernard, G.G. and Holm, L.W.: "Effect of Foam on Permeability of Porous Media to Gas," *SPEJ* (Sept. 1964) 267-274.
3. Bernard, G.G., Holm, L.W., and Jacobs, W.L.: "Effect of Foam on Trapped Gas Saturation and on Permeability of Porous Media to Water," *SPEJ* (Dec. 1965) 295-300.
4. Holm, L.W.: "The Mechanism of Gas and Liquid Flow Through Porous Media in the Presence of Foam," *SPEJ* (Dec. 1968) 359-369.
5. Kovscek, A.R., Patzek, T.W., and Radke, C.J.: "Simulation of Foam Displacement in Porous Media," paper SPE 26402 presented at the 1993 SPE Annual Technical Conference and Exhibition, Houston, Oct. 3-6.
6. Radke, C.J. and Gillis, J.V.: "A Dual Gas Tracer Technique for Determining Trapped Gas Saturation During Steady Foam Flow in Porous Media," paper SPE 20519 presented at the 1990 SPE Annual Technical Conference and Exhibition, New Orleans, Sept. 23-26.
7. Friedmann, F., Chen, W. H., and Gauglitz, P.: "Experimental and Simulation Study of High-Temperature Foam Displacement in Porous Media," *SPE* (Feb. 1991) 37-45.
8. Khatib, Z.I., Hirasaki, G.J., and Falls, A.H.: "Effects of Capillary Pressure on Coalescence and Phase Mobilities in Foams Flowing Through Porous Media," *SPE* (Aug. 1988) 919-926.
9. Lee, H.O., Heller, J.P., and Hoefer, A.M.W.: "Change in Apparent Viscosity of CO₂ Foam With Rock Permeability," *SPE* (Nov. 1991) 421-428.
10. Radke, C.J. *et al.*: *Colloids and Surfaces A* (1994) **83**, 109.
11. Yang, S.H. and Reed, R.L.: "Mobility Control Using CO₂ Foams," paper SPE 19689 presented at the 1989 SPE Annual Technical Conference and Exhibition, San Antonio, Oct. 8-11.
12. Tsau, J.S. *et al.*: "CO₂ Foam Field Verification Pilot Test at EVGSAU: Phase IIIA-Surfactant Performance Characterization and Quality Assurance," paper SPE 27785 presented at the 1994 SPE/DOE Symposium on Improved Oil Recovery, Tulsa, April 17-20.
13. Friedmann, F. *et al.*: "Steam Foam Mechanistic Field Trial in the Midway-Sunset Field," paper SPE 21780 presented at the 1991 SPE Western Regional Meeting, Long Beach, March 20-22.
14. Isaacs, E.E., McCarthy, F.C., and Maunder, J.D.: "Investigation of Foam Stability in Porous Media at Elevated Temperatures," *SPE* (May 1988) 565-572.
15. Albrecht, R.A. and Marsden, S.S.: "Foams as Blocking Agents in Porous Media," *SPEJ* (March 1970) 51-55.

16. Rossen, W.R.: "Theory of Mobilization Pressure Gradient of Flowing Foams in Porous Media," *J. Colloid and Interface Science* (April 1990) **136**, No. 1, 1-53.
17. Rossen, W.R.: "Modeling Foam Mobility in Porous Media," paper SPE 22627 presented at the 1991 SPE Annual Technical Conference and Exhibition, Dallas, Oct. 6-9.
18. Seright, R.S.: "Placement of Gels to Modify Injection Profiles," paper SPE/DOE 17332 presented at the 1988 SPE/DOE Symposium on Enhanced Oil Recovery, Tulsa, April 17-20.
19. Zhou, Z.H. and Rossen, W.R.: "Applying Fractional-Flow Theory to Foam Processes at the Limiting Capillary Pressure," paper SPE 24180 presented at the 1992 SPE/DOE Symposium on Enhanced Oil Recovery, Tulsa, April 22-24.
20. Kovscek, A.R., Patzek, T.W., and Radke, C.J.: "Mechanistic Prediction of Foam Displacement in Multidimensions: A Population Balance Approach," paper SPE 27789 presented at the 1994 SPE/DOE Symposium on Improved Oil Recovery, Tulsa, April 17-20.
21. Irani, C.A. and Easterly, R.A.: "Transporting Mobility Control Agents to Thief Zones," paper SPE 27701 presented at the 1994 SPE/DOE Symposium on Improved Oil Recovery, Tulsa, April 17-20.
22. Raza, S.H.: "Foam in Porous Media: Characteristics and Potential Applications," *SPEJ* (Dec. 1970) 328-336.
23. Hanssen, J.E.: "Foam as a Gas-Blocking Agent in Petroleum Reservoirs," *J. Petroleum Science & Engineering* (1993) **10**, 117-156.
24. Ekran, S. and Hanssen, J.E.: "Well Treatment Against Gas Coning Must Exploit Gravity Effects," paper FS11 presented at the 1993 NIPER/DOE Symposium on Field Application of Foams for Oil Production, Bakersfield, Feb. 11-12.
25. Persoff, P. *et al.*: "Aqueous Foams for Control of Gas Migration and Water Coning in Aquifer Gas Storage," *Energy Sources* (1990) **10**, 479-497.
26. Seright, R.S.: "Gel Placement in Fractured Systems," paper SPE 27740 presented at the 1994 SPE/DOE Symposium on Improved Oil Recovery, Tulsa, April 17-20.
27. Hanssen, J.E. and Haugum P.: "Gas Blockage by Nonaqueous Foams," paper SPE 21002 presented at the 1991 SPE International Symposium on Oilfield Chemistry, Anaheim, Feb. 20-22.
28. Karp, J.C., Lowe, D.K., and Marusov, N.: "Horizontal Barriers for Controlling Water Coning," *JPT* (July 1962) 783-90.
29. Seright, R.S., Liang, J., and Sun, H.: "Gel Treatments in Production Wells with Water Coning Problems," *In Situ* (1993) **17**, No.3, 243-272.
30. Liang, J., Lee, R.L., and Seright, R.S.: "Placement of Gels in Production Wells," *SPEPF* (Nov. 1993) 276-284; *Trans.*, AIME **295**.
31. Seright, R.S.: "Impact of Permeability and Lithology on Gel Performance," paper SPE 24190

presented at the 1992 SPE/DOE Symposium on Enhanced Oil Recovery, Tulsa, April 22-24.

32. Bernard, G.G. and Holm, L.W.: "Method for Storing Gas in Subterranean Formations," U.S. Patent 3,393,738, July 23, 1968.
33. Minssieux, L.: "Oil Displacement by Foams in Relation to Their Physical Properties in Porous Media," *JPT* (Jan. 1974) 100-108.
34. Robin, M.: "Laboratory Evaluation of Foaming Additives Used to Improve Steam Efficiency," paper SPE 16729 presented at the 1987 SPE Annual Technical Conference and Exhibition, Dallas, Sept. 27-30.
35. Manlowe, D.J. and Radke, C.J.: "A Pore-Level Investigation of Foam/Oil Interactions in Porous Media," *SPE* (Nov. 1990) 495-502.
36. Casteel, J.F. and Djabbarah, N.F.: "Sweep Improvement in CO₂ Flooding by Use of Foaming Agents," *SPE* (Nov. 1988) 1186-1192.
37. Hutchins, R.D. and Dovan, H.T.: "Method for Emplacement of a Gelatinous Foam in Gas Flooding Enhanced Recovery," U.S. Patent 4,694,906, Sept. 22, 1987.
38. Hutchins, R.D., Sandiford, B.B., and Dovan, H.T.: "Foamed Gels Having Selective Permeability," U.S. Patent 5,203,834, April 20, 1993.
39. Hazlett, R.D. and Shu, P.: "Amino Resin Modified Xanthan Polymer Foamed with a Chemical Blowing Agent," U.S. Patent 4,830,108, May 16, 1989.
40. Hazlett, R.D. and Strom, E.T.: "In-Situ Foaming of Polymer Profile Control Gels," U.S. Patent 4,844,163, July 4, 1989.
41. Hazlett, R.D.: "Use of Metal Silicate Foam with a Chemical Blowing Agent," U.S. Patent 4,848,465, July 18, 1989.
42. Milind, S. *et al.*: "Stability of Aqueous Foams with Polymer Additives," *J. Colloid and Interface Science* (Oct. 1990) **139**, No. 2, 519-526.
43. Sydansk, R.D.: "Foam for Improving Sweep Efficiency in Subterranean Oil-Bearing Formations," U.S. Patent 5,105,884, April 21, 1992.
44. Sydansk, R.D.: "Enhanced Liquid Hydrocarbon Recovery Process," U.S. Patent 5,129,457, July 14, 1992.
45. Sydansk, R.D.: "Polymer-Enhanced Foam: Laboratory Development and Evaluation," paper SPE 25168 presented at the 1993 SPE International Symposium on Oilfield Chemistry, New Orleans, March 2-5.
46. Sydansk, R.D.: "Polymer-Enhanced Foam Propagation Through High-Permeability Sandpacks," paper SPE 25175 presented at the 1993 SPE International Symposium on Oilfield Chemistry, New Orleans, March 2-5.

47. Miller, M.J. and Fogler, H.S.: "A Mechanistic Investigation of Waterflood Diversion Using Foamed Gels," paper SPE 24662 presented at the 1992 SPE Annual Technical Conference and Exhibition, Washington, D.C., Oct. 4-7.
48. Miller, M.J. and Fogler, H.S.: "A Model to Estimate the Performance of Foamed Gel for Conformance Control," SPE/DOE paper 27775 presented at the 1994 SPE/DOE Symposium on Improved Oil Recovery, Tulsa, April 17-20.
49. Myers, R.D. and Greebe, F.: "Method of Reducing Permeability in Subterranean Formation by Use of Alkali Metal Silicate Foam," U.S. Patent 4,676,318, Jan. 30, 1987.
50. Chan, K.S.: "Delayed Rigid Foam Systems and Applications in Particular for Selective Plugging Treatments in the Oil Industry,," U.S. Patent 5,103,910, April 4, 1992.
51. Craighead, M.S., Hossaini, M., and Freeman, E.R.: "Foam Fracturing Utilizing Delayed Crosslinked Gels," paper SPE 14437 presented at the 1985 SPE Annual Technical Conference and Exhibition, Las Vegas, Sept. 22-25.
52. Seright, R.S. and Martin, F.D.: "Impact of Gelation pH, Rock Permeability, and Lithology on the Performance of a Monomer-Based Gel," *SPE* (Feb. 1993) 43-50.
53. Seright, R.S.: "Reduction of Gas and Water Permeabilities Using Gels," paper SPE 25855 presented at the 1993 SPE Joint Rocky Mountain Regional and Low Permeability Reservoirs Symposium, Denver, April 26-28.
54. Liang, J., Sun, H., Seright, R.S.: "Why Do Gels Reduce Water Permeability More Than Oil Permeability?," paper SPE 27829 presented at the 1994 SPE/DOE Symposium on Improved Oil Recovery, Tulsa, April 17-20.
55. Gauglitz, P.A. *et al.*: "Field Optimization of Steam/Foam for Profile Control," paper SPE 25781 presented at the 1993 International Thermal Operations Symposium, Bakersfield, Feb. 8-10.
56. Stevens, J.E. and Martin, F.D.: "CO₂ Foam Field Verification Pilot Test at EVGSAU: Phase IIIB—Project Operations and Performance Review," paper SPE 27786 presented at the 1994 SPE/DOE Symposium on Improved Oil Recovery, Tulsa, April 17-20.
57. Harpole, K.J., Siemers, W.T., and Gerard, M.G.: "CO₂ Foam Field Verification Pilot Test at EVGSAU: Phase IIIC—Reservoir Characterization and Response to Foam Injection," paper SPE 27798 presented at the 1994 SPE/DOE Symposium on Improved Oil Recovery, Tulsa, April 17-20.
58. Hoefner, M.L. *et al.*: "CO₂ Foam: Results From Four Developmental Field Trials," paper SPE 27787 presented at the 1994 SPE/DOE Symposium on Improved Oil Recovery, Tulsa, April 17-20.
59. Kuehne, D.L. *et al.*: "Design and Evaluation of a Nitrogen-Foam Field Trial," *JPT* (April 1990) 504-512.
60. Seright, R.S.: "Impact of Dispersion on Gel Placement for Profile Control," *SPE* (Aug. 1991) 343-352.

61. Sorbie, K.S. and Seright, R.S.: "Gel Placement in Heterogeneous Systems with Crossflow," paper SPE 24192 presented at the 1992 SPE/DOE Symposium on Enhanced Oil Recovery, Tulsa, April 22-24.
62. Greaser, G.R. and Shore, R.A.: "Steamflood Performance in the Kern River Field," paper SPE 8834 presented at the 1980 SPE/DOE Symposium on Enhanced Oil Recovery, Tulsa, April 20-23.
63. Clampitt, R.L., Eson, R.L., and Cooke, R.W.: "Applying a Novel Steam-CO₂ Combination Process in Heavy Oil and Tar Sands," paper SPE 21547 presented at the 1991 International Thermal Operations Symposium, Bakersfield, Feb. 7-8.
64. Eson, R.L. and Cooke, R.W.: "A Successful High-Temperature Gel System to Reduce Steam Channeling," paper SPE 24665 presented at the 1992 SPE Annual Technical Conference and Exhibition, Washington, D.C., Oct. 4-7.
65. Hirasaki, G.J.: "The Steam-Foam Process," *JPT* (May 1989) 449-456.
66. Castanier, L.M. and Brigham, W.E.: "An Evaluation of Field Projects of Steam with Additives," *SPE* (Feb. 1991) 62-68.
67. Patzek, T.W. and Kolnis, M.T.: "Kern River Steam-Foam Pilots," *JPT* (April 1990) 496-503.
68. Heller, J.P., Boone, D.A., and Watts, R.J.: "Field Test of CO₂ Mobility Control at Rock Creek," paper SPE 14395 presented at the 1985 SPE Annual Technical Conference and Exhibition, Las Vegas, Sept. 22-25.
69. Chou, S.I. *et al.*: "CO₂ Foam Field Trial at North Ward-Estes," paper SPE 24643 presented at the 1992 SPE Annual Technical Conference and Exhibition, Washington, D.C., Oct. 4-7.
70. *Emulsions*, L.L. Schramm (ed.), Advances in Chemistry Series 231, ACS, Washington, D.C. (1992).
71. Soo, H. and Radke, C.J.: "The Flow Mechanism of Dilute, Stable Emulsions in Porous Media," *I&EC Fundamentals* (1984) **23**, 342-347.
72. Soo, H. and Radke, C.J.: "Flow of Dilute, Stable Liquid and Solid Dispersions in Underground Porous Media," *AIChE J.* (Nov. 1985) **31**, No. 11, 1926-1928.
73. Soo, H. and Radke, C.J.: "Velocity Effects in Emulsion Flow through Porous Media," *J. Colloid & Interface Science* (Dec. 1984) **102**, No. 2, 462-476.
74. Soo, H. and Radke, C.J.: "A Filtration Model for the Flow of Dilute, Stable Emulsions in Porous Media—I. Theory," *Chemical Engineering Science* (1986) **41**, No. 2, 263-272.
75. Soo, H., Williams, M.C., and Radke, C.J.: "A Filtration Model for the Flow of Dilute, Stable Emulsions in Porous Media—II. Parameter Evaluation and Estimation," *Chemical Engineering Science* (1986) **41**, No. 2, 273-281.
76. McAuliffe, C.D.: "Oil-in-Water Emulsions and Their Flow Properties in Porous Media," *JPT* (June

1973) 727-733.

77. Spielman, L.A. and Su, Y-P.: "Coalescence of Oil-in-Water Suspensions by Flow Through Porous Media," *I&EC Fundamentals* (1977) **16**, No. 2, 272-282.
78. Cartmill, J.C. and Dickey, J.C.: "Flow of a Disperse Emulsion of Crude Oil in Water Through Porous Media," *AAPG Bulletin* (Dec. 1970) **54**, No. 12, 2438-2447.
79. French, T.R.: "Use of Crude Oil Emulsions to Improve Profiles," *Surfactant-Based Mobility Control*, D.H. Smith (ed.), Symposium Series 373, ACS, Washington, D.C. (1988) 405-428.
80. Alvarado, D.A. and Marsden, S.S.: "Flow of Oil-in-Water Emulsions Through Tubes and Porous Media," *SPEJ* (Dec. 1979) 369-377.
81. Gogarty, W.B.: "Rheological Properties of Pseudoplastic Fluids in Porous Media," *SPEJ* (June 1967) 149-160.
82. Spielman, L.A. and Goren, S.L.: "Progress in Induced Coalescence and a New Theoretical Framework for Coalescence by Porous Media," *I&EC Chemistry* (Oct. 1970) **62**, No. 10, 10-24.
83. Devereux, O.F.: "Emulsion Flow in Porous Solids," *Chemical Engineering J.* (1974) **7**, 121-136.
84. Islam, M.R. and Farouq Ali, S.M.: "Numerical Simulation of Emulsion Flow Through Porous Media," *JCPT* (March 1994) **33**, No. 3., 59-63.
85. Varnon, J.E. *et al.*: "High Conformance Oil Recovery Process," U.S. Patent 4,159,037, June 26, 1979.
86. Schievelbein, V.H. and Park, J.H.: "High Conformance Oil Recovery Process," U.S. Patent 4,160,480, July 10, 1979.
87. Decker, R.M. and Flock, D.L.: "Thermal Stability and Application of Emulsion Composed Blocking Agents for Steamflooding," *JCPT* (Aug. 1988) **27**, No. 4, 69-78.
88. Eddins, W.N. and Lissant, K.J.: "Method of Reducing the Porosity of Subterranean Porous Formations, U.S. Patent 3,343,599, Sept. 26, 1967.
89. Tosch, W.C.: "Prevention of Salt Water Encroachment into Fresh Water Aquifers," U.S. Patent 3,587,737, June 28, 1971
90. Son, M.: "Use of Oil-External Micellar Dispersions as Plugging Agents in Subterranean Formations," U.S. Patent 3,604,508, Sept. 14, 1971.
91. Dauben, D.L.: "Miscible Flood Process," U.S. Patent 3,866,680, Feb. 18, 1975.
92. Wu, C.H. *et al.*: "High Vertical and Horizontal Conformance Thermal Oil Recovery Process," U.S. Patent 4,175,618, Nov. 27, 1979.
93. Morris, C.W. and Terry, R.E.: "Method for Permeability Correction by In Situ Genesis of

- Macroemulsions in Hard Brines," U.S. Patent 4,296,811, Oct. 27, 1981.
94. Brown, A. *et al.*: "High Sweep Efficiency Enhanced Oil Recovery Process," U.S. Patent 4,299,284, Nov. 10, 1981.
 95. Falk, D.O.: "Selectively Plugging Subterranean Formations with a Hydrocarbon Soluble Fluid," U.S. Patent 4,482,015, Nov. 13, 1984.
 96. Yeung, K. and Farouq Ali, S.M.: "How to Waterflood Reservoirs with a Water Leg," *JCPT* (Jan. 1994) **33**, No. 1, 50-55.
 97. McAuliffe, C.D.: "Crude-Oil-in-Water Emulsions to Improve Fluid Flow in an Oil Reservoir," *JPT* (June 1973) 721-726.
 98. Binder, G.G and Russell, C.D.: "Secondary Oil Recovery Process," U.S. Patent 3,149,669, Sept. 22, 1964.
 99. Hardy, W.C., Shepard, J.C., and Reddick, K.L.: "Secondary Recovery of Petroleum with a Preformed Emulsion Slug Drive," U.S. Patent 3,294,164, Dec. 27, 1966.
 100. Hardy, W.C. and Crawford, H.R.: "Secondary Recovery of Petroleum," U.S. Patent 3,358,758, Dec. 1967.
 101. Cooke, C.E., Williams, R.E., and Kolodzie, P.A.: "Oil Recovery by Alkaline Waterflooding," *JPT* (Dec. 1974) 1365-1374.
 102. Islam, M.R. and Farouq Ali, S.M.: "Mobility Control in Waterflooding Oil Reservoirs with a Bottom-Water Zone," *JCPT* (Nov.-Dec. 1987) **26**, 40-53.
 103. Islam, M.R. and Farouq Ali, S.M.: "Waterflooding Oil Reservoirs with Bottom Water," *JCPT* (May-June 1989) **28**, No. 3, 59-66.
 104. Breston, J.N.: "Selective Plugging of Waterflood Input Wells Theory, Methods and Results," *JPT* (March 1957) 26-31.
 105. Willman, B.T.: "Method for Control of Water Injection Profiles," U.S. Patent No. 3,251,414 (1966).
 106. Garland, T.M.: "Selective Plugging of Water Injection Wells," *JPT* (Dec. 1966) 1550-1560.
 107. Smith, L.R., Fast, C.R., and Wagner, O.R.: "Development and Field Testing of Large Volume Remedial Treatments for Gross Water Channeling," *JPT* (Aug. 1969) 1015-1025.
 108. White, N.F., Noles, J.R., and Walker, C.O.: "Method for Treating Underground Formations," U.S. Patent No. 4,261,422 (1981).
 109. Jennings, Jr., A.R.: "Disposal of Produced Formation Fines During Oil Recovery," U.S. Patent No. 4,787,452 (1988).
 110. Snowden, M.J., Vicent, B., and Morgan, J.C.: "Conformance Control In Underground Reservoirs,"

- U.K. Patent No. GB2262117A, (1993).
111. Thomeer, J.H. and Abrams, A.: "A Shallow Plugging-Selective Re-Entry Technique for Profile Correction," *JPT* (May, 1977) 571-578.
 112. Vetter, O.J., Kandarpa, V., Stratton, M., and Veith, E.: "Particle Invasion Into Porous Medium and Related Injectivity Problems," paper SPE 16255 presented at the 1987 International Symposium on Oilfield Chemistry, San Antonio, Feb. 4-6.
 113. Eleri, O.O. and Ursin, J-R.: "Physical Aspects of Formation Damage in Linear Flooding Experiments," paper SPE 23784 presented at the 1992 International Symposium on Formation Damage Control, Lafayette, Feb. 26-27.
 114. Barkman, J.H. and Davidson, D.H.: "Measuring Water Quality and Predicting Well Impairment," *JPT* (July 1972) 865-873.
 115. Abram, A.: "Mud Design To Minimize Rock Impairment Due to Particle Invasion," *JPT* (May 1977) 586-592.
 116. van Oort, E., van Velzen, J.F.G., and Leerlooijer, K.: "Impairment by Suspended Solids Invasion: Testing and Prediction," *SPEPF* (Aug. 1993) 178-184.
 117. Donaldson, E.C., Baker, B.A., and Carroll, H.B.: "Particle Transport in Sandstones," paper SPE 6905 presented at the 1977 SPE Annual Technical Conference and Exhibition, Denver, Oct. 9-12.
 118. Davidson, D.H.: "Invasion and Impairment of Formations by Particulates," paper SPE 8210 presented at the 1979 SPE Annual Technical Conference and Exhibition, Las Vegas, Sept. 23-26.
 119. Eylander, J.G.R.: "Suspended Solids Specifications for Water Injection From Coreflood Tests," *SPEPE* (Nov. 1988) 1287-1294.
 120. Kumar, T. and Todd, A.C.: "A New Approach for Mathematical Modeling of Formation Damage Due to Invasion of Solid Suspensions," paper SPE 18203 presented at the 1988 SPE Annual Technical Conference and Exhibition, Houston, Oct. 2-5.
 121. Baghdikian, S.Y., Sharma, M.M., and Handy, L.L.: "Flow of Clay Suspensions Through Porous Media," *SPEPE* (May 1989) 213-220.
 122. Todd, A.C., Kumar, T., and Mohammadi, S.: "The Value and Analysis of Core-Based Water-Quality Experiments as Related to Water Injection Schemes," *SPEFE* (June 1990) 185-191.
 123. Tien, C. and Payatakes, A.C.: "Advances in Deep Bed Filtration," *AIChE Journal* (1979) **25**, No. 5, 737-759.
 124. Hoefner, M.L., Seetharam, R.V., Shu, P., and Phelps, C.H.: "Selective Penetration of Biopolymer Profile-Control Gels: Experiment and Model," *Journal of Petroleum Science and Engineering* (1992) **7**, 53-66.
 125. Seright, R.S.: "Effect of Rheology on Gel Placement," *SPEPE* (May, 1991) 212-218.

126. Seright, R.S. and Martin, F.D.: "Fluid Diversion and Sweep Improvement with Chemical Gels in Oil Recovery Processes," second annual report (DOE/BC/14447-10), Contract No. DE-FG22-89BC14447, U.S. DOE (Nov. 1991) 86-110.
127. Vela, S., Peaceman, D.W., and Sandvik, E.I.: "Evaluation of Polymer Flooding in a Layered Reservoir With Crossflow, Retention, and Degradation," *SPEJ* (April 1976) 82-96.
128. Jennings, R.R., Rogers, J.H., and West, T.J.: "Factors Influencing Mobility Control By Polymer Solutions," *JPT* (March 1971) 391-401.
129. Zaitoun, A. and Kohler, N.: "The Role of Adsorption in Polymer Propagation Through Reservoir Rocks," paper SPE 16274 presented at the SPE International Symposium on Oilfield Chemistry, San Antonio, Oct. 4-6, 1987.
130. Seright, R.S. and Martin, F.D.: "Effect of Cr^{3+} on the Rheology of Xanthan Formulations in Porous Media: Before and After Gelation," *In Situ* (1992) **16**, No.1, 1-16.
131. Seright, R.S. and Martin, F.D.: "Fluid Diversion and Sweep Improvement with Chemical Gels in Oil Recovery Processes," first annual report (DOE/BC/14447-8), Contract No. DE-FG22-89BC14447, U.S. DOE (June 1991) 34-55.
132. Fletcher, J.P., Flew, S., Forsdyke, I.N., Morgan, J.C., Rogers, C., and Suttles, D.: "Deep Diverting Gels for Very Cost Effective Waterflood Control," *J. Petroleum Science & Engineering* (April 1992) **2**, Nos. 1,2, 33-43.
133. Matthews, C.S. and Russell, D.G.: *Pressure Buildup and Flow Tests in Wells*, Monograph Series, SPE, Richardson, TX (1967) 48.
134. Gabriel, G.A. and Erbstoesser, S.R.: "The Design of Buoyant Ball Sealer Treatments," paper SPE 13085 presented at the 1984 SPE Annual Technical Conference and Exhibition, Houston, Sept. 16-19.
135. Dullien, F.A.L.: *Porous Media: Fluid Transport and Pore Structure*, Academic Press, London (1979) 170-171.
136. van Velzen, J.F.G. and Leerlooijer, K.: "Impairment of a Water Injection Well by Suspended Solids: Testing and Prediction," paper SPE 23822 presented at the 1992 SPE International Symposium on Formation Damage, Lafayette, LA, Feb. 27-27.
137. Mack, J.C. and Smith, J.E.: "In-Depth Colloidal Dispersion Gels Improve Oil Recovery Efficiency," paper SPE 27780 presented at the 1994 SPE/DOE Symposium on Improved Oil Recovery, Tulsa, April 17-20.
138. Fielding, R.C., Gibbons, D.H., and Legrand, F.P.: "In-Depth Drive Fluid Diversion Using and Evolution of Colloidal Dispersion Gels and New Bulk Gels: An Operational Case History of North Rainbow Ranch Unit," paper SPE 27773 presented at the 1994 SPE/DOE Symposium on Improved Oil Recovery, Tulsa, April 17-20.

139. Hejri, S. *et al.*: "Permeability Reduction by a Xanthan/Cr(III) System in Porous Media," *SPE* (Nov. 1993) 299-304.
140. Todd, B.J., Green, D.W., and Willhite, G.P.: "A Mathematical Model of In-Situ Gelation of Polyacrylamide by a Redox Process," *SPE* (Feb. 1993) 51-58.
141. Burcik, E.J.: "The Mechanism of Microgel Formation in Partially Hydrolyzed Polyacrylamide," *JPT* (April 1969) 373-374.
142. Seright, R.S.: "The Effects of Mechanical Degradation and Viscoelastic Behavior on Injectivity of Polyacrylamide Solutions," *SPEJ* (June 1983) 475-85.
143. Seright, R.S., Maerker, J.M., and Holzwarth G.: "Mechanical Degradation of Polyacrylamides Induced by Flow Through Porous Media," *American Chemical Society Polymer Preprints* (Aug. 1981) **22**, 30-33.
144. Chauveteau, G. and Lecourtier, J.: "Propagation of Polymer Slugs Through Adsorbent Porous Media," *Water Soluble Polymers for Petroleum Recovery*, G.A. Stahl and D.N. Schulz (eds.), Plenum, New York (1988) 53-68.
145. Putz, A.G., Lecourtier, J.M., and Bruckert, L.: "Interpretation of High Recovery Obtained in a New Polymer Flood in the Chateaufrenard Field," paper SPE 18093 presented at the 1988 SPE Annual Technical Conference and Exhibition, Houston, Oct. 2-5.
146. Walsh, M.P. *et al.*: "Chemical Interactions of Aluminum-Citrate Solutions with Formation Minerals," paper SPE 11799 presented at the 1983 International Symposium on Oilfield Chemistry, Denver, June 1-3.
147. Rocha, C.A. *et al.*: "An Experimental Study of the Interactions of Aluminum Citrate Solutions and Silica Sand," paper SPE 18503 presented at the 1989 International Symposium on Oilfield Chemistry, Denver, Feb. 8-10.
148. Seright, R.S. and Liang, J.: "A Survey of Field Applications of Gel Treatments for Water Shutoff," paper SPE 26991 presented at the 1994 SPE III Latin American & Caribbean Petroleum Engineering Conference, Buenos Aires, April 27-29.
149. Sydansk, R.D.: "A Newly Developed Chromium (III) Gel Technology," *SPE* (Aug. 1990) 346-352.
150. Zaitoun, A. and Potie, B.: "Limiting Conditions for the Use of Hydrolyzed Polyacrylamides in Brines Containing Divalent Ions," paper SPE 11785 presented at the 1983 International Symposium on Oilfield Chemistry, Denver, June 1-3.
151. Moradi-Araghi, A. and Doe, P.H.: "Hydrolysis and Precipitation of Polyacrylamides in Hard Brines at Elevated Temperatures," *SPE* (May 1987) 189-198.
152. Muskat, M.: *The Flow of Homogeneous Fluids Through Porous Media*, McGraw-Hill Book Co. Inc., New York (1937) 164-165.

153. Needham, R.B., Threlkeld, C.B., and Gall, J.W.: "Control of Water Mobility Using Polymers and Multivalent Cations," paper SPE 4747 presented at the 1974 SPE-AIME Improved Oil Recovery Symposium, Tulsa, April 22-24.
154. Avery, M.R. and Wells, T.A.: "Field Evaluation of a New Gelant for Water Control in Production Wells," paper SPE 18201 presented at the 1988 SPE Annual Technical Conference and Exhibition, Houston, Oct. 2-5.
155. Sandiford, B.B. and Graham, G.A.: "Injection of Polymer Solutions in Producing Wells," AICHE Symposium Series, (1973) **69**, No. 127, 38.
156. Schneider, F.N. and Owens, W.W.: "Steady-State Measurements of Relative Permeability for Polymer/Oil Systems," *SPEJ* (Feb. 1982) 79.
157. Sparlin, D.D.: "An Evaluation of Polyacrylamides for Reducing Water Production," *JPT* (Aug. 1976) 906-914.
158. White, J.L., Goddard, J.E., and Phillips, H.M.: "Use of Polymers To Control Water Production in Oil Wells," *JPT* (Feb. 1973) 143-150.
159. Zaitoun, A. and Kohler N.: "Two-Phase Flow Through Porous Media: Effect of an Adsorbed Polymer Layer," paper SPE 18085 presented at the 1988 SPE Annual Technical Conference and Exhibition, Houston, Oct. 2-5.
160. Zaitoun, A. and Kohler N.: "Thin Polyacrylamide Gels for Water Control in High-Permeability Production Wells" paper SPE 22785 presented at the 1991 SPE Annual Technical Conference and Exhibition, Dallas, Oct. 6-9.
161. Liang, J., Sun, H., and Seright, R.S.: "Reduction of Oil and Water Permeabilities Using Gels," paper SPE 24195 presented at the 1992 SPE/DOE Symposium on Enhanced Oil Recovery, Tulsa, April 22-24.
162. Seright, R.S.: "Improved Techniques for Fluid Diversion in Oil Recovery," first annual report, DOE/BC/14880-5, U.S. DOE (Dec. 1993) 141-165.
163. Seright, R.S. and Martin, F.D.: "Fluid Diversion and Sweep Improvement with Chemical Gels in Oil Recovery Processes," final report, DOE/BC/14447-15, U.S. DOE (Sept. 1992) 28-58.
164. Zaitoun, A. and Kohler N.: "Modification of Water/Oil and Water/Gas Relative Permeabilities After Polymer Treatment of Oil or Gas Wells," *In Situ* (1989) **13**, No. 1&2, 55-77.

APPENDIX A

Effect of Formation Permeability on Degree of Permeability Reduction by Particulates

Tien *et al.*¹²³ conducted an extensive review of the deep-bed-filtration theory. The authors presented relationships between the amount of deposition and the changes of pressure gradient for two limiting cases of the deposition mechanisms.

Smooth-Coating Mode

In the smooth-coating mode, particles form a uniform smooth coating outside filter grains during the deposition process. All flow passages remain open until the pores are completely filled. The following equation relates the amount of deposit and the changes in pressure gradient,

$$\frac{(\Delta p / \Delta z)}{(\Delta p / \Delta z)_o} = \frac{1}{1 - \frac{s}{f_o(1 - f_d)}} + \frac{f_o^3}{(1 - f_d)(1 - f_o)^3} \quad (A1)$$

where

- p = pressure, psi
- z = axial distance, inches
- s = specific deposit (volume of deposited matter per unit volume of filter bed)
- f_o = porosity of clean filter bed
- f_d = porosity of deposits

In Eq. A1, f_o is the only term in the equation relating to the property of the clean filter bed. For a given amount of deposition, Eq. A1 shows that the degree of permeability reduction, $(\Delta p / \Delta z) / (\Delta p / \Delta z)_o$, increases with decreasing porosity of the clean filter bed. Assuming that the filter grains are uniform spheres, the relationship between the permeability and the porosity of the clean filter bed can be described by the Carman-Kozeny equation

$$k_o = \frac{1}{72\tau} \frac{f_o^3 d^2}{(1 - f_o)^2}, \quad (A2)$$

where

- k_o = clean filter permeability, md
- τ = tortuosity
- d = filter grain size or pore size, μm

According to Eq. A2, the clean filter bed permeability decreases with decreasing porosity. Therefore, for a given amount of deposition, the permeability reduction increases with decreasing clean bed permeability.

Blocking Mode

In the blocking mode, deposition occurs when particles are trapped by the pore constrictions. Assume that the filter bed is composed of a number of constricted tubes with the same dimensions. The following equation describes the relationship between the amount of deposit and the changes in pressure gradient,

$$\frac{(\Delta p / \Delta z)}{(\Delta p / \Delta z)_0} = 1 - \frac{3 a_c \beta}{2 (1 - \beta_d) r_c^3 (1 - \beta_o)^{1/3} N_o \beta^{2/3}} \beta^{-1} \quad (\text{A3})$$

where

a_c = collector radius, inches

β = adjustable parameter for the minimum amount of deposit to block off a constriction

r_c = radius of constrictions, inches

N_o = number of constricted tubes per unit sectional area of a clean filter bed

Eq. A3 shows that the degree of permeability reduction is a strong function of the radius of constrictions. The degree of permeability reduction, $(\Delta p / \Delta z) / (\Delta p / \Delta z)_0$, in this case increases with decreasing radius of constrictions. From Eq. A2, the permeability of the clean filter bed is proportional to the square of the pore size. Therefore, for a given amount of deposition, the permeability reduction increases with decreasing clean bed permeability.

The flow of particulates in the porous medium is very similar to the deep-bed-filtration process. From our analysis of the deep-bed-filtration theory, we conclude that the degree of permeability reduction by particulates increases with decreasing formation permeability.

APPENDIX B

Derivation of Eq. 37

Expression of Permeability Distribution

$$k_i = \frac{1}{\frac{\cos^2 \theta_i}{k_x} + \frac{\sin^2 \theta_i}{k_y}} \quad (\text{B1})$$

Derivation

$$u_x = \frac{k_x}{\cos^2 \theta_i} \frac{dp}{dr} + u_y \sin^2 \theta_i \quad (\text{B2})$$

$$u_y = - \frac{k_y}{\sin^2 \theta_i} \frac{dp}{dr} \quad (\text{B6})$$

Rearranging Eq. B2,

$$k_i = - \frac{u_i}{\frac{dp}{dr}} = - \frac{u_i^2}{u_i \frac{dp}{dr}} = - \frac{u_i^2}{\frac{dp}{dr} u_i} \quad (\text{B7})$$

Inputting Eqs. B3 through B6 into Eq. B7, yields

$$\begin{aligned}
 k_i &= -\frac{\frac{u_x \frac{\partial p}{\partial x} + u_y \frac{\partial p}{\partial y}}{u_i^2}}{\frac{u_i \cos^2 \theta_i \frac{\partial p}{\partial x} + u_i \sin^2 \theta_i \frac{\partial p}{\partial y}}{u_i^2}} = -\frac{\frac{\partial p}{\partial x} \cos^2 \theta_i + \frac{\partial p}{\partial y} \sin^2 \theta_i}{\frac{\partial p}{\partial x} \cos^2 \theta_i + \frac{\partial p}{\partial y} \sin^2 \theta_i}}{u_i} \\
 &= \frac{\frac{\partial p}{\partial x} \cos^2 \theta_i + \frac{\partial p}{\partial y} \sin^2 \theta_i}}{\frac{\frac{u_x \cos^2 \theta_i}{u_i} \frac{\partial p}{\partial x} + \frac{u_y \sin^2 \theta_i}{u_i} \frac{\partial p}{\partial y}}{u_i}} = \frac{1}{\frac{\cos^2 \theta_i}{k_x} + \frac{\sin^2 \theta_i}{k_y}} \\
 &= \frac{1}{\frac{\cos^2 \theta_i}{k_x} + \frac{\sin^2 \theta_i}{k_y}}
 \end{aligned} \tag{B8}$$

APPENDIX C

Derivation of Eq. 38

$$\frac{q_i}{k_i} \left[\frac{r_{pi}^2}{r_w^2} F_r \ln \left(\frac{r_{pi}}{r_w} \right) + \ln \left(\frac{r_e}{r_{pi}} \right) + \frac{1-F_r}{2} \left(\frac{r_w}{r_{pi}} \right)^2 \ln \left(\frac{r_e}{r_w} \right) + \frac{1-F_r}{2} \right] = \text{constant} \quad (38)$$

In Model 1 of Chapter 8, both the inner boundary (injection wellbore) and the outer drainage boundary are circular equipotential lines. Therefore, the equipotential curves in the drainage area should also be concentric circles. Since streamlines are always perpendicular to the equipotential curves, the streamlines in the drainage area should be radial.

Based on the above analysis, we can divide the drainage area into an infinite number of sector elements. Darcy's law can be applied to any one of these elements as follows:

$$u_i = - \frac{k_i}{\mu} \frac{dp}{dr} \quad (C1)$$

Rearranging,

$$dp = - u_i \frac{\mu}{k_i} dr \quad (C2)$$

Another expression for superficial velocity:

$$u_i = \frac{q_i}{r h} \quad (C3)$$

Inputting Eq. C3 into Eq. C2,

$$dp = - \frac{q_i}{r h k_i} dr \quad (C4)$$

Integrating the left side of Eq. C4 between p_w and p_r , while integrating the right side between r_w and r_{pi} ,

$$p_w - p_r = \frac{q_i}{h k_i} \ln \left(\frac{r_{pi}}{r_w} \right) \quad (C5)$$

Integrating the left side of Eq. C4 between p_r and p_e , while integrating the right side between r_{pi} and r_e ,

$$p_r - p_e = \frac{q_i}{h k_i} \ln \frac{r_e}{r_{pi}} \quad (C6)$$

Combining Eqs. C5 and C6,

$$p_w - p_e = \frac{q_i}{h k_i} \ln \frac{r_{pi}}{r_w} + \mu_p \ln \frac{r_e}{r_{pi}} \quad (C7)$$

Rearranging Eq. C3,

$$\frac{q_i}{h} = r u_i \quad (C8)$$

Another expression for v_i :

$$u_i = v_i = \frac{dr}{dt} \quad (C9)$$

Combining Eqs. C8 and C9,

$$\frac{q_i}{h} = r \frac{dr}{dt} \quad (C10)$$

Inputting Eq. C10 into Eq. C7 and replacing μ_p/μ_w with F_r ,

$$p_w - p_e = r \frac{dr}{dt} \frac{1}{k_i} \ln \frac{r_{pi}}{r_w} + \ln \frac{r_e}{r_{pi}} \quad (C11)$$

Rearranging,

$$\frac{1}{k_i} \ln \frac{r_{pi}}{r_w} + \ln \frac{r_e}{r_{pi}} F_r \frac{dr}{dt} = \frac{p_w - p_e}{r} \quad (C12)$$

Integrating between time 0 and t,

$$\int_0^t \frac{1}{k_i} \ln \frac{r_{pi}}{r_w} + \ln \frac{r_e}{r_{pi}} F_r \frac{dr}{dt} dt = \int_0^t \frac{p_w - p_e}{r} dt \quad (C13)$$

Simplifying and integrating with respect to r,

$$\frac{p_i}{k_i} \frac{r_{pi}}{r_w} F_r \ln \frac{r_{pi}}{r_w} + \ln \frac{r_e}{r_{pi}} r dr = \frac{p_w - p_e}{\mu} t \quad (C14)$$

Solving the integration and simplifying,

$$\frac{p_i}{k_i} \frac{r_{pi}^2}{r_w} F_r \ln \frac{r_{pi}}{r_w} + \ln \frac{r_e}{r_{pi}} + \frac{1 - F_r}{2} \frac{r_w^2}{r_{pi}^2} \ln \frac{r_e}{r_w} + \frac{1 - F_r}{2} = 2 \frac{p_w - p_e}{\mu} t \quad (C15)$$

At any given time, the right side of Eq. C15 is a constant under the conditions assumed here.

APPENDIX D

Derivations of Eqs. 39, 40, and 41

Equations for the superficial velocity and injectivity before and after gel forms (used in Chapter 8) are developed in this appendix.

Superficial Velocity Before Gel Forms

Along a given radial pathway,

$$p_w - p_e = q_{io} \frac{h}{k_i} F_r \ln \frac{r_{pi}}{r_w} + \ln \frac{r_e}{r_{pi}} \quad (D1)$$

Rearranging Eq. D1,

$$q_{io} = (p_w - p_e) \frac{k_i h}{F_r \ln \frac{r_{pi}}{r_w} + \ln \frac{r_e}{r_{pi}}} \quad (D2)$$

The superficial velocity can be expressed as

$$u_i = \frac{q_{io}}{h r} \quad (D3)$$

Inputting Eq. D2 into Eq. D3,

$$u_i = (p_w - p_e) \frac{k_i}{r F_r \ln \frac{r_{pi}}{r_w} + \ln \frac{r_e}{r_{pi}}} \quad (D4)$$

If $F_r=1$, Eq. D4 can be re-written as

$$u_i = (p_w - p_e) \frac{k_i}{r \ln \frac{r_e}{r_w}} \quad (D5)$$

Superficial Velocity After Gel Forms

For convenience, the following derivation assumes F_r is equal to 1.

Along a given pathway,

$$p_w - p_e = q_i \frac{h k_i}{r_w F_{rr}} \ln \frac{r_{pi}}{r_w} + \ln \frac{r_e}{r_{pi}} \quad (D6)$$

Rearranging,

$$q_i = (p_w - p_e) \frac{h k_i}{r_w F_{rr} \ln \frac{r_{pi}}{r_w} + \ln \frac{r_e}{r_{pi}}} \quad (D7)$$

So, superficial velocity can be expressed as

$$u_i = \frac{k_i}{r_w F_{rr}} \frac{p_w - p_e}{\ln \frac{r_{pi}}{r_w} + \ln \frac{r_e}{r_{pi}}} \quad (D8)$$

Injectivity Before and After Gel Forms

By rearranging Eq. D2, the fluid injectivity, I_{io} , in direction i before gel forms is expressed as

$$I_{io} = \frac{q_{io}}{p_w - p_e} = \frac{h k_i}{r_w F_{rr} \ln \frac{r_{pi}}{r_w} + \ln \frac{r_e}{r_{pi}}} \quad (D9)$$

By rearranging Eq. D7, the fluid injectivity, I_i , in direction i after gel forms is expressed as

$$I_i = \frac{q_i}{p_w - p_e} = \frac{h k_i}{r_w F_{rr} \ln \frac{r_{pi}}{r_w} + \ln \frac{r_e}{r_{pi}}} \quad (D10)$$

For the case of constant pressure drop between the injection well and the outer boundary, the overall injectivity ratio, I/I_o , or the ratio of the total injection rate after gel forms to the total injection rate before gel forms is expressed as

(D11)

APPENDIX E

Derivation of Eq. 42

Pressure Expression

In Model 2 of Chapter 8, the pressure before gelant injection can be expressed in the form of Fourier series as

$$p = \frac{\frac{m}{4} + n - p_w}{\log\left(\frac{r_e}{r_w}\right)} \log(r) + p_w - \log(r_w) - \frac{\frac{m}{4} + n - p_w}{\log\left(\frac{r_e}{r_w}\right)} \quad (E1)$$

$$+ \sum_{k=1,3,5,\dots} \frac{2m}{k^2 (r_w^{4k} r_e^{-2k} - r_e^{-2k})} r^{2k} + \sum_{k=1,3,5,\dots} \frac{2m}{k^2 (r_w^{-4k} r_e^{2k} - r_e^{-2k})} r^{-2k} \cos(2k\theta)$$

Prescribed boundary conditions

Inner boundary ($r=r_w$):

$$p = p_w \quad (E2)$$

Outer boundary ($r=r_e$):

$$p = m + n \quad \text{for } 0 \leq \theta \leq \frac{\pi}{2} \quad (E3)$$

where

- n = pressure at the intersecting point of the outer boundary and the x-axis, psi
- m = slope of the linear pressure distribution at the outer boundary

Derivation

At the outer boundary, pressure can be expressed in Fourier series as

$$p = \frac{w_0}{2} + \sum_{k=1,2,3,\dots} w_k \cos(2k\theta) \quad (E4)$$

where

$$w_k = \frac{-2m}{k^2} \quad k = 1, 3, 5, \dots \quad \frac{1}{4} \frac{m}{2} + n \quad \sin(2k?) = \frac{m}{k^2} \cos(k?) - 1? \quad k = 1, 2, 3, \dots \quad (E5)$$

$$= 0 \quad k = 2, 4, 6, \dots \quad (E6)$$

$$= \frac{m}{2} + 2n$$

Inputting Eqs. E5 and E6 into Eq. E4,

$$p = \frac{m}{4} + n + \sum_{k=1,3,5,\dots} \frac{-2m}{k^2} \cos(2k?) \quad (E7)$$

The general solution for Laplace equation is

$$p = c_0 \log(r) + \sum_0^{\infty} r^{\alpha} [a_{\alpha} \sin(\alpha?) + b_{\alpha} \cos(\alpha?)] + \sum_1^{\infty} r^{-\alpha} [c_{\alpha} \sin(\alpha?) + d_{\alpha} \cos(\alpha?)] \quad (E8)$$

Since pressure is a periodic function with period of p , Eq. E8 can be re-written as

$$p = c_0 \log(r) + b_0 + \sum_1^{\infty} [r^{2k} a_k + r^{-2k} c_k \sin(2k?) + r^{2k} b_k + r^{-2k} d_k \cos(2k?)] \quad (E9)$$

Comparing Eq. E9 to the inner boundary condition,

$$\begin{aligned}
 c_0 \log \frac{r_e}{r_w} + b_0 &= p_w \\
 r_w^{2k} a_k + r_w^{-2k} c_k &= 0 \quad k = 1, 2, 3, \dots \\
 r_w^{2k} b_k + r_w^{-2k} d_k &= 0
 \end{aligned}
 \tag{E10}$$

Comparing Eq. E9 to the outer boundary condition,

$$r_e^{2k} a_k + r_e^{-2k} c_k = \frac{2m}{2k^2} + n \quad k = 1, 2, 3, \dots
 \tag{E11}$$

$$= 0 \quad k = 2, 4, 6, \dots
 \tag{E13}$$

Solving the above two sets of equations, yields

$$\begin{aligned}
 b_k &= \frac{m \frac{2m}{2k^2} + n - p_w}{\log \frac{r_e}{r_w}} \quad k = 1, 3, 5, \dots \\
 &= 0 \quad k = 2, 4, 6, \dots
 \end{aligned}
 \tag{E15}$$

$$b_0 = p_w - \log \frac{r_e}{r_w} \frac{\frac{m}{4} + n - p_w}{\log \frac{r_e}{r_w}}
 \tag{E14}$$

$$a_k = 0 \quad k = 1, 2, 3, \dots$$

$$c_k = 0 \quad k = 1, 2, 3, \dots$$

$$d_k = \frac{2m}{k^2 \left(\frac{r_w^{-4k}}{r_e^{2k}} - r_e^{-2k} \right)} \quad k = 1, 3, 5, \dots \quad (E16)$$

$$= 0 \quad k = 2, 4, 6, \dots$$

Inputting the above coefficients into Eq. E9 and rearranging, Eq. E1 is obtained.

Pressure Gradient Expression

In polar coordinates, the gradient of pressure is expressed as

$$-p = \frac{\partial p}{\partial r} \cos \theta - \frac{1}{r} \frac{\partial p}{\partial \theta} \sin \theta \quad i + \frac{\partial p}{\partial r} \sin \theta + \frac{1}{r} \frac{\partial p}{\partial \theta} \cos \theta \quad j \quad (E17)$$

Differentiating Eq. E1,

$$\frac{\partial p}{\partial r} = m \frac{\partial}{\partial r} \left(\frac{r^2}{4} + n - p_w \right) \sin(2k\theta) + \frac{4m}{r^2} \left(\frac{r^{2k}}{r_w^{-2k} r_e^{2k}} + \frac{r^{-2k}}{r_w^{-4k} r_e^{2k} - r_e^{-2k}} \right) \cos(2k\theta) \quad (E19)$$

$$\frac{\partial p}{\partial \theta} = \frac{4m}{r^2} \left(\frac{r^{2k}}{r_w^{-2k} r_e^{2k}} - \frac{r^{-2k}}{r_w^{-4k} r_e^{2k} - r_e^{-2k}} \right) \sin(2k\theta) \quad (E18)$$

Inputting Eqs. E18 and E19 into Eq. D8 and rearranging, yields

$$-p = \frac{m}{4} \left(\frac{r^2}{r_w} + n - p_w \right) \cos \theta + \sum_{k=1,3,5,\dots} \frac{4m}{k} \cos \theta (2k+1) \frac{r^{2k-1}}{r_w^{4k} r_e^{-2k} - r_e^{2k}} - \cos \theta (2k-1) \frac{r^{-2k-1}}{r_w^{-4k} r_e^{2k} - r_e^{-2k}}$$

$$+ \frac{m}{4} \left(\frac{r^2}{r_w} + n - p_w \right) \sin \theta - \sum_{k=1,3,5,\dots} \frac{4m}{k} \sin \theta (2k-1) \frac{r^{2k-1}}{r_w^{4k} r_e^{-2k} - r_e^{2k}} - \sin \theta (2k+1) \frac{r^{-2k-1}}{r_w^{-4k} r_e^{2k} - r_e^{-2k}} \quad j$$

APPENDIX F

A Fortran Program to Determine the Profile of the Gelant Front: Supplement to Chapter 8

In this appendix, a Fortran program is used to determine the mathematical expression for the profile of the gelant front when gelant reaches the outer boundary in the x-direction.

Solution Method

In the following study, we only consider the first quadrant and assume that the gelant resistance factor, F_r , is equal to 1.

To determine the profile of the gelant front, we select several points along the injection wellbore, and we follow the trails of the flow path starting from the selected points. Since radial flow exists close to the injection wellbore, the gelant flows radially at the selected points. Starting from these points and using Darcy's law and the pressure gradient expression developed in Appendix E, we can calculate the positions of the gelant front after any given time step for any selected streamline. The profile of the gelant front is obtained by drawing a smooth curve through the positions of these gelant fronts.

If the calculation results do not meet the prescribed tolerances, the size of the time step is reduced. The program repeats the calculation process with smaller time steps until the tolerance is met.

After the profile of the gelant front is determined, the least-squares method is used to determine a mathematical expression. By fitting different forms of equations to the data of the gelant positions, we found that an equation of the form, $a^c x^c + b^c y^c = 1$ ($1 < c < 2$), fits the data best, where a is the distance of gelant penetration in the x-direction, and b is the distance of gelant penetration in the y-direction. Therefore, our objective is to determine the value of c that results in a minimum sum of residuals.

Program Structure

Main Program

1. Select the flow paths.
2. Loop to determine the positions of the gelant fronts.
 - 2.1. Loop to determine the time needed for the gelant to reach the outer boundary in the x-direction.
 - 2.1.1. If the positions do not meet the tolerance, reduce the time step and recalculate.
 - 2.1.2. Else, write the message and save the experienced time period.
 - 2.2. Loop to determine the positions of the other gelant fronts within the time period of step 2.1.1.
 - 2.2.1. If the positions do not meet the tolerance, reduce the time step and recalculate.
 - 2.2.2. Else, save the data of the gelant head positions in array.
3. Loop to fit the curve with least-squares method.
 - 3.1. Loop to calculate the sum of the residuals and save the results in an array.
 - 3.2. Determine the least sum of the residuals.
 - 3.3. Determine the degree of the mathematical expression of the profile of the gelant front which results in the least sum of the residuals (the least-squares fit).
4. Output the results.

Subroutine

1. Calculate the pressure gradient.
2. Return the results.

Fortran Program

```
C Global Variables
C RW = radius of the injection wellbore, ft
C RE = radius of the outer boundary, ft
C PW = pressure at the injection well, psi
C RN = pressure at the intersecting point of the outer boundary and the x-axis, psi
C RM = slope of the linear pressure distribution at the outer boundary
C PERM = permeability, md
C VISC = viscosity, cp
C INCRE = size of the time step, s
C TIME = initial value of the considered time period, s
C TTIME = time needed for the gelant to reach the outer boundary in the x-direction, s
C
C Variable declarations and data initialization
C Variables involved in this section
C LESS = the smaller value by comparing every two of the sum of the residuals
C T,C,O,CYCLE = loop variables
C SYM = a symbol stating if gelant reaches the outer boundary in the x-direction (SYM=1: C
      gelant reaches the outer boundary in the x-direction; SYM=0: gelant has not C
      reached the outer boundary in the x-direction)
C FOURI1, FOURI2 = name of the subroutines used to calculate the pressure gradient
C N = number of the selected streamlines
C M = number of the repeated process to calculate the degree of the gelant-front expression
C XX(N) = an array of N elements to save the x-coordinates of the gelant fronts
C YY(N) = an array of N elements to save the y-coordinates of the gelant fronts
C RAD(N) = an array of N elements to save the distances from the origin to the gelant fronts
C THETA(N) = an array of N elements to store the angles between the x-axis and the lines passing C
      through the origin and the gelant fronts
C XXX(2:N-1) = an array of N-2 elements to save the x-coordinates of the gelant fronts C
      in the least-squares fitting curve
C YYY(2:N-1) = an array of N-2 elements to save the y-coordinates of the gelant fronts in C
      the least-squares fitting curve
C LEAST(M) = an array of M elements to save the sums of residuals
C CALR(2:N-1) = an array of N-2 elements to save the distances from the origin to the C
      gelant fronts in the least-squares fitting curve
C
PROGRAM MAIN
REAL INCRE,LEAST,LESS
INTEGER T,C,O,CYCLE,SYM
DOUBLE PRECISION FOURI1,FOURI2
PARAMETER(RW=1./3.,RE=50.0,PW=3000.0,RN=1000.0,TIME=2000000)
PARAMETER(PERM=50.0,VISC=0.8)
```

```

PARAMETER(PI=3.1416,N=20,M=20)
DIMENSION XX(N),YY(N),XXX(2:N-1),YYY(2:N-1),RAD(N),THETA(N)
DIMENSION LEAST(M),CALR(2:N-1)
C Read pressure drop ratio (the ratio of the pressure drop in the x-direction to the pressure drop in the C
y-direction)
WRITE(*,*)'PRESSURE DROP RATIO = '
READ(*,*)RATIO
C Calculate the slope of the linear pressure distribution at the outer boundary
RM=(PW-(PW-RN)/RATIO-RN)*2/PI
TTIME=TIME
C Local variables
C E = the angle between the x-axis and the line passing through the origin and the considered C
gelant front
C EE = the initial value of E
C F = the distance between the origin and the considered gelant front
C RECE = the calculation result of E for a given time step
C RECF = the calculation result of F for a given time step
C
C Loop to process the selected flow paths one by one
DO 30 I=1,N
E=PI*(I-1)/(2*(N-1))
EE=E
RECF=0
RECE=0
C Loop to calculate the position of the gelant front for a given time step
DO 20 T=1,100000
C Local variables
C MM: number of time steps
C CO: x-coordinate of the considered gelant front
C DO: y-coordinate of the considered gelant front
INCRE=TTIME/(10000*T)
MM=10000*T
CO=RW*COS(EE)
DO=RW*SIN(EE)
E=EE
F=RW
DO 10 J=1,MM
GRADPX=FOURI1(E,F,RW,RE,RN,RM,PI,PW)
GRADPY=FOURI2(E,F,RW,RE,RN,RM,PI,PW)
CO=CO-0.000000073224*PERM/VISC*GRADPX*INCRE
DO=DO-0.000000073224*PERM/VISC*GRADPY*INCRE
F=SQRT(CO**2+DO**2)
E=ATAN(DO/CO)
C If gelant reaches the outer boundary in the x-direction, set SYM to 1, save the number of the
C experienced time steps and go to 11 to check if the result meets the tolerance
IF(ABS(CO-RE).LT.0.01) THEN
NEW=J
SYM=1
GO TO 11

```

```

C Else, continue the calculation
  ELSE
  SYM=0
  END IF
10 CONTINUE
C Check if the calculation result in the x-direction meets the tolerance
C If the tolerance is not met, reduce the size of the time step, save the result in RECF, and re-
C calculate
11 IF(I.EQ.1) THEN
  IF(ABS(F-RECF).GT.0.001) THEN
  RECF=F
  GO TO 20
C Else, write the message, save the coordinates of the gelant front to the arrays, and save the C
experienced time period
  ELSE
  WRITE(*,15)I,INCRE
  XX(I)=CO
  YY(I)=DO
  RAD(I)=F
  THETA(I)=E
  IF(SYM.EQ.1) THEN
  WRITE(*,*)'GELANT REACHES THE OUTER BOUNDARY IN THE X-DIRECTION'
  TTIME=INCRE*NEW
  ELSE
  WRITE(*,*)'GELANT HAS NOT REACHED THE OUTER BOUNDARY IN THE X-
% DIRECTION'
  END IF
  GO TO 30
  END IF
C Check if the calculation results of the other flow paths meet the tolerance
  ELSE
C If the tolerance is not met, reduce the size of the time step, save the results, and recalculate
  IF(ABS(F-RECF).GT.0.001 .OR. ABS(E-RECE).GT.0.008) THEN
  RECF=F
  RECE=E
  GO TO 20
C Else, write the message, and save the results to arrays
  ELSE
  WRITE(*,15)I,INCRE
15 FORMAT(1X,'FOR CURVE=',I3,'TIME INCREMENT=',F8.1)
  XX(I)=CO
  YY(I)=DO
  RAD(I)=F
  THETA(I)=E
  GO TO 30
  END IF
  END IF
20 CONTINUE
30 CONTINUE

```

```

C
C The following determines the degree of the mathematical expression of the profile of the gelant front
C by the least-squares method
C Loop to calculate the sum of the residuals and save the results to array
DO 60 O=1,M
  Z=0.1+0.1*(O-1)
  SUM=0
  DO 50 I=2,N-1
    CALR(I)=(1/((COS(THETA(I))/RAD(1))**Z
%   +(SIN(THETA(I))/RAD(N))**Z))**(1/Z)
    DEVI=(CALR(I)-RAD(I))**2
    SUM=SUM+DEVI
50 CONTINUE
  LEAST(O)=SUM
  WRITE(*,*)SUM
60 CONTINUE
C Determine the least sum of the residuals and save it to LESS
  LESS=LEAST(1)
  DO 70 C=2,M
    IF(LEAST(C).LT.LESS) LESS=LEAST(C)
70 CONTINUE
  WRITE(*,80) LESS
80 FORMAT(1X,'LEAST SQUARE=',1X,F13.8)
C Determine the degree of the gelant-front-profile expression which results in the least sum of residuals
DO 90 O=1,M
  IF(ABS(LEAST(O)-LESS).LT.0.000001) CYCLE=O
90 CONTINUE
  ORDER=0.1+0.1*(CYCLE-1)
  WRITE(*,100)ORDER
100 FORMAT(1X,'DEGREE OF THE OBJECTIVE FUNCTION=',1X,F6.3)
C Calculate the gelant-front position according to the least-square fitting curve
DO 110 I=2,N-1
  R=(1/((COS(THETA(I))/RAD(1))**ORDER
%   +(SIN(THETA(I))/RAD(N))**ORDER))**(1/ORDER)
  XXX(I)=R*COS(THETA(I))
  YYY(I)=R*SIN(THETA(I))
110 CONTINUE
C Output the results
  OPEN (UNIT=1, FILE='F2.DAT',STATUS='OLD')
  DO 200 I=1,N
    WRITE(1,150)XX(I),YY(I)
150 FORMAT(1X,E15.5E3,10X,E15.5E3)
200 CONTINUE
  CLOSE(1)
  OPEN(UNIT=2,FILE='F3.DAT',STATUS='OLD')
  DO 250 I=2,N-1
    WRITE(2,240)XXX(I),YYY(I)
240 FORMAT(1X,E15.5E3,10X,E15.5E3)
250 CONTINUE

```

```

CLOSE(2)
END
C The following subroutine calculates the pressure gradients
FUNCTION FOURI1(G,S,RW,RE,A,B,PI,PW)
F1=0
FO=0
DO 300 K=1,101,2
F1=F1+4*B*RE**(2*K)*(COS((2*K+1)*G)*S**(2*K-1)+RW**(4*K)*COS((2
% *K-1)*G)/S**(2*K+1))/(PI*K*(RW**(4*K)-RE**(4*K)))/RE**8
IF(ABS(F1-FO).LT.0.001) THEN
GO TO 400
ELSE
FO=F1
END IF
300 CONTINUE
400 FOURI1=(B*PI/4.0+A-PW)*COS(G)/(LOG10(RE/RW)*S)+F1*RE**8
END
FUNCTION FOURI2(G,S,RW,RE,A,B,PI,PW)
F2=0
FO=0
DO 500 L=1,101,2
F2=F2+4*B*RE**(2*L)*(S**(2*L-1)*SIN((2*L-1)*G)+RW**(4*L)*SIN((2
% *L+1)*G)/S**(2*L+1))/(PI*L*(RW**(4*L)-RE**(4*L)))/RE**8
IF (ABS(F2-FO).LT.0.001) THEN
GO TO 600
ELSE
FO=F2
END IF
500 CONTINUE
600 FOURI2=(B*PI/4.0+A-PW)*SIN(G)/(LOG10(RE/RW)*S)-F2*RE**8
END

```

APPENDIX G

Pressure Expression After Gel Forms for Near-Wellbore Gelant Placement: Supplement to Chapter 8

This appendix determines the coefficients of the general solution for the Laplace equation using material balance and the boundary conditions for the case of near-wellbore gelant placement.

Pressure Expressions for the Zone Swept by the Gelant

For the zone swept by the gelant, pressure can be expressed by Eq. G1.

$$p_1 = c_0 \log(r) + b_0 + \sum_{k=1}^{\infty} r^{2k} b_k + r^{-2k} d_k \cos(2k\theta) \quad (G1)$$

where

$$c_0 = \frac{F_{pr} \left[\frac{m}{4} + n - p_w \right] \left[(1 - F_{pr}) r_e^{4k} - r_0^{4k} \right] r_w^{2k} (1 + F_{pr}) + \frac{r_0^{2k}}{r_e^{2k}} r_0^{2k} (1 - F_{pr})}{k \log \frac{r_e}{r_0} - F_{pr} \log \frac{r_w}{r_0} \left[(1 + F_{pr}) r_0^{4k} - r_e^{4k} \right] + (F_{pr} - 1) \left[r_0^{8k} - r_e^{4k} r_w^{4k} \right]}$$

$$b_0 = p_w - \frac{F_{pr} \log \frac{r_w}{r_0} \left[\frac{m}{4} + n - p_w \right]}{\log \frac{r_e}{r_0} - F_{pr} \log \frac{r_w}{r_0}} \quad k = 1, 3, 5, \dots$$

$$d_k = \frac{m}{k^2} \left[(1 + F_{pr}) r_e^{-2k} r_w^{4k} - \frac{\left[(1 - F_{pr}) r_e^{4k} - r_0^{4k} \right] r_w^{2k} (1 + F_{pr}) + \frac{r_0^{2k}}{r_e^{2k}} r_0^{2k} (1 - F_{pr})}{\left[(1 + F_{pr}) r_0^{4k} - r_e^{4k} \right] + (F_{pr} - 1) \left[r_0^{4k} - r_e^{4k} r_w^{4k} \right]} \right]$$

$$k = 1, 3, 5, \dots$$

- p_1 = pressure in the zone swept by the gelant, psi
- r_0 = radius of the circular gelant penetration front, ft
- F_{rr} = residual resistance factor

Pressure Expression for the Zone Not Swept by the Gelant

For the zone that has not been swept by the gelant, the pressure can be expressed by Eq. G2.

$$p_2 = c_0 \log(r) + b_0 + \sum_{k=1}^{\infty} \left[r^{2k} b_k + r^{-2k} d_k \right] \cos(2k\theta) \tag{G2}$$

where

$$c_0 = \frac{m \left[\frac{r_w}{r_e} + \frac{r_w}{r_0} (1 - F_{rr}) \right] + \frac{r_0}{r_e} (1 - F_{rr}) \frac{2m}{k^2}}{\log \left[\frac{r_e}{r_w} F_{rr} \log \frac{r_w}{r_0} \right] + (1 + F_{rr}) \left[1 - \frac{r_w}{r_0} \right] + (F_{rr} - 1) \left[\frac{r_0}{r_e} - \frac{r_w}{r_0} \right]}$$

$$d_k = \frac{m \left[\frac{r_w}{r_e} + \frac{r_w}{r_0} (1 - F_{rr}) \right] + \frac{r_0}{r_e} (1 - F_{rr}) \frac{2m}{k^2}}{\log \left[\frac{r_e}{r_w} F_{rr} \log \frac{r_w}{r_0} \right] + (1 + F_{rr}) \left[1 - \frac{r_w}{r_0} \right] + (F_{rr} - 1) \left[\frac{r_0}{r_e} - \frac{r_w}{r_0} \right]}$$

$$k = 1, 3, 5, \dots$$

$$b_k = \frac{-2m}{k^2} r_e^{-2k} - \frac{\frac{r_w}{r_e} r_w^{2k} (1 + F_{rr}) + \frac{r_0}{r_e} r_0^{2k} (1 - F_{rr})}{(1 + F_{rr}) r_e^{4k} - r_w^{4k} + (F_{rr} - 1) r_0^{4k} - r_e^{4k} \frac{r_w}{r_0}}$$

$$k = 1, 3, 5, \dots$$

p_2 = pressure in the zone that has not been swept by the gelant, psi

Derivation

Since the pressure in this model is an even function with period of p , the general solution of the Laplace equation can be simplified to take the forms of Eqs. G1 and G2.

Inner boundary conditions:

$$c_0 \log \frac{r_w}{r_e} + b_0 = p_w \tag{G3}$$

$$r_w^{2k} b_k + r_w^{-2k} d_k = 0 \quad k = 1, 2, 3, \dots \tag{G4}$$

Outer boundary conditions:

$$r_0^{2k} \log \frac{r_0}{r_e} + \frac{r_0^{2k}}{b_0} = \frac{m}{4} + n \quad k = 2, 4, 6, \dots \quad (G5)$$

$$= \frac{-2m}{k^2} \quad k = 1, 3, 5, \dots \quad (G6)$$

Since the pressure has the same value at the interface of the two zones, we have

$$c_0 \log \frac{r_0}{r_e} + \frac{r_0^{2k}}{b_0} = c_0 \log \frac{r_0}{r_e} + \frac{r_0^{2k}}{b_0} \quad k = 1, 2, 3, \dots \quad (G8)$$

Based on material balance, the normal components of the velocity flowing into and out from the interface should be equal. So,

$$|u_1| \cos \theta_1 = |u_2| \cos \theta_2$$

Incorporating Darcy's law, yields

$$k_1 | -p_1 | \cos \theta_1 = k_2 | -p_2 | \cos \theta_2 \quad (G9)$$

where

- k_1 = permeability in the zone swept by the gelant, md
- k_2 = permeability in the zone which has not been swept by the gelant, md
- p_1 = gradient of the pressure in gelant swept zone, psi/ft
- p_2 = gradient of the pressure in the zone not swept by the gelant, psi/ft
- θ_1 = the angle between the velocity direction flowing from the gelant swept zone to a given point at the interface and the normal direction at this point
- θ_2 = the angle between the velocity direction flowing from the interface to the zone not swept by the gelant at a given point at the interface and the normal direction at this point

We also have

$$| -p_1 | \cos \theta_1 = \frac{-p_1 \dot{n}}{|\dot{n}|}$$

$$| -p_2 | \cos \theta_2 = \frac{-p_2 \dot{n}}{|\dot{n}|}$$

Inputting the above two equations into Eq. G9 yields

$$k_1 - p_1 \dot{n} = k_2 - p_2 \dot{n} \quad (G10)$$

where

\dot{n} : vector expression of the normal at any given point at the interface

For a circular curve, the normal vector can be expressed as

$$\dot{n} = \cos \theta \mathbf{i} + \sin \theta \mathbf{j}$$

Let

$$\begin{aligned} \underline{k} p_1 &= F_{\pi} p_{1x} \mathbf{i} + p_{1y} \mathbf{j} \\ \underline{k} p_2 &= -p_{2x} \mathbf{i} + -p_{2y} \mathbf{j} \end{aligned}$$

Inputting the above equations into Eq. G10, Eq. G10 can be re-written as

$$-p_{1x} \cos \theta + -p_{1y} \sin \theta = F_{\pi} [-p_{2x} \cos \theta + -p_{2y} \sin \theta] \quad (G11)$$

In polar coordinates, gradient of pressure is expressed as

$$-\underline{p} = \frac{\partial p}{\partial r} \cos \theta - \frac{\partial p}{\partial r} \frac{\sin \theta}{r} \mathbf{i} + \frac{\partial p}{\partial r} \sin \theta + \frac{\partial p}{\partial r} \frac{\cos \theta}{r} \mathbf{j} \quad (G12)$$

For p_1 , let

$$\frac{\partial p_1}{\partial r} = \frac{\partial p_1}{\partial r} \cos \theta - \frac{\partial p_1}{\partial r} \frac{\sin \theta}{r} \quad (G13)$$

$$\frac{\partial p_1}{\partial r} = \frac{\partial p_1}{\partial r} \sin \theta + \frac{\partial p_1}{\partial r} \frac{\cos \theta}{r} \quad (G14)$$

Differentiating Eq. G1,

$$\frac{\partial p_1}{\partial r} = \frac{c_0}{r} + \sum_{k=1}^{\infty} 2k \frac{\partial}{\partial r} r^{2k-1} b_k - r^{-2k-1} d_k \cos(2k\theta) \quad (G15)$$

$$\frac{\partial p_1}{\partial r} = c_0 \log(r) - \sum_{k=1}^{\infty} 2k \frac{\partial}{\partial r} r^{2k} b_k + r^{-2k} d_k \sin(2k\theta) \quad (G16)$$

Inputting Eqs. G15 and G16 into Eq. G13 and rearranging,

$$-p_{1x} = \frac{c_0}{r} \cos \theta - \log(r) \sin \theta + \sum_{k=1}^{\infty} 2k \frac{\partial}{\partial r} r^{2k-1} b_k \cos(2k-1)\theta - r^{-2k-1} d_k \cos(2k+1)\theta$$

Inputting Eqs. G15 and G16 into Eq. G14 and rearranging,

$$-p_{1y} = \frac{c_0}{r} \sin \theta + \log(r) \cos \theta + \sum_{k=1}^{\infty} 2k r^{-2k-1} b_k \sin(2k-1)\theta - r^{-2k-1} d_k \sin(2k+1)\theta$$

Combining the above two equations,

$$-p_{1x} \cos \theta + -p_{1y} \sin \theta = \frac{c_0}{r} + \sum_{k=1}^{\infty} 2k r^{2k-1} b_k - r^{-2k-1} d_k \cos(2k\theta) \quad (G17)$$

For the same reason, we also have

$$-p_{2x} \cos \theta + -p_{2y} \sin \theta = \frac{c_0}{r} + \sum_{k=1}^{\infty} 2k r^{2k-1} b_k - r^{-2k-1} d_k \cos(2k\theta) \quad (G18)$$

Comparing Eqs. G17 and G18 to Eq. G11, at the interface of the two zones, the following relations exist:

$$r_0^{2k-1} b_k = F_{kr} r_0^{-2k-1} d_k = F_{tr} r_0^{2k-1} b_k - r_0^{-2k-1} d_k \quad (G19)$$

Solving Eqs. G3 through G8 and Eqs. G19 and G20, the coefficients are determined.

APPENDIX H

Pressure Expression After Gel Forms When the Gelant Reaches the Outer Boundary in the x-Direction: Supplement to Chapter 8

In this appendix, we use material balance, pressure continuity, and boundary conditions to solve the pressure expressions for the zone swept and not swept by the gelant after gel forms when the gelant reached the outer boundary in the x-direction.

Since the expression for the gelant front in this case is a function of two independent variables (r and θ), simplification of the Fourier terms is more difficult than that given in Appendix G. Therefore, we must use finite numbers of the Fourier terms to approximate the infinite Fourier series and use Gaussian elimination to solve the linear equation set.

Derivation

Boundary conditions:

$$c_{e0} \log \frac{r}{r_0} + \sum_{k=1}^{\infty} \frac{b_k}{r^{2k}} = \frac{p_0}{\rho_0 g} - \frac{h}{r_0} \sum_{k=1}^{\infty} \frac{(-1)^k}{k} \quad k = 1, 2, 3, \dots$$

Rearranging the above equations,

$$\frac{b_k}{r^{2k}} = \frac{\rho_0 g}{h} \left[\frac{p_0}{\rho_0 g} - \frac{h}{r_0} \sum_{k=1}^{\infty} \frac{(-1)^k}{k} - c_{e0} \log \frac{r}{r_0} \right] \quad k = 1, 2, 3, \dots$$

Inputting the above four equations into the general pressure expressions (Eqs. G1 and G2) yields

$$p_p = c_0 \log\left(\frac{r}{r_w}\right) + \frac{m}{4} c_0 \log\left(\frac{r_e}{r_w}\right) + \sum_{k=1,2,3,\dots} \left[\frac{r^{2k} - r_e^{-2k} r_w^{4k}}{r^{2k} - r_e^{-2k}} b_k \cos(2k\theta) \right] \quad (\text{H1})$$

$$+ \sum_{k=1,2,3,\dots} \left[\frac{r^{2k} - r_e^{-2k} r_w^{4k}}{r^{2k} - r_e^{-2k}} b_k \cos(2k\theta) \right] \quad (\text{H2})$$

Since pressure has the same value at the interface,

$$c_0 \log\left(\frac{r}{r_w}\right) + \frac{m}{4} c_0 \log\left(\frac{r_e}{r_w}\right) + \sum_{k=1,2,3,\dots} \left[\frac{r^{2k} - r_e^{-2k} r_w^{4k}}{r^{2k} - r_e^{-2k}} b_k \cos(2k\theta) \right] - \sum_{k=1,2,3,\dots} \left[\frac{r^{2k} - r_e^{-2k} r_w^{4k}}{r^{2k} - r_e^{-2k}} b_k \cos(2k\theta) \right]$$

$$= - \sum_{k=1,2,3,\dots} \frac{m}{k^2} r^{-2k} r_e^{2k} (-1)^k \cos(2k\theta) + m \frac{m}{4} + n - p_w \quad (\text{H3})$$

From Appendix F, the expression for the gelant front is

$$\frac{x^c}{a^c} + \frac{y^c}{b^c} = 1 \quad (\text{H4})$$

where

- a = distance of gelant penetration in the x-direction, ft
- b = distance of gelant penetration in the y-direction, ft
- c = degree of the expression

Differentiating,

$$\frac{x^{(c-1)}}{a^c} \frac{dx}{a} + \frac{y^{(c-1)}}{b^c} \frac{dy}{b} = 0 \quad (\text{H5})$$

Inputting Eqs. H10 through H13 into Eq. H9, yields

$$\begin{aligned}
 -p_{2x} = & \frac{c_0}{r} \cos \theta - p_1 \log \left(\frac{c_0}{r} \right) \sin \theta + \log \left(\frac{r}{r_0} \right) \sin \frac{2m}{k} r^{2k} r^{-2k-1} [1 - (-1)^k] \cos(2k+1)\theta \\
 & + \sum_{k=1,2,3,\dots} \frac{2k}{r} r^{2k-1} \cos(2k-1)\theta + \sum_{k=1,2,3,\dots} \frac{2k}{r} r^{-2k-1} \cos(2k+1)\theta b_k
 \end{aligned} \tag{H14}$$

$$\begin{aligned}
 -p_{2y} = & \frac{c_0}{r} \sin \theta - p_1 \log \left(\frac{c_0}{r} \right) \cos \theta + \log \left(\frac{r}{r_0} \right) \cos \frac{2m}{k} r^{-2k-1} r^{2k} [1 - (-1)^k] \sin(2k+1)\theta \\
 & + \sum_{k=1,2,3,\dots} \frac{2k}{r} r^{-2k-1} \sin(2k+1)\theta - \sum_{k=1,2,3,\dots} \frac{2k}{r} r^{2k-1} \sin(2k-1)\theta b_k
 \end{aligned} \tag{H15}$$

From material balance,

$$-p_{1x} n_x + -p_{1y} n_y = F_{rr} [-p_{2x} n_x + -p_{2y} n_y] \tag{H18}$$

Inputting Eqs. H14 through H17 into Eq. H18 and rearranging, the left side of Eq. H18 is

The right side of Eq. H18 is

$$\begin{aligned}
 -p_{2x} n_x + -p_{2y} n_y = & \frac{c_0}{r} b^c \cos^c + a^c \sin^c + \log(r) a^c \cos \sin^{(c-1)} - b^c \sin \cos^{(c-1)} \\
 + \sum_{k=1,2,3,\dots} \frac{2m}{k} r^{2k} r^{-2k-1} & (-1)^k b^c \cos(2k+1) \cos^{(c-1)} + a^c \sin(2k+1) \sin^{(c-1)} \\
 + \sum_{k=1,2,3,\dots} 2k b^c \cos^{(c-1)} & r^{2k-1} \cos(2k-1) + r^{-2k-1} r^{4k} \cos(2k+1) b^c \\
 - \sum_{k=1,2,3,\dots} 2k a^c \sin^{(c-1)} & r^{2k-1} \sin(2k-1) - r^{-2k-1} r^{4k} \sin(2k+1) a^c
 \end{aligned}$$

Rearranging Eq. H18,

$$c_0 FF_1 - F_{rr} FF_1 c_0 + \sum_{k=1,2,3,\dots} FF_2 b_k - \sum_{k=1,2,3,\dots} F_{rr} FF_5 b_k = F_{rr} FF_4 \tag{H19}$$

where

$$\begin{aligned}
 FF_5 = & 2k b^c \cos^{(c-1)} r^{2k-1} \cos(2k-1) + r^{-2k-1} r^{4k} \cos(2k+1) \\
 FF_4 = & 2k a^c \sin^{(c-1)} r^{2k-1} \sin(2k-1) - r^{-2k-1} r^{4k} \sin(2k+1) \\
 FF_2 = & \frac{2m}{k} r^{2k} r^{-2k-1} (-1)^k b^c \cos(2k+1) \cos^{(c-1)} + a^c \sin(2k+1) \sin^{(c-1)} \\
 FF_1 = & \frac{c_0}{r} b^c \cos^c + a^c \sin^c + \log(r) a^c \cos \sin^{(c-1)} - b^c \sin \cos^{(c-1)} \\
 FF_4 = & -2k a^c \sin^{(c-1)} r^{2k-1} \sin(2k-1) - r^{-2k-1} r^{4k} \sin(2k+1) \\
 FF_5 = & -2 \frac{k}{r} a^c \sin^{(c-1)} r^{2k} \sin(2k-1) - r^{-2k-1} r^{4k} \sin(2k+1)
 \end{aligned}$$

Based on Eqs. H3 and H19, we can establish a linear equation set and solve for the coefficients of c_0 , c_0' , b_k , b_k' as shown in the following Fortran program.

A Fortran Program to Solve for the Coefficients of the Fourier Series

- C The program solves for the coefficients of the Fourier series by Gaussian elimination
- C The involved variables:
- C RN = the pressure at the intersecting point of the outer boundary and the x-axis, psi

C RM = the slope of the linear pressure distribution at the outer boundary
 C N = number of equations in the set
 C K = number of finite Fourier terms
 C A = K*K coefficient matrix
 C B = vector of K elements, initially used to store the right side constants of the equations,
 C and is used to store the solutions of the equation set
 C AA = distance of the gelant penetration in the x-direction when gelant reaches the outer C
 boundary in the x-direction, ft
 C BB = distance of the gelant penetration in the y-direction when gelant reaches the outer C
 boundary in the x-direction, ft
 C C = degree of the mathematical gelant-front expression
 C KWJI = a signal used to show if the solutions are found
 C TRYR = radius of the test point used to perform the convergence analysis, ft
 C BELTA = the angle between the x-axis and the line passing through the origin and the test point
 C PRES2 = pressure at the test point, psi
 C
 C The following assigns the values to the coefficient matrix:
 DOUBLE PRECISION A,B,SUM,PRES2
 DOUBLE PRECISION GS1,FF1,FF2,FF4,FF5,F1,F2,F3
 PARAMETER(RW=1.0/3.0,RE=50.0,PW=3000.0,RN=1000.0)
 PARAMETER(RATIO=10.0,FRR=10.,AA=49.992,BB=25.362,C=1.2)
 PARAMETER(K=11,N=2*K+2)
 PARAMETER(TRYR=50.0,BELTA=0.0)
 DIMENSION A(N,N),B(N)
 DIMENSION THETA(K+1),R(K+1)
 RM=(PW-(PW-RN)/RATIO-RN)*2/3.1416
 DO 5 I=1,K+1
 THETA(I)=3.1416/2*(1-I/(K+2.))
 R(I)=(AA*BB)*(BB**C*(COS(THETA(I)))**C+
 % AA**C*(SIN(THETA(I)))**C)**(-1.0/C)
 5 CONTINUE
 DO 6 I=1,K+1
 A(I,1)=LOG10(R(I)/RW)
 A(I,2)=LOG10(RE/R(I))
 B(I)=F3(R(I),THETA(I),RE,K,RM)+RM*3.1416/4.0+RN-PW
 DO 7 J=3,K+2
 A(I,J)=F1(R(I),THETA(I),RW,J-2)
 7 CONTINUE
 DO 8 J=K+3,2*K+2
 A(I,J)=F2(R(I),THETA(I),RE,J-K-2)
 8 CONTINUE
 6 CONTINUE
 DO 9 I=K+2,2*K+2
 A(I,1)=FF1(R(I-K-1),THETA(I-K-1),AA,BB,C)
 A(I,2)=-1.0*FRR*A(I,1)
 B(I)=FRR*FF4(R(I-K-1),THETA(I-K-1),AA,BB,K,RE,RM,C)
 DO 10 J=3,K+2
 A(I,J)=FF2(R(I-K-1),THETA(I-K-1),AA,BB,J-2,RW,C)
 10 CONTINUE

```

DO 11 J=K+3,2*K+2
A(I,J)=FF5(R(I-K-1),THETA(I-K-1),AA,BB,J-K-2,RE,C)*(-1.0)*FRR
11 CONTINUE
9 CONTINUE
C Call the subroutine to solve the simultaneous linear equation set
CALL GS1(N,A,B,0.1E-100,KWJI)
C Write the results
WRITE(*,*)'SOLUTIONS ARE:'
DO 8060 I=1,11
WRITE(*,*)B(I)
8060 CONTINUE
DO 8061 I=12,K+2
B(I)=B(I)/RE**(2*(I-2))
WRITE(*,*)B(I)
8061 CONTINUE
DO 8065 I=K+3,2*K+2
B(I)=B(I)/(RE**(2*(I-K-2)))
WRITE(*,*)B(I)
8065 CONTINUE
WRITE(*,*)'MARK'
WRITE(*,*)KWJI
C The following calculates the pressure value at the test point based on the above solutions
BO=RM*3.1416/4.0+RN-B(2)*LOG10(RE)
SUM=B(2)*LOG10(TRYR)+BO
DO 8070 I=1,K
PRES2=RM/(3.1416*I**2)*TRYR**(-2.0*I)*((-1)**I-1)
% *RE**(2*I)*COS(2*I*BELTA)+(TRYR**(2*I)-TRYR**(-2.0*I)
% *RE**(4*I))*B(I+K+2)*COS(2*I*BELTA)
SUM=SUM+PRES2
8070 CONTINUE
C Output the results
OPEN (UNIT=30,FILE='TRY.DAT',STATUS='OLD')
DO 9000 I=1,N
WRITE(30,*)B(I)
9000 CONTINUE
CLOSE(30)
END
C
C The following procedures calculate the values of the coefficients:
FUNCTION FF1(R,THETA,AA,BB,C)
FF1=1/R*(BB**C*(COS(THETA))**C+AA**C*(SIN(THETA))**C
% +LOG10(R)*(AA**C*(COS(THETA))*(SIN(THETA))**C-1)-BB**C*
% SIN(THETA)*(COS(THETA))**C-1))
END
FUNCTION FF2(R,THETA,AA,BB,K,RW,C)
FF2=2*K/R*(BB**C*(COS(THETA))**C-1)*(R**(2*K)*
% COS((2*K-1)*THETA)+R**(-2.0*K)*RW**(4*K)*
% COS((2*K+1)*THETA))-AA**C*(SIN(THETA))**C-1*(R**(2*K)*
% SIN((2*K-1)*THETA)-R**(-2*K)*RW**(4*K)*SIN((2*K+1)*THETA)))

```

```

END
FUNCTION FF4(R,THETA,AA,BB,K,RE,RM,C)
SUM=0
DO 600 I=1,K
FF4=2*RM/(3.1416*I)*RE**(2*I)*R**(-2.0*I-1)*(1-(-1)**I)*
% (BB**C*COS((2*I+1)*THETA)*(COS(THETA))**(C-1)+AA**C*
% SIN((2*I+1)*THETA)*(SIN(THETA))**(C-1))
SUM=SUM+FF4
600 CONTINUE
FF4=SUM
END
FUNCTION FF5(R,THETA,AA,BB,K,RE,C)
FF5=2.0*K*(BB**C*(COS(THETA))**(C-1)*((R/RE)**(2*K)/R*
% COS((2*K-1)*THETA)+R**(-2.0*K-1)*RE**(2*K)*COS((2*K+1)*THETA))
% -AA**C*(SIN(THETA))**(C-1)*((R/RE)**(2*K)/R*SIN((2*K-1)*THETA)-
% R**(-2.0*K-1)*RE**(2.0*K)*SIN((2*K+1)*THETA)))
END
FUNCTION F1(R,THETA,RW,K)
F1=(R**(2*K)-R**(-2.0*K)*RW**(4*K))*COS(2*K*THETA)
END
FUNCTION F2(R,THETA,RE,K)
F2=(R**(-2.0*K)*RE**(2*K)-(R/RE)**(2*K))*COS(2*K*THETA)
END
FUNCTION F3(R,THETA,RE,K,RM)
SUM=0
DO 700 I=1,K
F3=RM/(3.1416*I**2)*R**(-2.0*I)*RE**(2.0*I)*((-1)**I-1)
% *COS(2*I*THETA)
SUM=SUM+F3
700 CONTINUE
F3=SUM
END

```

C

C This subroutine solves N simultaneous equations by Gaussian elimination to create an upper triangular C system, followed by back-substitution to obtain the solution. To improve the accuracy, the program C looks through all the columns and rows in the coefficient matrix to determine a coefficient with the C largest absolute value as the pivot.

```

SUBROUTINE GS1(N,A,B,EP,KWJI)
DOUBLE PRECISION A,B
DIMENSION A(N,N),B(N),M(100)

```

C Look for a larger potential pivot, save its column and row number.

```

DO 10 I=1,N
10 M(I)=I
DO 20 K=1,N
P=0.0
DO 30 I=K,N
DO 30 J=K,N
IF(ABS(A(I,J)).LE.ABS(P)) GO TO 30
P=A(I,J)

```

```

    IO=I
    JO=J
30 CONTINUE
C If the values of the coefficients are less than EP, the equation set is considered to have no solution.
  IF(ABS(P)-EP) 200,200,300
200 KWJI=1
    RETURN
C Interchange the coefficient positions to make sure the pivot occupies the position at which the column
C number and the row number are the same. Save the original position in M.
300 IF(JO.EQ.K) GO TO 400
    DO 40 I=1,N
      T=A(I,JO)
      A(I,JO)=A(I,K)
40  A(I,K)=T
      J=M(K)
      M(K)=M(JO)
      M(JO)=J
400 IF(IO.EQ.K) GO TO 500
    DO 50 J=K,N
      T=A(IO,J)
      A(IO,J)=A(K,J)
50  A(K,J)=T
      T=B(IO)
      B(IO)=B(K)
      B(K)=T
C Convert the equation set into new set, where the coefficient matrix is an upper triangular matrix
500 P=1/P
    IN=N-1
    IF(K.EQ.N) GO TO 600
    DO 60 J=K,IN
60  A(K,J+1)=A(K,J+1)*P
600 B(K)=B(K)*P
    IF(K.EQ.N) GO TO 20
    DO 70 I=K,IN
      DO 80 J=K,IN
80  A(I+1,J+1)=A(I+1,J+1)-A(I+1,K)*A(K,J+1)
70  B(I+1)=B(I+1)-A(I+1,K)*B(K)
20 CONTINUE
C Solve the new set by back-substitution
    DO 90 I1=2,N
      I=N+1-I1
      DO 90 J=I,IN
90  B(I)=B(I)-A(I,J+1)*B(J+1)
C Based on M, arrange the solutions in the original order
    DO 1 K=1,N
      I=M(K)
1  A(1,I)=B(K)
    DO 2 K=1,N
2  B(K)=A(1,K)

```

```
KWJI=0  
RETURN  
END
```

Convergence Analysis

Fig. H1 shows the convergence trend for the pressure value at the intersecting point of the outer boundary and the x-axis.

When the number of the Fourier terms increases, the numerical range of the coefficients increases. When the number of the Fourier terms exceeds 11, the required numerical range exceeds the intrinsic numerical range of the IBM PC that we used, which is between 10^{-38} and 10^{+38} . Therefore, we must use 11 Fourier terms to represent the infinite series. This results in a relative error of 3%.

APPENDIX I

Data Supplement to Chapter 9

Table I-1a. Summary of Residual Saturations (S_{wr} , S_{or}) and Endpoint Permeabilities (k_r , k_{ro}) Obtained Before Gel Treatment (Core SSH-64, Berea Sandstone, Strongly Water-Wet, 41°C)

Stage	S_{wr}	k
After 1st oilflood	0.27	576
After 2nd oilflood	0.27	566
Stage	S_{or}	k
After 1st waterflood	0.34	110

Table I-1b. Summary of Residual Saturations (S_{wr} , S_{or}) and Endpoint Permeabilities (k_r , k_{ro}) Obtained Before Gel Treatment (Core SSH-69, Berea Sandstone, Strongly Water-Wet, 41°C)

Stage	S_{wr}	k
After 1st oilflood	0.28	626
After 2nd oilflood	0.30	596
Stage	S_{or}	k
After 1st waterflood	0.36	100

Table I-1c. Summary of Residual Saturations (S_{wr} , S_{or}) and Endpoint Permeabilities (k_r , k_{ro}) Obtained Before Gel Treatment (Core SSH-78, Berea Sandstone, Strongly Water-Wet, 41°C)

Stage	S_{wr}	k
After 1st oilflood	0.26	676
Stage	S_{or}	k
After 1st waterflood	0.33	132

Table I-1d. Summary of Residual Saturations (S_{wr} , S_{or}) and Endpoint Permeabilities (k, k) Obtained Before Gel Treatment (Core SSH-85, Berea Sandstone, Strongly Water-Wet, 41°C)

Stage	S_{wr}	k
After 1st oilflood	0.30	500
Stage	S_{or}	k
After 1st waterflood	0.34	140

Table I-1e. Summary of Residual Saturations (S_{wr} , S_{or}) and Endpoint Permeabilities (k, k) Obtained Before Gel Treatment (Core SSH-86, Berea Sandstone, Strongly Water-Wet, 41°C)

Stage	S_{wr}	k
After 1st oilflood	0.27	474
After 2nd oilflood	0.28	483
Stage	S_{or}	k
After 1st waterflood	0.67	188
After 2nd waterflood	0.65	150

Table I-1f. Summary of Residual Saturations (S_{wr} , S_{or}) and Endpoint Permeabilities (k, k) Obtained Before Gel Treatment (Core SSH-S2, Berea Sandstone, Strongly Water-Wet, 41°C)

Stage	S_{wr}	k
After 1st oilflood	0.28	513
Stage	S_{or}	k
After 1st waterflood	0.28	140

Table I-2a—Core SSH-S2
Residual Resistance Factors for Brine (F_{rw}) and for Soltrol-130 (F_{ro})
Core: High-permeability Berea sandstone
Gel: 0.5% HPAM (Alcoflood 935®) + 0.0417% Cr(III)-acetate + 1% NaCl (pH=5.6)

Stage	Flux, ft/d	1st segment (short)		2nd segment (long)	
		F_{rw}	F_{ro}	F_{rw}	F_{ro}
1st waterflood after gel treatment $F_{rw}=1,016u^{-0.34}$, $r=0.999$ (For all the readings for the long segment.)	0.023	1,325		5,188	
	0.047	1,133		3,850	
	0.023	1,774		4,826	
	0.093	1,096		2,633	
	0.047	1,637		3,320	
	0.023	2,418		4,396	
	0.187	746		1,789	
	0.093	1,343		2,228	
	0.047	2,016		2,846	
	0.023	2,733		3,661	
	0.187	926		1,813	
1st oilflood after gel treatment $F_{ro}=15u^{-0.37}$, $r=0.977$ (For all the readings for the long segment.)	23.337		23		5
	11.68		25		6
	5.834		27		7
	3.112		27		9
	1.556		26		12
	0.778		36		15
	0.389		57		18
	0.187		61		30
	0.093		88		49
23.337		24		6	

Table I-2a (continued)—Core SSH-S2
Residual Resistance Factors for Brine (F_{rw}) and for Soltrol-130 (F_{ro})
Core: High-permeability Berea sandstone
Gel: 0.5% HPAM (Alcoflood 935®) + 0.0417% Cr(III)-acetate + 1% NaCl (pH=5.6)

Stage	Flux, ft/d	1st segment (short)		2nd segment (long)	
		F_{rw}	F_{ro}	F_{rw}	F_{ro}
2nd waterflood after gel treatment $F_{rw}=4.4$ (Average of all the readings for the long segment.)	23.337	4		4	
	11.68	4		4	
	5.834	5		4	
	3.112	6		4	
	1.556	7		4	
	0.778	9		5	
	0.389	12		5	
	0.187	17		5	
	0.093	28		5	
	23.337	5		4	
2nd oilflood after gel treatment $F_{ro}=4.9$ (Average of all the readings for the long segment.)	23.337		14		5
	11.68		16		5
	5.834		20		5
	3.112		24		5
	1.556		41		5
	0.778		55		5
	23.337		11		4

Table I-2b—Core SSH-64
Residual Resistance Factors for Brine (F_{rrw}) and for Soltrol-130 (F_{rro})
Core: High-permeability Berea sandstone
Gel: 2% hydroxystearic acid in Soltrol-130

Stage	Flux, ft/d	1st segment (short)		2nd segment (long)	
		F_{rrw}	F_{rro}	F_{rrw}	F_{rro}
1st oilflood after gel treatment $F_{rro}=26$ (Last reading for the long segment at this stage.)	0.05		81		58
	0.101		161		58
	0.05		103		59
	0.202		190		59
	0.101		173		60
	0.05		93		62
	0.394		197		54
	0.202		151		54
	0.101		111		59
	0.05		37		56
	0.787		193		52
	0.394		180		54
	0.202		149		57
	0.101		95		59
	0.05		87		61
	1.575		166		51
	0.05				56
	3.15		15		30
	1.575		14		30
	0.787		13		30
	0.394		7		31
	0.202		2		31
	0.101				31
0.05		21		28	
1.575		11		26	

Table I-2b (continued)—Core SSH-64
 Residual Resistance Factors for Brine (F_{rrw}) and for Soltrol-130 (F_{rro})
 Core: High-permeability Berea sandstone
 Gel: 2% hydroxystearic acid in Soltrol-130

Stage	Flux, ft/d	1st segment (short)		2nd segment (long)	
		F_{rrw}	F_{rro}	F_{rrw}	F_{rro}
1st waterflood after gel treatment $F_{rrw}=1$ (For the long segment.)	1.575	1		1	
	15.75	1		1	
	6.3	1		1	
	3.15	1		1	
	1.575	1		1	
	0.787	2		1	
	3.15	2		1	
2nd oilflood after gel treatment $F_{rro}=3.3$ (Average of all the readings for the long segment.)	15.75		1		3
	7.87		1		3
	3.94		1		4

Table I-2c—Core LSH-67
Residual Resistance Factors for Brine (F_{rrw}) and for Soltrol-130 (F_{rro})
Core: 32-md Indiana limestone
Gel: 1.39% HPAM (Marathon) + 0.0212% Cr(III)-acetate + 1% NaCl (pH=6.0)

Stage	Flux, ft/d	1st segment (short)		2nd segment (long)	
		F_{rrw}	F_{rro}	F_{rrw}	F_{rro}
1st waterflood after gel treatment $F_{rrw}=47u^{-0.51}$, $r=0.997$ (For the last five readings for the long segment.)	0.025	1,240		293	
	0.05	481		291	
	0.025	911		362	
	0.101	510		182	
	0.05	331		292	
	0.025	885		349	
	0.197	118		137	
	0.101	157		189	
	0.05	296		271	
	0.025	548		357	
	0.394	86		78	
	0.197	111		107	
	0.101	58		153	
	0.05	403		206	
	0.025	44		327	
1st oilflood after gel treatment $F_{rro}=4$ (Average of all readings for the long segment.)	15.75		2		3
	12.6		1		3
	6.3		2		3
	3.15		2		4
	1.575				4
	0.787				5
	0.394				6

Table I-2c (continued)—Core LSH-67
 Residual Resistance Factors for Brine (F_{rrw}) and for Soltrol-130 (F_{rro})
 Core: 32-md Indiana limestone
 Gel: 1.39% HPAM (Marathon) + 0.0212% Cr(III)-acetate + 1% NaCl (pH=6.0)

Stage	Flux, ft/d	1st segment (short)		2nd segment (long)	
		F_{rrw}	F_{rro}	F_{rrw}	F_{rro}
2nd waterflood after gel treatment $F_{rrw}=18u^{-0.52}$, $r=0.994$ (For all the readings for the long segment.)	3.15	6		11	
	1.575	5		14	
	0.787	9		19	
	0.394	11		26	
	0.197			39	
	0.101			57	
	0.05			87	
	0.025			139	

Table I-2d—Core SSL-68
 Residual Resistance Factors for Brine (F_{rrw}) and for Soltrol-130 (F_{rro})
 Core: 123-md low-permeability Berea sandstone
 Gel: 1.39% HPAM (Marathon) + 0.0212% Cr(III)-acetate + 1% NaCl (pH=6.0)

Stage	Flux, ft/d	1st segment (short)		2nd segment (long)	
		F_{rrw}	F_{rro}	F_{rrw}	F_{rro}
1st waterflood after gel treatment (See next page for more readings at this stage.)	0.025	15		25	
	0.05	12		19	
	0.025	15		24	
	0.101	10		23	
	0.05	14		32	
	0.025	15		38	
	0.197	8		22	
	0.101	9		26	
	0.05	10		39	
	0.025	11		55	
	0.394	6		17	
	0.197	7		20	
	0.101	8		27	
	0.05	8		37	
	0.025	10		70	
	0.787	5		16	
	0.394	6		16	
	0.197	6		20	
	0.101	5		25	
	0.05	7		37	
0.025	8		40		

Table I-2d (continued)—Core SSL-68
Residual Resistance Factors for Brine (F_{rw}) and for Soltrol-130 (F_{ro})
Core: 123-md low-permeability Berea sandstone
Gel: 1.39% HPAM (Marathon) + 0.0212% Cr(III)-acetate + 1% NaCl (pH=6.0)

Stage	Flux, ft/d	1st segment (short)		2nd segment (long)	
		F_{rw}	F_{ro}	F_{rw}	F_{ro}
1st waterflood after gel treatment $F_{rw}=12u^{-0.26}$, $r=0.96$ (For the last seven readings for the long segment.)	1.575	4		12	
	0.787	5		12	
	0.394	5		14	
	0.197	6		16	
	0.101	6		20	
	0.05	7		31	
	0.025	7		29	
1st oilflood after gel treatment $F_{ro}=4$ (For the long segment.)	1.575		2		4
2nd waterflood after gel treatment $F_{rw}=9$ (For the long segment.)	1.575	5		9	

Table I-2e—Core SSH-78
Residual Resistance Factors for Brine (F_{rw}) and for Soltrol-130 (F_{ro})
Core: High-permeability Berea sandstone
Gel: 0.75% HPAM (Alcoflood 935®), 0.0625% Cr(III)-acetate

Stage	Flux, ft/d	1st segment (short)		2nd segment (long)	
		F_{rw}	F_{ro}	F_{rw}	F_{ro}
1st waterflood after gel treatment $F_{rw}=300 u^{-0.35}$, $r=0.991$ (For the last five readings for the long segment.)	0.025	7900		2370	
	0.05	2020		1730	
	0.025	2570		2040	
	0.101	1430		1230	
	0.05	2230		1490	
	0.025	3190		1820	
	0.197	230		540	
	0.101	240		640	
	0.05	480		840	
	0.025	810		1120	
	0.101	410		700	
1st oilflood after gel treatment $F_{ro}=23$ (Average of all the readings for the long segment.)	25.2		15		19
	12.6		16		22
	6.3		17		24
	3.15		18		25
	1.575		18		26
	0.787		19		26
	0.394		22		25
	0.202		26		26
	0.101		36		25
	0.05		54		22
	0.025		90		15

Table I-2e (continued)—Core SSH-78
Residual Resistance Factors for Brine (F_{rw}) and for Soltrol-130 (F_{ro})
Core: High-permeability Berea sandstone
Gel: 0.75% HPAM (Alcoflood 935®), 0.0625% Cr(III)-acetate

Stage	Flux, ft/d	1st segment (short)		2nd segment (long)	
		F_{rw}	F_{ro}	F_{rw}	F_{ro}
2nd waterflood after gel treatment $F_{rw}=30 u^{-0.18}$, $r=0.909$ (For all the readings for the long segment.)	6.3	35		27	
	3.15			26	
	1.575	41		27	
	0.787	43		28	
	0.394	53		32	
	0.202	75		34	
	0.101	100		43	
	0.05	140		50	
	0.025	170		77	
	6.3	24		27	
2nd oilflood after gel treatment $F_{ro}= 17$ (Average of all the readings for the long segment.)	15.75		10		17
	12.6		10		17
	6.3		10		17
	3.15		10		17
	1.575		10		17
	0.787		11		17
	0.394		12		17
	0.202		16		18
	0.101		26		15
	15.75		10		15

Table I-2e (continued)—Core SSH-78
 Residual Resistance Factors for Brine (F_{rrw}) and for Soltrol-130 (F_{rro})
 Core: High-permeability Berea sandstone
 Gel: 0.75% HPAM (Alcoflood 935®), 0.0625% Cr(III)-acetate

Stage	Flux, ft/d	1st segment (short)		2nd segment (long)	
		F_{rrw}	F_{rro}	F_{rrw}	F_{rro}
3rd waterflood after gel treatment $F_{rrw}=23 u^{-0.10}$, $r=0.967$ (For all the readings for the long segment.)	6.3	24		20	
	3.15	26		20	
	1.575	29		21	
	0.787	32		22	
	0.394	36		24	
	0.202	50		28	
	0.101	55		30	
	0.05	60		32	
	0.025	75		35	
	6.3	27		21	

Table I-2f—Core SSH-86
Residual Resistance Factors for Brine (F_{rw}) and for Soltrol-130 (F_{ro})
Core: High-permeability Berea sandstone
Gel: 18% 12-hydroxystearic acid in Oil A

Stage	Flux, ft/d	1st segment (short)		2nd segment (long)	
		F_{rw}	F_{ro}	F_{rw}	F_{ro}
1st waterflood after gel treatment $F_{rw}= 5$ (For all the readings for the long segment.)	0.025	5		5	
	0.05	5		5	
	0.101	5		5	
1st oilflood after gel treatment $F_{ro}= 225$ (For the long segment.)	0.025		200		225
2nd waterflood after gel treatment $F_{rw}= 14$ (Average of all the readings for the long segment.)	0.05	19		10	
	0.101	21		16	
	0.05	42		14	
	0.197	20		14	

Table I-3a. Pore-Volume Determination from Water-Tracer Studies and Residual-Saturation Determination from Material Balance Calculations
Core SSH-64 (Oil Phase: Oil A, Gelant: 2% 12-hydroxystearic acid in Soltrol-130)

Water-tracer study	V_p/V_{po}	$1-V_p/V_{po}$	S_{or}
After 1st waterflood before gel	0.66	0.34	0.34
After 1st waterflood after gel	0.81	0.19	

Table I-3b. Pore-Volume Determination from Oil-Tracer Studies and Residual-Saturation Determination from Material Balance Calculations
Core SSH-64 (Oil Phase: Oil A, Gelant: 2% 12-hydroxystearic acid in Oil A)

Oil-tracer study	V_p/V_{po}	$1-V_p/V_{po}$	S_{wr}	S_{gel}
After 1st oilflood before gel	0.76	0.24	0.27	
After 2nd oilflood before gel	0.77	0.23	0.27	
After 1st oilflood after gel	0.85	0.15		
After 2nd oilflood after gel	0.83	0.17		

Table I-3c. Pore-Volume Determination from Water-Tracer Studies and Residual-Saturation Determination from Material Balance Calculations
Core LSH-67 [Oil Phase: Oil A, Gelant: 1.39% HPAM, 0.0212% Cr(III)-acetate]

Water-tracer study	V_p/V_{po}	$1-V_p/V_{po}$	S_{or}
After 1st waterflood before gel	0.78	0.22	0.30
After 2nd waterflood before gel	0.53	0.47	0.31
After 3rd waterflood before gel	0.49	0.51	0.34
After 4th waterflood before gel	0.49	0.51	0.36

Table I-3d. Pore-Volume Determination from Oil-Tracer Studies and Residual-Saturation Determination from Material Balance Calculations
Core LSH-67 [Oil Phase: Oil A, Gelant: 1.39% HPAM, 0.0212% Cr(III)-acetate]

Oil-tracer study	V_p/V_{po}	$1-V_p/V_{po}$	S_{wr}	$S_{o(trap)}$
After 1st oilflood before gel	0.61	0.39	0.36	
After 2nd oilflood before gel	0.56	0.44	0.37	
After 3rd oilflood before gel	0.47	0.53	0.40	
After 4th oilflood before gel	0.48	0.52	0.38	
After 1st oilflood after gel	0.24	0.76	0.43*	0.33

* $S_{wr}+S_{gel}$

Table I-3e. Pore-Volume Determination from Water-Tracer Studies and

Residual-Saturation Determination from Material Balance Calculations
 Core SSL-68 [Oil Phase: Oil A, Gelant: 1.39% HPAM (Marathon), 0.0212% Cr(III)-acetate]

Water-tracer study	V_p/V_{po}	$1-V_p/V_{po}$	S_{or}	S_{gel}
After 1st waterflood before gel	0.65	0.35	0.42	
After 2nd waterflood before gel	0.61	0.39	0.43	
After 3rd waterflood before gel	0.59	0.41	0.43	
After 4th waterflood before gel	0.60	0.40	0.41	
After 1st waterflood after gel			0.39	
After 2nd waterflood after gel			0.40	

Table I-3f. Pore-Volume Determination from Oil-Tracer Studies and
 Residual-Saturation Determination from Material Balance Calculations
 Core SSL-68 [Oil Phase: Oil A, Gelant: 1.39% HPAM (Marathon), 0.0212% Cr(III)-acetate]

Oil-tracer study	V_p/V_{po}	$1-V_p/V_{po}$	S_{wr}
After 1st oilflood before gel	0.72	0.28	0.28
After 2nd oilflood before gel	0.72	0.28	0.27
After 3rd oilflood before gel	0.71	0.29	0.27
After 4th oilflood before gel	0.73	0.27	0.28
After 1st oilflood after gel			0.37*

* $S_{wr}+S_{gel}$

Table I-3g. Pore-Volume Determination from Water-Tracer Studies and
 Residual-Saturation Determination from Material Balance Calculations
 Core SSH-69 (Oil Phase: Oil A, Gelant: 4% 12-hydroxystearic acid in Oil A)

Water-tracer study	V_p/V_{po}	$1-V_p/V_{po}$	S_{or}
After 1st waterflood before gel	0.63	0.37	0.36
After 1st waterflood after gel			0.33*

* $S_{or}+S_{gel}$

Table I-3h. Pore-Volume Determination from Oil-Tracer Studies and Residual-Saturation Determination from Material Balance Calculations
Core SSH-69 (Oil Phase: Oil A, Gelant: 4% 12-hydroxystearic acid in Oil A)

Oil-tracer study	V_p/V_{po}	$1-V_p/V_{po}$	S_{wr}
After 1st oilflood before gel	0.76	0.24	0.28
After 2nd oilflood before gel	0.76	0.24	0.30
After 1st oilflood after gel			0.22
After 2nd oilflood after gel			0.30

Table I-3i. Pore-Volume Determination from Water-Tracer Studies and Residual-Saturation Determination from Material Balance Calculations
Core SSH-78 [Oil Phase: Oil A, Gelant: 0.75% HPAM (Alcoflood 935®), 0.0625% Cr(III)-acetate]

Water-tracer study	V_p/V_{po}	$1-V_p/V_{po}$	S_{or}
After 1st waterflood before gel	0.70	0.30	0.33
After 1st waterflood after gel			0.33
After 2nd waterflood after gel			0.35
After 3rd waterflood after gel			0.36

Table I-3j. Pore-Volume Determination from Oil-Tracer Studies and Residual-Saturation Determination from Material Balance Calculations
Core SSH-78 [Oil Phase: Oil A, Gelant: 0.75% HPAM (Alcoflood 935®), 0.0625% Cr(III)-acetate]

Oil-tracer study	V_p/V_{po}	$1-V_p/V_{po}$	S_{wr}
After 1st oilflood before gel	0.76	0.24	0.26
After 1st oilflood after gel			0.54
After 2nd oilflood after gel			0.53

Table I-3k. Pore-Volume Determination from Water-Tracer Studies and Residual-Saturation Determination from Material Balance Calculations
Core SSH-85 (Oil Phase: Oil A, Gelant: 18% 12-hydroxystearic acid in Oil A)

Water-tracer study	V_p/V_{po}	$1-V_p/V_{po}$	S_{or}
After 1st waterflood before gel	0.69	0.31	0.34

Table I-3l. Pore-Volume Determination from Oil-Tracer Studies and Residual-Saturation Determination from Material Balance Calculations
Core SSH-85 (Oil Phase: Oil A, Gelant: 18% 12-hydroxystearic acid in Oil A)

Oil-tracer study	V_p/V_{po}	$1-V_p/V_{po}$	S_{wr}
After 1st oilflood before gel	0.78	0.22	0.30

Table I-3m. Pore-Volume Determination from Water-Tracer Studies and Residual-Saturation Determination from Material Balance Calculations
Core SSH-86 (Oil Phase: Oil A, Gelant: 18% 12-hydroxystearic acid in Oil A)

Water-tracer study	V_p/V_{po}	$1-V_p/V_{po}$	S_{or}
After 1st waterflood before gel	0.64	0.36	0.33
After 2nd waterflood before gel	0.61	0.39	0.35

Table I-3n. Pore-Volume Determination from Oil-Tracer Studies and Residual-Saturation Determination from Material Balance Calculations
Core SSH-86 (Oil Phase: Oil A, Gelant: 18% 12-hydroxystearic acid in Oil A)

Oil-tracer study	V_p/V_{po}	$1-V_p/V_{po}$	S_{wr}
After 1st oilflood before gel	0.77	0.23	0.27
After 2nd oilflood before gel	0.75	0.25	0.28

Table I-3o. Pore-Volume Determination from Water-Tracer Studies and Residual-Saturation Determination from Material Balance Calculations
Core SSH-S2 [Oil Phase: Oil A, Gelant: 0.5% HPAM (Alcoflood 935®), 0.0417% Cr(III)-acetate]

Water-tracer study	V_p/V_{po}	$1-V_p/V_{po}$	S_{or}	S_{gel}
After 1st waterflood before gel	0.72	0.28	0.28	
After 1st waterflood after gel	0.64	0.36	0.30	0.06
After 2nd waterflood after gel	0.64	0.36	0.35	0.01

Table I-3p. Pore-Volume Determination from Oil-Tracer Studies and Residual-Saturation Determination from Material Balance Calculations
Core SSH-S2 [Oil Phase: Oil A, Gelant: 0.5% HPAM (Alcoflood 935®), 0.0417% Cr(III)-acetate]

Oil-tracer study	V_p/V_{po}	$1-V_p/V_{po}$	S_{wr}	$S_{o(trap)}$
After 1st oilflood before gel	0.74	0.26	0.28	
After 1st oilflood after gel	0.33	0.67	0.53*	0.14
After 2nd oilflood after gel	0.42	0.58	0.44*	0.14

* $S_{wr}+S_{gel}$

Table I-4a. Relative Dispersivities from Water-Tracer Studies
Core SSH-64 (Oil Phase: Oil A, Gelant: 2% 12-hydroxystearic acid in Soltrol-130)

Water-tracer study	$a/a_o(10/90)$	$a/a_o(20/50)$
After 1st waterflood before gel	35	43
After 1st waterflood after gel	1	2

Table I-4b. Relative Dispersivities from Oil-Tracer Studies
Core SSH-64 (Oil Phase: Oil A, Gelant: 2% 12-hydroxystearic acid in Soltrol-130)

Oil-tracer study	$a/a_o(10/90)$	$a/a_o(20/50)$
After 1st oilflood before gel	1	1
After 2nd oilflood before gel	1	1
After 1st oilflood after gel	9	10
After 2nd oilflood after gel	6	6

Table I-4c. Relative Dispersivities from Water-Tracer Studies
Core LSH-67 [Oil Phase: Oil A, Gelant: 1.39% HPAM (Marathon), 0.0212% Cr(III)-acetate]

Water-tracer study	$a/a_o(10/90)$	$a/a_o(20/50)$
After 1st waterflood before gel	13	6
After 2nd waterflood before gel	12	9
After 3rd waterflood before gel	11	7
After 4th waterflood before gel	13	8

Table I-4d. Relative Dispersivities from Oil-Tracer Studies
Core LSH-67 [Oil Phase: Oil A, Gelant: 1.39% HPAM (Marathon), 0.0212% Cr(III)-acetate]

Oil-tracer study	$a/a_o(10/90)$	$a/a_o(20/50)$
After 1st oilflood before gel	1	1
After 2nd oilflood before gel	2	2
After 3rd oilflood before gel	2	1
After 4th oilflood before gel	3	2
After 1st oilflood after gel	4	3

Table I-4e. Relative Dispersivities from Water-Tracer Studies
 Core SSL-68 [Oil Phase: Oil A, Gelant: 1.39% HPAM (Marathon), 0.0212% Cr(III)-acetate]

Water-tracer study	$a/a_o(10/90)$	$a/a_o(20/50)$
After 1st waterflood before gel	51	10
After 2nd waterflood before gel	46	9
After 3rd waterflood before gel	51	10
After 4th waterflood before gel	35	15

Table I-4f. Relative Dispersivities from Oil-Tracer Studies
 Core SSL-68 [Oil Phase: Oil A, Gelant: 1.39% HPAM, 0.0212% Cr(III)-acetate]

Oil-tracer study	$a/a_o(10/90)$	$a/a_o(20/50)$
After 1st oilflood before gel	1	1
After 2nd oilflood before gel	1	1
After 3rd oilflood before gel	1	1
After 4th oilflood before gel	1	1

Table I-4g. Relative Dispersivities from Water-Tracer Studies
 Core SSH-69 (Oil Phase: Oil A, Gelant: 4% 12-hydroxystearic acid in Oil A)

Water-tracer study	$a/a_o(10/90)$	$a/a_o(20/50)$
After 1st waterflood before gel	68	53

Table I-4h. Relative Dispersivities from Oil-Tracer Studies
 Core SSH-69 (Oil Phase: Oil A, Gelant: 4% 12-hydroxystearic acid in Oil A)

Oil-tracer study	$a/a_o(10/90)$	$a/a_o(20/50)$
After 1st oilflood before gel	1	1
After 2nd oilflood before gel	1	1

Table I-4i. Relative Dispersivities from Water-Tracer Studies
 Core SSH-78 [Oil Phase: Oil A, Gelant: 0.75% HPAM (Alcoflood 935®), 0.0625% Cr(III)-acetate]

Water-tracer study	$a/a_o(10/90)$	$a/a_o(20/50)$
After 1st waterflood before gel	76	77

Table I-4j. Relative Dispersivities from Oil-Tracer Studies
 Core SSH-78 [Oil Phase: Oil A, Gelant: 0.75% HPAM (Alcoflood 935®), 0.0625% Cr(III)-acetate]

Oil-tracer study	$a/a_o(10/90)$	$a/a_o(20/50)$
After 1st oilflood before gel	1	1

Table I-4k. Relative Dispersivities from Water-Tracer Studies
 Core SSH-85 (Oil Phase: Oil A, Gelant: 18% 12-hydroxystearic acid in Oil A)

Water-tracer study	$a/a_o(10/90)$	$a/a_o(20/50)$
After 1st waterflood before gel	75	39

Table I-4l. Relative Dispersivities from Oil-Tracer Studies
 Core SSH-85 (Oil Phase: Oil A, Gelant: 18% 12-hydroxystearic acid in Oil A)

Oil-tracer study	$a/a_o(10/90)$	$a/a_o(20/50)$
After 1st oilflood before gel	1	1

Table I-4m. Relative Dispersivities from Water-Tracer Studies
 Core SSH-86 (Oil Phase: Oil A, Gelant: 18% 12-hydroxystearic acid in Oil A)

Water-tracer study	$a/a_o(10/90)$	$a/a_o(20/50)$
After 1st waterflood before gel	41	33
After 2nd waterflood before gel	71	25

Table I-4n. Relative Dispersivities from Oil-Tracer Studies
 Core SSH-86 (Oil Phase: Oil A, Gelant: 18% 12-hydroxystearic acid in Oil A)

Oil-tracer study	$a/a_o(10/90)$	$a/a_o(20/50)$
After 1st oilflood before gel	1	1
After 2nd oilflood before gel	1	1

Table I-4o. Relative Dispersivities from Water-Tracer Studies
 Core SSH-S2 [Oil Phase: Oil A, Gelant: 0.5% HPAM (Alcoflood 935®), 0.0417% Cr(III)-acetate]

Water-tracer study	$a/a_o(10/90)$	$a/a_o(20/50)$
After 1st waterflood before gel	5	6
After 1st waterflood after gel	28	22
After 2nd waterflood after gel	26	57

Table I-4p. Relative Dispersivities from Oil-Tracer Studies
 Core SSH-S2 [Oil Phase: Oil A, Gelant: 0.5% HPAM (Alcoflood 935®), 0.0417% Cr(III)-acetate]

Oil-tracer study	$a/a_o(10/90)$	$a/a_o(20/50)$
After 1st oilflood before gel	1	1
After 1st oilflood after gel	10	8
After 2nd oilflood after gel	7	6

APPENDIX J

Technology Transfer

PROJECT REVIEW MEETINGS

November 10, 1994 in Socorro. 20 people from 10 oil companies in attendance.

February 8, 1994 in Socorro. 17 people from 9 oil companies in attendance.

May 19, 1993 in Socorro. 14 people from 8 oil companies in attendance.

November 5, 1992 in Socorro. 14 people from 8 oil companies in attendance.

May 21, 1992 in Socorro. 13 people from 7 oil companies in attendance.

May 13, 1991 in Socorro. 12 people from 7 oil companies in attendance.

June 4, 1990 in Socorro. 8 people from 6 oil companies in attendance.

ORGANIZATIONS CURRENTLY SUPPORTING THE PROJECT

Arco Exploration and Production Technology Co.,
British Petroleum Company,
Chevron Petroleum Technology Co.,
Conoco Inc.,
Exxon Production Research Company,
Marathon Oil Co.,
Mobil Research and Development Corp.,
Phillips Petroleum Co. (including Drilling Specialties),
Texaco Inc.,
Unocal,
United States Department of Energy,
State of New Mexico.

PAPERS RESULTING FROM DOE PROJECTS DE-AC22-92BC14880 AND DE-FG22-89BC14447

Seright, R.S. and Liang, J.: "A Comparison of Different Types of Blocking Agents," paper SPE 30120 presented at the 1995 SPE European Formation Damage Control Conference, The Hague, May 15-16.

Seright, R.S.: "Gel Placement in Fractured Systems," paper SPE 27740 presented at the 1994 SPE/DOE Symposium on Improved Oil Recovery, Tulsa, OK, April 17-20.

Liang, J., Sun, H., Seright, R.S.: "Why Do Gels Reduce Water Permeability More Than Oil Permeability?," paper SPE 27829 presented at the 1994 SPE/DOE Symposium on Improved Oil Recovery, Tulsa, OK,

April 17-20.

Seright, R.S. and Liang, J.: "A Survey of Field Applications of Gel Treatments for Water Shutoff," paper SPE 26991 presented at the 1994 SPE Permian Basin Oil & Gas Recovery Conference, Midland March 16-18.

Liang, J., Lee, R.L., Seright, R.S.: "Placement of Gels in Production Wells," *SPE Production & Facilities* (Nov. 1993) 276-284; *Transactions AIME* **295**.

Seright, R.S.: "Effect of Rock Permeability on Gel Performance in Fluid-Diversion Applications," *In Situ* (1993) **17**, No.4, 363-386.

Seright, R.S., Liang, J., and Sun, H.: "Gel Treatments in Production Wells with Water Coning Problems," *In Situ* (1993) **17**, No.3, 243-272.

Seright, R.S.: "Reduction of Gas and Water Permeabilities Using Gels," paper SPE 25855 presented at the 1993 SPE Joint Rocky Mountain Regional and Low Permeability Reservoirs Symposium, Denver, CO, April 26-28.

Seright, R.S. and Martin, F.D.: "Impact of Gelation pH, Rock Permeability, and Lithology on the Performance of a Monomer-Based Gel," *SPE Reservoir Engineering* (Feb. 1993) 43-50.

Seright, R.S.: "Impact of Permeability and Lithology on Gel Performance," paper SPE 24190 presented at the 1992 SPE/DOE Symposium on Enhanced Oil Recovery, Tulsa, OK, April 22-24.

Sorbie, K.S. and Seright, R.S.: "Gel Placement in Heterogeneous Systems with Crossflow," paper SPE 24192 presented at the 1992 SPE/DOE Symposium on Enhanced Oil Recovery, Tulsa, OK, April 22-24.

Liang, J., Sun, H., Seright, R.S.: "Reduction of Oil and Water Permeabilities Using Gels," paper SPE 24195 presented at the 1992 SPE/DOE Symposium on Enhanced Oil Recovery, Tulsa, OK, April 22-24.

Seright, R.S. and Martin, F.D.: "Effect of Cr^{3+} on the Rheology of Xanthan Formulations in Porous Media: Before and After Gelation," *In Situ* (1992) **16**, No.1, 1-16.

Seright, R.S.: "Impact of Dispersion on Gel Placement for Profile Control," *SPE Reservoir Engineering* (Aug. 1991) 343-352.

Seright, R.S.: "Effect of Rheology on Gel Placement," *SPE Reservoir Engineering* (May 1991), 212-218; *Transactions AIME* **291**.

PRESENTATIONS (WITHOUT PAPERS)

"Cost Effective Methods to Reduce Water Production," SPE Distinguished Lecture presented at the following local sections of the Society of Petroleum Engineers (costs paid by the SPE Foundation):

1. New Plymouth, New Zealand, April 15, 1994.
2. Darwin, Australia, April 13, 1994.
3. Perth, Australia, April 12, 1994.
4. Adelaide, Australia, April 8, 1994.
5. Melbourne, Australia, April 7, 1994.
6. Sydney, Australia, April 6, 1994.
7. Brisbane, Australia, April 5, 1994.
8. Roswell, New Mexico, March 22, 1994.
9. Midland, Texas, March 17, 1994.
10. Bakersfield, California, March 10, 1994.
11. Santa Maria, California, March 9, 1994.
12. Edmonton, Alberta, Canada, March 8, 1994.
13. Ponca City, Oklahoma, February 17, 1994.
14. Bartlesville, Oklahoma, February 17, 1994.
15. Grayville, Illinois, February 16, 1994.
16. Pittsburgh, Pennsylvania, February 15, 1994.
17. Traverse City, Michigan, February 14, 1994.
18. Liberal, Kansas, January 21, 1994.
19. Gillette, Wyoming, January 19, 1994.
20. Rock Springs, Wyoming, January 18, 1994.
21. Farmington, New Mexico, January 17, 1994.
22. Beijing, China, November 25, 1993.
23. Jakarta, Indonesia, November 22, 1993.
24. Ahmedabad, India, November 18, 1993.
25. Karachi, Pakistan, November 15, 1993.
26. Muscat, Oman, November 14, 1993.
27. Doha, Qatar, November 10, 1993.
28. Dhahran, Saudi Arabia, November 9, 1993.
29. Cairo, Egypt, November 8, 1993.
30. Lubbock, Texas, October 21, 1993.
31. Mobile, Alabama, October 20, 1993.
32. Shreveport, Louisiana, October 19, 1993.
33. Abilene, Texas, October 18, 1993.
34. Port of Spain, Trinidad, September 27, 1993.
35. Maracaibo, Venezuela, September 22, 1993.
36. Santa Cruz, Bolivia, September 21, 1993.
37. Buenos Aires, Argentina, September 16, 1993.
38. Quito, Ecuador, September 14, 1993.
39. Bogota, Colombia, September 13, 1993.
40. Socorro, New Mexico (NM Tech), September 8, 1993.

Other Recent Presentations

"Overview of Conformance and Sweep Improvement Techniques," presented at the Permian Basin Conformance Control and Sweep Improvement Seminar, Midland, TX, October 26, 1994.

"Challenges of Gel Placement in Oil Recovery," presented at the University of Kansas, Department of Chemical and Petroleum Engineering, Lawrence, KS, September 21, 1994.

"Use of Gels to Reduce Water Production During Oil Recovery," presented at the Lawrence Berkeley Laboratory, Berkeley, CA, December 10, 1993.

"Disproportionate Permeability Reduction by Gels," (Jenn-Tai Liang) presented at the SPE Forum, *Advances in Conformance Control*, Snow Mass, CO, August 11, 1993.

PREVIOUS REPORTS FROM DOE PROJECTS DE-AC22-92BC14880 AND DE-FG22-89BC14447

Seright, R.S.: "Improved Techniques for Fluid Diversion in Oil Recovery Processes," first annual report (DOE/BC/14880-5), Contract No. DE-AC22-92BC14880, U.S. DOE (Dec., 1993).

Seright, R.S. and Martin, F.D.: "Fluid Diversion and Sweep Improvement with Chemical Gels in Oil Recovery Processes," final report (DOE/BC/14447-15), Contract No. DE-FG22-89BC14447, U.S. DOE (Sept, 1992).

Seright, R.S. and Martin, F.D.: "Fluid Diversion and Sweep Improvement with Chemical Gels in Oil Recovery Processes," second annual report (DOE/BC/14447-10), Contract No. DE-FG22-89BC14447, U.S. DOE (Nov. 1991).

Seright, R.S. and Martin, F.D.: "Fluid Diversion and Sweep Improvement with Chemical Gels in Oil Recovery Processes," first annual report (DOE/BC/14447-8), Contract No. DE-FG22-89BC14447, U.S. DOE (June 1991).